Chronological, magmatological and geochemical study of post-collisional basaltic volcanism in Central Anatolia and its spatio-temporal evolution

Gullu Deniz Doğan Külahci Doğan

N° d'Ordre : D.U. 2593

UNIVERSITE BLAISE PASCAL

U.F.R. Sciences et Technologies

ECOLE DOCTORALE DES SCIENCES FONDAMENTALES

N° 830

THESE

présentée pour obtenir le grade de

DOCTEUR D'UNIVERSITE

***Spécialité** : Géochimie - Volcanologie*

Par :

KÜLAHCI DOĞAN G. Deniz

Master

Le volcanisme basaltique post-collisionnel d'Anatolie Centrale
Etude chronologique, magmatologique et géochimique
Evolution spatio-temporelle

Soutenue publiquement le 1 Septembre 2015, devant le commission d'examen

President	: **LE PENNEC Jean-Luc**	Université Blaise Pascal Clermont-Ferrand
Rapporteur	: **GUILLOU Hervé**	LSCE CEA-CNRS- Gif-Sur-Yvette
Rapporteur	: **SEYİTOĞLU Gürol**	Université d'Ankara - Ankara
Examinateur	: **KÜRKÇÜOĞLU Biltan**	Université Hacettepe- Ankara
Examinateur	: **MURATÇAY VAROL Elif**	Université Hacettepe- Ankara
Directeur de thèse	: **TEMEL Abidin**	Université Hacettepe- Ankara
Co-directeur de thèse	: **GOURGAUD Alain**	Université Blaise Pascal Clermont-Ferrand

Le volcanisme basaltique post-collisionnel d'Anatolie Centrale
Etude chronologique, magmatologique et géochimique
Evolution spatio-temporelle

Résumé

Cette thèse est consacrée à la caractérisation pétrologique et géochimique des basaltes quaternaires post-collisionnels d'Anatolie centrale (strato-volcans Erciyes et Hasandağ et volcanisme dispersé d'Obruk-Zengen et de Karapınar), en se focalisant sur l'évolution spatio-temporelle de ce magmatisme de la Cappadoce (Turquie).

Par la géochronologie K-Ar, la coexistence de basaltes alcalins et calco-alcalins a été démontrée, parfois dans un même lieu et à la même époque. Par ailleurs, nos résultats montrent aussi que ces basaltes peuvent être très jeunes (quelques milliers d'années seulement).

La minéralogie des basaltes quaternaires de la Cappadoce est la suivante : plagioclase, olivine, clinopyroxène, orthopyroxène et oxydes (magnétite, ilménite). Pourtant, seuls les basaltes de l'Erciyes contiennent de l'orthopyroxène, alors que ceux du Hasandağ et du volcanisme dispersé d'Obruk-Zengen et de Karapınar en sont dépourvus. Les phénocristaux de plagioclases présentent souvent des figures de déséquilibre, attribuées au processus de mélange magmatique : zonages complexes (normaux, inverses, oscillatoires), richesse en inclusions vitreuses, figures de résorption. Toutefois, la minéralogie observée est compatible avec un processus de cristallisation fractionnée dominant. Les géobaromètres utilisés montrent que l'origine des magmas de l'Erciyes est plus superficielle que celle des autres sites.

Les résultats en géochimie confirment la dualité minéralogique observée entre l'Erciyes et les autres secteurs, ainsi que les caractères alcalins (néphéline normative) et calco-alcalins de basaltes parfois contemporains. Tous les basaltes étudiés sont enrichis en LREE et LILE. Les données isotopiques (Sr, Nd, Pb, O) montrent l'importance de la source lithosphérique enrichie. L'ensemble des données géochimiques montre aussi la signature d'autres sources et processus comme la contamination par la croûte continentale et l'héritage d'une ancienne subduction.

Mots Clés: *Turquie, Anatolie Centrale, post-collisionnel, Quaternaire, basaltes, âge K-Ar, minéralogie, pétrologie, géochimie.*

Chronological, magmatological and geochemical study of post-collisional Basaltic volcanism in Central Anatolia and Its spatio-temporal evolution

Abstract

This thesis revealed the petrological and geochemical characterization of post-collisional Quaternary basalts of Central Anatolia (Erciyes and Hasandağ stratovolcanoes, and dispersed volcanisms of Obruk-Zengen and Karapınar), focusing on the spatiotemporal evolution of the magmatism in Cappadocia (Turkey).

K-Ar geochronology indicated the coexistence of alkaline and calc-alkaline basalts from the same location and age. Moreover, the results also show that these basalts may be very young (a few thousand years).

The mineralogy of Quaternary basalts from the Cappadocia is as follows: plagioclase, olivine, clinopyroxene, orthopyroxene and oxides (magnetite, ilmenite). Orthopyroxene is observed only in basalts of Erciyes, while it is lacking in Hasandağ and dispersed volcanisms of Obruk-Zengen and Karapınar. The plagioclase phenocrysts often exhibit disequilibrium features attributed to magma mixing process: complex zoning (normal, inverse, oscillatory), concentric zones rich in melt inclusions, resorption features. However, the observed mineralogy is consistent with a dominant fractional crystallization process. The estimated geobarometer show that the origin of magmas of Erciyes is shallower than the other settings.

The results in geochemistry confirm not only the mineralogical duality between Erciyes and the other settings but also the coexistence of alkaline (normative nepheline) and calc-alkaline characters of contemporary basalts. All studied basalts are enriched in LREE (Light Rare Earth Elements) and LILE (Large Ion Lithophile Elements). The isotopic data (Sr, Nd, Pb, O) indicate the importance of enriched lithospheric source. All geochemical data also display the signature of other sources and processes such as contamination by the continental crust and heritage of a former subduction.

Keywords: *Turkey, Central Anatolia, post-collisional, Quaternary, basalts, K-Ar age, mineralogy, petrology, geochemistry.*

Orta Anadolu'daki çarpışma sonrası bazaltik volkanizmanın kronolojik, Magmatolojik ve jeokimyasal incelemesi, Zamansal ve mekansal evrimi

Özet

Bu tez Orta Anadolu'daki (Erciyes ve Hasandağ stratovolkanları ile Obruk-Zengen ve Karapınar dağınık volkanizmaları) çarpışma sonrası Kuvaterner bazaltlarının petrolojik ve jeokimyasal özelliklerini ortaya koymuş, Kapadokya'daki magmatizmanın zamansal-mekansal evrimine odaklanmıştır.

K-Ar jeokronolojisi, aynı konum ve yaşta olan alkali ve kalkalkali bazaltların birlikte varolduğuna işaret etmektedir. Ayrıca, sonuçlar bu bazaltların çok genç (bir kaç bin yıl) olabileceklerini göstermiştir.

Kapadokya'daki Kuvaterner bazaltlarının mineralojisi aşağıdaki gibidir: plajiyoklaz, olivin, klinopiroksen, ortopiroksen ve oksitler (manyetit, ilmenit). Ortopiroksen sadece Erciyes bazaltlarında görülürken, Hasandağ ve Obruk-Zengen ve Karapınar volkanizmalarında yoktur. Plajiyoklaz fenokristalinin çoğunlukla dengesiz özellikler göstermesi magma karşım sürecine işaret etmektedir: karmaşık zonlanma (normal, ters, osilasyonlu), eriyik kapanımlarınca zengin konsantrik zonlar, soğurulma özellikleri. Bununla birlikte, gözlemlenen mineraloji, baskın fraksiyonel kristallenme süreciyle de uyumludur. Hesaplanan jeobarometre Erciyesideki magma kökeninin diğer yerlerden daha sığ'da yer aldığını göstermektedir.

Jeokimyasal sonuçlar Erciyes ve diğer yerlerin sadece mineralojik farklılığını değil, aynı zamanda yaştaş alkali ve kalkalkali bazaltların birlikteliğini de ortaya koymuştur. Çalışılan tüm bazaltlar LREE (Hafif Nadir Toprak Elementler) ve LILE'ce (İri Katyonlu Litofil Elementler) zengindirler. İzotopik veriler (Sr, Nd, Pb, O) zenginleşmiş litosferik kaynağın önemini göstermiştir. Tüm jeokimyasal veriler ayrıca kıtasal kabuk ve daha önceki bir dalma-batmanın kalıntısı ile kontaminasyon gibi süreçleri ve başka kaynakların izlerini de göstermektedir.

Anahtar Kelimeler: *Türkiye, Orta Anadolu, çarpışma sonrası, Kuvaterner, bazaltlar, K-Ar yaşı, mineraloji, petroloji, jeokimya.*

ACKNOWLEDGEMENTS

I would like to thank TUBITAK (The Scientific and Technological Research Council of Turkey) for financial support during my research, Research Project No: 109Y064.

Firstly, I would like to express my sincere gratitude to my advisors Prof. Dr. Abidin TEMEL in Turkey and Prof.Dr. Alain GOURGAUD in France for the continuous support, motivation, and immense knowledge during my Ph.D study and related research.

Besides my advisors, I would like to thank Dr. Catherine DENIEL. Her guidance helped me while researching for and writing this thesis in all the time of research and writing of this thesis.

I would like to thank the rest of my thesis committee: Prof.Dr.Gürol SEYİTOĞLU, Assoc.Prof.Dr.Biltan KÜRKÇÜOĞLU, Assoc.Prof.Dr. Elif VAROL MURATÇAY, Dr.Hervé GUILLOU and Dr. Jean-Luc LE PENNEC for their insightful comments and encouragement.

My sincere thanks also goes to Prof.Dr. Nilgün GÜLEÇ, who supported me throughout my thesis and made constructive criticism to make my manuscript better.

I would like to thank Dr. Christian Pin who always smiled when he saw me at the lab, and gave his positive energy.

I am also grateful to my friend Assis.Prof.Dr. Altuğ Hasözbek who supported me throught this thesis.

My dear “la salle des thésards a Clermont-Ferrand” friends Aude de la Rupelle Asmaa Boujibar, Amelie Didier, Baptiste Debret, Oscar Laurent, Gareth-Engille Mae-Pagucian Fabro, Yannic Guéhenneux, Camille Tiécar, Wu Jia, Elodie Brothelande, Manon Hardigon, Gabrielle Menard and Sarah B. Cichy. Thank you very much for your friendship and many things that make me happy... Je t’embrasse trés trés fort!

I am also grateful to Dr.Marie-Christine Gerbe, Jean-Luc Devidal, Mhammed Benbakkar, Chantal Bosq, Delphine Auclair, Eric Brut and Verenique Gimmenez.

I wish to express my sincere thanks to Burcu Üstün, Sevgi Telsiz, Burcu Kahraman, Yağmur İnal Emiroğlu, Tahir İnan Turan, Erman Özsayın, İnan Ulusoy, and Evren Çubukçu.

If “Çokyılmaz Family” were not in Clermont-Ferrand probaby I would have been cold during my stay at the dormitory. You are very special for me... Thank you very much!

Last but not the least, I would like to thank my family: my parents (Naime-H.Hüseyin) and to my brother (Cem) for supporting me spiritually throughout writing this thesis and the whole of my life.

And my lovely husband Tunca, thank you very much for supporting and convincing me to get married in the most difficult period of my thesis...

TABLE OF CONTENTS

1 INTRODUCTION 4

1.1. PURPOSE AND SCOPE 4

1.2. STUDIED AREAS 5

1.3. PREVIOUS STDUDIES IN CAPPADOCIA 10

1.4. LABORATORY STUDIES AND ANALYTICAL METHODS 13

1.4.1. Mineraology and Petrography 13

1.4.2. Geochemical Analyses 13

1.4.3. K-Ar Dating Method 18

2 GENERAL GEOLOGY 19

2.1. GENERAL SETTING OF THE STUDIED AREAS IN CAPPADOCIA 19

2.2. OVERVIEW ON POST-COLLISIONAL MAGMATISM 26

2.3. THE BASEMENT ROCKS OF CAPPADOCIA 28

2.4. BRIEFLY OVERVIEW OF THE MAJOR ELEMENT ANALYSIS AND THE CLASSIFICATION OF THE ERCİYES STRATOVOLCANO AND SOUTHWESTERN CAPPADOCIA SAMPLES 28

2.5. THE ERCİYES STRATOVOLCANO 31

2.6. THE SOUTHWESTERN CAPPADOCIA VOLCANISM 35

2.6.1. Hasandağ Basaltic Volcanism 36

2.6.2. The Obruk-Zengen Dispersed Volcanism 38

2.6.3. The Karapınar Dispersed Volcanism 40

2.7. CONCLUSION 40

3 MINERALOGY AND PETROGRPHY 42

3.1. THE BASALTS S.L. OF ERCİYES STROTOVOLCANO 42

3.2. THE BASALTS S.L. OF SOUTHWESTERN CAPPADOCIA 48

3.2.1. The Basalts s.l. of Hasandağ Stratovolcano 48

3.2.2. The Basalts s.l. of the Obruk-Zengen Dispersed Volcanism 53

3.2.3. Basalts s.l. of the Karapınar Dispersed Volcanism 56

3.3. CONCLUSION 59

4 MINERAL CHEMISTRY 61

4.1. MINERAL CHEMISTRY OF THE BASALTS S.L. OF THE ERCİYES STROTOVOLCANO 61

4.2. MINERAL CHEMISTRY OF THE BASALTS S.L OF THE SOUTHWESTERN CAPPADOCIA VOLCANISM 68

4.2.1. The Hasandağ Stratovolcano 68

4.2.2. The Obruk-Zengen Dispersed Volcanism ... *71*
4.2.3. The Karapınar Dispersed Volcanism ... *74*
4.3. CRYSTAL-LIQUID EQUILIBRIUM ... 76
4.3.1. Erciyes Stratovolcano ... *76*
4.3.1.1. Olivine-Liquid Equilibrium ... *76*
4.3.1.2. Clinopyroxene-Liquid Equilibrium ... *78*
4.3.1.3. Feldispar-Liquid Equilibrium ... *79*
4.3.2. Southwestern Cappadocia Volcanism ... *80*
4.3.2.1. Olivine-Liquid Equilibrium ... *80*
4.3.2.2. Clinopyroxene-Liquid Equilibrium ... *81*
4.3.2.3. Feldspar-Liquid Equilibrium ... *82*
4.4. GEOTHERMOMETER AND GEOBAROMETER CALCULATION ... 83
4.4.1. Erciyes Stratovolcano ... *84*
4.4.1.1. Olivine-Liquid Geothermometer ... *85*
4.4.1.2. Clinopyroxene-Liquid Geothermometer ... *85*
4.4.1.3. Clinopyroxene-Orthopyroxene Geothermometer ... *86*
4.4.1.4. Plagioclase-Liquid Geothermometer ... *86*
4.4.2. The Soutwestern Cappadocia ... *87*
4.4.2.1. Olivine-Liquid Geothermometer ... *88*
4.4.2.2. Clinopyroxene-Liquid Geothermometer ... *89*
4.4.2.3. Plagioclase-Liquid Geothermometer ... *90*
4.4.3. Conclusion ... *91*

---

5 GEOCHEMISTRY ... **93**
5.1. MAJOR, TRACE AND RARE EARTH ELEMENT (REE) ANALYSIS ... 93
5.1.1. Erciyes Strotovolcano ... *93*
5.1.2. Southwestern Cappadocia Volcanism ... *108*
5.2. ISOTOPE GEOCHEMISTRY ... 125
5.2.1. Sr-Nd-Pb-O Isotope Geochemistry ... *125*
5.2.1.1. Erciyes Stratovolcano ... *125*
5.2.1.2. Southwestern Cappadocia Volcanism ... *137*
5.3. CONCLUSION ... 148

---

6 DISCUSSION and CONCLUSION ... **153**
6.1. ERCİYES STRATOVOLCANO ... 153
6.1.1. Partial Melting ... *154*
6.1.2. Fractional Crystallization ... *157*
6.1.3. Crustal Contamination and AFC
(Assimilation Fractional Crystallization) ... *159*
6.1.3.1. Potential Contaminants and AFC modeling ... *165*
6.1.4. Mixing Sources ... *167*
6.2. SOUTHWESTERN CAPPADOCİA VOLCANISM ... 169

6.2.1. Partial Melting *170*
6.2.2. Fractional Crystallization *171*
6.2.3. Crustal Contamination-AFC *174*
6.2.3.1. Potential Contaminants and AFC modeling *178*
6.2.4. Mixing Souces *180*
6.3. TECTONICS 181
6.4. POSSIBLE MAGMA SOURCES 185
6.5. COMPARISON OF ES, HS, OZ AND K 192
6.6. TEMPORAL AND SPATIAL EVOLUTION OF MAGMA 194

APPENDIX **199**

REFERENCES **208**

1. INTRODUCTION

1.1. Purpose and Scope

The purpose of the thesis is to present new geochronological, mineralogical and geochemical (major, trace and isotope elements) data on the Quaternary post collisional basaltic volcanism of Central Anatolia, to emphasize possible temporal and spatial evolution, and to evaluate the lithosphere-asthenosphere interactions.

Several studies have been performed about Mio-Pliocene acidic volcanism which is located in the Cappadocia region and cover large areas, and Quaternary Hasandağ and Erciyes stratovolcanoes (Ayrancı, 1969; Keller, 1974; Batum, 1978; Ercan et al., 1990); Aydar, 1992; Le Pennec et al., 1994; Notsu et al; Şen, 1997; Temel, 1992; Temel et al., 1998; Deniel et al., 1998; Kürkçüoğlu, 2000; Alıcı Şen, 2002; Le Pennec et al., 2005). Significant contributions have been proposed in the literature about the geochronology, stratigraphy, petrology and geochemistry, but there are no adequate data on the basaltic volcanism spreading over large areas in Cappadocia.

The purpose of sampling was to collect Quaternary basaltic volcanics that represents the post-collisional characteristics of the Central Anatolia. On this basis, total 63 samples were collected from the study area. Fresh and unaltered 43 samples have been selected for thin section. These 43 thin sections were examined under the microscope and 34 samples among them were selected for geochemical studies (major and trace element analyses).

According to major and trace element analyses, LOI contents, hand specimen and thin section observations of the samples and the previous workers studies, 29 unaltered samples were decided to the analyses of mineral chemistry and for geochronological studies. In the light of preliminary data of mineral chemistry and petrography; K-Ar dating, radiogenic $^{206}Pb/^{204}Pb$, $^{207}Pb/^{204}Pb$, $^{208}Pb/^{204}Pb$, $^{87}Sr/^{86}Sr$, $^{143}Nd/^{144}Nd$ and stable isotope (oxygen) analyses were conducted. All these analyses were financed by TUBITAK (The Scientific and Technological Research Council of Turkey; Research Project 109Y064).

1.2. Studied Areas

The studied areas are located in 1/100 000 scaled Kayseri L-34, K-34, L-35, K-35, Aksaray L-32 and Karaman M-32, M-31 sheets and are given in Figure 1.1. These regions are in the Southern part of the Central Anatolian Volcanic Complex. Four zones are considered: Erciyes stratovolcano at east (Figure 1.2), Hasandağ stratovolcano at southwest (Figure 1.3), dispersed volcanism of Obruk-Zengen, at south of Hasandağ (Figure 1.4) and dispersed volcanism of Karapınar, at the south-west of Hasandağ (Figure 1.5). Volcanics in the region crop out in the form of ignimbritic shields, stratovolcanoes, and dispersed volcanism (maar, dome, lava flow and scoria cones).

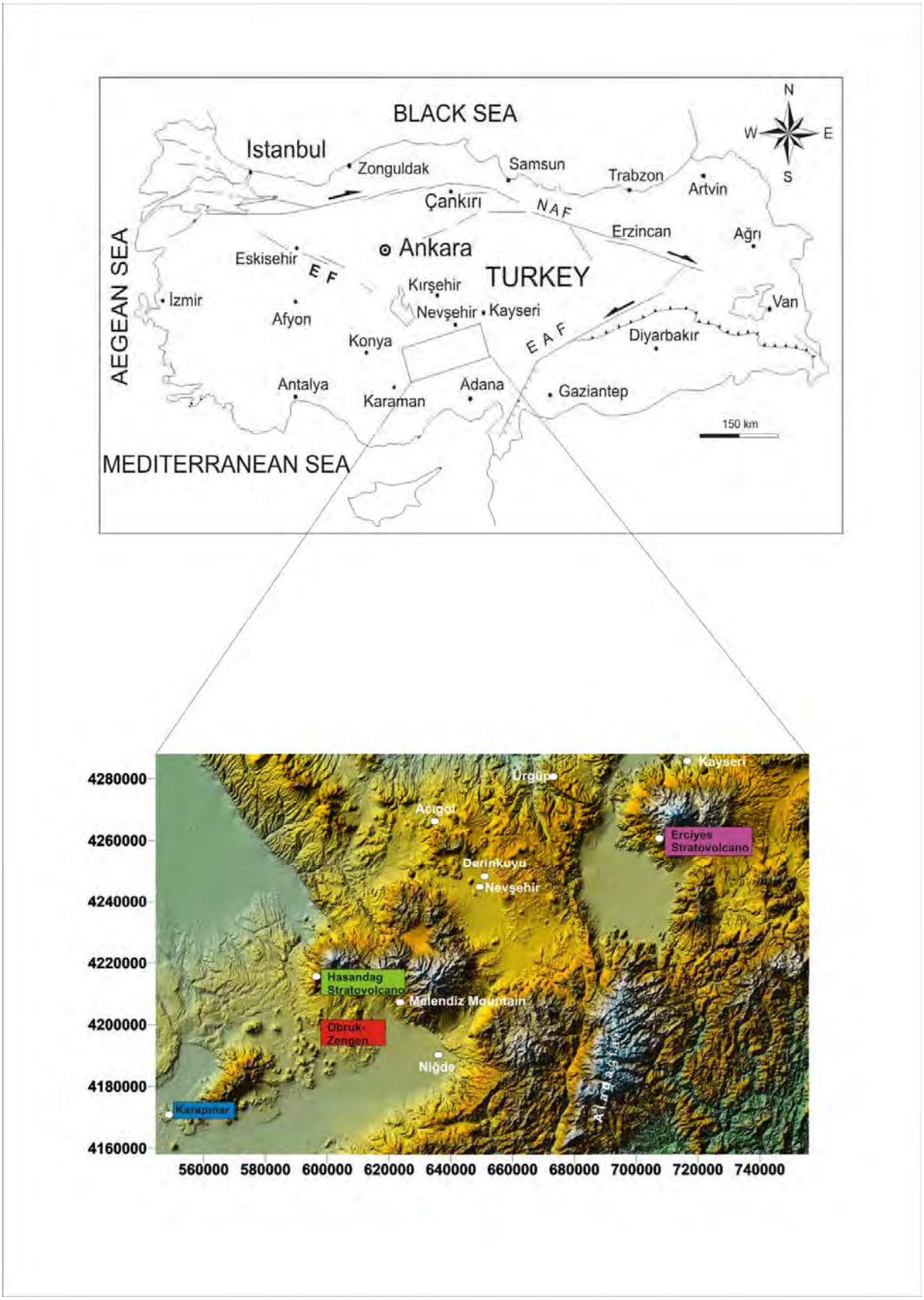

Figure 1.1: Location map of the studied areas (http://www2.jpl.nasa.gov/srtm/)

Figure 1.2: Erciyes stratovolcano (photo from G.Deniz Külahcı)

Figure 1.3: Hasandağ stratovolcano (photo from G.Deniz Külahcı)

Figure 1.4: Karnıyarık scoria cone in the Obruk-Zengen area (photo from Prof.Dr. Abidin Temel)

a)

b)

Figure 1.5: Karapınar area: (a) Meke mountain (b) scoria cone (Meke) in a maar crater (lake) (Photos from Prof.Dr. Abidin Temel)

1.3. Previous Studies in Cappadocia

Central Anatolia (Cappadocia) is a region which is located between the Africa-Arabic and the Eurasian convergent plates. Widespread volcanism that developed after continental collision between the Afro-Arabian and Eurasian plates that began during the early to middle Miocene (Şengör, 1980; Şengör and Yılmaz, 1981; Dewey et al., 1986). The Cappadocian volcanism cropped out as stratovolcanoes and basaltic and rhyolitic monogenic vents in Miocene-Quaternary times (Aydar et al., 1994).

The asidic ignimbritic volcanism in Cappodocia is very spectacular and bulky in Mio-Pliocene. The ignimbrites covered area of approximately 40.000 km^2 and 1000 km^3 in volume (Temel, 1992; Le Pennec et al., 1994; Temel et al., 1998). Pasquare (1968) mapped ignimbrite units in Central Anatolia and exhibited their stratigraphy. Le Pennec et al. (1994) reviewed the stratigraphical sequences of ignimbrites presented in previous studies (Pasquare, 1968; Pasquare et al., 1988; Schumacher et al., 1990) and estimated the volumes of the different ignimbritic units. Some other previous workers performed K/Ar dating on ignimbrites in the region. Innocenti et al. (1975) presented the age of the Valibaba ignimbrite is 2.7-3.0 ± 0.1 Ma, Şen et al. (2003) also dated the Valibaba ignimbrite at 2.8 Ma and Ayrancı (1969) dated ignimbrite located around Erkilet, at 8.53 ± 0.47 Ma.

Erciyes and Hasandağ stratovolcanoes, Obruk-Zengen and Karapınar dispersed (Keller, 1974) volcanisms are significant part of Quaternary basaltic volcanism in Central Anatolia. Moreover, the basaltic volcanism accompanied with the large rhyolitic ignimbritic volcanism for more than 10 Ma helps us to understand the nature and the spatio-temporal processes of the mantellic sources of this post-collisional volcanism. The first detailed stratigraphic studies for the Erciyes and Hasandağ stratovolcanoes were made by Şen (1997) and Aydar (1992), respectively. Ercan et al. (1990) mapped different rock types around Hasandağ stratovolcano. The volcanological and petrological characteristics of Karataş basalts (northwest of Hasandağ stratovolcano) presented by Aydar et al. (1997). Besides, Şen et al. (2002; 2003) studied the products related to the Dikkartın Mountain and Koçdağ from Erciyes.

Geochemical, isotopic and radiometric data from various types of volcanic rocks on Erciyes and Hasandağ stratovolcano, Karapınar and monogenic centers presented by many workers; Pasquare (1968), Innocenti et al.(1975), Ercan et al. (1990; 1994), Notsu et al. (1995), Aydar et al. (1995), Aydar and Gourgaud (1998), Kürkçüoğlu et al. (1998; 2001; 2004; 2010), Şen et al (2003), Alıcı Şen et al. (2004), Deniel et al. (1998), Doğan (2010), Gençalioğlu-Kuşcu (2010) and Gençalioğlu-Kuşçu and Geneli (2010). These previous workers discussed the geodynamical processes related to the formation of the contemporaneous Quaternary alkaline and calc-alkaline magmatism in Central Anatolia. According to Pasquare (1968) and Innocenti et al. (1975), volcanic activity was related to subduction event. On the other hand, Aydar et al. (1995), Notsu et al. (1995) and Kürkçüoğlu et al. (1998; 2001; 2004; 2010) stated that this magmatism was related to intracontinental activity. Deniel et al. (1998) stated that the strong calc-alkaline character of Hasandağ lavas, in the absence of contemporaneous subduction, must be related to the heritage of the early subduction. İlbeyli (2004) also asserted that alkaline and calc-alkaline magmatisms indicated that mantle source before collision was heterogeneous under the Central Anatolian area and the magmas derived from an enriched source, with traces of a previous subduction. Alıcı Şen et al. (2004) revealed that the Central Anatolian volcanism derived from a lithospheric mantle source in which the effects of an ancient subduction occurred. Güçtekin and Köprübaşı (2009) also support this and they claimed that Central Anatolia volcanics were formed by the partial melting of a metasomatized lithospheric mantle. Doğan et al. (2013) and Gençalioğlu-Kuşçu (2010) added, Erciyes mafic lavas and monogenic basalts of Cora Maar (Northwest of Erciyes) formed by shallow melting of a garnet-free lithospheric mantle, respectively. On the other hand, Kürkçüoğlu et al. (2004) claimed that calc-alkaline magmas are related to the partial melting of depleted and enriched asthenospheric sources. They stated that the partial melting was followed by AFC process and the resulting magmas did not derive directly from a melting of subducting slice but from a tholeiitic component.

According to mineralogical and petrological data (Aydar and Gourgaud, 1998) both magma mixing and fractional crystallization are the main petrological processes leading to andesitic and dacitic rocks at Hasandağ stratovolcano. Other study in

Central Anatolia (Siebel et al., 2011) is the rhyolitic Acıgöl area and they claimed that crustal melting, fractional crystallization at high rate and finally mixing with basaltic/andesitic magmas occurred in the genesis of the rhyolites. However, Dogan et al. (2013) claimed that magma mixing process is the major process for the genseis of the Erciyes silicic lavas. Güçtekin and Köprübaşı (2009) emphasized fractional crystallization is an effective processes not only for Hasandağ tholeiitic, alkaline and calc-alkaline rocks but also for Erciyes alkaline and calc-alkaline rocks. Aydar et al. (1994) mentioned that fractional crystallization was the predominant process during the magma evolution of Erciyes and Hasandağ stratovolcanoes, but magma mixing was also effective. Moreover, they stated that when the crustal effect is not considered, the basalts exhibit the mineralogy and chemistry of intra- plate basalts (Aydar et al., 1997). Isobaric and isenthalpic magma mixture of basalt and rhyolite were the main process of the magmatic evolution at Hasandağ stratovolcano (Doğan et al., 2008; Üstünışık and Kılınç (2011).

Toprak and Göncüoğlu (1993) defined 2 different fault systems in Neogene–Quaternary Central Anatolian Volcanic Province. The first system covers Tuz gölü fault, which is a right lateral strike slip fault, and the Ecemiş Fault, which is a left lateral strike slip fault. Other faults run parallel to these 2 fault systems. They claimed that volcanic centers (as Hasandağ, Keçiboyduran and Melendiz stratovolcanoes) were in the juxtaposition of these two fault systems. Ecemiş Fault Zone had gained its main strike slip in pre-Lutetian times and had an offset of 80±10 km (Yetiş and Demirkol, 1984). Extensional strike slip faults in Northern Ecemiş Fault Zone were synchronous (Early Messinien and Early Pleistocene) with Erciyes Basin. That means that Ecemiş Fault Zone was kinematically associated with Erciyes Basin Jaffrey et al. (2004). Dirik and Göncüoğlu (1996) stated that the Tuz gölü and Sultansazlığı basins along with the Ecemiş Fault Zone is an active pull apart basin since the Early Quaternary. They emphasized that seismic activities, which occurred in recent times, indicate that Central Anatolia is tectonically active. Besides, Özsayın et al. (2013) emonstrated that the average vertical displacement rates are different at eastern and western flanks of Tuz Gölü Lake. According to their study NNW–SSE to NE–SW contraction ended by 6.81 ± 0.24 Ma and was followed by N–S to NE–SW

extension during the Pliocene–Quaternary periods. According to Temel et al. (1998) from Miocene (11.2 Ma) to Quaternary times, decreasing $^{87}Sr/^{86}Sr$ ratio of ignimbritic rocks may be linked with the transition from collisional to extensional tectonics. In addition, the transition from calc-alkaline to alkaline compositions through time is related to the development of extensional tectonics in Central Anatolia in the Late Miocene (Deniel et al., 1998). Based on DEM (Digital Elevation Modeling) and field data of Dhont et al. (1998) also support this review.

1.4. Laboratory Studies and Analytical Methods

1.4.1 Mineralogy and Petrography

- **Polarized microscope**

Samples collected from the studied area were cut and left for drying. Later on these samples were carefully studied under the daylight and parts considered as altered were then rasped in cutting machine in "*Magmas et Volcans" laboratory, Blaise Pascal University (Clermont-Ferrand/France)*. After this process, thin sections were prepared. Thin sections were polished at 3 different processes with 10 minute periods each in Mecatech 334 brand machine.

- ***Electron Probe Micro Analyses (EPMA)***

In order to determine the chemical compositions of minerals, a Cameca SX-100 brand electron microscope was used at "*Magmas et Volcans"* laboratory*, Blaise Pascal University (Clermont-Ferrand/ France).* Analyses were made at 15 kv, 10-12 nA and 10 s for phenocrysts, microphenocrysts and microlites, and at 15 kv, 4 nA and 5μm, 10 s for glass analyses. Na and K elements were analyzed first, in order to prevent to the migration of these mobile alkaline elements.

1.4.2. Geochemical Analyses

- **Major and trace elements analytical methods**

For the accuracy of the analyses, fresh and unaltered samples were selected. Selected samples were cut and made into small chips in jaw crusher. Afterwards, small chips milled in agate mortar. The trace and rare earth element analyses have been made at the *Center of Petrographic and Geochemical Research (Centre de Recherches Pétrographiques et Géochimiques) (Nancy/ France).* Main

element dissolutions were expressed in oxide %. Trace and rare earth element analyses were expressed in ppm (parts per million).

- ***ICP-AES (Inductively Coupled Plasma - Atomic Emission Spectrometry)***

Major element (Si, Al, Fe, Mn, Mg, Ca, Na, K, P, and Ti) analyses have been performed at *Service d'Analyse des Roches et des Minéraux, CRPG – CNRS (Nancy/France)* using Jobin-Yvon JY 70. Powdered samples (200 mg) were molten by $LiBO_2$ (Lithium metaborate) and dissolved by HNO_3. Prepared solutions were analyzed by the automatic procedure installed in the system. Detection limits and uncertainties at given intervals for major elements were given in Table1.1 (http://helium.crpg.cnrs-nancy.fr/SARM/pages/roches.html).

Table 1.1: Detection limits for major element analyses for ICP-AES

Major element content

Oxides%	>10%	>5%	>1%	>0.5%	>0.1%	>0.05%	>0.01%	>0.005%	Limit%
SiO_2	<1%	-	-	<10%	-	-	-	-	0.5
Al_2O_3	<1%	-	-	<10%	-	-	-	-	0.02
Fe_2O_3	-	-	<2%	-	<5%	<15%		-	0.01
MnO	-	-	<1%	-	<5%	-	<10%	-	0.0005
MgO	-	<2%	<5%	-	-	<10%	-	-	0.02
CaO	-	<2%	-	<5%	<10%	-	-	-	0.035
Na_2O	-	<2%	-	-	<15%	-	-	-	0.03
K_2O	-	<2%	-	<5%	<10%	<15%	-	-	0.01
TiO_2	-	-	-	<5%	-	<10%	-	-	0.001
P_2O_5	-	-	<5%	-	<10%	-	-	-	0.05

- ***ICP-MS (Inductively Coupled Plasma - Mass Spectrometry)***

Trace element analyses have been conducted in *Service d'Analyse des Roches et des Minéraux, CRPG – CNRS (Nancy, France)* using Perkin Elmer 5000 Mass Spectrometer. The detection limits and uncertainties at given intervals, for trace elements, are given in Table 1.2 (http://helium.crpg.cnrs-nancy.fr/SARM/pages/roches.html).

Table 1.2: Detection limits for trace element analyses and uncertainties for given concentrations

Trace Element Content

	>50 ppm	>10 ppm	>1 ppm	>0.1 ppm	>0.01 ppm	Limit ppm
As	**<5%**	**<10%**	-	-	-	1.10
Ba	**<5%**	**<10%**	-	-	-	**1.50**
Be	**<5%**	**<10%**	-	-	-	**0.40**
Bi	-	**<5%**	**<10%**	-	-	**0.10**
Cd	-	**<5%**	**<15%**	-	-	**0.12**
Ce	-	**<5%**	**<10%**	-	-	**0.10**
Co	**<5%**	**<10%**	**<15%**	-	-	**0.35**
Cr	**<5%**	**<10%**		-	-	**4.00**
Cs		**<5%**	**<10%**	-	-	**0.15**
Cu	**<5%**	**<10%**	-	-	-	**4.50**
Dy	-	-	**<5%**	**<10%**	**<15%**	**0.007**
Er	-	-	**<5%**	**<10%**		**0.003**
Eu	-	-	-	**<5%**	**<10%**	**0.004**
Ga	-	**<5%**	**<8%**	-	-	**0.20**
Gd	-	-	-	**<5%**	**<10%**	**0.02**
Ge	-	**<5%**	**<8%**		-	**0.11**
Hf	-	**<5%**	**<10%**	**<15%**	-	**0.030**
Ho	-	-	**<5%**	**<10%**	-	**0.001**
In	-	-	**<5%**	-	-	**0.10**
La	-	-	**<5%**	**<10%**	-	**0.06**
Lu	-	-	-	**<5%**	**<10%**	**0.001**
Mo	-	**<5%**	**<10%**	-	-	**0.30**

	>50 ppm	>10 ppm	>1 ppm	>0.1 ppm	>0.01 ppm	Limit ppm
Nb	-	**<5%**	**<10%**	**<15%**	-	**0.06**
Nd	-	-	**<5%**	**<10%**	-	**0.03**
Ni	**<5%**	-	-	-	-	**4.50**
Pb	-	**<5%**	**<10%**	-	-	**0.90**
Pr	-	-	**<5%**	**<10%**	-	**0.008**
Rb	-	**<5%**	**<10%**	-	-	**0.30**
Sb	-	**<5%**	**<10%**	-	-	**0.10**
Sm	-	-	**<5%**	**<10%**	-	**0.007**
Sn	**<5%**	**<10%**	**<15%**	-	-	**0.40**
Sr	**<5%**	**<10%**	-	-	-	**1.40**
Ta	-	-	**<10%**	**<15%**	-	**0.015**
Tb	-	-	-	**<5%**	**<10%**	**0.004**
Th	-	**<5%**	**<10%**	**<15%**	-	**0.02**
Tm	-	-	**<5%**	**<10%**	-	**0.005**
U	**<5%**	**<10%**	-	**<15%**	-	**0.03**
V	**<5%**	**<10%**	-	-	-	**0.45**
W	**<5%**	**<10%**	**<15%**	-	-	**0.20**
Y	-	**<5%**	-	-	-	**0.40**
Yb	-	-	**<5%**	**<10%**	-	**0.003**
Zn	**<10%**	-	-	-	-	**14.00**
Zr	**<8%**	-	-	-	-	**0.80**

- **Isotope analyses**

Sr-Nd-Pb

During the selection of the sample for isotope analysis, hand specimen and thin section observations, major and trace element results, LOI contents and previous wrokers studies were taken into consideration. The Sr, Nd and Pb isotope analyses were performed by C.Deniel, both at UMR 6524 Clermont-Ferrand (Sr and Nd) and ENS Lyon (Pb).

Isotopic analyses for Sr and Nd were made using Thermo-Finnigan Triton (TI) brand mass spectrometer at the "*Magmas et Volcans" laboratory, Blaise Pascal University (Clermont-Ferrand/France)*.

Samples selected for isotope analyses were prepared in 4 different data sets and measurements have been completed at different periods. Selected samples were first crushing by jaw crusher at the laboratory *"Magmas et Volcans"*, quartered then approximately 50 mg of it was separated (hand picked selection of unaltered chips). A part of 0.5 mg was selected from unaltered crushed small chips that have no sign of cutting or alteration. Then, 0.2 mg of the selected 0.5 mg grains were

weighed then put into teflon beakers. These separated samples were first washed for 10 minutes by 2N HCl, then was cleaned by distilled water. Later, 1 ml HNO_3+4 ml HF was added and placed on a hot plate at 90°C. During 2 days, three times a day (morning, noon and night) ultrasonic bath were applied then they were again put onto the hot plate. After dissolution process had been completed, Pb, Sr and Nd elements were separated by the method of ion exchange chromatography.

Solutions obtained were taken into a solution by 0.05M HNO_3 and loaded into single Re (Rhenium) filaments with 2 µl Ta_2O_5 activator and 3 drop of 3M H_3PO_4 for Sr isotope measurements. However, for Nd isotope measurements solutions obtained were taken into a solution by 0.05M HNO_3 then loaded into dual W (Tungsten) filament (except the 4th series onto double Re filament) with a drop of 1M H_3PO_4. For the isotopic measurements of Sr and Nd, National Bureau of Standards NBS 987 and JNDi standards have been used, respectively to evaluate the accuracy and reproducibility of the mass spectrometer. Over the period of measurements, replicate analyses of standards gave for the NBS 987, $^{87}Sr/^{86}Sr=0.710238 \pm 5.5.10^{-6}$ (2σ) (N=19) and for JNDi, $^{143}Nd/^{144}Nd=0.512102 \pm 7.2.10^{-6}$ (2σ) (N=24). The $^{87}Sr/^{86}Sr$ ratios were normalized to $^{87}Sr/^{86}Sr$ =0.1194, and $^{143}Nd/^{144}Nd$ ratios were normalized to$^{143}Nd/^{144}Nd$ =0.7219. Total blanks were 0.05-0.1 ng for Sr and 0.09-0.4 ng for Nd. The samples HA15 and ER27 were duplicated to check the reproducibility of the chemical preparation.

Pb isotope analyses were carried out at *Ecole Normale Supérieure de Lyon* (France) using MC-ICP-MS (Multicollector mass spectrometer) (Nu instrument 041). In order to follow the mass fractionation in Pb isotope measurements Tl (thallium) spike has been added (White et al., 2000). The Pb isotopic ratios were corrected for instrumental fractionation using average measured values of the NBS981 standard. Total blank levels were less than 50 pg.

O (Oxygen)

Based on the handspecimen, thin section, major and trace element results of the samples, low LOI contents and unaltered samples were selected for stable isotope analysis. 0.7 mg of powder samples, which milled in agate mortar were manupulated for oxygen isotope analyses.

Oxygen isotope analyses have been performed at the Stable Isotope Laboratory of Jean-Monnet University by Marie-Christine Gerbe, Laboratory of Lithospheric Transfers (LTL) (Saint-Etienne, France).

The extraction of oxygen from the whole rocks and minerals is performed on a conventional extraction line type by reaction at high temperature with BrF_5 (Bromine pentafluoride) and oxygen is converted to CO_2 (Clayton and Mayeda, 1963). The performance of each analysis was calculated by systematically measuring the volume of CO_2 obtained during the conversion reaction. For oxygen isotope measurement of each series, MQ laboratory standard (Université de Capedown, South Africa, Murchinson Quartz) used regularly. MQ results calibrated according to the suggested international quartz standard NBS-28 10.1±0.2 (Vennemann et Smith, 1990). The average of the repetitive measurements (*N*=16) of MQ value was determined as (10.01±0.10). This value is very close to the recommended value. The accuracy and preciseness of analyses were 0.3‰ (2 sigma) during the separation of oxygen from silicates in LTL.

Oxygen isotope analyses were performed on a micromass isoprime triple collector-dual inlet mass spectrometer. In order to correlate the oxygen gas of samples in measurements, the references NBS19 and CO8 carbonate gases were used. The measurement results were normalized as δ18O‰=(R sample/R standard-1)×10^3, R=($^{18}O/^{16}O$) according to the Standard Mean Ocean Water (VSMOW) (Coplen, 1993). Duplicates were made for 12 whole rock samples to determine the average reproducibility of analyzes of our samples. It is ± 0.3 ‰ for whole rock (2 sigma).

1.4.3. K-Ar Dating Method

The selection of the samples for the analysis of K-Ar dating; major and trace elements results, LOI values, macroscopic (hand specimen)-microscopic (thin section) observations and the previous studies were taken into account.

The dating of selected samples has been performed in Laboratoire des Sciences du Climat et de l'Environnement by Hervé Guillou, Unité Mixte de Recherche CEA-CNRS (LSCE) in Gif-sur-Yvette, France.

Samples were crushed (nearly 500 g) and sieved to 0.25 - 0.125 mm size fraction. Approximately, 60 g of fractioned samples were washed in ultrasonic bath with $HC_2H_3O_2$. Groundmass of the rocks was separated following the procedure detailed in Guillou et al. (1998). Initially, magnetic separation was made and later phenocrysts and microphenocrysts were removed by means of heavy liquids (diodomethane). K analyses have been made in the "*Centre de Recherches Pétrographiques et Géochimiques" at Nancy, France.* Ar extraction and the method of analysis are presented in Carbit et al. (1998). The Isotopic composition of Ar and total Ar content were determined applying the unspiked K-Ar technique, (see Cassignol et al. (1982) and Carbit et al. (1998)). For calibration reference materials, analytical procedure and the settings of the mass spectrometers used refer to Guillou et al. (1998) and references therein.

2. GENERAL GEOLOGY

2.1. General Setting of the Studied Areas in Cappadocia

The tectonic regime changed as a result of the collision of the Eurasian and Arabian plates in the Middle (Early) Miocene, marking the beginning of neotectonic times (Şengör, 1980; Şengör and Yılmaz, 1981). Due to the effects of this collision in Eastern Anatolia, deformations started on the continental crust along the Bitlis Suture Belt. The shortening and thickening of the crust with time was not able to compensate for the deformations, and the Anatolian block started to move westward along the NAF (North Anatolian Fault) and EAF (East Anatolian Fault), which are strike-slip faults (McKenzie, 1972; Şengör et al., 1985; Dewey et al., 1986). Intraplate deformations developed in the Anatolian Block during this period as well as pull apart basins and thrust faults (Şengör, 1980; Dhont et al., 1998; Seyitoğlu et al., 2009).

The Anatolian Plate was the scene of intense volcanic activity, mainly concentrated in three regions: West, Central and East Anatolia. This thesis considers the Quaternary Erciyes and Hasandağ stratovolcanoes and the dispersed volcanism of Obruk-Zengen and Karapınar, from Central Anatolia, Cappadocia. However, easy to make comparison for regions, Hasandağ stratovolcano, Obruk-Zengen and the Karapınar dispersed volcanisms are collected under the *Southwestern Cappadocia volcanism* title.

A geological map of the studied area was prepared by reference to Pasquare et al. (1988), Le Pennec et al. (1994) and Temel et al. (1998) (Figure 2.1). However, in order to investigate volcanic units in more detail, the geological maps that former investigators prepared for the Erciyes and Hasandağ stratovolcanoes were used, and also the 1/500 000 scaled geological maps of Turkey of MTA (*The General Directorate of Mineral Research and Exploration*) for the Karapınar and Obruk-Zengen dispersed volcanism. Geological maps related to the studied areas were superposed with SRTM (*Shuttle Radar Topography Mission*) images. Sampling locations were noted in Figure 2.2 for Erciyes stratovolcano, in Figure 2.3 for Hasandağ stratovolcano, in Figure 2.4 for Obruk-Zengen dispersed volcanism and in Figure 2.5 for Karapınar dispersed volcanism.

The first detailed stratigraphic studies for the Erciyes and Hasandağ stratovolcanoes were made by Şen (1997) and Aydar (1992), respectively.

UTM coordinates of 29 samples, and of other samples belonging to the four regions for which the ages had been determined using K/Ar dating, are given in Table 2.1. Colors representing the four different regions in Table 2.1 will always be used to indicate the same regions throughout the thesis. Purple represents Erciyes stratovolcano, green represents Hasandağ stratovolcano, red for the Obruk-Zengen volcanism and blue for the Karapınar area. Some modifications were made to the stratigraphical sections prepared by former investigators using the new geochronological data obtained in this study.

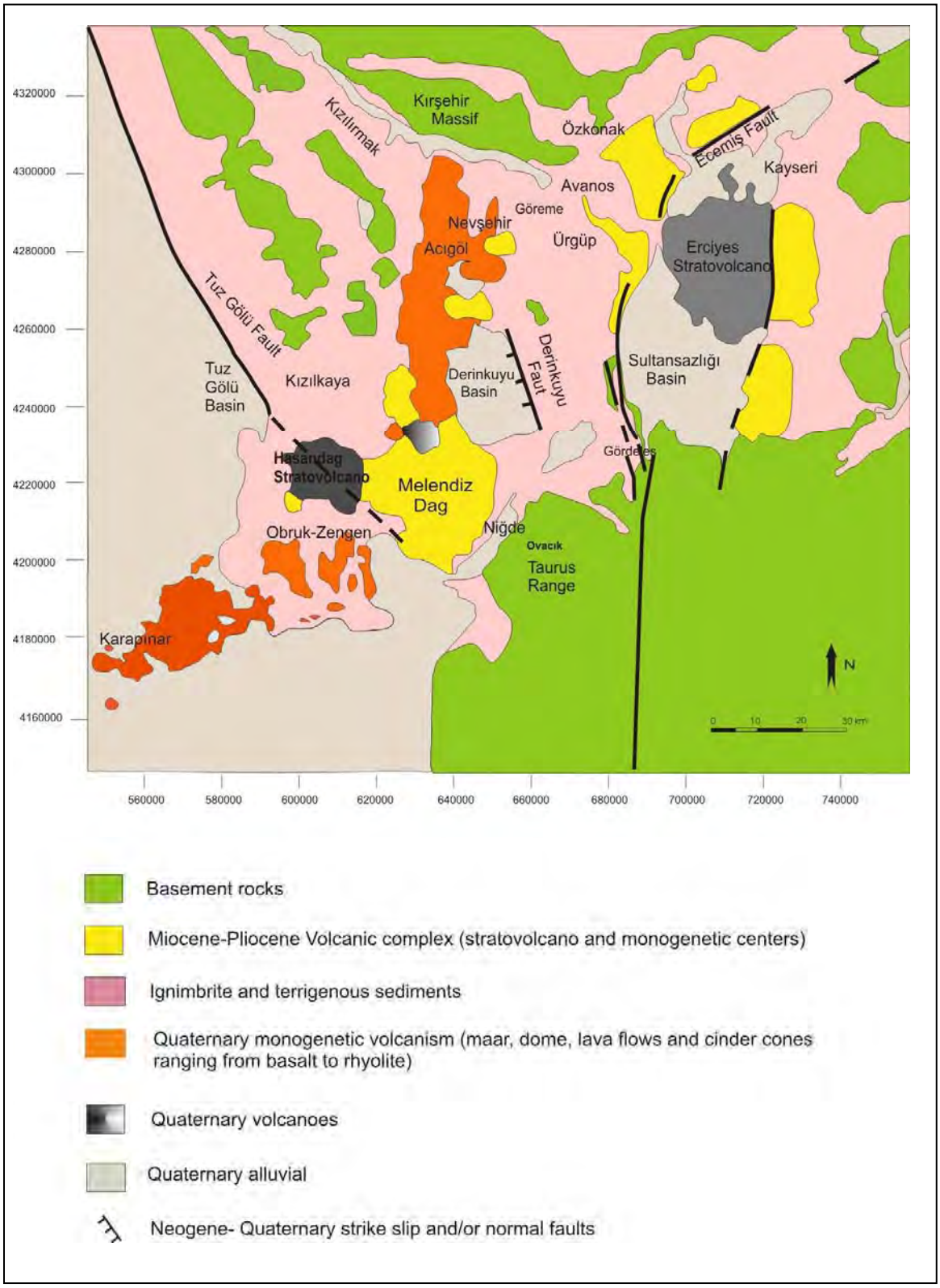

Figure 2.1: Geological map of the studied areas (modified from Pasquare et al., 1988; Le Pennec et al., 1994; Temel et al., 1998)

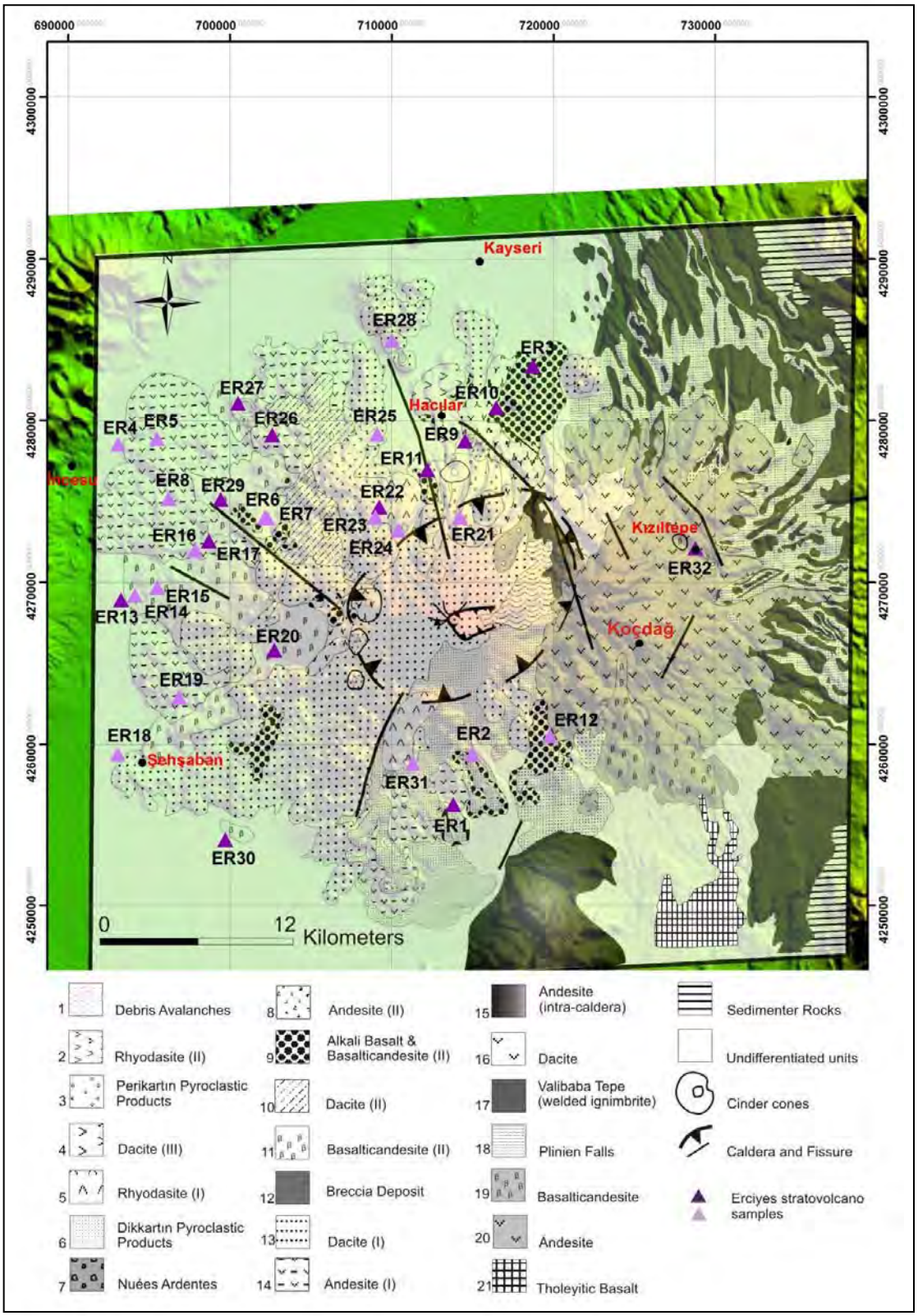

Figure 2.2: Geological map of the Erciyes stratovolcano (modified from Şen, 1997 and Kürkçüoğlu, 2000), superimposed with SRTM images and with sampling locations. Legend: 21-14: Koçdağ stage; 13-1: Erciyes stage. (purple triangle: dated Erciyes stratovolcano samples, pink triangle: undated Erciyes stratovolcano samples)

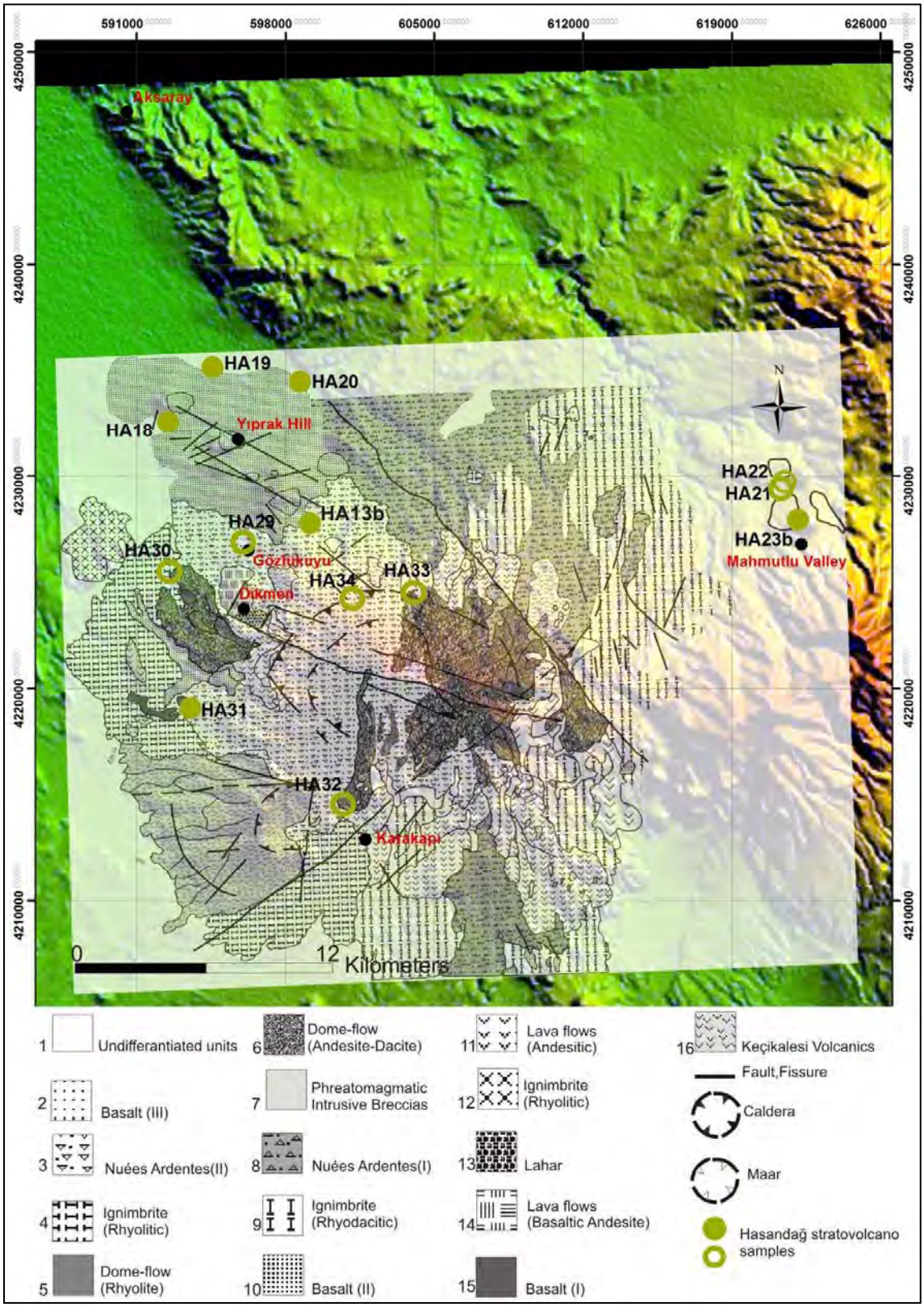

Figure 2.3: Geological map of the Hasandağ stratovolcano (modified from Aydar and Gourgaud, 1998), superimposed with SRTM images and with sampling locations. Legend: 16-12: Paleovolcano; 11-9: Mesovolcano ; 9-1: Neovolcano. (green-solid circles: dated HS samples, green-blank circles: undated HS samples)

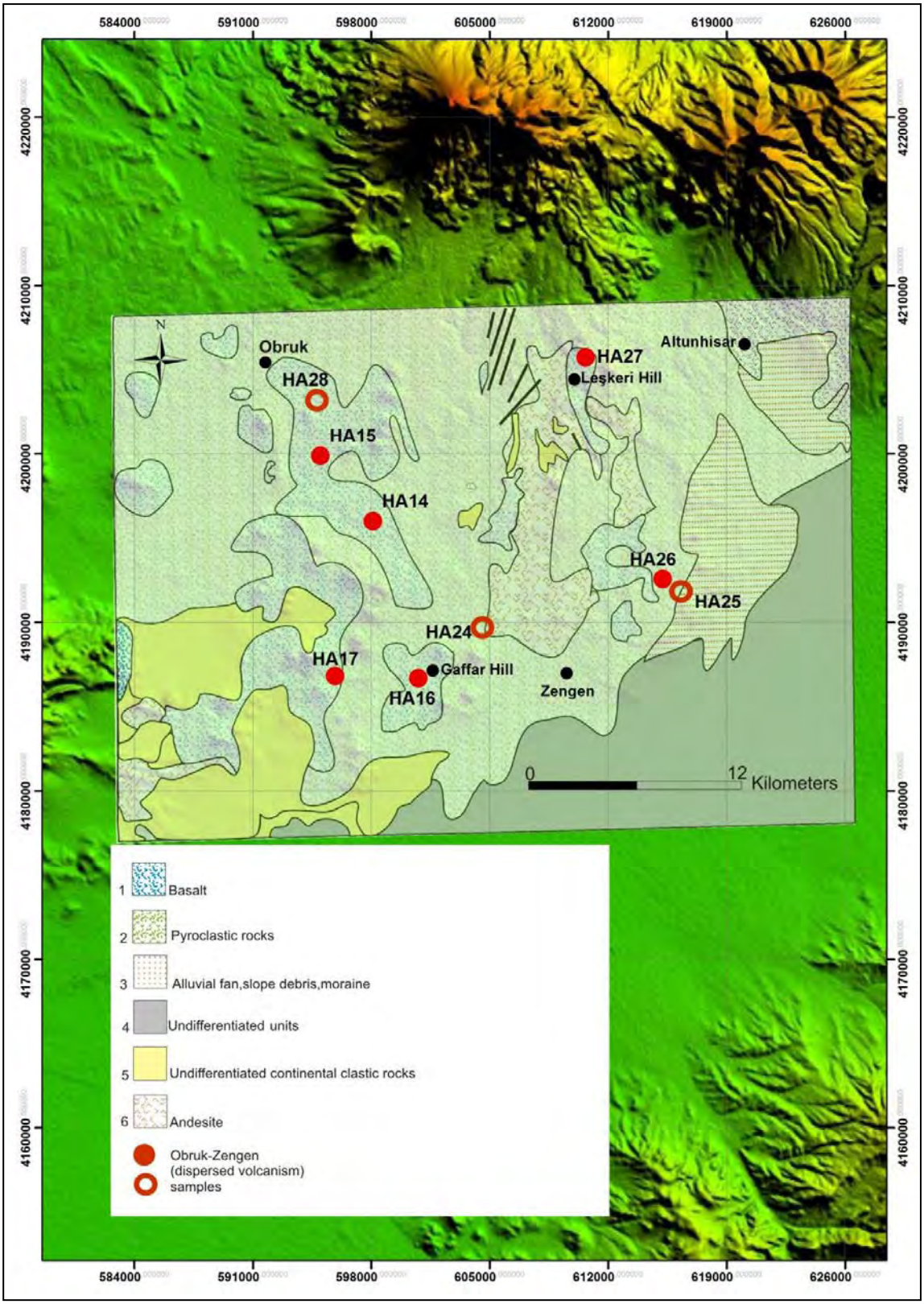

Figure 2.4: Geological map of the Obruk-Zengen dispersed volcanism (from MTA 1/500.000 geological map), superimposed with SRTM images and with sampling locations Legend: 6: Pliocene, 5: Upper Miocene–Pliocene, 4-1: Quaternary. (red-solid circles: dated OZ samples, red-blank circles: undated OZ samples)

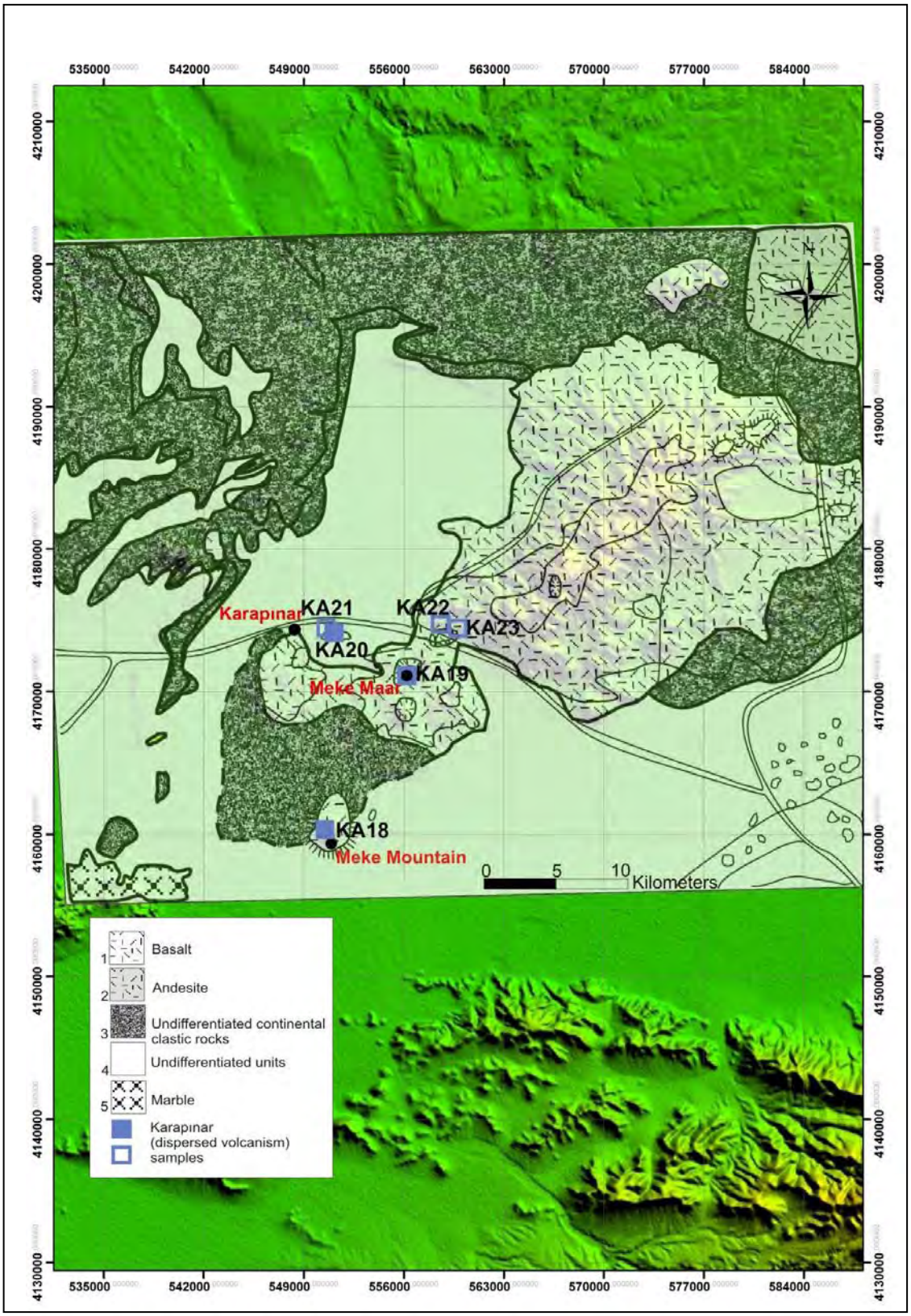

Figure 2.5: Geological map of the Karapınar dispersed volcanism (from MTA 1/500.000 geological map), superimposed with SRTM images, with sampling locations. Legend: 5: Middle Jurassic–Cretaceous, 4-1: Quaternary. (blue-solid squares: dated K samples, blue-blank square: undated K sample)

These re-organized successions are shown in Figure 2.7 for the Erciyes stratovolcano and in Figure 2.8 for the Hasandağ stratovolcano, Obruk-Zengen and Karapınar dispersed volcanisms.

Table 2.1: Dated samples of each group are colored. Puple: Erciyes stratovolcano, green: Hasandag stratovolcano, red: Obruk-Zengen, Blue: Karapınar

Erciyes Stratovolcano

Samples	
ER 1	Scoria cone-(lava flow) N of Develi
ER 2	Scoria cone-(basalt) N of Develi
ER 3	Scoria cone-basaltic bomb- W of Ali Dag
ER 4	Basaltic lava flow (İncesu-Kızılören)
ER 5	Basaltic lava flow (İncesu-Kızılören)
ER 6	Scoria Cone-basaltic bomb- Abas Hill
ER 7	Scoria Cone-basaltic bomb- Abas Hill
ER 8	Basaltic lava flow (Kocaoğlan)
ER 9	Basaltic lava flow (E of Hcalılar)
ER 10	Basaltic lava flow (W of Kızıltepe)
ER 11	Scoria cone-(lava flow) S of Hacılar
ER 12	Lava flow-Develi Road
ER 13	Basaltic Lava (SE of İncesu)
ER 14	Basaltic Lava (SE of İncesu)
ER 15	Basaltic Lava (SE of İncesu)
ER 16	Olivine-Basaltic Lava (SE of İncesu)
ER 17	Basaltic Lava (Sürtme Plateau)
ER 18	Andesite-(Şeyhşaban)
ER 19	Basaltic Lava (Şeyhşaban)
ER 20	Basaltic Lava (Şeyhşaban)
ER 21	Rhyodacite (S of Erciyes)
ER 22	Fissure eruption basalt (Karagüllü)
ER 23	Scoria cone-(basalt)
ER 24	Rhyodacite (S of Erciyes)
ER 25	Scoria cone-(lava flow) Siharslan Hill
ER 26	Scoria cone-(lava flow) Avşar Village
ER 27	Cora Maar
ER 28	Dacite
ER 29	Scoria Cone-basaltic bomb
ER 30	Scoria Cone-basaltic bomb(S of Erciyes)
ER 31	Fissure eruption basalt (Diikartın)
ER 32	Scoria Cone (Kızıltepe)

Hasandağ stratovolcano and Obruk-Zengen

Samples	
HA 13b	Lava Flow-Anasultan Hill
HA 14	Olivine Basalt (Aksaray-Adana Road)
HA 15	Scoria Cone-basaltic bomb-(Gamaz)
HA 16	Scoria cone-(lava flow) Gaffar Hill
HA 17	Olivine Basalt (Obruk)
HA 18	Scoria cone-(lava flow) Near Kızıltepe
HA 19	Olivine Basalt (NE of Kızıltepe)
HA 20	Olivine Basalt (Ulugüney)
HA 21	Olivine Basalt (NW Çardak)
HA 22	Scoria Cone-basaltic bomb-(Mahmutlu)
HA 23	Basaltic Block (Mahmutlu Valley)
HA 24	Scoria cone- bomb- (S of Hasandag)
HA 25	Scoria cone- bomb- (Çukurkuyu)
HA 26	Scoria cone- bomb- (Çukurkuyu)
HA 27	Basaltic lava flow (W of Altınhisar)
HA 28	Basaltic lava flow (Aksaray-Adana Road)
HA 29	Basaltic Block (Gözlükuyu)
HA 30	Andesite (Taşpınar)
HA 31	Scoria cone- (Karacaören)
HA 32	Andesite (N of Karaköy)
HA 33	Andesite (Hasandağ)
HA 34	Andesite (Hasandağ)

Karapınar

Samples	
KA 18	Scoria cone-(lava flow) Meke Mountain
KA 19	Scoria cone-(lava flow) Meke Maar
KA 20	Dyke-Karapınar Exit
KA 21	Scoria cone- bomb- (Kumsivri Hill)
KA 22	Dacite
KA 23	Basaltic bomb-Acıgöl maar

2.2. Overview on Post-Collisional Magmatism

Post-collisional magmatism is one of the common features of many orogens around the world (Dewey, 1988). Post-collisional settings are identified as a “relaxation phase” after collision (Liégeois et al., 1998). According to Liégeois et al.

(1998), post-collisional geodynamic settings are not completely understood. However, Wang et al. (2004) state that, petrogenetic studies of post-collisional magmatism provide to understand the geodynamic processes such as; interruption of collision, beginning of extension and reveal changes in magma source regions associated with such processes.

One of the widespread characteristics of post-collisional magmatism is its subduction-related geochemical characteristics despite subduction processes having been terminated as a result of continental collision (Wang et al., 2004; Seyitoğlu et al., 1992; Seyitoğlu et al., 1997). In addition, the subduction-related signatures are attributed to metasomatism by slab-derived fluids of the mantle lithosphere prior to collision (Pearce et al., 1990; Turner et al., 1992, 1993, 1996; Platt & England, 1993, Peccerillo,1999).

Post-collisional magmatism has been observed in Neogene-Quaternary times in Turkey, Italy, Spain and the North Africa (Halloul and Gourgaud, 2012). The formation of the Neotethys Ocean which was opened in Triassic and started to close in Late Cretaceous has a great significance on the development of Anatolia in Turkey (Şengör and Yılmaz, 1981). The closure of Neotethys led to the collision and continued during Paleocene to Early Eocene times (Şengör and Yılmaz, 1981; Koçyiğit et al., 1995; Koçyiğit et al., 2003). In Neogene-Quaternary times, the post-collisional volcanism occured in Central Anatolia Volcanic Province (CAVP), as mentioned above. Mostly this post-collisional volcanism is bimodal and characterized by calc-alkaline andesites-dacites, with subordinate tholeiitic-transitional-mildly alkaline basaltic volcanism of the monogenetic cones (Kuşçu and Geneli, 2010). Another example for bimodal character of post-collisional volcanism is the Foça Volcanic Center (FVC) from Western Anatolia (Altunkaynak et al., 2010). In FVC the older units were identified high-K calc-alkaline basalt, andesite, trachyandesite, rhyolite, and associated pyroclastic rocks and the younger sequences include shoshonitic–alkaline basalt lavas and dikes, trachytes, phonolites, and phonolitic ignimbrites that formed strombolian cones.

According to El Bakkali et al. (1998) and Maury et al. (2000), there is a strong relationship between the tectonics and the timing of the magmatism. Besides, the

major tectonic elements and some local faults are active in Neogene-Quaternary times in Central Anatolia and volcanism is related to an ancient subduction (Deniel et al., 1998; Temel et al, 1998; Alıcı Şen, 2004; Kürkçüoğlu et al., 2010). The study of Altunkaynak et al. (2010) proposes spatio-temporal evolution of volcanism in western Anatolia (FVC) during Miocene times. They stated that the changes in geochemical nature of the volcanism and tectonic regimes might have been caused by successive thermal relaxations associated with possible 'piecemeal' removal of the base of subcontinental lithospheric mantle beneath western Anatolia.

Accordingly, the purpose of the thesis is to emphasize possible temporal and spatial evolution of the Quaternary post collisional basaltic volcanism in Central Anatolia.

2.3. The Basement Rocks of Cappadocia

Basement rocks in the Central Anatolian Volcanic Complex are related to Paleozoic–Mesozoic metamorphic series (quartzite and crystalline schists), to Mesozoic–Early Tertiary magmatic series (acidic–intermediate granite and granodiorites, intermediate–basic granitic and gabbroic intrusive, gabbro and ophiolites) and by Lower Miocene sediments (sandstones intercalating with carbonates, semi-metamorphosed limestones, sandy and clayey marls and sediments with gypsum) (Ayrancı, 1991).

2.4. Briefly Overview of the Major Element Analysis and the Classification of the Erciyes Stratovolcano and Southwestern Cappadocia Samples

In order to understand the revisions made on the stratigraphic sections (Figure 2.7 and Figure 2.8), it will be important to look briefly the major element features and the classification of the samples. The major element analysis and the classification diagram of the samples from the study area can be seen in Table 2.2 and Figure 2.6, respectively. According to Figure 2.6, mostly the samples of the Erciyes stratovolcano are calc-alkaline. On the other hand, Southwestern Cappadocia volcanism samples are alkaline in features. The detail geochemical features of the samples, essential diagrams and related considirations are in Chapter 5.

Table 2.2: Major element analysis of Erciyes stratovolcano and Southwestern Cappadocia volcanics

	ER1	ER2	ER3	ER4	ER5	ER9	ER10	ER11	ER13	ER16	ER17	ER18	ER20	ER22	ER25	ER26	ER27	ER29	ER30	ER32
Major element(%)																				
SiO2	54.34	55.33	53.13	62.02	60.25	57.34	53.09	56.70	48.89	62.70	55.46	55.13	54.53	57.37	57.15	56.43	55.01	52.45	55.07	56.22
Al2O3	17.17	17.32	16.52	16.67	16.19	17.64	16.95	17.65	17.06	16.38	17.57	16.96	17.56	18.24	17.57	17.98	17.42	17.68	17.40	17.78
Fe2O3	6.88	6.97	8.24	4.87	5.55	7.07	8.39	7.22	11.99	4.85	7.27	7.43	7.24	6.27	6.70	6.57	6.81	8.96	7.94	6.55
MgO	6.10	5.62	6.54	3.00	4.06	4.21	6.65	4.04	5.44	2.86	4.95	5.16	5.88	4.67	4.59	4.59	5.62	4.78	4.84	5.12
CaO	8.32	8.13	8.54	6.14	6.74	7.18	8.54	7.06	8.46	5.95	7.54	7.58	8.22	8.03	7.58	8.20	8.28	7.54	7.42	7.93
Na2O	3.48	3.66	3.62	3.72	3.67	4.08	3.81	4.08	4.17	3.71	3.97	4.23	3.70	3.52	3.74	3.80	3.64	4.31	4.06	3.65
K2O	1.24	1.37	1.02	1.67	1.63	1.23	0.96	1.24	0.94	1.74	1.54	2.05	1.36	1.10	1.18	1.31	1.14	1.65	1.62	0.95
TiO2	0.96	1.04	1.30	0.66	0.78	1.07	1.36	1.05	2.40	0.65	1.11	1.49	1.10	0.79	0.89	1.04	1.01	1.54	1.39	0.94
MnO	0.11	0.11	0.13	0.08	0.09	0.12	0.13	0.12	0.18	0.08	0.12	0.13	0.12	0.10	0.11	0.11	0.11	0.15	0.13	0.10
P2O5	0.36	0.33	0.37	0.19	0.23	0.37	0.40	0.45	0.51	0.19	0.38	0.33	0.36	0.25	0.37	0.34	0.33	0.66	0.41	0.28
LOI	0.23	0.28	-0.16	1.14	0.99	-0.19	-0.10	0.30	-0.32	1.09	0.30	0.18	0.29	0.47	0.50	0.08	0.42	0.15	0.50	0.58
Mg#	69.06	66.99	66.61	61.59	65.60	60.78	66.60	59.28	53.29	61.38	63.17		67.13	66.00	64.08	63.72	67.27	58.18	61.34	66.31
Total	99.19	100.15	99.25	100.15	100.19	100.12	100.18	99.91	99.73	100.22	100.20	100.65	100.36	100.81	100.39	100.42	99.79	99.87	100.79	100.09

	Hasandag stratovolcano						Obruk-Zengen						Karapınar		
	HA13 b	HA18	HA19	HA20	HA23b	HA31	HA14	HA15	HA16	HA17	HA26	HA27	KA18	KA19	KA21
Major element(%)															
SiO2	49.33	51.06	50.43	50.36	50.90	49.24	48.99	49.38	48.81	48.88	49.39	56.24	49.75	50.87	52.40
Al2O3	16.08	16.86	16.56	16.25	16.22	17.80	16.24	16.40	15.79	15.30	16.23	17.08	16.48	17.65	15.99
Fe2O3	8.88	8.72	8.87	9.14	8.86	9.57	9.01	9.42	8.97	8.60	9.39	7.31	8.53	9.17	8.20
MgO	8.52	7.31	7.99	8.75	7.35	6.01	8.52	8.71	10.18	10.92	8.81	4.07	8.12	5.69	8.54
CaO	9.78	8.76	9.42	9.85	9.32	10.68	9.28	8.98	10.43	10.86	9.47	7.57	11.02	9.52	9.11
Na2O	3.44	3.86	3.64	3.64	3.68	3.70	3.65	3.71	3.43	3.00	3.73	4.19	3.36	3.96	3.50
K2O	1.15	1.46	1.26	1.12	1.10	0.97	1.45	1.23	0.80	0.88	1.15	1.86	0.95	1.13	1.12
TiO2	1.19	1.43	1.33	1.21	1.23	1.34	1.40	1.50	1.10	1.06	1.49	1.25	1.03	1.27	1.00
MnO	0.15	0.14	0.15	0.15	0.15	0.16.	0.15	0.15	0.15	0.14	0.15	0.13	0.14	0.15	0.14
P2O5	0.44	0.43	0.44	0.43.	0.37	0.38.	0.43	0.41	0.37	0.25	0.41	0.31	0.30	0.35	0.33
LOI	-0.14	-0.43	-0.58	-0.27	0.00	-0.06	-0.35	-0.28	-0.32	-0.23	0.22	0.24	-0.32	-0.38	0.12
Mg#	69.16	67.82	67.79	69.11	65.98	59.50	70.41	68.37	72.62	74.80	68.68	59.19	68.99	60.97	72.38
Total	98.72	99.88	99.72	100.64	98.97	99.51	98.69	99.32	99.75	99.83	100.42	100.23	99.35	99.38	100.43

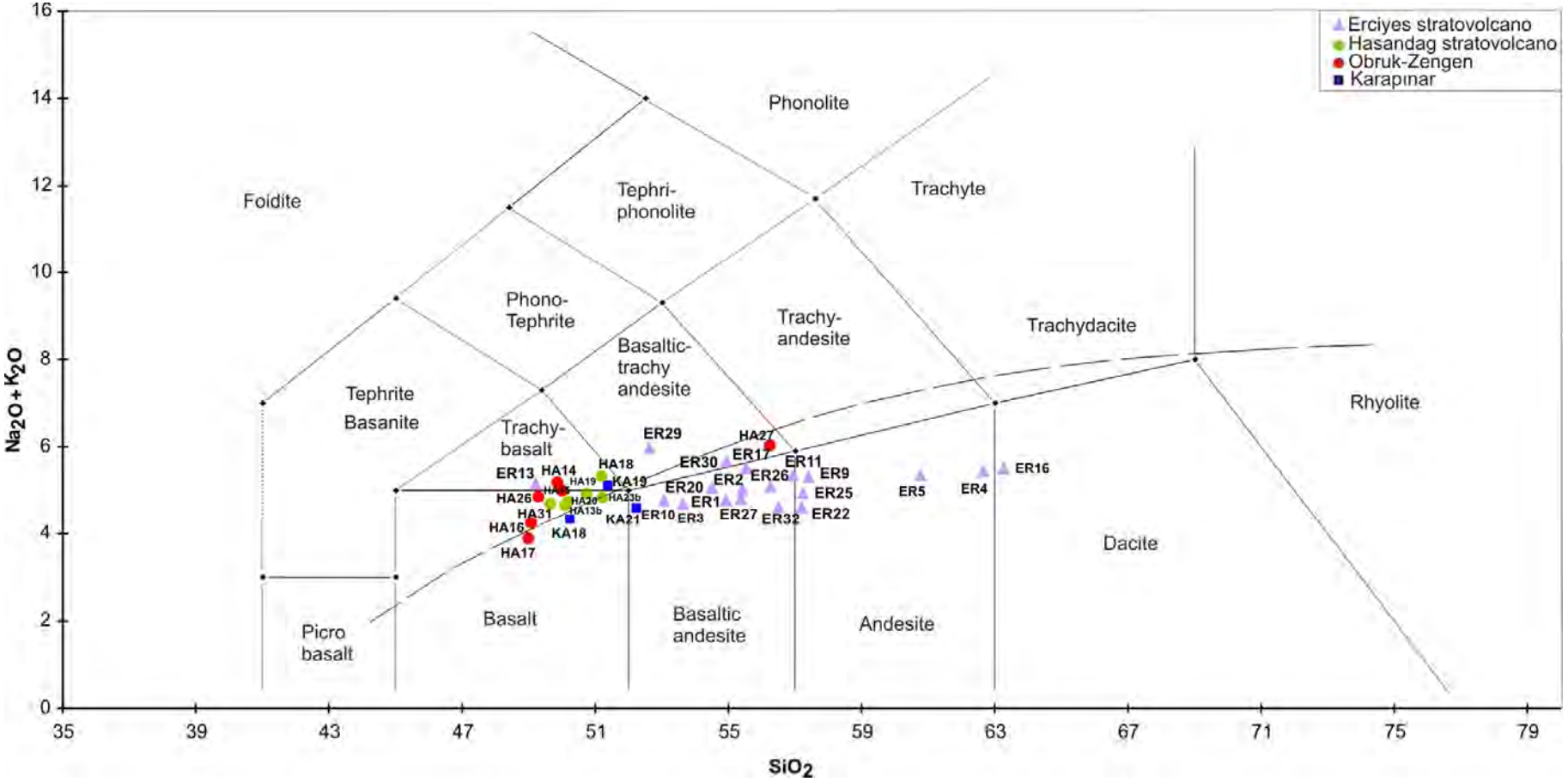

Figure 2.6: TAS (Total-Alkali Silis) diagram of Erciyes stratovolcano and Southwestern Cappadocia volcanics (Hasandağ stratovolcano, Obruk-Zengen and Karapınar)

2.5. The Erciyes Stratovolcano

The Quaternary Erciyes stratovolcano (3916 m), located 15 km south of Kayseri city, is the highest volcano of Central Anatolia and covers an area of 3300 km^2.

The Erciyes volcanic system consists of a large volcanic cone of various pyroclastics and lavas, with numerous monogenic vents (dome, cinder cone and maar). According to Şen (1997), the history of the Erciyes is divided in two evolutionary stages, the Koçdağ and Erciyes s.s. stages (Figure 2.2). New K/Ar dating analyses on Erciyes stratovolcano are given in Table 2.3.

Hervé Guillou previous unpublished dating (samples TU-ER23, TU-ER45 and TU-ER-30) are also compiled in Table 2.3. Detailed information about the K/Ar dating method is given in Section 1.4.3.

The volcanic activity of the Koçdağ evolutionary stage was first effusive with tholeiitic basalts and then continues with intermediate lavas. Later, monogenetic scoria cones emplaced generally basaltic andesitic in composition. The age of the calc-alkaline basaltic andesite sample ER32 (Kızıltepe, scoria cone) in this study is 0.707± 0.015 Ma. This information considered ER32 is young and belongs to the post Koçdağ evolutionary stage.

The ultimate products of the Koçdağ stage consist of pyroclastics, mainly Plinian pumice fall-out and ignimbrites of the Valibaba sequence (Şen, 1997). The ages of the Valibaba ignimbrite are 2.7±0.1, 2.8±0.1 and 3.1±0.1 Ma, according to Innocenti et al. (1975). This ignimbritic sequence is related to the collapse of a caldera, and followed by sub-contemporaneous dacitic domes and intracaldera andesitic lavas, with a K/Ar age of 2.544±0.306 Ma (Notsu et al., 1995). So, the Koçdağ stage ends with the collapse of the caldera and then the beginning of the Erciyes s.s. stage started at the west of Koçdağ.

Table 2.3: New K-Ar ages from the Erciyes stratovolcano. (a and b represent the 1st and 2nd analyses of the samples)

Sample names		Molten weight (g)	40Ar* (%)	40Ar* (10^{-13} mol/g)	40Ar* weighted mean(± 1s)	K* (wt.%)	Age ± 2σ Ma
ER9 ***(TU-ER-23)***	a	1.00232	-0.376	<0		1.212 ± 0.012	**<0.001**
	b	0.93462	-0.214	<0			
ER11	a	1.00758	-0.393	<0		1.046 ± 0.011	**<0.001**
	b	1.00562	-0.097	<0			
ER29	a	1.04062	0.085	0.276	0.292 ± 0.057	1.345 ± 0.013	**0.013 ± 0.005**
	b	1.50364	0.107	0.318			
ER26 ***(TU- ER-45)***	a	1.49077	0.209	0.42	0.471 ± 0.107	1.104 ± 0.011	**0.025 ± 0.008**
	b	1.41079	0.22	0.523			
ER22	a	1.00075	0.247	0.619	0.638 ± 0.052	0.930 ± 0.009	**0.040 ± 0.007**
	b	1.01479	0.289	0.66			
ER17	a	1.00525	1.145	1.107	0.999 ± 0.058	1.287 ± 0.013	**0.045 ± 0.005**
	b	1.50996	0.581	0.921			
ER1	a	1.0115	0.209	1.65	1.670 ± 0.097	1.038 ± 0.010	**0.093 ± 0.011**
	b	1.00877	0.199	1.722			
ER30 ***(TU-ER-30)***	a	1.50434	0.905	2.731	2.578 ± 0.115	1.453 ± 0.015	**0.102 ± 0.007**
	b	1.4951	0.856	2.414			
ER20	a	1.00569	0.566	2.239	2.295 ± 0.062	1.146 ± 0.011	**0.115 ± 0.007**
	b	1.00353	0.524	2.328			
ER10	a	0.49442	1.033	4.619	4.403 ± 0.105	0.855 ± 0.009	**0.297 ± 0.015**
	b	0.50032	1.177	4.373			
ER3	a	0.49442	1.033	4.619	4.403 ± 0.105	0.855 ± 0.009	**0.352 ± 0.009**
	b	0.50032	1.177	4.373			
ER32	a	1.01111	6.358	10.061	10.280 ± 0.044	0.836 ± 0.008	**0.707 ± 0.015**
	b	1.5034	7.08	10.487			
ER13	a	0.49576	17.302	24.527	24.406 ± 0.105	0.830 ± 0.083	**1.695 ± 0.037**
	b	1.01285	25.758	24.315			

Kürkçüoğlu (2000) stated that basalts were the first products of the Erciyes s.s. stage. Besides, he indicated that he did not encounter the basaltic products at the western and southwestern parts of the Erciyes stratovolcano that mentioned from (Notsu et al., 1995). On the other hand, Notsu et al. (1995), emphasized that their sample ER24 (1.734±0.069 Ma), which is an alkaline basalt, was located on the southwestern of Erciyes stratovolcano (*precise UTM coordinates were not indicated, only coordinates given as* Şeyhşaban, Figure 2.2). In this study, our sample *ER13* (1.695±0.037 Ma) is an alkaline, trachybasalt (Figure 2.6) from a basaltic lava flow at southeastern part of İncesu town (Figure 2.2). Although there are some differences between major elements of both samples, the ages of ER24 (Notsu et al., 1995) and *ER13* are at the same age interval and both located on the western flank of the Erciyes stratovolcano. This information indicates the presence of a basaltic lava flow across these areas.

This basaltic unit is overlain by the first generation of andesitic various products and after the first generation of dacitic domes and flows occurred. The K/Ar age of these dacites is 0.9±0.2 Ma (Innocenti et al., 1975). Dacites are followed by basaltic andesite and blocky lavas at 0.53 ± 0.04 and 0.29 ± 0.04 Ma (Ercan et al., 1994) and by calc-alkaline *ER3* (0.352 ± 0.009 Ma) and *ER10* (0.297±0.015 Ma) basaltic-andesites, according to this study. These units are covered by the second generation of dacites dated at 0.3 ± 0.1 Ma (Innocenti et al., 1975), flowing towards the northwest. It is followed by the second basaltic generation, dated at 0.15 ± 0.07 Ma K/Ar by Ercan et al. (1994). The calc-alkaline samples of this study *ER20* (0.115 ± 0.007 Ma), *ER30* (0.102±0.007 Ma) and *ER1* (0.093±0.011 Ma) are at the same time interval (Figure 2.7). The occurrence of alkaline and calc-alkaline basalts at this stage of the Erciyes stratovolcano has been noted by Kürkçüoğlu, (2000). These basaltic lavas are overlain by the second generation of andesites dated at 0.171 ± 0.12 Ma K/Ar by Notsu et al. (1995) (Figure 2.7).

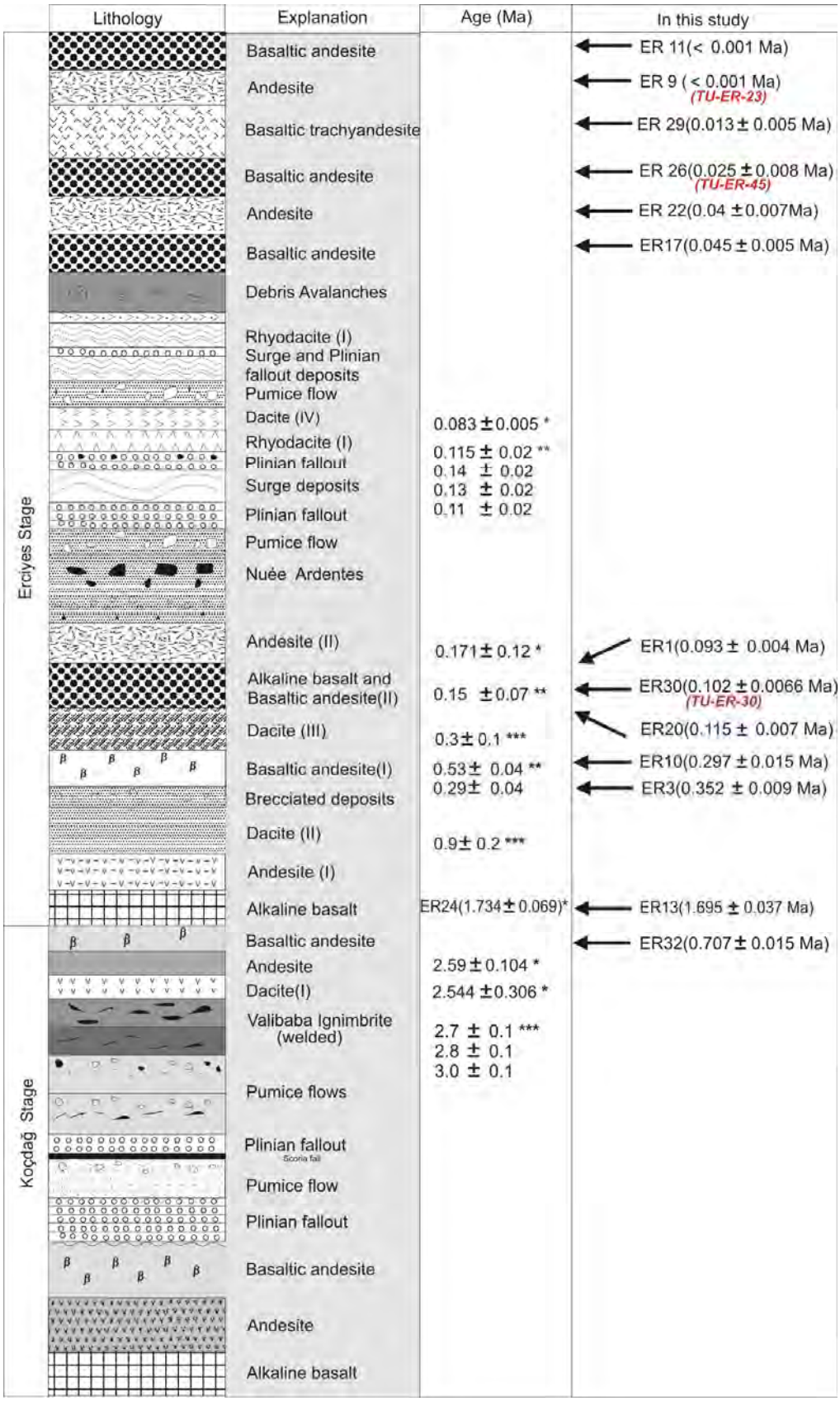

Figure 2.7: Synthetic stratigraphic section of the Erciyes stratovolcano (not to scale). (Modified from Şen , 1997 and Kürkçüoğlu, 2000) . (*Notsu et al., 1995; ** Ercan et al., 1994; ***Innocenti et al., 1975)

The volcanic activity, which became more explosive in character after the andesitic period, continued with dacitic and rhyodacitic extrusive, eruptions (Şen, 1997). Volcanic activity continued in recent times as rhyodactic pumice flows, base surge and plinian fallouts spread over large areas around a dome. Ercan et al. (1994) gave an age 0.14 ± 0.02 and 0.11 ± 0.03 Ma K/Ar for these products (Figure 2.6). Later, 0.083 ± 0.005 Ma dacites (*around Hacılar, Figure 2.2)* occur as the last dated products of the Erciyes volcanism (Notsu et al., 1995). Şen (1997) stated that an undated debris avalanche is more recent. Kürkçüoğlu [12] suggested that the activity following the dacitic and rhyodacitic units could be followed by alkaline basaltic products. However, there were no available radiometric datings for these volcanic products. New geochronological data were obtained on these basalts s.l. in the course of this thesis. They are calc-alkaline *ER17* (0.045±0.005 Ma), *ER26* (0.025±0.008 Ma),*ER11* (<0.001 Ma) and alkaline *ER29* (0.013±0.005 Ma). Moreover other young andesites such as *ER22* (0.04±0.007 Ma) and *ER9* (<0.001 Ma) suggested volcanic activity in historical times, as suggested by Strabo (Ayrancı,1991).

2.6. The Southwestern Cappadocia Volcanism

The southwestern volcanism of Cappadocia consists in 3 distinct areas:
1) The Hasandağ is a double-peaked Quaternary stratovolcano. It covers an area of 760 km^2 and the estimated volume is 354 km^3 (Aydar, 1992). The 2 peaks are 3253 m and 3069 m height, respectively (Photo in Figure 1.3).

2) The Obruk-Zengen dispersed volcanism exhibits basaltic scoria cones (and related lava flows) and maars which spread towards the south and southwest of the main cone of Hasandağ stratovolcano (Photo in Figure 1.4).

3) The Karapınar dispersed volcanism is located at the southwestern extreme part of the studied area, and consists of basaltic scoria cones (and related lava flows) and maars as Meke (Photo in Fig.1.5 and Figure 2.5).

The new K/Ar age dating performed on samples belonging to Hasandağ, Obruk-Zengen and Karapınar dispersed volcanism are given in Table 2.4. The sample CK-89-19, of Kayahan Olanca (Olanca, 1994) is considered as equivalent of

KA18. These two samples are at the same location and they closely resemble to each other in terms of major element contents. Detailed information about the method of K/Ar dating analysis is given in section 1.4.3.

2.6.1. Hasandağ Basaltic Volcanism

The volcanic history of the Hasandağ stratovolcano is divided in three successive phases: Paleovolcano, Mesovolcano and Neovolcano (Aydar, 1992).

The Paleovolcano is represented by Keçikalesi volcanic units, dated at 13.7±0.3 and 12.4±4 Ma (Besang et al., 1977) and by basaltic andesites dated at 7.21±0.09 Ma (K/Ar) (Aydar and Gourgaud, 1998) that flowed in the sedimentary basin. The most voluminous phase of this stage is a rhyolitic ignimbrite dated at 6.31±0.20 Ma (Deniel et al., 1998). The emplacement of two different ignimbritic units was related to the collapse of a caldera.

The Mesovolcano is represented by andesitic lava flows, domes and block-and-ash flow deposits. These products filled the first caldera that collapsed at the Paleovolcano stage and created a new volcanic cone. Voluminous rhyodacitic ignimbrites and plinian fallout caused the collapse of the second caldera. The post caldera activity was mainly related to dome growing and block-and-ash flow emplacement, and andesitic lava flows, that built a new cone.

However, the Neovolcano stage, defined as the third stage, started with Pelé-type eruptions that filled the second caldera, as well as the next extrusive and explosive activities producing andesitic and dacitic domes, rhyolitic domes, block-and-ash flows, phreatomagmatic breccias and rhyolitic ignimbrite (Aydar, 1992). A new and last caldera collapse occurred, filled by domes and related block-and-ash flows.

Table 2.4: New K-Ar ages of volcanic samples from Hasandağ stratovolcano, Obruk-Zengen and Karapınar dispersed volcanisms. (a and b represent the 1st and 2nd analyses of the samples)

	Sample names		Molten weight (g)	40Ar* (%)	40Ar* (10^{-13} mol/g)	40Ar* weighted mean(± 1s)	K* (wt.%)	Age ± 2σ Ma
Hasandağ stratovolcano	HA31	a	1.05637	0.018	0.038	0.031 ± 0.052	0.847 ± 0.009	**0.002 ± 0.007**
		b	1.50318	0.022	0.028			
	HA13b	a	0.99537	0.816	0.373	0.355 ± 0.042	1.079 ± 0.011	**0.019 ± 0.005**
		b	1.50806	0.797	0.343			
	HA20	a	1.00576	1.15	0.989	1.028 ± 0.047	1.038 ± 0.010	**0.057 ± 0.005**
		b	1.00321	0.879	1.049			
	HA19	a	1.00486	1.927	1.592	1.540 ± 0.041	1.129 ± 0.011	**0.079 ± 0.004**
		b	1.28385	2.132	1.518			
	HA18	a	1.00058	1.774	2.237	2.199 ± 0.052	1.212 ± 0.012	**0.105 ± 0.005**
		b	1.50051	2.412	2.136			
	HA23b	a	0.99697	9.86	9.3	9.377 ± 0.031	0.996 ± 0.010	**0.543 ± 0.012**
		b	2.00253	8.005	9.446			
Obruk-Zengen	HA17							**0.066± 0.007**
	HA27	a	1.0037	1.85	9.364	9.300 ± 0.046	1.619 ± 0.016	**0.331 ± 0.007**
		b	1.02372	1.616	9.214			
	HA14	a	0.5015	4.09	8.455	8.415 ± 0.059	1.229 ± 0.012	**0.395 ± 0.01**
		b	1.03149	4.938	8.41			
	HA15	a	1.02037	5.091	7.547	7.568 ± 0.049	1.079 ± 0.011	**0.404 ± 0.01**
		b	1.49874	5.675	7.573			
	HA26	a	0.4802	5.862	12.135	12.155 ± 0.070	1.038±0.01	**0.675 ±0.016**
		b	0.93817	4.847	12.16			
	HA16	a	1.00134	12.273	9.055	9.086 ± 0.071	0.656 ± 0.007	**0.799 ± 0.02**
		b	1.50996	4.996	9.106			
Karapınar	KA19							**<0.001**
	KA21	a	0.50028	0.756	3.152	3.162 ± 0.091	1.121 ± 0.012	**0.163 ± 0.01**
		b	0.50674	0.855	3.26			
	KA18 *(CK89-19)*							**0.280 ± 0.0071**

The age interval of the dome and blocky flows near *Karakapı village* (Figure 2.3) has been determined as 0.08–0.58 Ma (Ercan et al., 1990). In this study, the alkali basalt *HA23b* (0.543±0.012 Ma) taken from the blocky flow from *Mahmutlu Valley* (Figure 2.3), can also be placed within this same age interval.

This unit is followed by basaltic cones (0.065–0.12 Ma by Ercan et al. 1990) located at the northeast of *Gözlükuyu village* (Figure 2.3) and lava flows (0.034 Ma by Aydar and Gourgaud 1998 from *the Yıprak Hill* (Figure 2.3). Our samples alkaline trachy-basalt *HA18* (0.105±0.01 Ma), alkali basalts *HA19* (0.079±0.004 Ma) and *HA20* (0.057±0.005 Ma), which are located on the same region, northeastern part of the Hasandağ. In this case, it was determined that the age interval for this unit, formed by basaltic scoria cones and related lava flows, was older than the age given by previous workers. The post-caldera activity continued with domes and block-and-ash flows. For this unit, the andesitic dome was dated <0.006 Ma (Aydar and Gourgaud, 1998) and the basaltic andesites located around Dikmen (Figure 2.3) were dated at 0.029–0.033 Ma (Kuzucuoğlu et al., 1998). The alkali basalts *HA13b* and *HA31* located to the north and west of the Hasandağ (Figure 2.3) were dated at 0.019±0.005 Ma and 0.002±0.007 Ma, respectively.

2.6.2. The Obruk-Zengen Dispersed Volcanism

Radiometric ages of the Obruk-Zengen dispersed volcanism are presented in Table 2.4. According to Table 2.4, except calc-alkaline basalt HA17 (0.066±0.007 Ma), the others are older than Hasandağ stratovolcano samples. The oldest two samples are the alkaline basalts HA16 (0.799±0.02 Ma) and HA26 (0.65±0.016 Ma). The others are alkaline basalt *HA15* (0.404±0.01Ma), trachybasalt *HA14* (0.395±0.01Ma) and calc-alkaline basaltic trachyandesites HA27 (0.331±0.007 Ma).

There are few studies on the basaltic volcanism in the Obruk-Zengen region. One of the previous studies in the region belongs to Ercan et al. (1990) but there are some doubts about the data were given in that study. Consequently, the K-Ar ages given in this study are very important to understand spatio-temporal evaluation of the magmatism in the region.

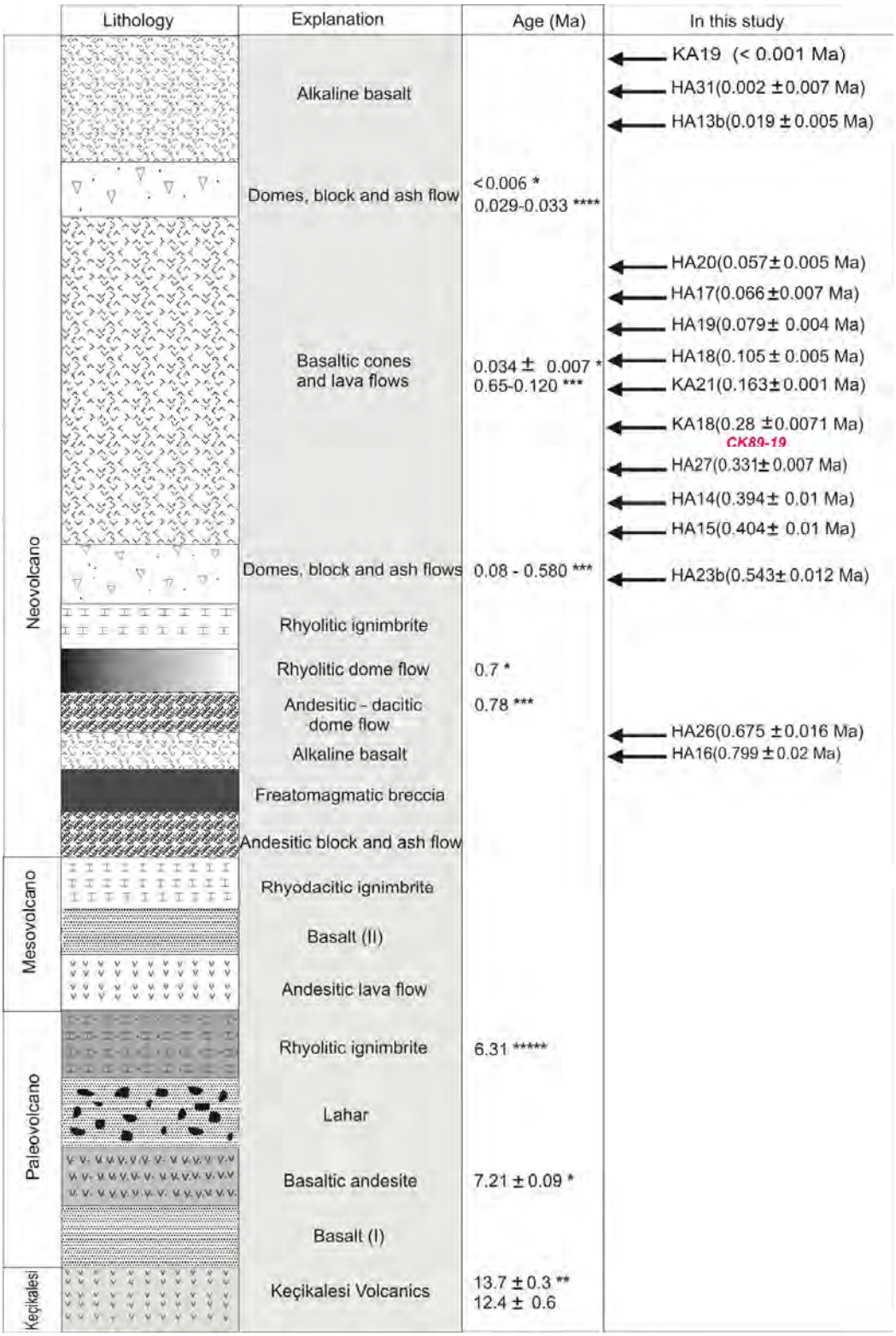

Figure 2.8: Synthetic stratigraphic columnar section of the Southwestern Cappadocia (not to scale), including Hasandag stratovolcano, Obruk-Zengen and Karapınar dispersed volcanism. (Modified from Aydar and Gourgaud, 2002). (* Aydar and Gougaud, 1998; ** Besang et al., 1977; ***Ercan et al., 1992; ****Kuzucuoğlu et al., 1998; ***** Deniel et al., 1998)

2.6.3. The Karapınar Dispersed Volcanism

The first volcanic products near Karapınar town, comprised trachyandesitic and andesitic lavas. Karapınar volcanics are basaltic lava flows (Ercan et al., 1990), but also explosive products as scoria and phreatomagmatic ejectas. The calc-alkali basalt *KA18* (0.28±0.0071 Ma) from the Meke Mountain (Figure 2.5) and the calc-alkali basaltic andesite *KA21* (0.163±0.01 Ma) are related to basaltic scoria cones and lava flows (Figure 2.8).

The most recent products are basalts of the Meke Maar area (Ercan et al., 1990). There is a 50 m high scoria cone with a small related lava flow (Figure 1.5) inside the Meke maar, which is 900 m long and 550 m wide. The age of the alkali trachybasalt *KA19* taken from Meke maar (<0.001 Ma) (Figure 2.5) in this study also verifies the interpretation of (Ercan et al., 1990).

During excavations at Çatalhöyük, a picture of an active volcano was found on the walls of a temple which is considered to have been built in 6200 BC (Mellart, 1967). The picture, thought to have been drawn 8000–8200 years ago, could depict the Hasandağ in activity or the activity of the Meke volcano that was the closest volcanic area.

2.7. Conclusion

New K-Ar dating analyses were carried out on 24 samples of Erciyes stratovolcano, Hasandağ stratovolcano, Obruk-Zengen and Karapınar dispersed volcanisms. Our data contribute significantly to the findings of previous studies carried out in the region and to the age of Quaternary basalts in the area. We emphasize the very young ages (in historical times) of some samples.

1. At Erciyes stratovolcano, according to our new radiometric aging, the oldest sample is related to a basaltic lava flow sample *ER13* (1.695±0.037 Ma) which exhibits an alkaline character (trachybasalt). The youngest samples, however, are the calc-alkaline basaltic andesite *ER11* (<0.001 Ma) and the andesite *ER9* (<0.001 Ma), located at the south of Hacılar (Figure 2.2) Recent ages obtained from the Erciyes stratovolcano and the sample locations were assessed

altogether, and we emphasize that most samples aged 0.045 Ma and younger, are located to the northeast and northwest of the volcano.

2. At Hasandağ stratovolcano, the oldest sample is the alkaline basalt, *HA23b* (0.543±0.012 Ma), located to the northwest of the main cone (Mahmutlu Valley) and the youngest is *HA31* the alkaline basalt (0.002±0.007Ma), located to the west of the main cone. When considering all basaltic samples belonging to the Hasandağ stratovolcano, we emphasize that except *HA23b,* all other samples were ~0.1 Ma or much younger.

3. However, considering the basalts of the Obruk-Zengen dispersed volcanism, it is observed that all samples, except HA17, are older than those of Hasandağ stratovolcano. The oldest sample is from Gaffar Hill, *HA16* (0.799±0.02 Ma), and the youngest is *HA17* (0.066±0.007 Ma), located to the west of Gaffar Hill (Figure 2.4).

4. The oldest sample taken of the Karapınar dispersed volcanism is calc-alkaline basalt, *KA18* (0.28±0.0071 Ma) taken from Meke Mountain, and the youngest is alkaline trachybasalt KA19 (<0.001 Ma), taken from Meke Maar. The number of the studied sample is limited in this area in order to be observed the expected magmatic transition.

Moreover, we emphasize the new very young ages concerning Erciyes, Hasandağ stratovolcanoes and Karapınar area. These new ages reveal that historical eruptions occurred in Cappadocia. Such new data are very important for assessment of volcanic hazards.

3. MINERALOGY and PETROGRAPHY

In order to determine the mineralogical and petrographical properties of basalts of Cappadocia, 32 samples were collected from Erciyes stratovolcano and 28 samples from Southwestern Cappadocia, including Hasandağ stratovolcano, Obruk-Zengen and Karapınar. Totally 43 thin sections were prepared in the Laboratory *"Magmas et Volcans"* at Blaise Pascal University (Clermont-Ferrand, France). Informations related to the analytical methods are given in section 1.4.1. Most of studied samples are basalts s.l. (including trachybasalts, basaltic andesites and rarely andesites), collected as scoria ejecta (from strombolian scoria cones), phreatomagmatic bombs and fragments of lava flows.

3.1. The Basalts s.l. of Erciyes Stratovolcano

Optical microscopic studies show that the common mineralogical assemblage of Erciyes samples is plagioclase + olivine + clinopyroxene and oxide minerals. Sometimes, orthopyroxene occurs. The majority of samples display a porphyritic texture. Some phenocrysts contain glassy inclusions, reaction belts and exhibit strong zoning. Table 3.1 summarizes the description of 21 samples.

Plagioclase (Plg) crystals are observed as subhedral, prismatic and sometimes as gnawed, varying from a few hundred microns to few millimeters in size. Plagioclases are in equilibrium and/or in disequilibrium in the groundmass. We emphasize that both conditions are present together in the samples. Equilibrium plagioclases are present as phenocrysts, microphenocrysts and microlites, and display concentric zoning. However, other plagioclases are mostly observed as phenocrysts and display various disequilibrium textures. Some of them are gnawed and fragmented, or exhibit a clear zone at centre with a sieve texture surrounding this central zone (Figure 3.1) and others display sieve texture only (Figure 3.2). Glomeroporpyhritic texture is also observed. In some thin sections, clinopyroxene (ophitic texture) (Figure 3.3), apatite and oxide minerals are present as inclusions in and around the plagioclase phenocrysts.

Table 3.1: Petrographic description of samples of Erciyes stratovolcano

Samples	Macroscopic features	Freshness	Rock Texture	Major crystals	Groundmass	Alteration
ER1	Dark gray colored with alkaline feldspars and small white inclusions Moderately vesicular	×	Hypocrystalline porphyritic, Embayed, gnawed and skeletal triangular shape ol phenocrysts. Moderately vesicular	Plg Ol Cpx	pilotaxitic plg, ol oxide and cpx	serpentinization, oxidation
ER2	Consolidated, bright grey colored with very small white inclusions	×	Hypocrystalline porphyritic Mostly embayed, gnawed and skeletal triangular shape ol phenocrysts Less vesicular than ER1	Plg Ol Cpx	pilotaxitic plg, ol oxide and cpx	serpentinization, oxidation
ER3	Light grey colored with alkaline feldspars and very small, white inclusions Highly vesicular	×	Hypocrystalline porphyritic Mostly embayed, gnawed and skeletal triangular shape ol phenocrysts. Highly vesicular	Plg Ol Cpx Opx	pilotaxitic plg, ol. oxide and pyx	oxidation
ER4	Dark grey colored with alkaline feldspars and very small, white inclusions Highly vesicular	×	Hypocrystalline porphyritic, Mostly spongy cellular, gnawed euhedral plg phenocrysts, with spiky cpx. Highly vesicular	Plg Cpx	pilotaxitic plg, oxide and cpx	oxidation
ER5	Consolidated, light grey colored with small white inclusions	×	Hypocrystalline porphyritic Spongy cellular, gnawed, euhedral plg phenocrysts and some of them show oscillatory zoning Glomeroporphyritic texture Moderately vesicular	Plg Cpx Opx Ol	pilotaxitic plg, oxide and cpx	oxidation
ER8	Consolidated, dark grey colored with alkaline feldspars	×	Hypocrystalline porphyritic Spongy cellular, gnawed euhedral plg phenocrysts and some of them show oscillatory zoning Glomeroporphyritic texture Moderately vesicular	Plg Cpx Opx? Ol	pilotaxitic plg and oxide.	oxidation
ER9	Consolidated, dark grey colored with small white inclusions	×	Hypocrystalline porphyritic, Gnawed euhedral plg microphenocrysts. Glomeroporphyritic texture	Plg Opx Cpx?	glassy with few phenocrysts	dusty zones
ER10	Consolidated, light grey colored with small olivine, pyroxene and some brownish staffs	×	Hypocrystalline porphyritic. Spongy cellular, gnawed euhedral plg phenocrysts Skeletal olivine phenocrysts. Glomeroporphyritic texture (cpx)	Plg Ol Cpx	pilotaxitic plg, ol, cpx and oxide	serpentinization

Table 3.1: continued

ER11	Consolidated, dark grey colored, small alkaline phenocrysts	×	Hypocrystalline porphyritic Spongy cellular, gnawed euhedral plg phenocrysts and some of them show oscillatory zoning	Plg Cpx (few) Opx Ol (few)	pilotaxitic plg, oxide, cpx	oxidation
ER11M	Consolidated, enclave is dark brown and the matrix is light-grey colored with small white inclusions.	×	Hypocrystalline porphyritic Enclave is formed with plg and ol aggregates with black matrix. Outside of enclave is formed of few gnawed plg and cpx, ol phenocrysts. The intersection part of enclave and the whole-rock is light brown colored with plg microlites	Plg Cpx Ol	pilotaxitic plg, cpx, ol and oxide	
ER13	Light grey colored with white phenocrysts Moderately vesicular	×	Holocrystalline porphyritic Embayed ol phenocrysts Moderately vesicular	Plg Ol Cpx	pilotaxitic plg, oxide, cpx, ol	oxidation and iddingsite
ER16	Dark grey colored. with some small, white inclusions and brownish staffs. Moderately vesicular	×	Hypocrystalline porphyritic, Spongy cellular, gnawed euhedral plg, ol phenocrysts Moderately vesicular	Plg Ol Amp?	pilotaxitic plg, oxide, cpx (few)	oxidation
ER17	Consolidated dark grey colored olivine phenocrysts	×	Hypocrystalline porphyritic Spongy cellular, gnawed plg phenocrysts, with euhedral and skeletal olivine phenocrysts Less vesicular	Plg Ol	pilotaxitic plg, oxide, cpx (few)	oxidation
ER20	This sample is similar to ER-17.	×	Hypocrystalline porphyritic Ol phenocrysts and some of them are skeletal texture. Less vesicular.	Plg Ol Pyx	pilotaxitic plg, pyx, oxide	oxidation
ER22	Mostly consolidated and dark grey colored, with big white and green crystals	×	Hypocrystalline porphyritic Spongy cellular, gnawed euhedral plg phenocrysts and some of them show oscillatory zoning. Glomeroporphyritic texture	Plg Ol (few)	pilotaxitic plg, ol, oxide, cpx (few)	oxidation
ER25	Consolidated, dark grey colored with small white inclusions	×	Hypocrystalline seriate porphyritic Spongy cellular, gnawed euhedral plg phenocrysts with Ol microphenocrysts	Plg Ol	pilotaxitic plg, ol, oxide, cpx? (few)	oxidation

ER26	Light grey colored. with some small, white inclusions and small greenish staffs	×	Hypocrystalline porphyritic Gnawed euhedral plg phenocrysts Glomeroporphyritic texture Moderately vesicular	Plg Cpx	pilotaxitic plg, cpx and oxide	oxidation
ER27	Banded texture, one part is dark colored and the other part has white veins. Highly vesicular,	×	Hypocrystalline porphyritic One part is darker than the other part with cpx phenocrysts and skeletal olivine phenocrysts More vesicular than ER26	Plg Ol Cpx	pilotaxitic plg, cpx, ol (few) and oxide	oxidation
ER29	Dark grey colored, Highly vesicular	×	Hypocrystalline porphyritic Few plg phenocrysts Highly vesicular	Plg Ol	pilotaxitic plg, cpx (few) and oxide	
ER30	Consolidated, light grey colored with some small, white inclusions	~	Hypocrystalline porphyritic Spongy cellular, gnawed euhedral plg phenocrysts Glomeroporphyritic texture Moderately vesicular	Plg Ol Cpx	pilotaxitic plg, cpx (few) and oxide	oxidation
ER32	Consolidated, dark grey and black colored, with some small, white inclusions	×	Hypocrystalline porphyritic Glomeroporphyritic texture Moderately vesicular	Plg Ol Opx Cpx?	pilotaxitic plg, oxide	few oxidation

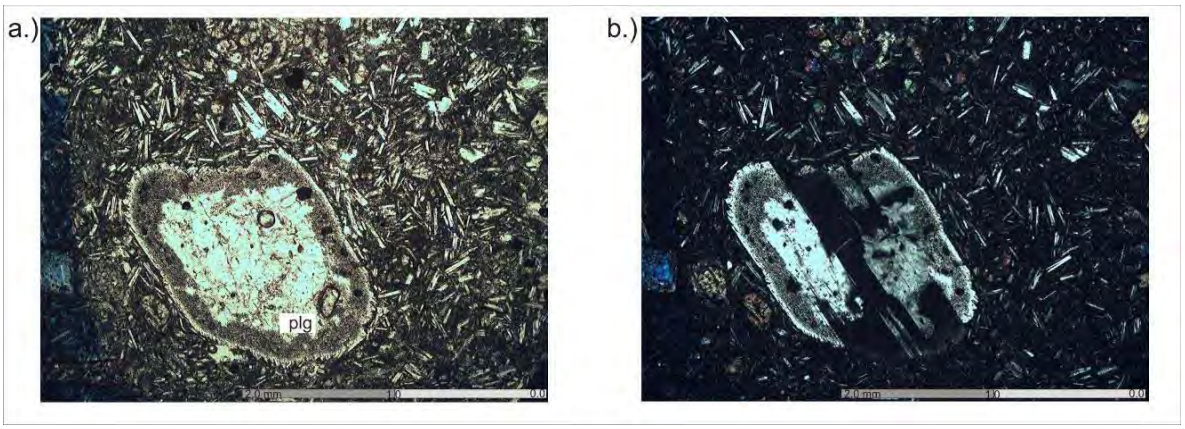

Figure 3.1: Plagioclase phenocryst displaying sieve texture and concentric zoning with glassy inclusions around its margins and centre (ER10, (a) I. Nicol, (b) II. Nicol) (plg: plagioclase)

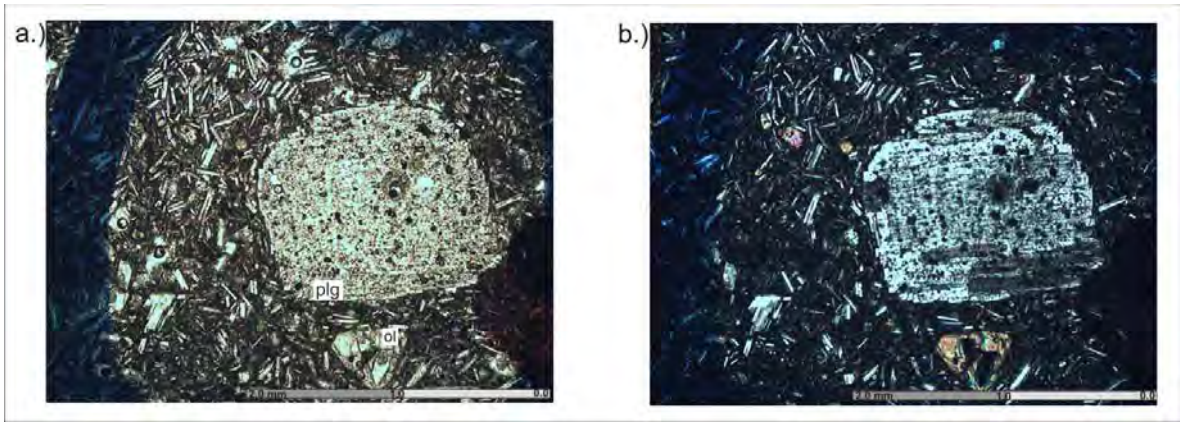

Figure 3.2: Plagioclase phenocryst with glassy inclusions and triangular shaped olivine phenocryst with gnawed structures starting from its centre (ER10, (a) I. Nicol, (b) II. Nicol) (plg: plagioclase, ol: olivine)

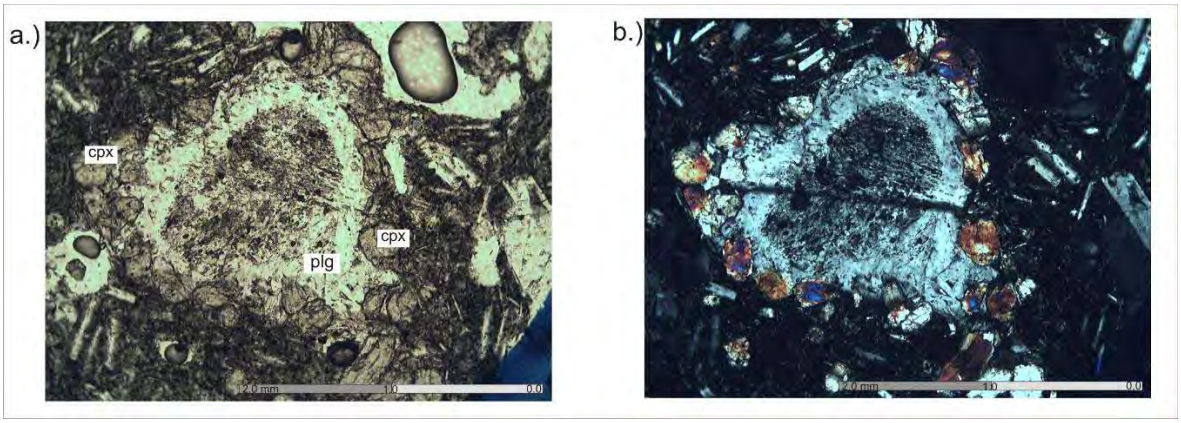

Figure 3.3: Plagioclase phenocryst with glassy inclusion in its central part and clinopyroxene microphenocrysts and microlites surrounding it (ER26, (a) I.Nikol, (b) II.Nikol) (plg: plagioclase, cpx: clinopyroxene)

Olivine (Ol) crystals are present at size interval varying from a few hundred microns to few millimeters. There are also samples containing both of these types of olivine crystals (Figure 3.4). Olivine that crystallized in equilibrium conditions is usually subhedral or anhedral, rounded, as phenocrysts, microphenocrysts and microlites. However, olivine that crystallized under disequilibrium conditions is skeletal, displaying gnawed structures starting from their central part (Figure 3.4). We observed also olivine crystals which are surrounded by a reaction belt. In some sections, iddingsitization is observed around margins of olivine crystals.

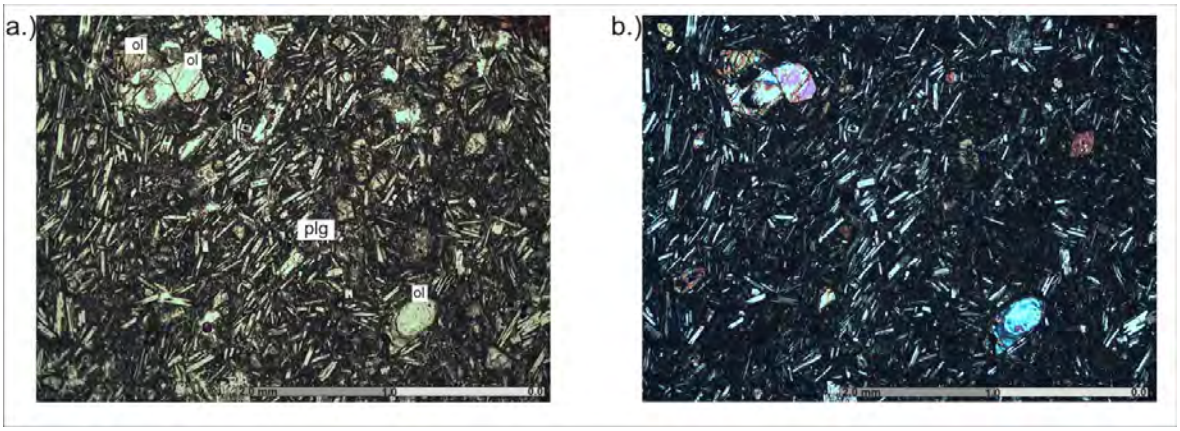

Figure 3.4: Equilibrium olivine (below right) and gnawed olivine microphenocryst (upper left). Plagioclase microlites (trachytic texture), pyroxene and olivine microlites are observed in the matrix. (ER10, (a) I. Nicol, (b) II. Nicol) (plg: plagioclase, ol: olivine)

Clinopyroxene (Cpx) crystals are observed as microlites in the groundmass, and as microphenocrysts of few hundred micron size. Clinopyroxene in equilibrium in the groundmass is euhedral or subhedral. When it was formed under disequilibrium conditions, the crystals are fragmented. Sometimes, Cpx is present in glomeroporphyritic grains (Figure 3.5).

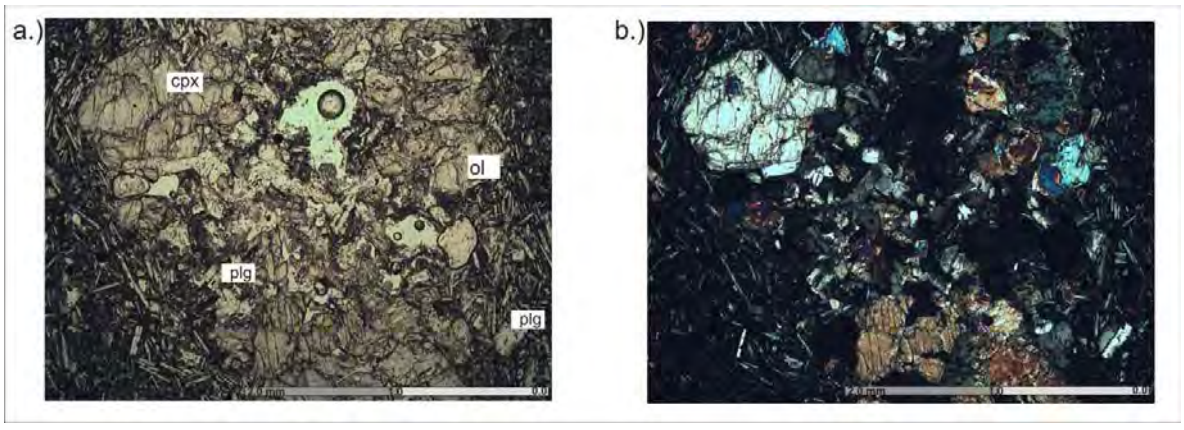

Figure 3.5: Clinopyroxene, plagioclase and olivine phenocrysts and microphenocrysts exhibiting glomeroporphyritic texture. (ER10, (a) I. Nicol, (b) II. Nicol) (plg: plagioclase, cpx: clinopyroxene, ol: olivine)

Orthopyroxene (Opx) crystals are observed together with clinopyroxene as phenocrysts, microphenocrysts and microlites in some samples. While the sizes of phenocrysts are few millimeters, sizes of microphenocrysts and microlites vary around few hundred microns. Phenocrysts and microphenocrysts are subhedral.

Orthopyroxene is present especially in ER9 and displays glomeroporphyritic texture (Figure 3.6).

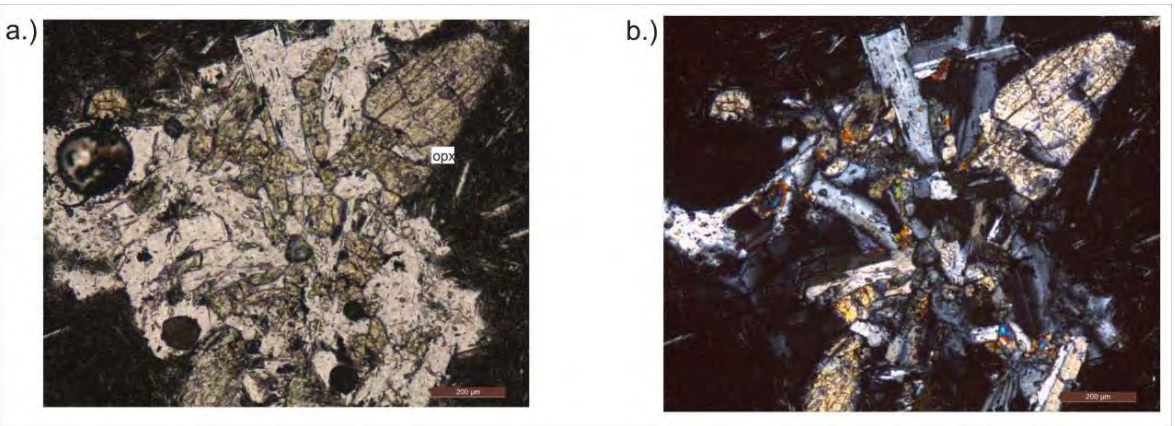

Figure 3.6: Orthopyroxene, plagioclase and olivine phenocrysts and microphenocrysts exhibiting glomeroporphyritic texture. (ER9, (a) I. Nicol, (b) II.Nicol) (opx: orthopyroxene)

The matrix is blackish and mainly consists of the microlites of the above mentioned minerals (Figure 3.4). Euhedral plagioclase microlites form sometimes trachytic textures.

3.2. The Basalts s.l. of Southwestern Cappadocia

These basalts s.l. were collected on scoria cones, related lava flows, and maar vents of 3 distinct areas: Hasandağ stratovolcano, Obruk-Zengen dispersed volcanism and Karapinar dispersed volcanism.

3.2.1. The Basalts s.l. of Hasandağ Stratovolcano

Samples of basalt collected on the flanks of Hasandağ stratovolcano revealed their mineralogical assemblage: plagioclase, olivine, clinopyroxene and oxides. The texture is hypocrystalline and porphyritic. The description of the basalts s.l. of Hasandağ volcano is given in Table 3.2.

Plagioclase (Plg) crystals were formed under equilibrium or disequilibrium conditions. Plagioclases formed under equilibrium conditions are euhedral microphenocrysts and microlites. Plg formed under disequilibrium conditions display sometimes sieve textures. Plg is also present in glomeroporphyritic globules, with olivine (Figure 3.7).

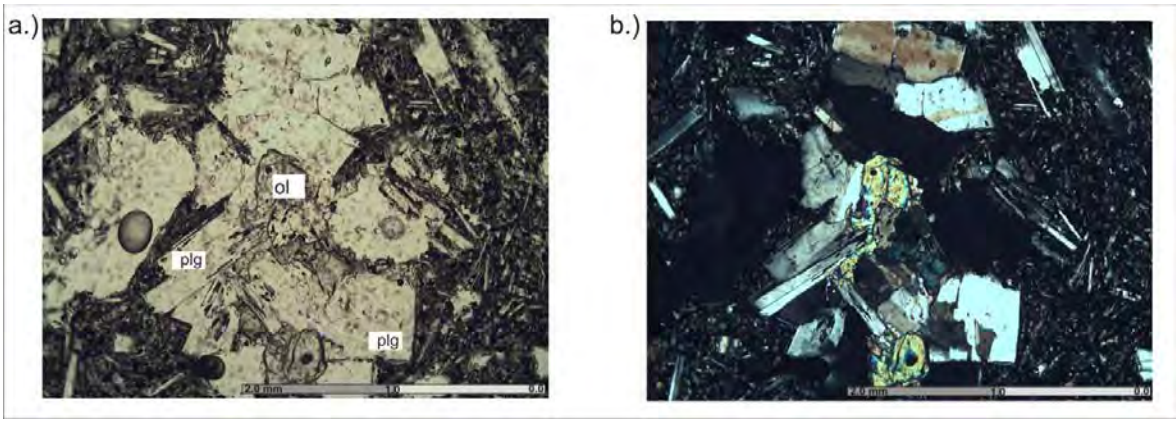

Figure 3.7: Plagioclase phenocrysts displaying glomeroporphyritic textures and olivine microphenocrysts (HA31, (a) I. Nicol, (b) II. Nicol) (plg: plagioclase, ol: olivine)

Olivine (Ol) crystals formed under equilibrium and disequilibrium conditions were observed together in most of the samples. Crystals formed under equilibrium conditions are usually euhedral phenocrysts and microphenocrysts. The ones formed under disequilibrium conditions are also phenocrysts but with greater sizes and skeletal features with gnawed features beginning from their central parts (Figure 3.8). Olivine is also observed in glomeroporphyritic grains. Sometimes, olivine contains opaque mineral inclusions of spinel. Iddingsitization is sometimes developed within fractures and in central parts of olivine.

Table 3.2: Petrographic description of basalts s.l. of Hasandağ stratovolcano, Obruk-Zengen and Karapınar dispersed volcanism area

Hasandag stratovolcano	Macroscopic features	Freshness	Rock Texture	Major crystals	Groundmass	Alteration
HA13 a	Dark grey colored with olivine phenocrysts and some very small, white inclusions Highly vesicular	×	Hypocrystalline porphyritic. Glomeroporphyritic texture Moderately vesicular	Plg Cpx Ol	pilotaxitic plg, cpx, ol and oxide	Oxidation, serpentinization
HA13 b	Consolidated, light grey colored with small white inclusions Less vesicular	×	Hypocrystalline porphyritic Skeletal olivine phenocrysts and some of them are disequilibrium Less vesicular than HA13a	Plg Ol Cpx	pilotaxitic plg, cpx, ol and oxide	serpentinization
HA18	Consolidated, with some vesicles Light brown and grey colored with olivine phenocrysts	×	Hypocrystalline porphyritic Embayed olivines, phenocrysts Moderately vesicular.	Plg Ol Cpx	pilotaxitic plg, ol, cpx? and oxide	oxidation, serpentinization
HA19	Light grey colored with olivine crystals Highly vesicular	×	Hypocrystalline porphyritic Embayed, gnawed and skeletal olivines phenocrysts Highly vesicular	Plg Ol Cpx	pilotaxitic plg, ol and oxide	oxidation, serpentinization
HA20	Consolidated with some vesicles Light grey, olivine phenocrysts	×	Hypocrystalline porphyritic Mostly embayed and gnawed olivines phenocrysts Less vesicular.	Plg Ol Cpx	pilotaxitic plg, ol and oxide	oxidation
HA22	Dark grey-black colored. Highly vesicular,	×	Hypocrystalline porphyritic. . Anhedral spongy cellular plg phenocrysts Highly vesicular	Plg Ol Cpx	pilotaxitic plg, ol, cpx and oxide	oxidation, serpentinization
HA23b	Consolidated, light grey colored with very white inclusions Moderately vesicular	×	Hypocrystalline porphyritic Cloudy texture plg phenocrysts with gnawed olivine and cpx phenocrysts Moderately vesicular	Plg Ol Cpx	pilotaxitic plg, ol, cpx and oxide	oxidation
HA31	Consolidated, light grey colored with small white inclusions	×	Hypocrystalline porphyritic Glomeroporphyritic texture	Plg Ol Cpx	pilotaxitic plg and few ol, cpx and oxide	

Table 3.2: continued

Obruk-Zengen	Macroscopic features	Freshness	Rock Texture	Major crystals	Groundmass	Alteration
HA14	Dark grey colored with olivine phenocrysts and small, white inclusions Highly vesicular	×	Hypocrystalline porphyritic Glomeroporphyritic texture Highly vesicular	Plg Ol Cpx	pilotaxitic plg, cpx, ol and oxide	oxidation
HA15	Highly vesicular Dark grey colored with olivine phenocrysts and small, white inclusions	×	Hypocrystalline porphyritic Glomeroporphyritic texture Highly vesicular	Plg Ol Cpx	pilotaxitic plg, cpx, ol and oxide	oxidation
HA16	Consolidated, light grey colored with small white inclusions Less vesicular	×	Hypocrystalline porphyritic Embayed and gnawed olivine phenocrysts Less vesicular	Plg Ol Cpx	pilotaxitic plg, cpx, ol and oxide	oxidation and iddingsite
HA17	Dark grey colored with olivine phenocrysts and some small, white inclusions Moderately vesicular	×	Hypocrystalline porphyritic Embayed and gnawed olivine phenocrysts Moderately vesicular	Plg Ol Cpx	pilotaxitic plg, cpx, ol and oxide	
HA24	Light grey-brown colored Highly vesicular	×	Hypocrystalline porphyritic Dark brown colored part is with ol and cpx. Outside of dark brown part is formed of the same crystals Highly vesicular	Plg Ol Cpx	pilotaxitic plg, ol, cpx and oxide	oxidation
HA26	Dark brown colored Highly vesicular	×	Hypocrystalline porphyritic Gnawed ol and cpx phenocrysts Highly vesicular	Ol Cpx Plg	pilotaxitic plg, ol, cpx and oxide	oxidation, serpentinization
HA27	Light grey colored with alkaline feldspars Moderately vesicular	×	Hypocrystalline porphyritic Spongy cellular plg phenocrysts and microphenocrysts Moderately vesicular	Plg Ol Cpx	pilotaxitic plg, ol, cpx and oxide	oxidation, iddingsite

Table 3.2: continued

Karapınar	Macroscopic features	Freshness	Rock Texture	Major crystals	Groundmass	Alteration
KA18	Consolidated Light grey colored with small white inclusions	×	Hypocrystalline porphyritic	Plg Ol Cpx	pilotaxitic plg, ol, cpx and oxide	
KA19	Light grey colored Highly vesicular	×	Hypocrystalline porphyritic Spongy cellular plg phenocrysts with gnawed ol Glomeroporphyritic texture with cpx, ol and plg	Plg Ol Cpx	pilotaxitic plg, ol, cpx and oxide	
KA21	Consolidated Dark grey colored with alkaline feldspars phenocrysts	×	Hypocrystalline porphyritic Spongy cellular plg phenocrysts with gnawed ol phenocrysts	Plg Ol Cpx	pilotaxitic plg, ol, cpx and oxide	oxidation

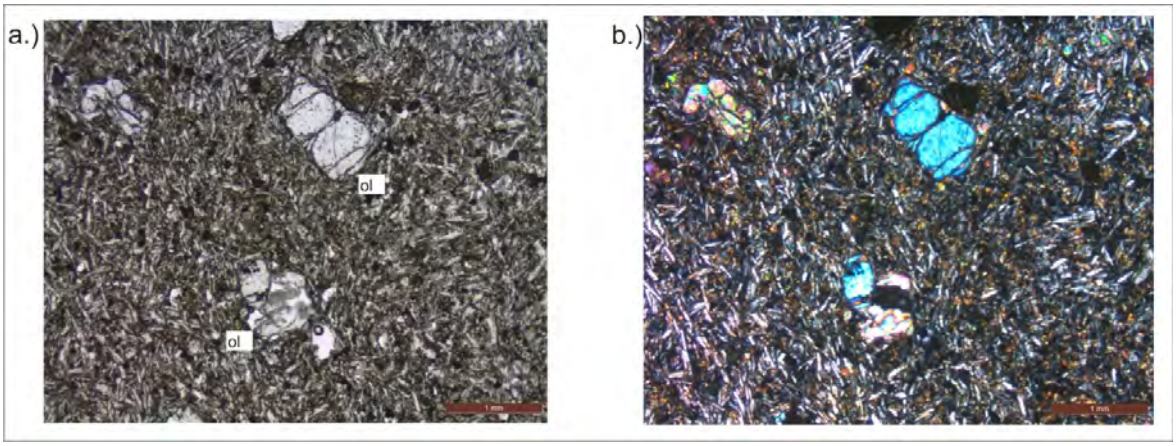

Figure 3.8: Olivine phenocrysts and microphenocrysts under equilibrium (upper right) and disequilibrium (lower left) conditions (HA20, (a) I. Nicol, (b) II. Nicol) (ol: olivine)

Clinopyroxene (Cpx) crystals are observed as prismatic microlites in the matrix and/or as phenocrysts, microphenocrysts (Figure 3.9). Fractured Cpx crystals are formed under disequilibrium conditions. Some Cpx microphenocrysts are observed at the margins of plagioclase. Sometimes, Cpx occurs in glomeroporphyritic grains. In few samples “sector zoning” and local serpentinization were observed.

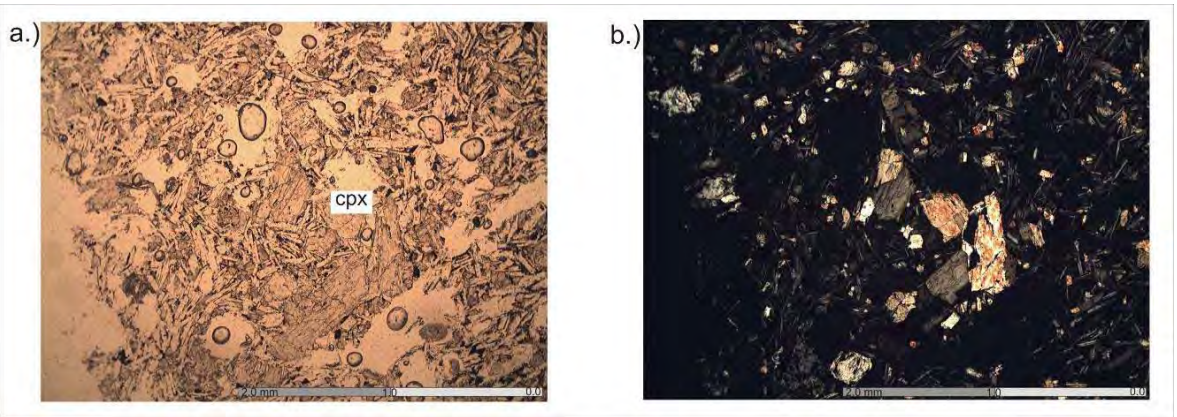

Figure 3.9: Clinopyroxene microphenocrysts and microlites in a glomeroporphyritic grain (HA13, (a) I.Nicol, (b) II. Nicol) (cpx: clinopyroxene)

Matrix commonly exhibit microlites of the above mentioned minerals (Fig 3.10). The matrix is blackish.

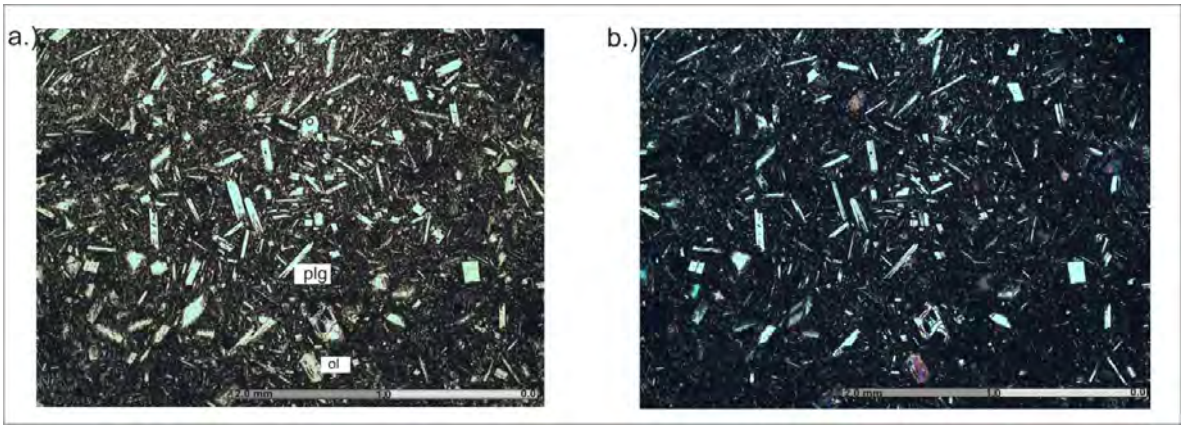

Figure 3.10: Plagioclase microlites with pyroxene and olivine crystals within the matrix. (HA31, (a) I. Nicol, (b) II. Nicol) (plg: plagioclase, ol: olivine)

3.2.2. The Basalts s.l. of the Obruk-Zengen Dispersed Volcanism

Basalts of the Obruk-Zengen area, at South of Hasandağ stratovolcano, exhibit the following mineralogical assemblage: plagioclase, olivine, clinopyroxene and oxide minerals. The textures are hypocrystalline and porphyritic. The description of the studied samples is given in Table 3.2.

Plagioclase (Plg) crystals are usually observed as microphenocrysts and microlites, sometimes as phenocrysts in HA27 (Figure 3.11). Plg phenocrysts in HA27 are subhedral, prismatic and sometimes gnawed and vary from a few hundred microns to few millimeters in size. Plagioclases in equilibrium and in disequilibrium are both present in HA27 (Figure 3.11). Plg formed under

disequilibrium conditions display sieve textures (Figure 3.11). Plagioclase is also present in glomeroporphyritic grains.

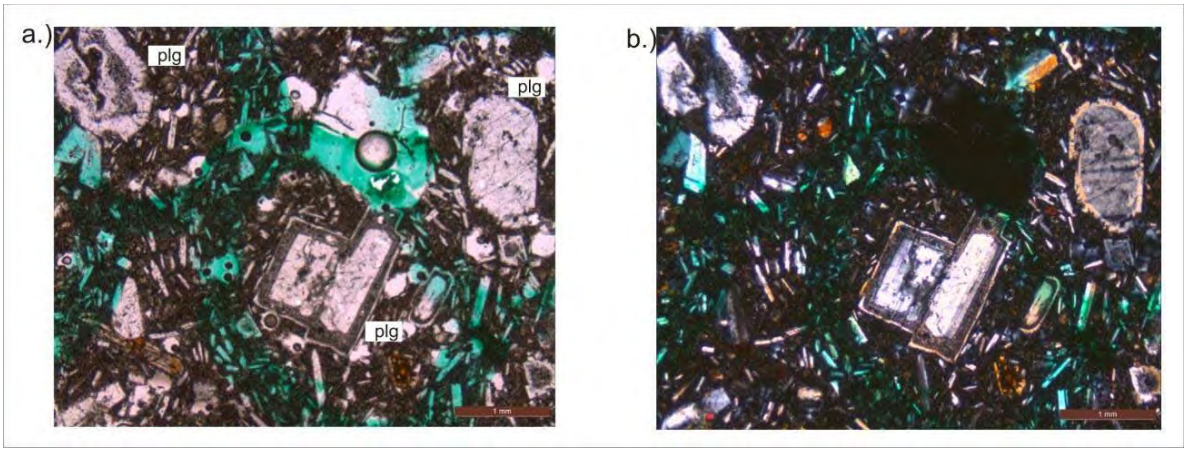

Figure 3.11: Plagioclase phenocrysts and microphenocrysts under equilibrium and disequilibrium conditions. The ones formed under disequilibrium conditions display sieve textures. (HA27, (a) I.Nicol, (b) II. Nicol) (plg: plagioclase)

Olivine (Ol) crystals exhibit equilibrium and disequilibrium features and are both observed in most of the samples (Figure 3.12). Olivine is present as phenocrysts, microphenocrysts and microlites. The sections formed under disequilibrium conditions are phenocrysts with greater sizes displaying skeletal habitus with gnawed features beginning from their central parts (Figure 3.13). Olivine is also observed in glomeroporphyritic grains. Some olivine sections contain opaque mineral inclusions of spinel. In some disequilibrium conditions, olivines display iddingsitization.

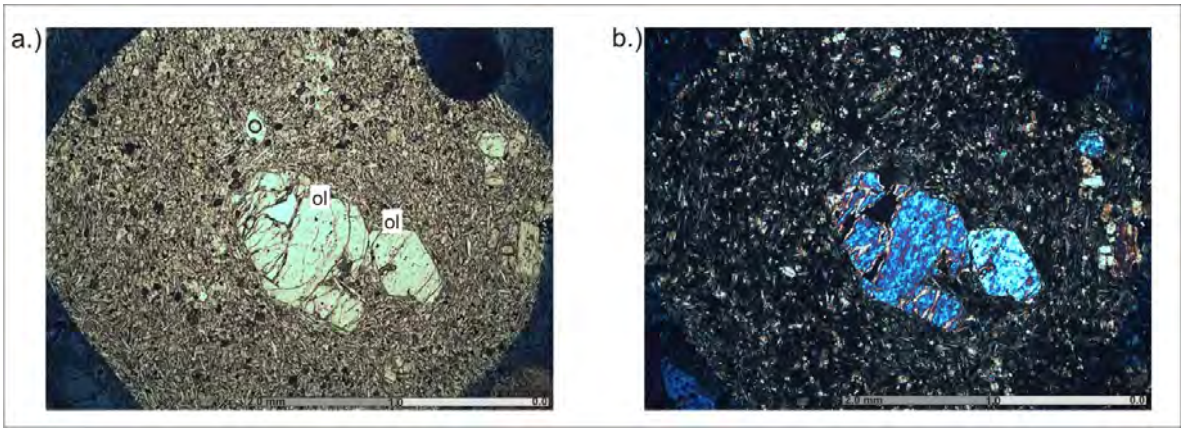

Figure 3.12: Equilibrium olivine microphenocrysts and disequilibrium olivine phenocrysts (HA16, (a) I.Nicol, (b) II. Nicol) (ol: olivine)

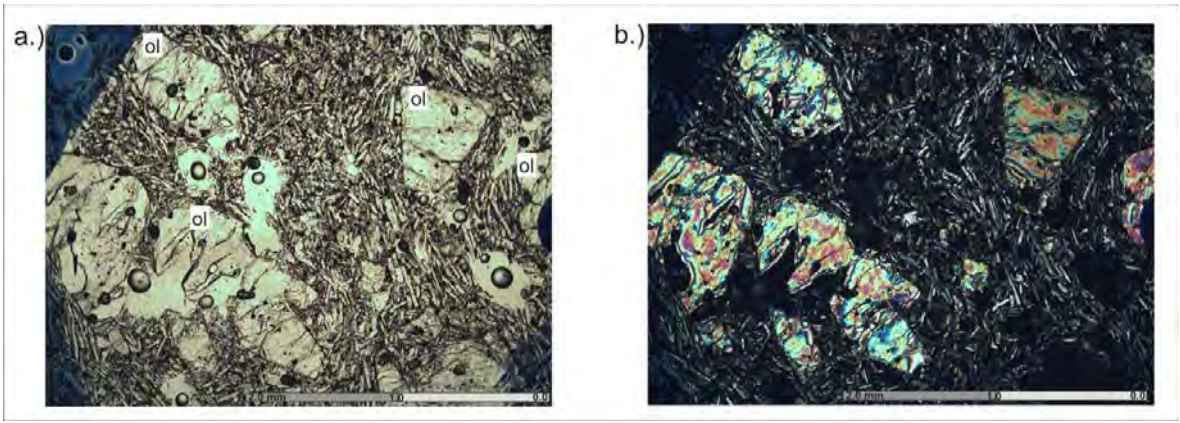

Figure 3.13: Gnawed, fractured olivine phenocrysts (HA17, (a) I.Nicol, (b) II. Nicol) (ol: olivine)

Clinopyroxene (Cpx) are common as prismatic microlites in the matrix and as phenocrysts and microphenocrysts (Figure 3.14). They are generally subhedral prismatic and a few millimeters in size. Some crystals formed under disequilibrium conditions are gnawed and fragmented. Cpx is also present in glomeroporphyritic grains.

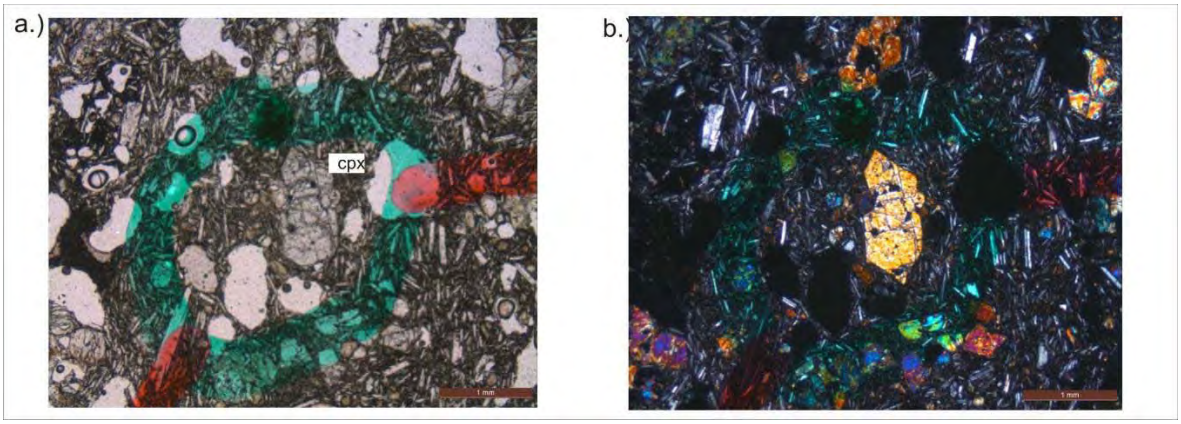

Figure 3.14: Fractured clinopyroxene phenocrysts and microphenocrysts (HA26, (a) I.Nicol, (b) II. Nicol) (cpx: clinopyroxene)

Matrix is commonly made of the microlites of the above mentioned minerals (Figure 3.15). Euhedral plagioclase display sub-trachytic texture olivine, and clinopyroxene microlites are present in a granular blackish matrix.

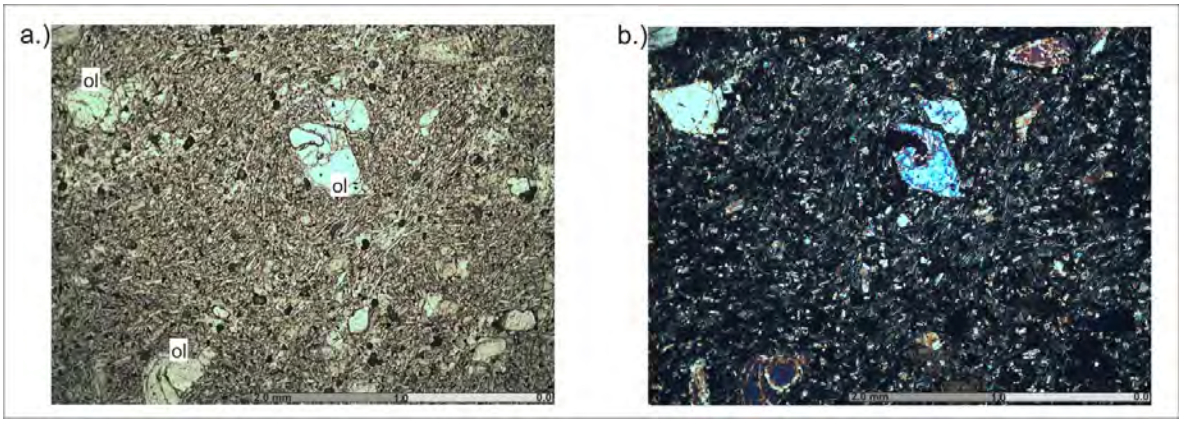

Figure 3.15: Equilibrium (upper left) and disequilibrium (lower left) olivine microphenocrysts. Plagioclase microphenocrysts displaying sub-trachytic texture, pyroxene and olivine microlites in the matrix (HA16, (a) I.Nicol, (b) II. Nicol) (ol: olivine)

3.2.3. Basalts s.l. of the Karapınar Dispersed Volcanism

The samples of Karapınar exhibit the following mineralogical assemblage: plagioclase, olivine, clinopyroxene and oxides. Their texture is hypocrystalline porphyritic. Table 3.2 shows the description of the Karapınar samples.

Plagioclase (Plg) crystals are subhedral, prismatic and sometimes gnawed. Their size varies between a few hundred microns to millimeters. Plagioclase is formed under equilibrium and disequilibrium conditions, as in KA19 and KA21 samples (Figure 3.16 and 3.17). Plagioclases are found as phenocrysts, microphenocrysts and microlites in KA19 and KA21 samples, but usually as microphenocrysts and microlites as in KA18. The Plg formed under disequilibrium conditions display sieve textures and cloudy zone in all Karapınar samples (Figure 3.16). Plagioclase is also observed in glomeroporphyritic aggregates.

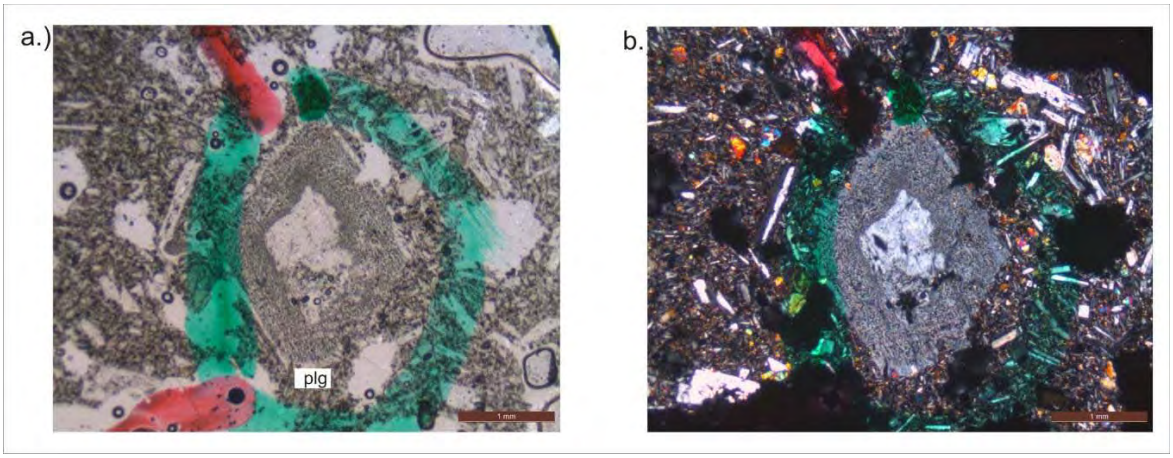

Figure 3.16: Plagioclase phenocryst displaying sieve texture (KA19, (a) I.Nicol, (b) II. Nicol) (plg: plagioclase)

Olivine (Ol) crystals exhibit both equilibrium and disequilibrium features. Olivines crystallized in equilibrium conditions are usually phenocrysts, microphenocrysts and microlites, but also as subhedral or anhedral crystals with rounded shapes (Figure 3.17). The olivine formed under disequilibrium conditions is present also as phenocrysts and microphenocrysts but display gnawed features. In KA21 sample, some olivine sections contain opaque mineral inclusions of spinel.

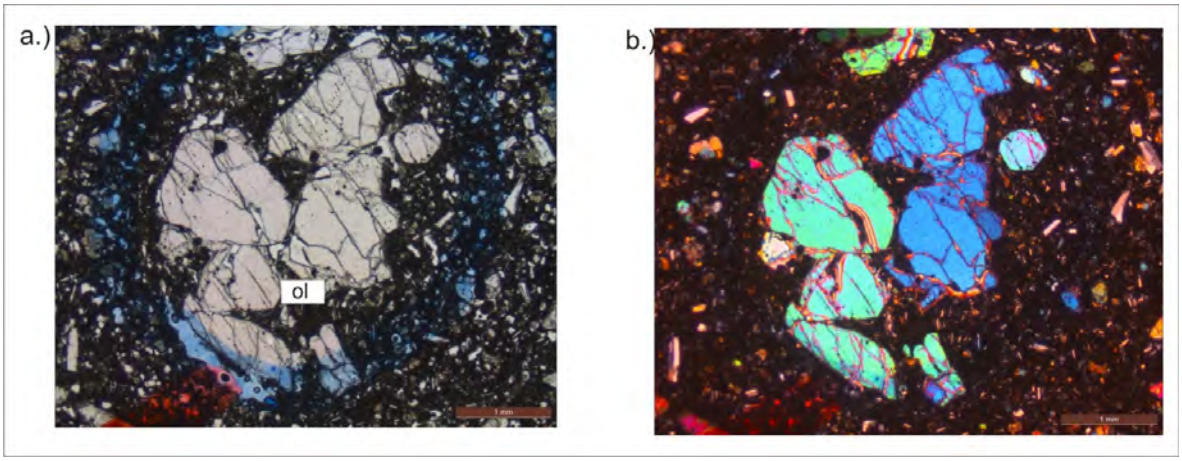

Figure 3.17: Olivine phenocrysts, microphenocrysts and microlites with subhedral or anhedral crystals with rounded shapes (KA21, (a) I. Nicol, (b) II. Nicol) (ol: olivine)

Clinopyroxene (Cpx) is present mainly as phenocrysts, but also as microphenocrysts and microlites (Figure 3.18). Cpx sections are subhedral, prismatic and sometimes gnawed, and are a few millimeters in size. Cpx occur sometimes in glomeroporphyritic aggregates.

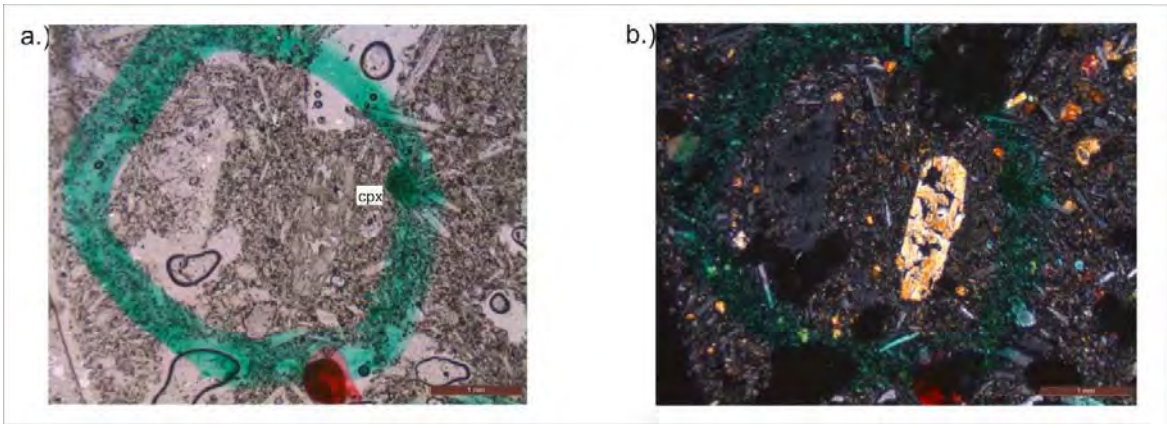

Figure 3.18: Clinopyroxene phenocrysts, microphenocrysts and microlites (KA19, (a) I. Nicol, (b) II. Nicol) (cpx: clinopyroxene)

The groundmass commonly exhibits microlites of plagioclase, clinopyroxene, olivine and oxides. Sometimes, plagioclase sections display a sub-trachytic texture, as in KA18 and KA19, but granular textures are common. The matrix of KA21 is blackish, but in KA18 and KA19, the matrix is light colored to brownish (Figure 3.19)

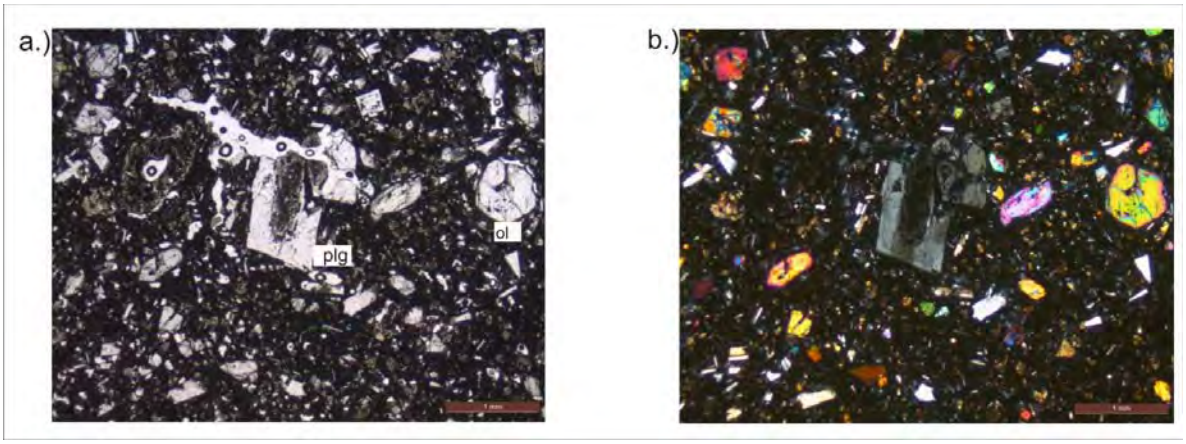

Figure 3.19: The matrix is blackish and mainly consists of microlites of plagioclase, clinopyroxene and olivine (KA21, (a) I. Nicol, (b) II. Nicol) (plg: plagioclase, ol: olivine)

3.3. Conclusion

As a result of our mineralogical and petrographical studies, from Erciyes and Hasandağ stratovolcanoes and from Obruk-Zengen and Karapınar dispersed volcanism, the following mineralogical assemblages are emphasized:

- Erciyes stratovolcano: Plagioclase + Olivine + Clinopyroxene ± Orthopyroxene + Opaque minerals.
- Hasandağ stratovolcano: Plagioclase + Olivine + Clinopyroxene + Opaque minerals
- Obruk-Zengen dispersed volcanism: Plagioclase + Olivine + Clinopyroxene + Opaque minerals.
- Karapınar dispersed volcanism: Plagioclase + Olivine + Clinopyroxene + Opaque minerals.
- So, 2 different mineralogical groups are proposed: Erciyes where orthopyroxene (Opx) occurs and other areas without Opx. We emphasize also the coexistence of mineralogical equilibrium and out of equilibrium features in most phenocrysts:

1. The samples have both cpx and opx are mainly located on the NW of the Erciyes stratovolcano. Their ages are between (0.115 — < 0.001 Ma). On the other hand ER3 (0.352 Ma) and the ER1 (0.093 Ma) are located N and the S of the main cone, respectively (Figure 2.2). ER9 (< 0.001 Ma) and ER32 (0.707 Ma) only have opx and they are located NE and E of the main cone, respectively. The other samples without opx are located on the NW of the Erciyes stratovolcano except ER10 (0.297Ma) and ER30 (0.102 Ma) which are located N and SW of the main cone. According to these informations, there isn't any systematic relationship between locations, ages and the mineral assemblages.

2. Both equilibrium and disequilibrium mineral sections were observed in the 4 areas: Erciyes stratovolcano, Hasandağ stratovolcano, Obruk-Zengen dispersed volcanism and Karapınar dispersed volcanism. However, it was observed that plagioclase of Erciyes and Karapınar exhibits more equilibrium features compared to the other regions. Such disequilibrium conditions are related essentially to sieve, spongy and cloudy features.

Besides, some plagioclases of Erciyes are locally surrounded by microcrysts and microlites of clinopyroxene. The occurrence of both plagioclases, in equilibrium and out of equilibrium, in the same sample let us consider that the genesis conditions were not homogenous.

3. The association of both equilibrium and disequilibrium olivines were observed in all regions. While some equilibrium olivines were observed as euhedral to subhedral shapes, disequilibrium olivine minerals were also observed as corroded, fragmented and as skeletal sections. The associations of both olivines were mainly observed in Hasandağ stratovolcano and Obruk-Zengen. Such association of different olivine crystals let us anticipate that olivine was generated under complex processes.

4. Clinopyroxene (Cpx) mineral is observed mainly as phenocryst in Karapınar region, and as microlites in Hasandağ stratovolcano and Obruk-Zengen However, Cpx occurs mainly as microlites and microphenocrysts in the Erciyes stratovolcano samples.

5. Orthopyroxene (Opx) was only detected in some samples of Erciyes stratovolcano, as phenocrysts, microphenocrysts and microlites. This is a major mineralogical feature, comparatively to the mineralogy of the 3 other studied areas where Opx is lacking. Generally, Opx phenocrysts occur in calc-alkaline mafic and intermediate lavas and not in alkaline ones.

4. MINERAL CHEMISTRY

Electron microprobe analyses have been performed at Blaise Pascal University, in “Laboratoire Magmas et Volcans”. Analyses have been performed upon the core and the rim of the phenocrysts, microphenocrysts and the microlites.

The microprobe data are plotted in mineral classification diagrams and mineral-liquid equilibrium diagrams. By the help of these diagrams and equations from the literature, order estimated temperatures and barometers are calculated. The evolution of temperatures with the different minerals changing host rock in SiO_2 contents, are also presented. Informations related to the analytical methods are given in section 1.4.1.

Table 4.1 shows the compositions of the minerals of the four studied areas. Representative mineral data set can be found in Appendix.

4.1. Mineral Chemistry of the Basalts s.l. of the Erciyes Stratovolcano

Feldspars

Plagioclase (Plg) is the dominant mineral in all Erciyes basaltic (s.l.) rocks. Plagioclases (An_{35-85}) range in composition (Table 4.1) from albite through andesine to bytownite (Figure 4.1). However, most plagioclases are andesine-labrodorite. Like phenocrysts and microphenocrysts, microlites have a large compositional range $An_{(39-70)}$ (Table 4.1). Generally, plagioclases display normal zoning but in some samples, such as ER1, ER3, ER9, ER10, ER11, ER22, ER27 and ER30, reversed zoning also occurs. As can be seen in Figure 4.1, the An compositions of ER3 and ER10 are very similar. The location of these two samples (Figure 2.2) and their ages are very close to each other (Table 2.3).

Olivine

The Fo% compositions of olivine (Ol) for Erciyes basaltic (s.l.) rocks are listed in Table 4.1. Olivine occurs as phenocrysts, microphenocrysts and microlites (Figure 4.2). Generally, they display a wide compositional range, Fo% ($_{57-86}$) for phenocrysts and microphenocrysts, and Fo% ($_{66-83}$) for microlites.

Table 4.1: Average minerals compositions of basalts s.l. in the 4 studied areas

	Erciyes stratovolcano	Hasandag stratovolcano	Obruk-Zengen	Karapınar
Plg (Phenocrysts & microphenocrysts)	An $(_{35-85})$	An $(_{37-85})$	An $(_{35-78})$	An $(_{34-76})$
Plg (Microlites)	An $(_{39-70})$	An $(_{52-72})$	An $(_{52-73})$	An $(_{45-70})$
Olivine (Phenocrysts & microphenocrysts)	Fo% $(_{57-86})$	Fo% $(_{68-86})$	Fo% $(_{57-90})$	Fo% $(_{68-89})$
Olivine (Microlites)	Fo% $(_{66-83})$	Fo% $(_{53-75})$	Fo% $(_{57-87})$	Fo% $(_{47-70})$
Cpx(Phenocrysts & microphenocrysts)	$Wo_{(33-46)}$ $En_{(42-52)}$ $Fs_{(9-22)}$	$Wo_{(42-47)}$ $En_{(41-47)}$ $Fs_{(8-16)}$	$Wo_{(40-49)}$ $En_{(41-48)}$ $Fs_{(8-17)}$	$Wo_{(41-46)}$ $En_{(40-48)}$ $Fs_{(9-16)}$
Cpx (Microlites)	$Wo_{(23-47)}$ $En_{(31-52)}$ $Fs_{(7-22)}$	$Wo_{(41-45)}$ $En_{(39-46)}$ $Fs_{(10-17)}$	$Wo_{(40-48)}$ $En_{(35-46)}$ $Fs_{(10-19)}$	$Wo_{(41-46)}$ $En_{(40-48)}$ $Fs_{(9-17)}$
Opx(Phenocrysts & microphenocrysts)	$Wo_{(2-13)}$ $En_{(65-83)}$ $Fs_{(14-30)}$	—	—	—
Opx (Microlites)	$Wo_{(3-9)}$ $En_{(66-79)}$ $Fs_{(18-29)}$	—	—	—
Ti-Magnetite	$Usp_{(35-73)}$	$Usp_{(57-62)}$	$Usp_{(38-58)}$	$Usp_{(40-63)}$
Ilmenite	$Ilm_{(98)}$	$Ilm_{(94)}$	*	*
Spinel	*	*	*	*

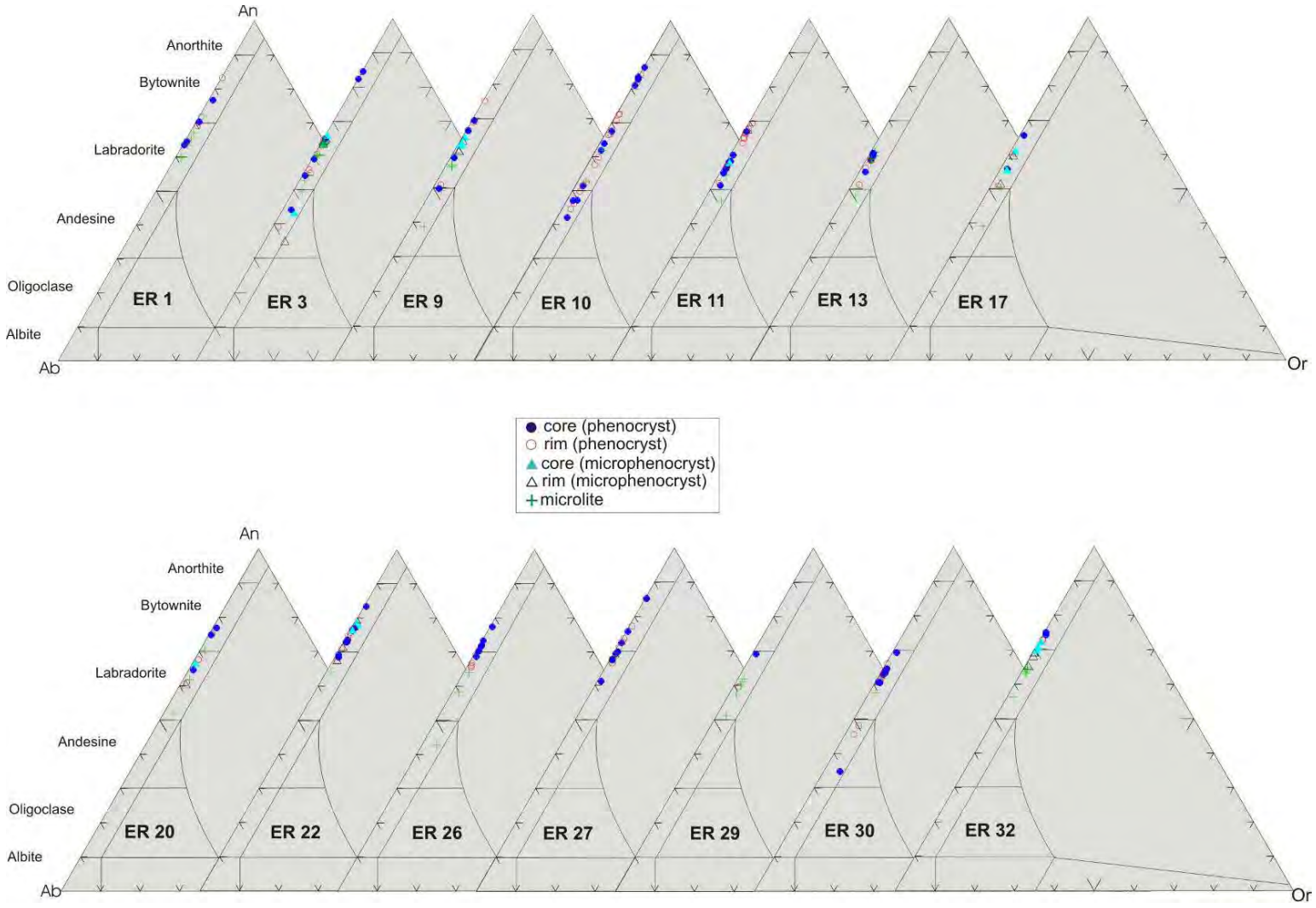

Figure 4.1: Compositions of feldspars (mole %) from Erciyes stratovolcano basalts s.l. (An: Anhortite, Ab: Albite, Or: Orthoclase)

On the other hand, the oldest sample ER13 (1.695±0.037 Ma) has few olivine sections and the compositional range is restricted (Figure 4.2). Most of olivines are normally zoned with respect to Mg, Fe, but some exhibit reversed zone such as ER10, ER17, ER22, ER27 and ER30.

Clinopyroxene

Clinopyroxene (Cpx) occurs as needle-like microphenocrysts and microlites but they have been observed also as phenocrysts in ER10 ER22, ER26 and ER27. Most phenocrysts are diopside and augite in composition (Figure. 4.3) (Morimoto, 1989). Cpx occurs only as microlites in ER13 and ER29 and ER30 (Figure 4.3). The composition of clinopyroxene is $Wo_{(33-46)}$, $En_{(42-52)}$, $Fs_{(9-22)}$ for phenocrysts and microphenocrysts and $Wo_{(23-47)}$, $En_{(31-52)}$, $Fs_{(7-22)}$ for microlites (Table 4.1). The Mg-numbers of clinopyroxenes display a wide range (59-87). Oscillatory zoning clinopyroxenes are common but some clinopyroxenes are weakly zoned. Normal-zoned clinopyroxene phenocrysts, with Mg-rich cores, coexist with reversed-zoned clinopyroxene phenocrysts with Mg-rich rims, in the samples ER10, ER17, ER26 and ER27.

Orthopyroxene

The compositions of Opx are listed in Table 4.1. Orthopyroxene (Opx) minerals are usually present as phenocrysts, microphenocrysts and microlites (Figure 4.3). Opx and Cpx coexist in samples ER1, ER3, ER11, ER17, ER20 and ER22. Cpx of these samples are augite and/or diopside with composition $Wo_{(23-44)}$, $En_{(42-57)}$, $Fs_{(9-23)}$ and Opx are enstatite and pigeonite with composition $Wo_{(3-9)}$, $En_{(65-82)}$, $Fs_{(15-30)}$. Except ER3 (0.352±0.009 Ma), the other samples with Opx and Cpx coexisting are younger and their ages vary between 0.115 and <0.001 M. ER9 and ER32 have only Opx (enstatite) (Figure 4.3). Normally zoned Opx phenocrysts, with Mg-rich cores, coexist with reversed-zoned Opx phenocrysts, with Mg-rich rims, in ER3, ER9 and ER32. The Mg-numbers of orthopyroxene are ranging between 69 and 84.

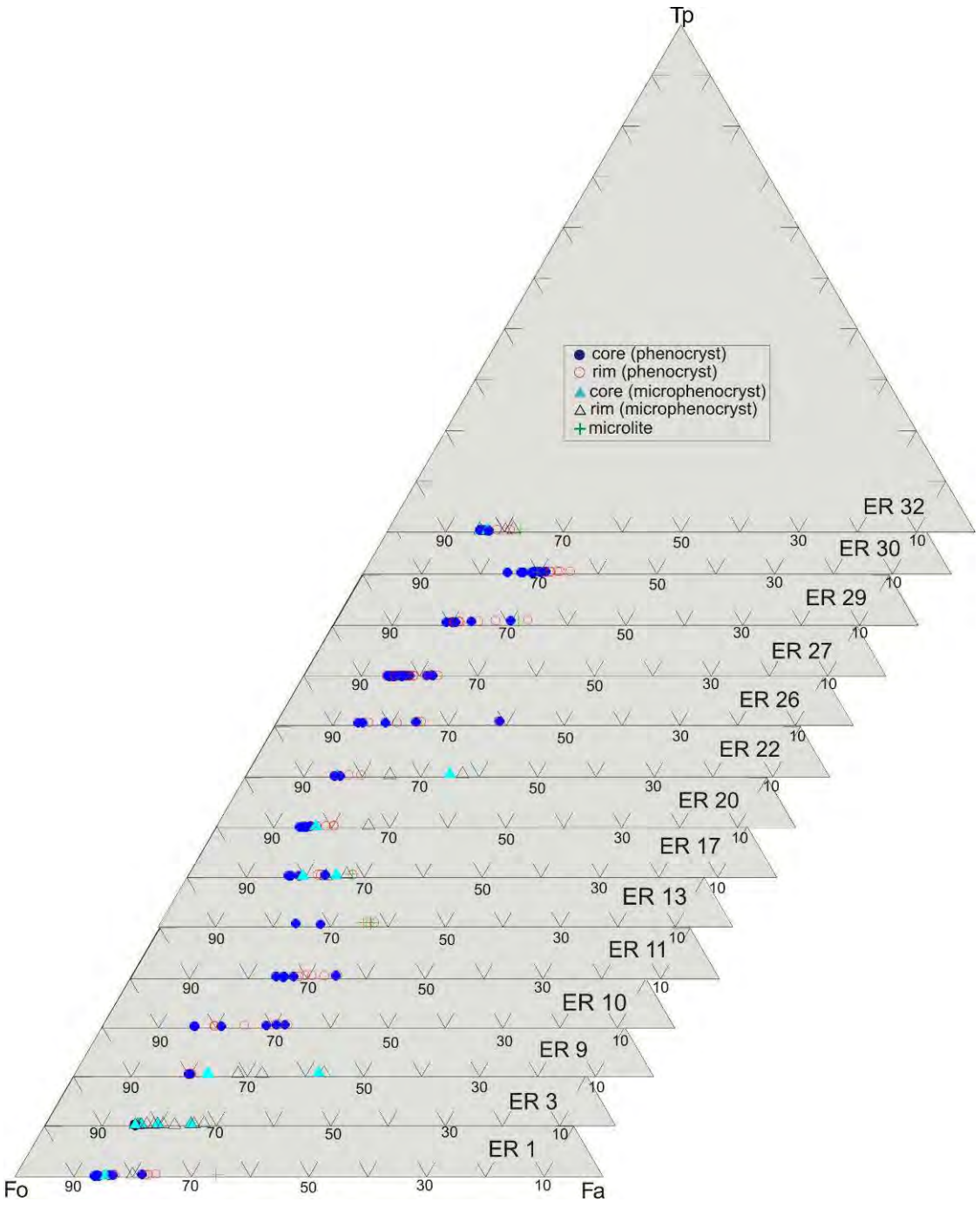

Figure 4.2: Compositional variations of olivine of the basaltic (s.l.) rocks from Erciyes stratovolcano. (Tp: Tephroite, Fo: Forsterite, Fa: Fayalite)

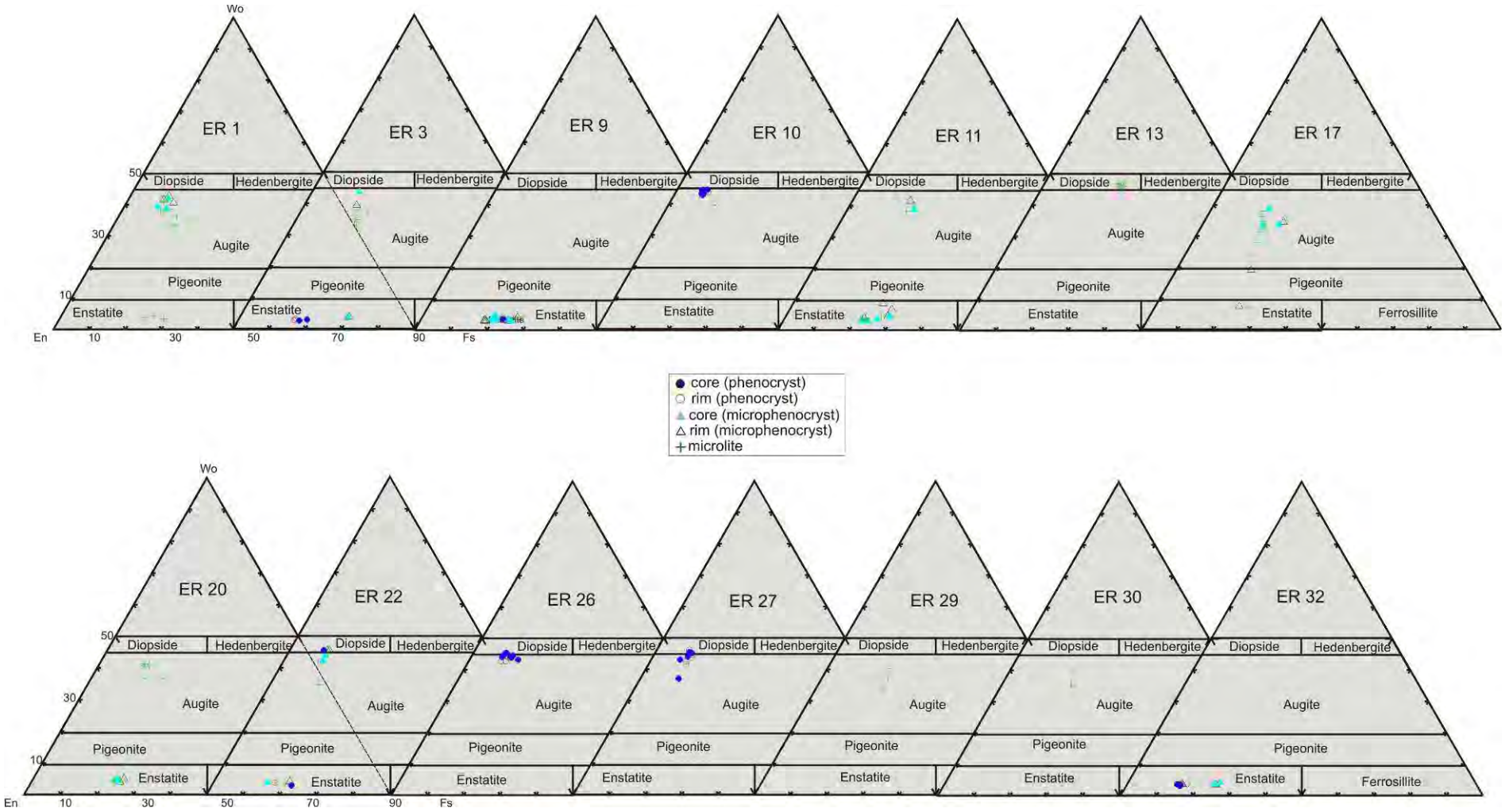

Figure 4.3: Compositional variations of pyroxenes in Wo-En-Fs diagrams (Morimoto, 1989). (En: Enstatite, Wo: Wollastonite, Fs: Ferrosillite)

Oxide Minerals

Oxide minerals are generally observed as microlites in the groundmass. The Fe-Ti oxides are essentially magnetite and secondary ilmenite (Figure 4.4a). According to Melluso et al. (1988), spinels are Cr-spinels in sample ER17 (Figure 4.4b).

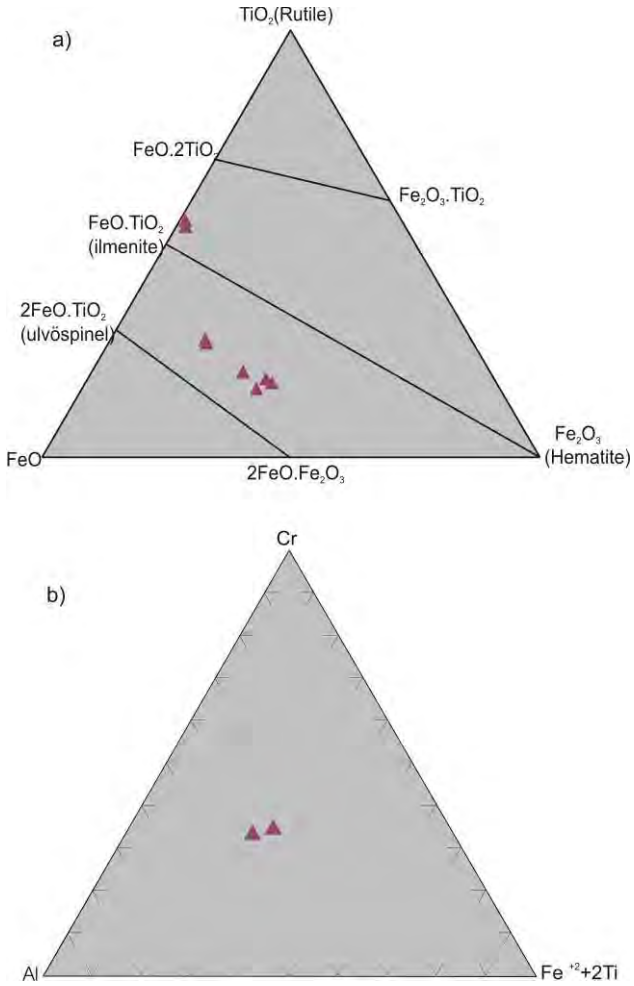

Figure 4.4: (a) Composition of Fe-Ti oxides (Bacon and Hirschmann, 1988) of basalts s.l. of Erciyes stratovolcano (b) Cr-Al-(Fe^{+2} + 2Ti) triangular diagram (Melluso et al., 1988)

Volcanic Glass

Microprobe analyses of glass can only be carried out on ER27 and ER30 samples. The SiO_2 content is between 66 and 68% in ER27, and 69-71% in ER30.

4.2. Mineral Chemistry of the Basalts s.l. of the Southwestern Cappadocia Volcanism

4.2.1. The Hasandağ Stratovolcano

Feldspars

While the composition of plagioclase (Plg) displays a wide range $An_{(37-85)}$ for phenocrysts and microphenocrysts, it is limited $An_{(52-72)}$ for microlites (Table 4.1). Generally reverse zoning is observed in all samples but normal zoning also occured. Plg is labradorite in composition for the samples HA13b, HA19 and HA20, andesine-labradorite for HA18 and HA23b, labradorite-bytownite for HA31 (Figure 4.5). While the phenocrysts of the youngest sample (HA31) are more calcic, the oldest sample (HA23b) phenocrysts are more sodic (Table 2.4).

Olivine

Olivine occurs as phenocrysts, microphenocrysts and microlites. In Table 4.1, we emphasize that the compositional range of olivine is Fo% ($_{68-86}$) for phenocrysts and microphenocrysts, and Fo% ($_{53-75}$) for microlites. The microlites of the oldest sample HA23b (Table 2.4) show a restricted range Fo% ($_{53-57}$). Generally, normal zoning with Fo-rich core olivines occur in all samples.

Clinopyroxene

Clinopyroxene (Cpx) usually occurs as needle-like microphenocrysts and microlites but the oldest sample HA23b exhibits clinopyroxene phenocrysts. All phenocrysts, microphenocrysts and microlites are diopside and augite in composition (Figure 4.7). The composition of Cpx is $Wo_{(42-47)}$, $En_{(41-47)}$,$Fs_{(8-16)}$ for phenocrysts and microphenocrysts and $Wo_{(41-45)}$, $En_{(39-46)}$ $Fs_{(10-17)}$ for microlites (Table 4.1). Clinopyroxene occurs only as microlites in basalt samples HA19 and HA31. The Mg-number of Cpx displays a limited range (72-85). Usually clinopyroxenes display normal zoning but some reverse-zoned clinopyroxene phenocrysts and microphenocrysts are present in HA20 and HA23b samples.

Oxides

The compositions of oxides of all Southwestern Cappadocia samples are plotted in Figure 4.8a-b. Oxides occur as magnetite and secondary ilmenite microlites in the groundmass (Figure 4.8a). Spinels are observed in olivine phenocrysts and/or

microphenocrysts of HA13b, HA19 and HA23b samples. They are Cr-spinel and Al-chromite spinel (Figure 4.8b).

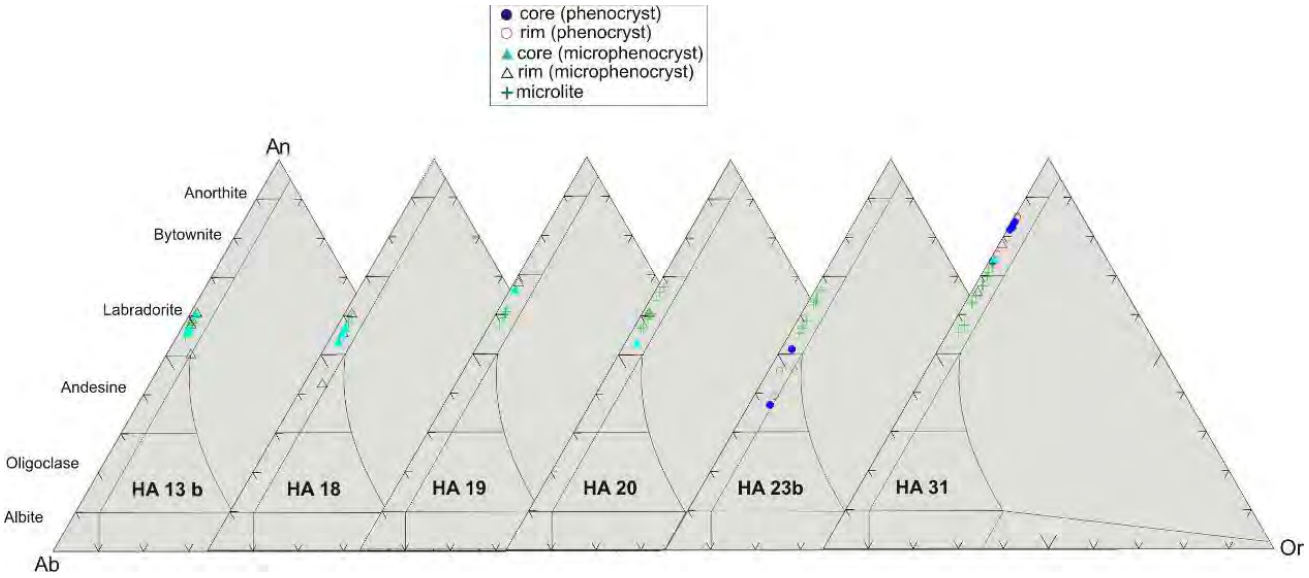

Figure 4.5: Compositions of feldspars from basalts s.l. of Hasandağ stratovolcano (An: Anhortite, Ab: Albite, Or: Orthoclase)

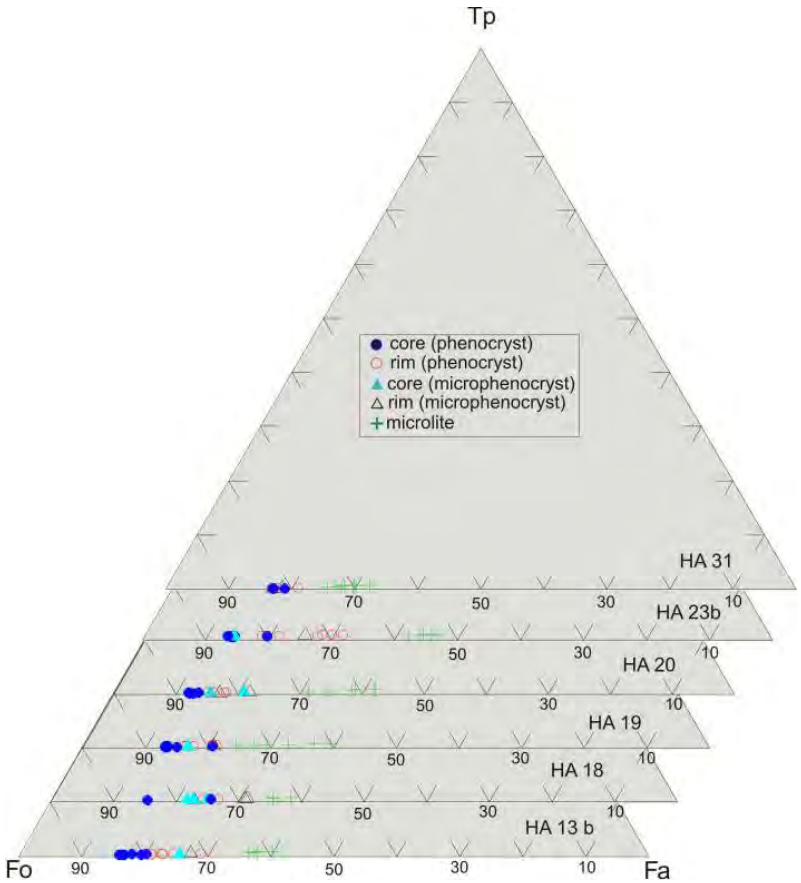

Figure 4.6: Composition of olivine from basalts s.l. of Hasandağ stratovolcano. (Tp: Tephroite, Fo: Forsterite, Fa: Fayalite)

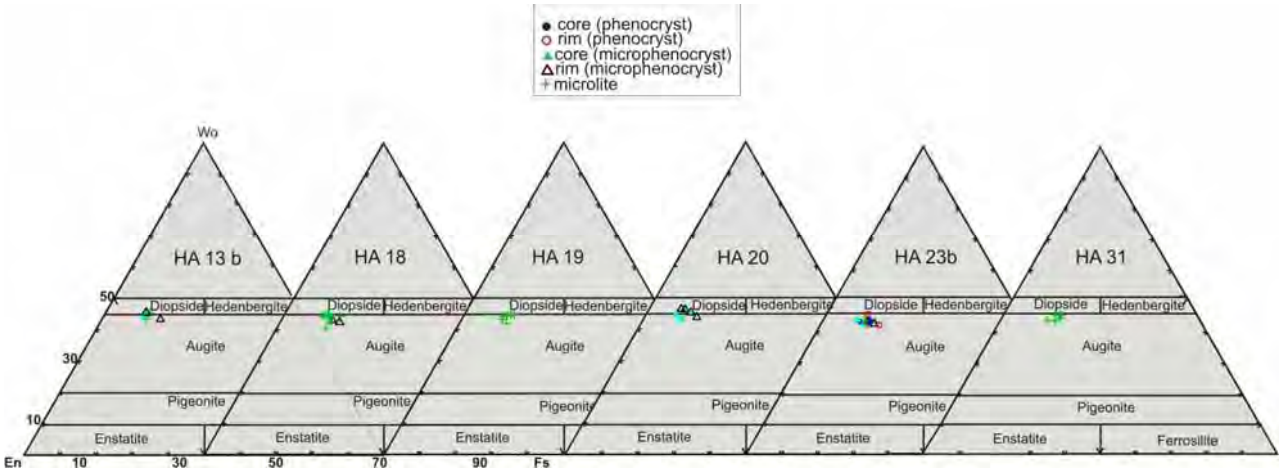

Figure 4.7: Compositions of pyroxenes from basalts s.l. of Hasandağ stratovolcano, (Morimoto, 1989) (En: Enstatite, Wo: Wollastonite, Fs: Ferrosillite)

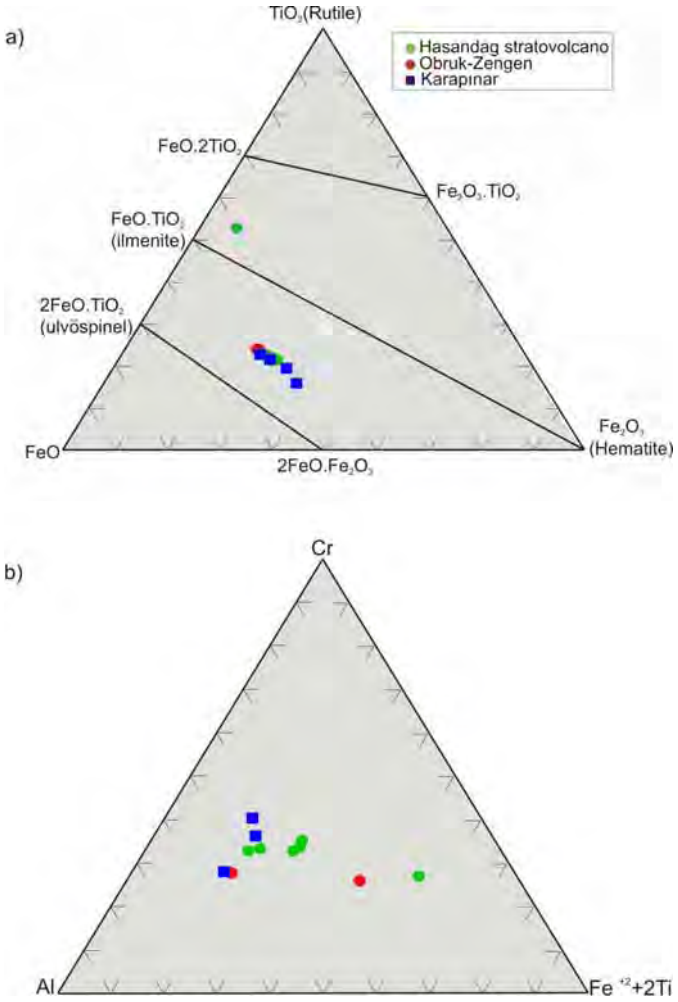

Figure 4.8: (a) Compositions of Fe-Ti oxides from basalts of Southwestern Cappadocia volcanism (Bacon and Hirschmann, 1988) (b) Cr-Al-(Fe^{+2} + 2Ti) triangular diagram (Melluso et al., 1988)

4.2.2. The Obruk-Zengen Dispersed Volcanism

Feldspars

Table 4.1 summarizes the feldspar composition of the basalts s.l. of the Obruk-Zengen dispersed volcanism. Generally plagioclase (Plg) occurs as microcrysts and microlites. However, plg occurs as phenocryst in HA14, HA26 and HA27. The plg phenocrysts of the more differentiated sample HA27 display a wide compositional range $An_{(35-77)}$ and they are andesine-bytownite in composition (Figure 4.9). HA27 is the only sample that presents sieve texture. Except HA27, the compositional range is $An_{(35-78)}$ for phenocrysts and microcrysts and $An_{(52-73)}$ for microlites. In Figure 4.9, the Plg of HA14, HA15, HA16, HA26 are labrodorite and bytownite in composition. The youngest sample HA17 (Table 2.4) is bytownite in composition. Reverse zoning is observed in HA26 and HA27 samples, but others samples show normal zoning.

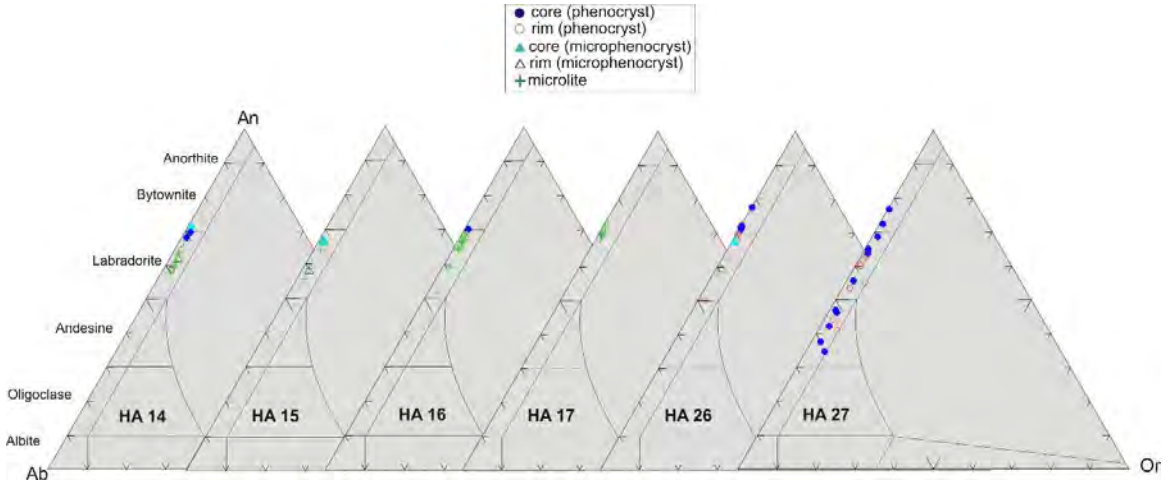

Figure 4.9: Composition of the feldspars from basalts s.l. of the Obruk-Zengen dispersed volcanism, in Ab-An-Or diagrams. (An: Anhortite, Ab: Albite Or: Orthoclase)

Olivine

Olivine is the most abundant mineral in all Obruk-Zengen samples. It occurs as phenocrysts, microphenocrysts and microlites (Figures 4.10). Equilibrium and disequilibrium features usually coexist in all samples. It could be related to the compositional variations and the probable occurrence of primary and secondary generations of olivine. The compositional range is wide Fo% 59-90 for phenocrysts and microphenocrysts, and Fo $\%_{(57-87)}$ for microlites. Most sections

are normally zoned with Fo-rich cores but in HA14 and HA27 samples, reversely zoned olivine occurs.

Clinopyroxene

Clinopyroxene (Cpx) occurs as phenocrysts and microphenocrysts in samples HA16, HA26 and HA27. The composition of Cpx is $Wo_{(40-49)}$, $En_{(41-48)}$, $Fs_{(8-17)}$ for phenocrysts and microcrysts (Figure 4.11). Cpx microlites are only present as needle-like and aggregates in the sample HA14, HA15 and HA17. The composition of microlites is $Wo_{(40-48)}$, $En_{(35-46)}$, $Fs_{(10-19)}$. All clinopyroxenes are diopside and augite in composition. The Mg-number displays a wide range between 65 and 84.

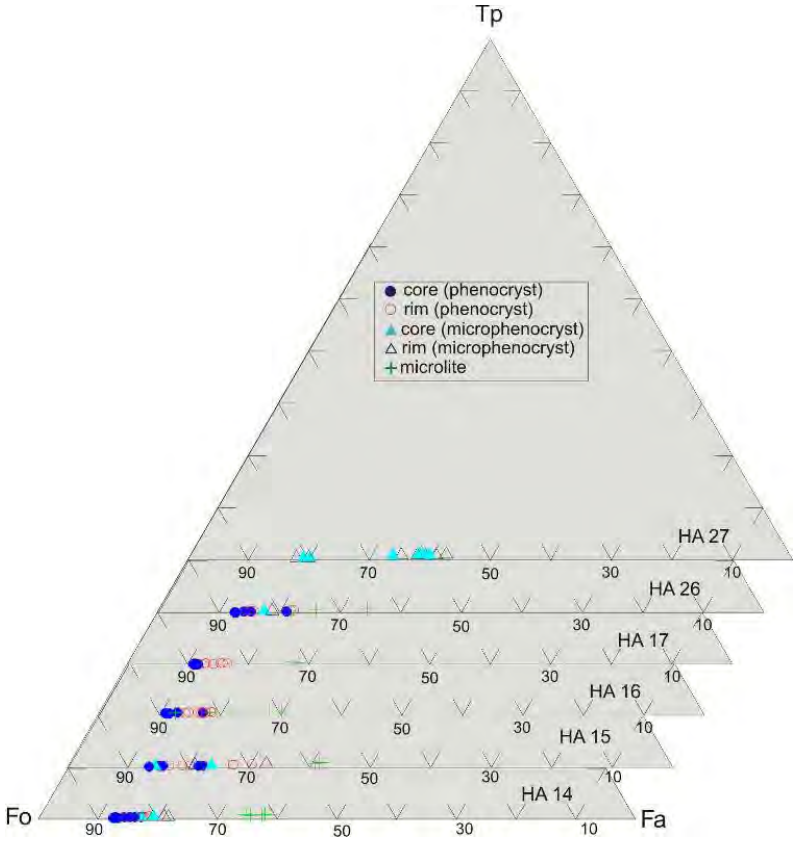

Figure 4.10: Composition of olivine from the basalts s.l. of the Obruk-Zengen dispersed volcanism (Tp: Tephroite, Fo: Forsterite, Fa: Fayalite)

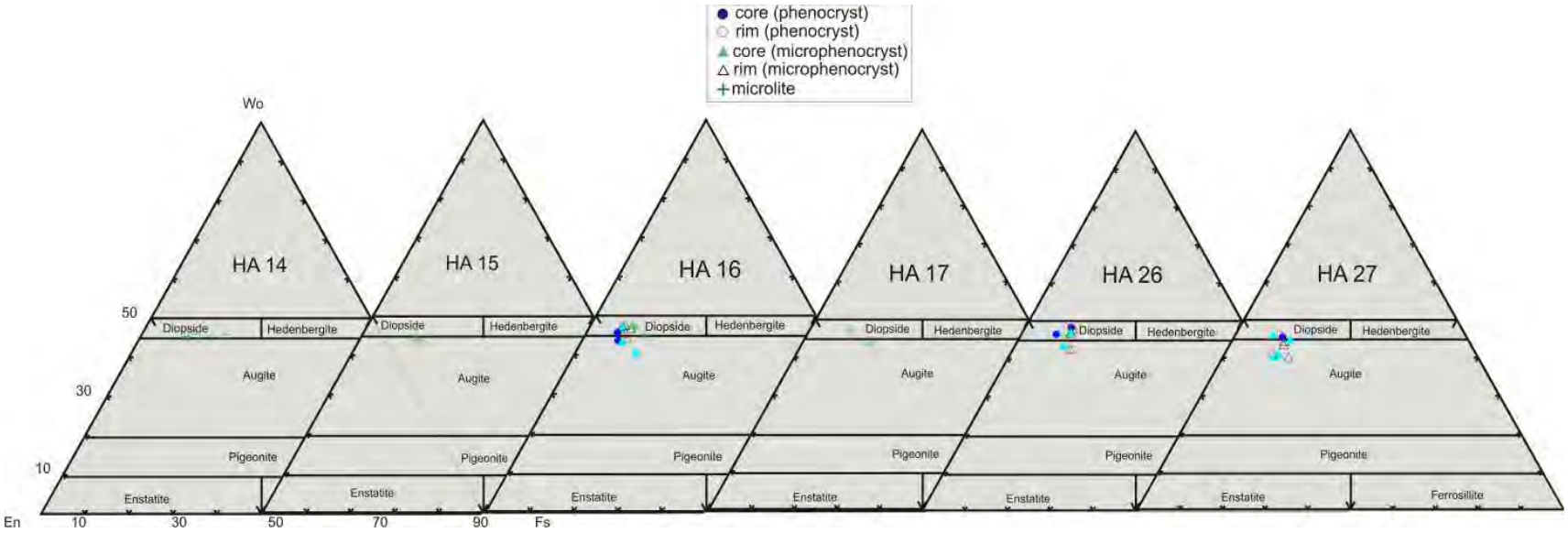

Figure 4.11: Composition of the pyroxenes from basalts s.l. of the Obruk-Zengen dispersed volcanism (Morimoto, 1989). (En: Enstatite, Wo: Wollastonite, Fs: Ferrosillite)

Oxides

Fe-Ti oxides occur as magnetite and ilmenite microlites. (Figure 4.8a). Cr-spinel and Al-chromite are determined in samples HA15 and HA26 (Figure 4.8b; Melluso et al., 1988).

4.2.3.The Karapınar Dispersed Volcanism

Feldspars

Plagioclase displays a wide compositional range, $An_{(3-76)}$ for phenocrysts and microcrysts and a more restricted range, $An_{(45-70)}$ for microlites (Table 4.1). The composition of Plg in KA18 and KA19 is andesine to bytownite; in KA21, it is labrodorite and bytownite Plg display generally normal and oscillatory zoning, but reverse-zoned plagioclase phenocrysts are observed in contemporaneous samples KA18 and KA21 (Table 2.4).

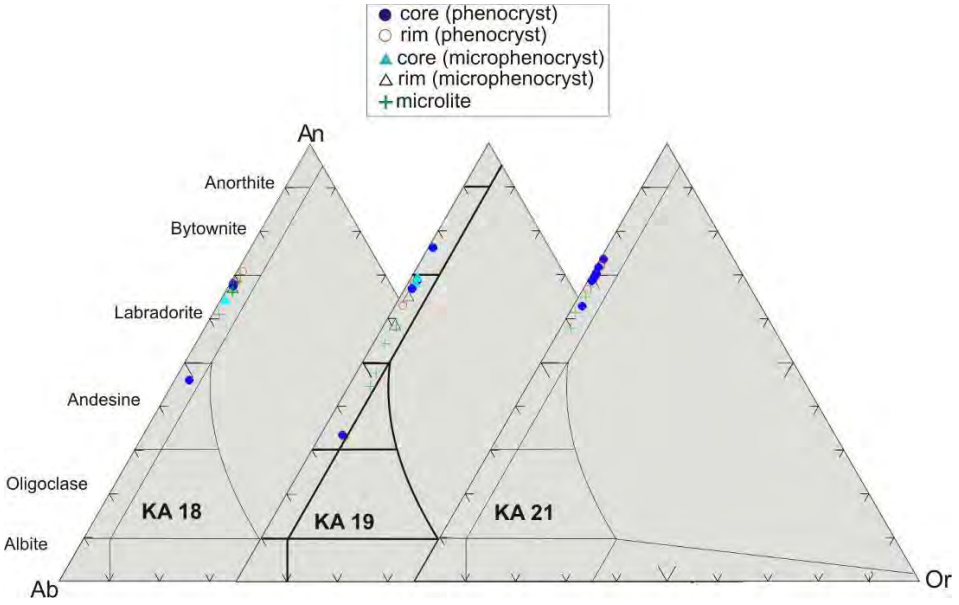

Figure 4.12: Compositions of feldspars from basalts s.l. of the Karapınar dispersed volcanism

Olivine

Olivine displays as phenocrysts, microcrysts and microlites (Figure 4.13). Equilibrium and disequilibrum features are both observed in all samples. The youngest sample KA19 (<0.001 Ma) has a wide range olivine composition for phenocyrsts and microcrysts (Fo% 68-86). However, the others are ranging between Fo% 77 and 89. Considering the olivine microlites, the composition of

oldest sample KA18 (0.280±0.0071 Ma) has Fo%($_{47-56}$) slightly lower than the KA19 and KA21, Fo%($_{62-70}$). All samples are normally zoned with Fo-rich cores.

Clinopyroxene

All Clinopyroxenes (Cpx) are diopside and augite in composition (Figures 4.14). They usually occur as phenocrysts and less microcrysts and microlites. The composition of Cpx is Wo($_{41-46}$), En($_{40-48}$), Fs($_{9-17}$) for phenocrysts and microphenocrysts and Wo($_{41-46}$), En($_{40-48}$), Fs($_{9-16}$) for microlites (Table 4.1). The Mg-number displays a restricted range (71-84). Phenocrysts and microcrysts are normally zoned with Mg-rich cores.

Oxides

Oxide occurs as magnetite microlites in KA19 (Figure 4.8a). However, there are Cr-spinel and Al-chromite in KA19 and KA21 (Figure 4.8b).

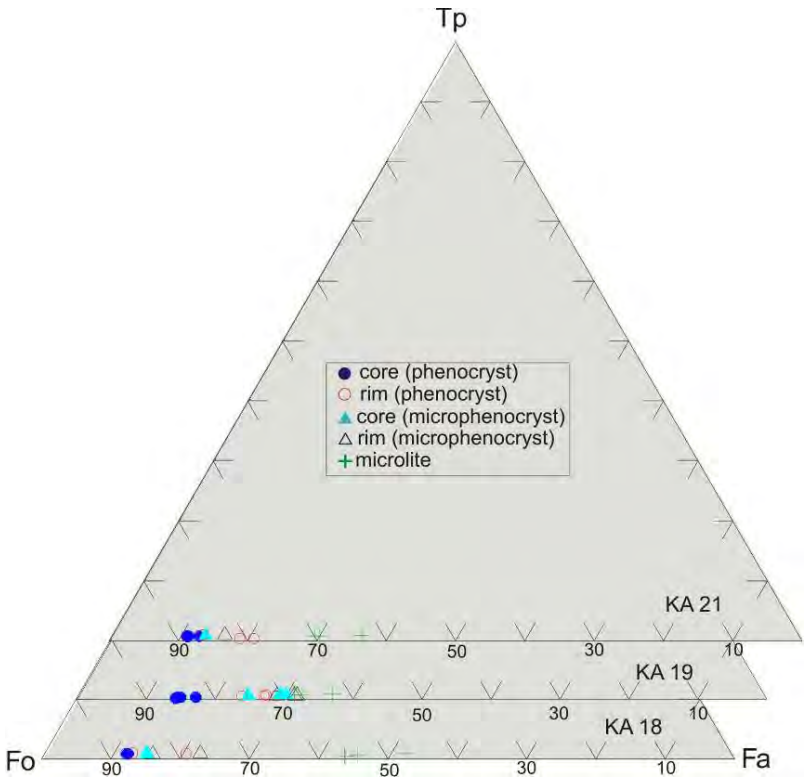

Figure 4.13: Composition of olivine from basalts s.l. of the Karapınar dispersed volcanism. (Tp: Tephroite, Fo: Forsterite, Fa: Fayalite)

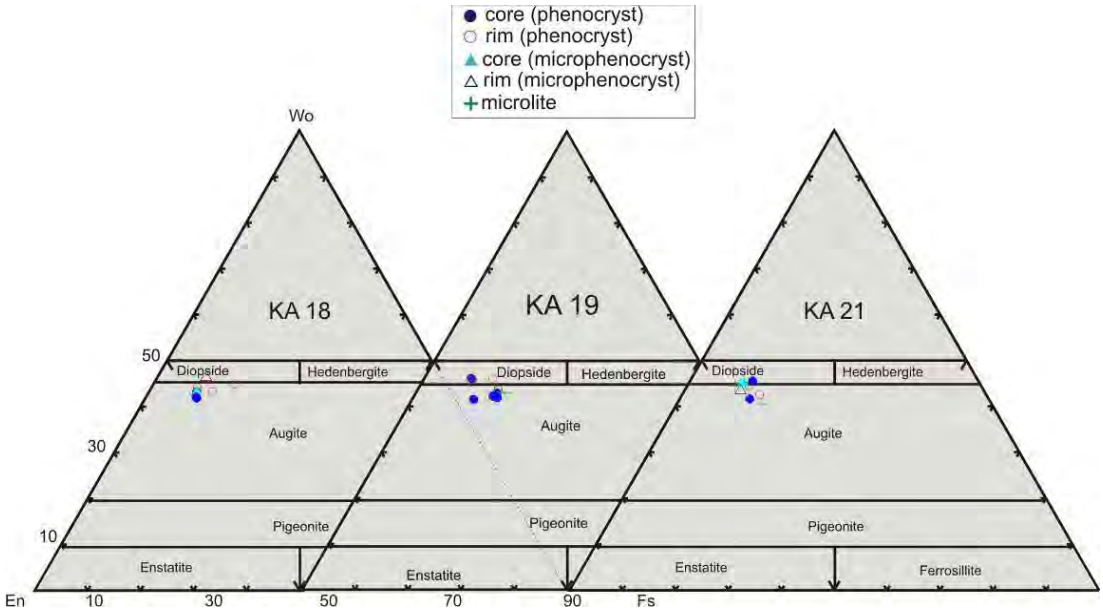

Figure 4.14: Composition of the pyroxenes from the basalts s.l. of the Karapınar dispersed volcanism (Morimoro, 1989). (En: Enstatite, Wo: Wollastonite, Fs: Ferrosillit)

4.3. Crystal-Liquid Equilibrium

According to Damasceno et al. (2002), magmatic systems are sensitive to changes in the composition of the phenocrysts and the mineral-liquid equilibrium. If phenocrysts and microcrysts are in equilibrium with liquid, they can be used to estimate the temperature (and sometimes pressure) of the magma.

4.3.1. Erciyes Stratovolcano

4.3.1.1. Olivine- Liquid Equilibrium

Chemical equilibrium between olivine and liquid has been the subject of considerable attention. In multi-component systems, the temperature dependence of Mg and Fe partitioning between olivine and liquid are very similar (Toplis, 2005). The ratio of the partition coefficients of iron and magnesium is called the exchange coefficient:

$$K_{DOl-liq}^{Mg-Fe} = \frac{X_{liq}^{Mg} / X_{Ol}^{Mg}}{X_{liq}^{Fe^{+2}} / X_{Ol}^{Fe^{+2}}}$$

Where X represents the molar fractions of respective components in either liquid (liq) or olivine (ol). The distribution coefficient between olivine and basaltic liquid is 0.3 ± 0.03 and is independed of temperature. This constant presented by Roeder and Emslie (1970) by experimental studies.

Figure 4.15 shows that olivine-melt equilibrium relations are best depicted in a plot of whole rock Mg number [100 x (Mg+2/Mg+2 + Fe+2)] versus forsterite content of olivine (e.g. Garcia, 1996) with the equilibrium field (KD = 0.3 ± 0.03) shown as the blue band (Damasceno et al, 2002).

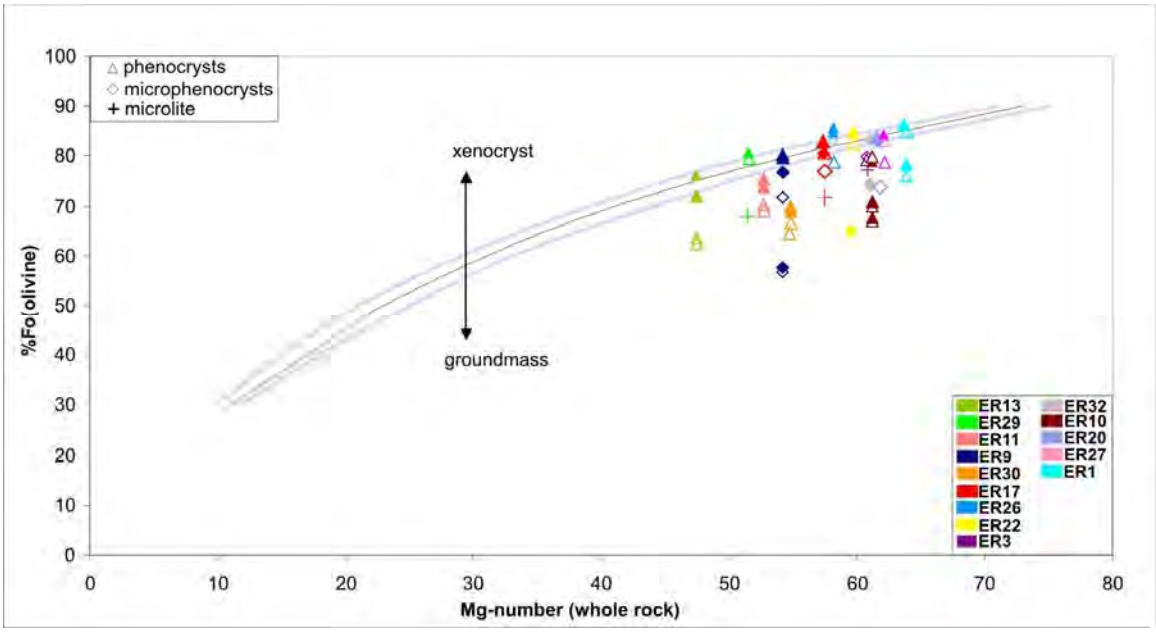

Figure 4.15: Olivine-melt Fe/Mg equilibrium diagram. Whole rock Mg-numbers versus Fo content of olivine is plotted for basalts s.l. of Erciyes. Mg-number = $100*Mg^{+2}/ (Mg^{+2} + Fe^{+2})$ is calculated assuming Fe^{+3}/Fe^{+2} =0.1. The equilibrium field for Fe/Mg exchange between olivine and the melt (0.3 ± 0.03; Roeder and Emslie, 1970) is shown. Arrows indicate the xenocryst addition and groundmass crystallization

As shown in Figure 4.15, core and rim compositions of phenocrysts and microcrysts of ER1, ER3, ER9, ER10, ER13, ER17, ER20, ER22, ER26, ER27 and ER29 samples are plotted in the equilibrium field, but not microlites. Therefore, none of the cores and rims compositions of ER11 and ER30 are in the equilibrium field. Mineral chemistry data confirm the mineralogical and petrographical observations as mentioned in Chapter 3.

4.3.1.2. Clinopyroxene- Liquid Equilibrium

The Fe/Mg exchange distribution coefficient between clinopyroxene and basaltic liquid is less constrained than that of olivine-liquid, due to the presence of ferric iron in clinopyroxene and in the melt (Damasceno et al., 2002). However, according to experimental studies (Grove and Bryan, 1983; Toplis and Carroll, 1995) the distribution coefficient between clinopyroxene and the basaltic liquid is 0.23 ± 0.05 (Hoover and Irvine, 1977; Damasceno et al., 2002). Figure 4.16 illustrates the relationship between Mg-numbers of whole rock and clinopyroxenes. Equilibrium field is drawn according to KD = 0.23 ± 0.05 (Toplis and Carroll, 1995).

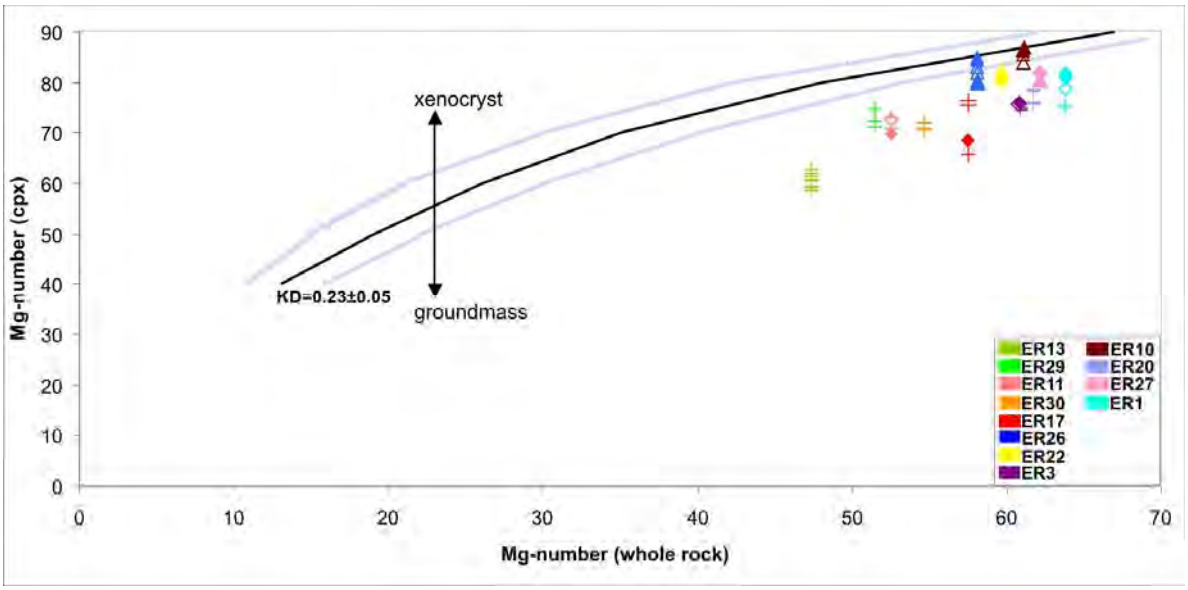

Figure 4.16: Variation of clinopyroxene compositions versus nominal whole rock geochemistry. Cpx - melt Fe/Mg equilibrium diagram. Whole rock Mg-numbers versus Mg-numbers of cpx is plotted. Mg-number = 100*Mg+2/ (Mg+2 + Fe+2) is calculated assuming Fe^{+3}/Fe^{+2} = 0.1. The equilibrium field for Fe/Mg exchange between Cpx and the melt (0.23 ± 0.05; (Toplis and Carroll, 1995) is shown. Arrows indicate the relative effects of xenocryst addition and groundmass crystallization. Symbols as in Figure 4.15

ER10 and ER26 are the only samples plotted in the equilibrium field (Figure 4.16). Mostly the clinopyroxenes of Erciyes stratovolcano samples are not in the equilibrium field (Figure 4.16). The samples ER9 and ER32 are not plotted in Figure 4.16 because they only have orthopyroxene.

4.3.1.3. Feldspar - Liquid Equilibrium

In Figure 4.17, some of the plagioclase phenocrysts of the samples ER9, ER11, ER20, ER22, ER26, ER27, ER30 and ER32 are in the liquid equilibrium field (Figure 4.17). The conditions are assumed under almost dry (KD = 1-3) and at low pressure (<2 kbar) (Sisson and Grove, 1993; Feeley and Dungan, 1996; Ferla and Meli, 2006).

On the other hand, the composition of plg microcrysts and microlites of ER3, ER10, ER13, ER17 and ER29 are out of the equilibrium field. As can be seen from the Figure 4.17, the rim composition of ER1 is plotted in the equilibrium field while the cores are out of that field.

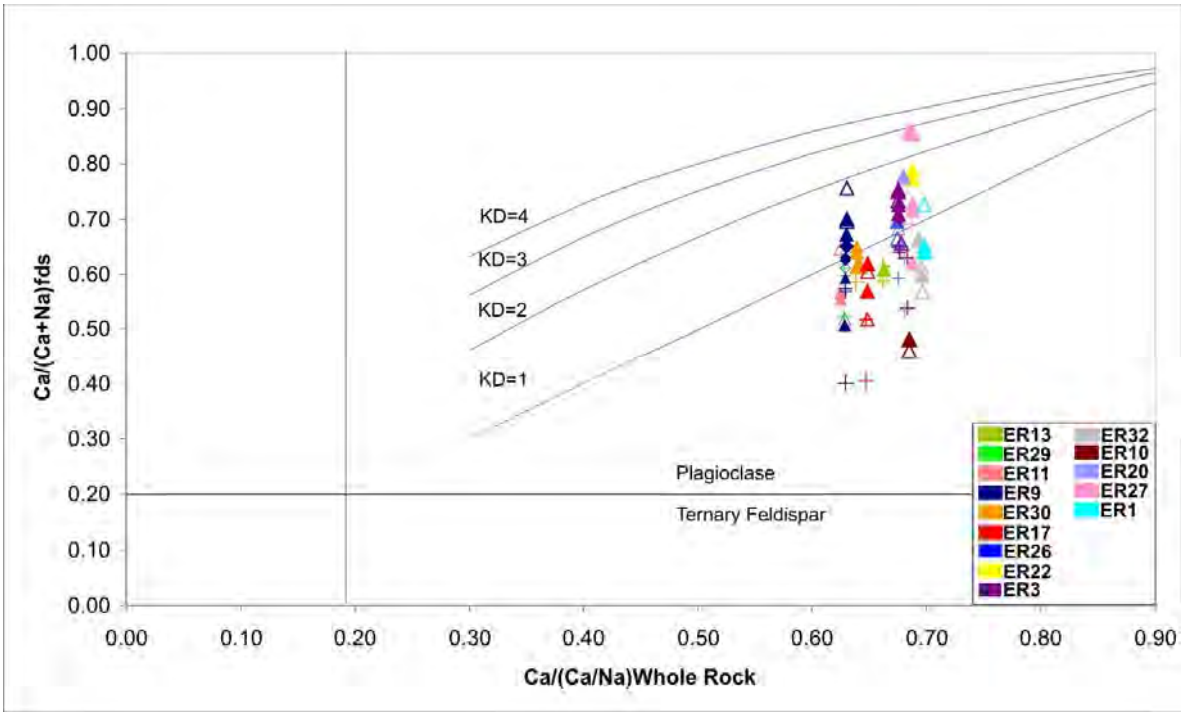

Figure 4.17: Feldspar - melt equilibria. (a) Plagioclase - melt equilibria for Erciyes stratovolcano; KD values are from Sisson and Grove (1993). Symbols as in Figure 4.15

4.3.2. Southwestern Cappadocia Volcanism

4.3.2.1. Olivine- Liquid Equilibrium

- ✓ ***Hasandağ stratovolcano***

As mentioned before in the section 4.3.1.1, in multi-component systems, the temperature dependence of Mg and Fe partitioning between olivine and liquid is very similar (Toplis, 2005) and the distribution coefficient between olivine and basaltic liquid is experimentally presented 0.3 ± 0.03 (Roeder and Emslie, 1970).

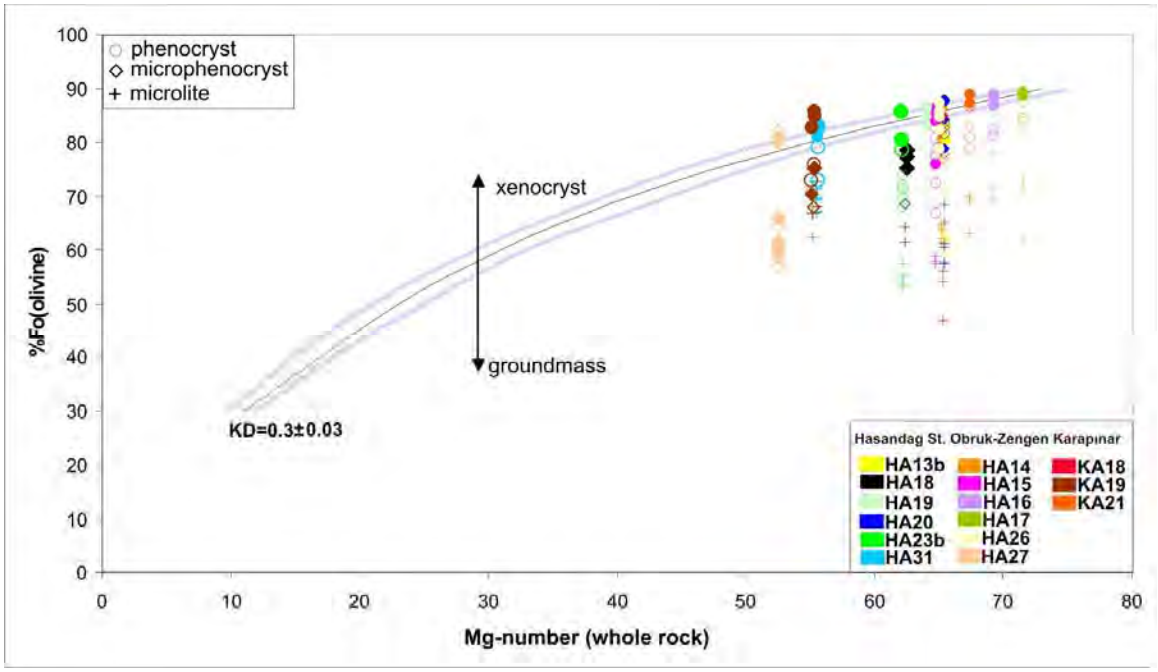

Figure 4.18: Olivine-melt Fe/Mg equilibrium diagram: Whole rock Mg-numbers versus Fo content of olivine. Mg-number = $100*Mg^{+2}/(Mg^{+2} + Fe^{+2})$ is calculated assuming Fe^{+3}/Fe^{+2} =0.1. The equilibrium field for Fe/Mg exchange between olivine and the melt (0.3 ± 0.03; (Roeder and Emslie, 1970) is shown. Arrows indicate the relative effects of xenocryst addition and groundmass crystallization.

As shown in Figure 4.18, except the samples HA13b and HA18, the other Hasandağ samples have some cores and rims in the equilibrium field.

Generally Hasandag samples are more mafic than the Erciyes samples (48 %< SiO2 <57%). So, the amount of olivine crystals in Hasandağ samples is higher than in Erciyes and their size is quite big, ranging between few µm to mm. According to the diagrams, Hasandag samples are rather in equilibrium with melt.

- ✓ ***Obruk-Zengen***

As mentioned in chapter 3, Olivine crystals exhibit equilibrium and disequilibrium features (Figure 3.12). Mostly, the phenocrysts rim and core compositions are in the equilibrium field (Figure 4.18). On the other hand microlites are out of equilibrium as expected. Except HA27, the others % Fo are high. HA27 is the most differentiated samples among Obruk-Zengen samples.

Karapınar

The phenocryst compositions of all Karapınar samples are mostly in the equilibrium field. The youngest sample, KA19 (Table 2.4) is different from the KA18 and KA21. The Mg number and the %Fo values are lower than the others.

4.3.2.2. Clinopyroxene- Liquid Equilibrium

- ✓ ***Hasandağ stratovolcano***

In Figure 4.19, none of the clinopyroxenes phenocrysts, microphenocrysts and microlites is in the equilibrium field. This information is in accord with the mineralogical-petrographical observations. The serpentinization of Cpx is common feature of this group (Table 3.2).

- ✓ ***Obruk-Zengen***

Except HA27 Cpx microcrysts, none of the other Cpx minerals of the Obruk-Zengen volcanics are plotted in the equilibrium field (Figure 4.19). According to mineralogical data, clinopyroxenes are mainly microlites and serpentinization occurs (Table 3.2).

- ✓ ***Karapınar***

As seen from the Figure 4.19, some of the clinopyroxenes phenocrysts in KA19 are plotted in the equilibrium field. On the other hand, none of the Cpx phenocrysts and/or microcrysts of KA18 and KA21 are in the equilibrium field. As a result of the mineralogical observations only KA21 has some oxidation (Table 3.2).

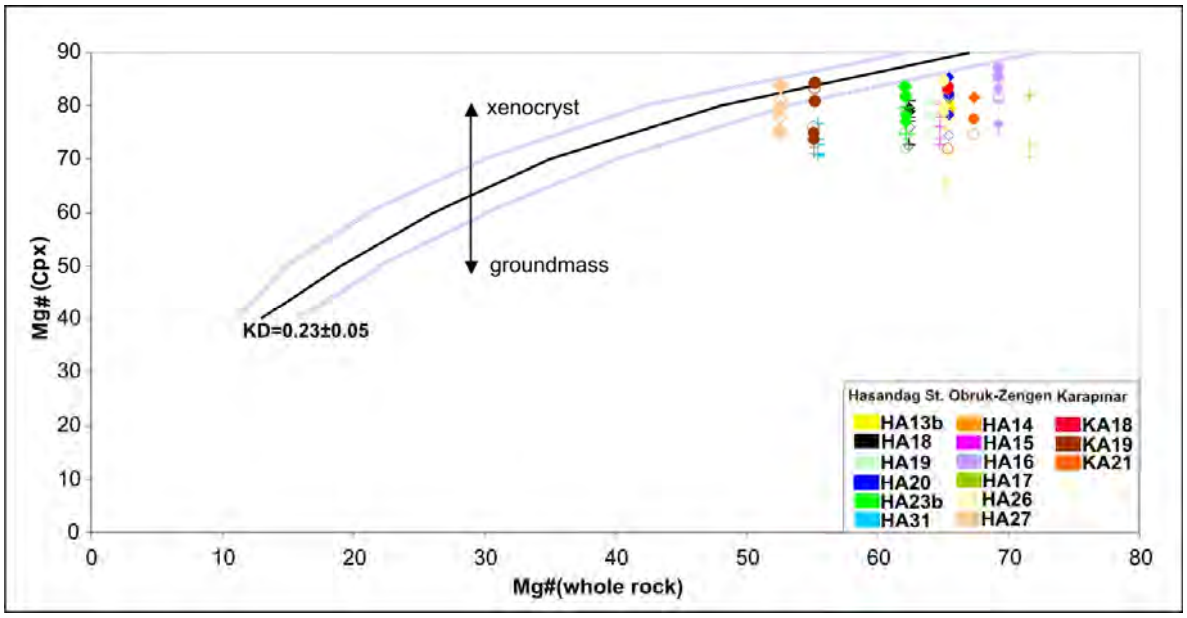

Figure 4.19: Variation of clinopyroxene compositions versus nominal whole rock geochemistry in a Cpx - melt Fe/Mg equilibrium diagram. Whole rock Mg-numbers versus Mg-numbers of Cpx Mg-number = 100*Mg+2/ (Mg+2 + Fe+2) is calculated assuming Fe+3/Fe+2 = 0.1. The equilibrium field for Fe/Mg exchange between cpx and the melt (0.23 ± 0.05; Toplis and Carroll, 1995) is shown. Arrows indicate the relative effects of xenocryst addition and groundmass crystallization. Symbols as in Figure 4.18

4.3.2.3. Feldspar Liquid Equilibrium

- ✓ **Hasandag stratovolcano**

In Figure 4.20, most of the samples of plagioclase phenocrysts, microphenocrysts and microlites, as cores and rims are not plotted in the equilibrium field, except HA31. As previously noted in the mineralogy and petrography chapter, Plagioclase phenocrysts of HA31 are under equilibrium conditions (Figure 3.7). On the other hand, the other samples crystallized under disequilibrium conditions.

- ✓ ***Obruk-Zengen***

The plagioclase phenocrysts and microphenocrysts of the HA14, HA26 and HA27 are plotted in the equilibrium field (Figure 4.20). The other samples (HA15, HA16, and HA17) of the Obruk-Zengen area are outside of the equilibrium field.

✓ **Karapınar**

Most of the plagioclase phenocrysts of KA19 and KA21 are plotted in the equilibrium field (Figure 4.20). The other sample KA18 is out of the equilibrium field.

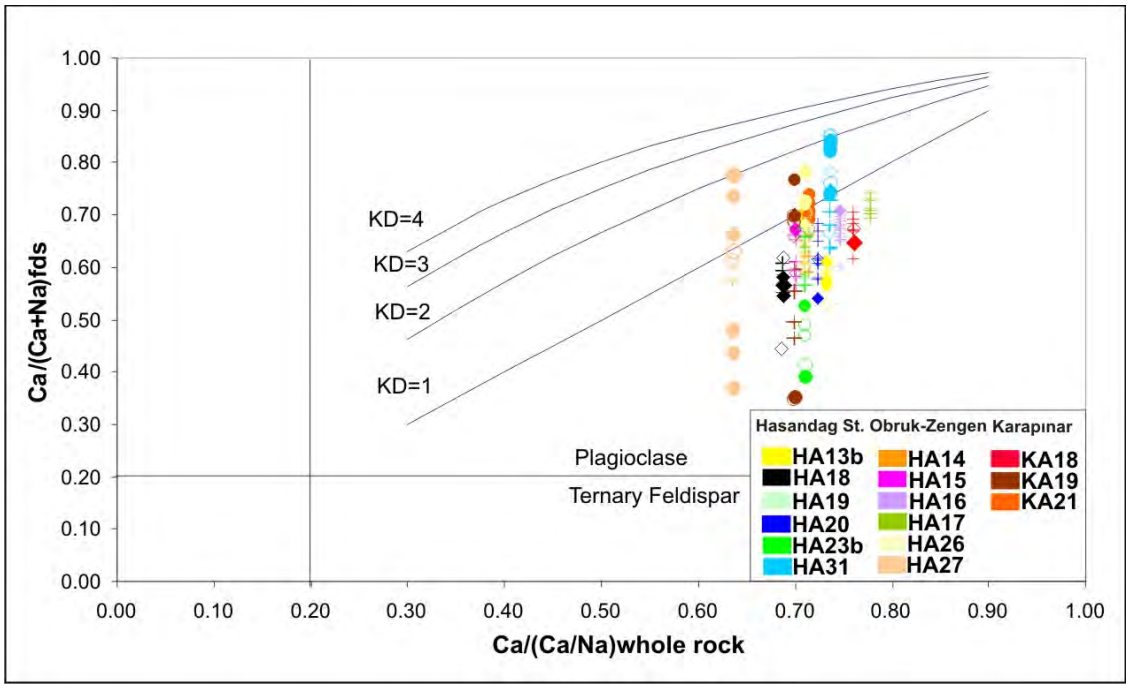

Figure 4.20: Feldspar-melt equilibria. (a) Plagioclase - melt equilibria of Southwestern Cappadocia; KD values are from Sisson and Grove (1993). Symbols same as in Figure 4.18

4.4. Geothermometer and Geobarometer Calculation

Magma temperatures for the basalts s.l. of Erciyes and Hasandağ stratovolcanoes, and for dispersed volcanism of Obruk-Zengen and Karapınar were estimated.

Mineral-mineral and mineral-liquid temperature estimations were performed for each rock sample. According to the chemistry of the samples, it was not possible to measure glass analyses for each rock samples. For this reason, instead of glass compositions, the whole rock compositions were used for liquid composition. The geothermometer calculations were done by the help of the Putirka (2008).

4.4.1. Erciyes Stratovolcano

The geothermometer calculations were performed on olivine-liquid, clinopyroxene-liquid, two-pyroxene and plagioclase-liquid pairs. Estimated geothermometers and the evolution of temperatures with changing SiO_2 contents are in Table 4.2 and Figure 4.21, respectively.

Table 4.2: Calculated geothermometer and geobarometer values of Erciyes stratovolcano

			Temperature				Pressure
Samples	SiO_2		Putirka 2008 Eq (32d-33-34) clinopyroxene-liquid Kd=(0.18-0.28)	Putirka 2008 olivine-liquid Eq 22	Putirka 2008 two-pyroxene Mean Eq 36 -37 Kd=0.95-1.23	Putirka 2008 Eq 23 plagioclase T>1050 °C = 0.1+/-0.11 T<1050 °C = 0.25+/-0.05	Putirka 2008 clinopyroxene-liquid (mean Eq (32a-32b-32c)) P(kbar)
ER1	54.34	Basaltic andesite	—	1218	—	—	—
ER3	53.13	Basaltic andesite	—	1260	1024	1180	—
ER9	57.09	Andesite	—	1215	—	1178	—
ER10	53.09	Basaltic andesite	1167	—	—	—	4.20
ER11	56.70	Basaltic andesite	—	—	—	1148	—
ER13	48.89	Trachybasalt	—	1242	—	—	—
ER17	55.46	Basaltic andesite		1183	—	—	—
ER20	54.53	Basaltic andesite	—	—	—	1177	—
ER22	57.37	Andesite	—	1197	1024	1174	—
ER26	56.43	Basaltic andesite	1138	—	—	1183	4.90
ER27	55.01	Basaltic andesite	—	—	—	1171	—
ER29	52.45	Basaltic trachyandesite	—	1212	—	1166	—
ER30	55.07	Basaltic trachyandesite	—	1200	—	1146	—
ER32	56.22	Basaltic andesite	—	1160	—	—	—

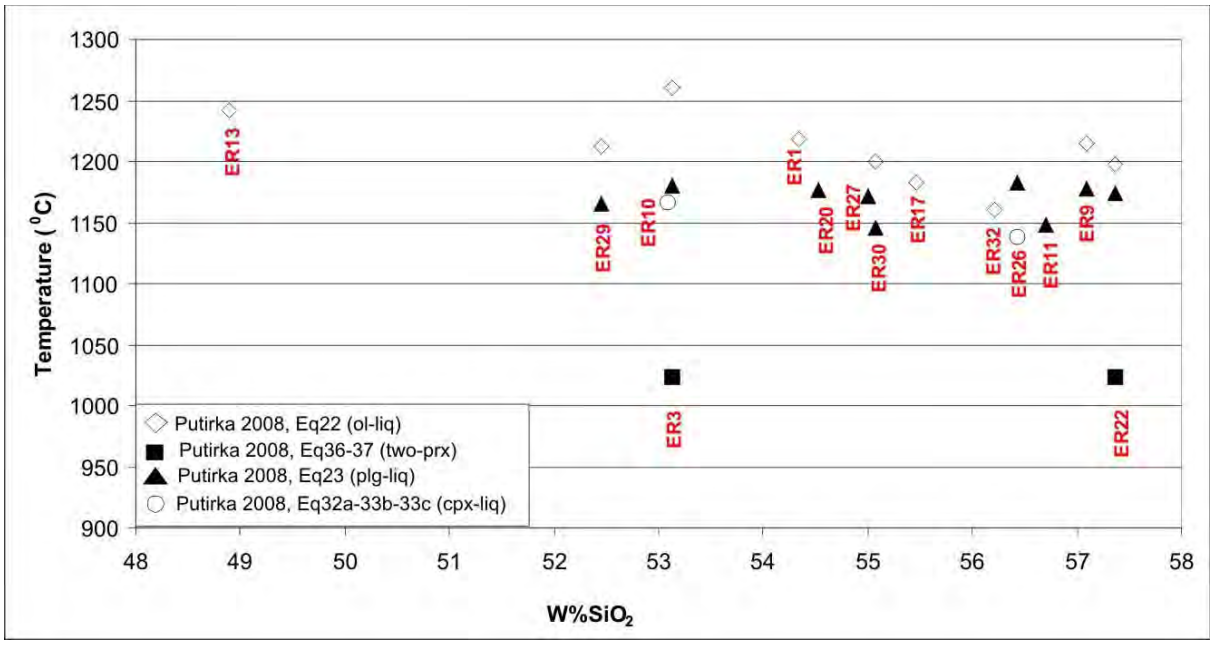

Figure 4.21: Temperature vs. SiO_2 of Erciyes volcanics

4.4.1.1. Olivine - Liquid Geothermometer

Olivine is the first crystallizing phase from basalts of different composition. Experimental studies present the composition of coexisting olivine and basaltic melts as a function of temperature (Roder and Emslie 1970). Based on this information olivine–liquids pairs of equilibrium (Figure 4.15) allows understanding of equilibrium and fractional crystallization in basaltic magmas (Roder and Emslie 1970).

The equilibrium conditions of considered minerals are the most important parameter for geothermometer calculations (Putirka, 2008). Putirka et al. (2007) present many equations for geothermometer calculations but the Equation 22 gives the best estimates when water is present and H_2O ranges from 0-18.6% for the test data set (Putirka, 2008). Accordingly Equation 22 is chosen for Erciyes samples. The water content of Erciyes basaltic samples is < 1% (Table 2.2). Estimated temperatures of the less differentiated samples (ER13, ER1, ER3 and ER29) vary between 1212 and 1260 ^{o}C (Table 4.2). On the other hand, the estimated temperature of more differentiated samples ranges between 1160 and 1215 ^{o}C (Table 4.2). Less differentiated samples estimated temperatures are higher than that of the differentiated samples.

4.4.1.2. Clinopyroxene- Liquid Geothermometer

Clinopyroxene is the common mineral in igneous rocks and it is useful for understanding the magmatic processes and crystallization conditions (Masotta et al., 2013). For this reason many models asserted before by Nimis 1995; Nimis and Ulmer, 1998; Nimis and Taylor 2000; Putirka et al., 1996, 2003; Putirka 2008. The models of thermometer or barometers use either clinopyroxene alone or clinopyroxene-liquid equilibria. In this work we use clinopyroxene-liquid equilibria (Putirka 2008). In Figure 4.16, the phenocrysts of ER10 and ER26 are in equilibrium field. Due to that only these samples clinopyroxene-liquid pairs were calculated. The estimated temperatures are 1167 ^{o}C and 1138 ^{o}C, respectively (Table 4.2). The estimated depth of ER10 is 17 km and it is 10.5 km for ER26 according to Putirka (2008) (Table 4.2).

4.4.1.3. Clinopyroxene- Orthopyroxene Geothermometer

Two pyroxene geothermometer calculations can be applied only on the samples where two pyroxenes coexist in equilibrium conditions. From the literature, Ca content of high-Ca pyroxene decreases with increasing temperature, while the low-Ca phase increases. ER3 and ER22 are suitable for two pyroxene calculations (Figure 4.16). According to Putirka (2008), based on the partitioning of enstatite + ferrosilite (=$Fm2Si_2O_6$ = EnFs; FmO = FeO + MgO + MnO) between clinopyroxene and orthopyroxene increases precision for the available experimental data (Equation 36). A global regression (Eqn. 36) provides somewhat greater precision, but precision is improved further if the calibration data base is restricted to include only Mg-rich systems, in this case defined as those cpx-opx pairs where Mg# *cpx* > 0.75. The models perform best for mafic systems where Mg# *cpx* > 0.75. A separate regression using only experiments with Mg# *cpx* > 0.75 (Eqn 37). However, Erciyes basaltic samples Mg# *cpx are* > 0.75 (Appendix). Estimated two pyroxene geothermometers of ER3 and ER22 are 1035 ^oC and 1025 ^oC for Eq 36 and 1012 ^oC and 1022 ^oC for Eq37, respectively (Table 4.2)

4.4.1.4. Plagioclase-Liquid Geothermometer

The first plagioclase-liquid geothermometer was presented by Kudo and Weill (1970). [106]. Many previous workers (e.g., Mathez 1973; Drake 1976; Loomis 1979; Glazner 1984; Ariskin and Barmina 1990; Marsh et al. 1990) showed attention about plagioclase thermometry. Later on, Putirka's (2005) stated that the calibration of Sugawara (2001) and the MELTS/pMELTS models of Ghiorso et al. (2002) are the most accurate predictors of *T* for existing models. However, these models failed at low *T* (<1100 °C) and for hydrous systems. According to Putirka (2008),as a test for plagioclase-liquid equilibrium, *T* from Equations (23) or (24a) can be compared to the *T* required for a liquid to reach plagioclase saturation. Due to that, Equation 23 was used for plagioclase-liquid geothermometer. The samples with plagioclases in equilibrium are selected for plagioclase-liquid geothermometer calculations (Figure 4.17). The minimum estimated temperature is 1146 ^oC for ER30 and the maximum temperature is 1183 ^oC for ER26 (Table 4.2).

4.4.2. The Southwestern Cappadocia

The geothermometer calculations were performed on olivine-liquid, plagioclase-liquid and clinopyroxene-liquid pairs. Differently from Erciyes Stratovolcano, none of the samples from Southwestern Cappadocia exhibit two pyroxenes. Estimated geothermometers of Southwestern Cappadocia are presented in Table 4.3. The evolution of temperatures according to changing host rock SiO_2 contents, are also presented in Figure 4.22.

Table 4.3: Calculated geothermometry and geobarometry values of Southwestern Cappadocia volcanics

			Temperature			Pressure
Samples	SiO_2		Putirka 2008 Eq (32d-33-34) clinopyroxene-liquid Kd=(0.18-0.28)	Putirka 2008 olivine-liquid Eq 22Kd=0.27-0.33	Putirka 2008 Eq 23 plagioclase T>1050 °C = 0,1+/-0.11 T<1050 °C = 0.25+/-0.05	Putirka 2008 clinopyroxene-liquid (mean Eq (32a-32b-32c)) P(kbar)
Hasandag Stratovolcano						
HA13b	49.33	Basalt	—	—	—	
HA18	51.06	Trachybasalt	—	—	—	
HA19	50.43	Basalt	—	1259	—	
HA20	50.36	Basalt	1208	1273	—	4.66
HA23b	50.90	Basalt	—	1233	—	
HA31	49.24	Basalt	—	1199	1250	
Obruk-Zengen						
HA14	48.99	Trachybasalt	—	1274	1207	
HA15	49.38	Basalt	—	1291	—	
HA16	48.81	Basalt	1233	1296	—	7.79
HA17	48.88	Basalt	—	1293	—	
HA26	49.39	Basalt	—	1266	1176	
HA27	56.24	Basaltic trachyandesite	1120	1135	1164	
Keretepe						
KA18	49.75	Basalt	—	1262	—	
KA19	50.87	Trachybasalt	1172	—	1228	5.30
KA21	52.40	Basaltic andesite	—	1263	1171	

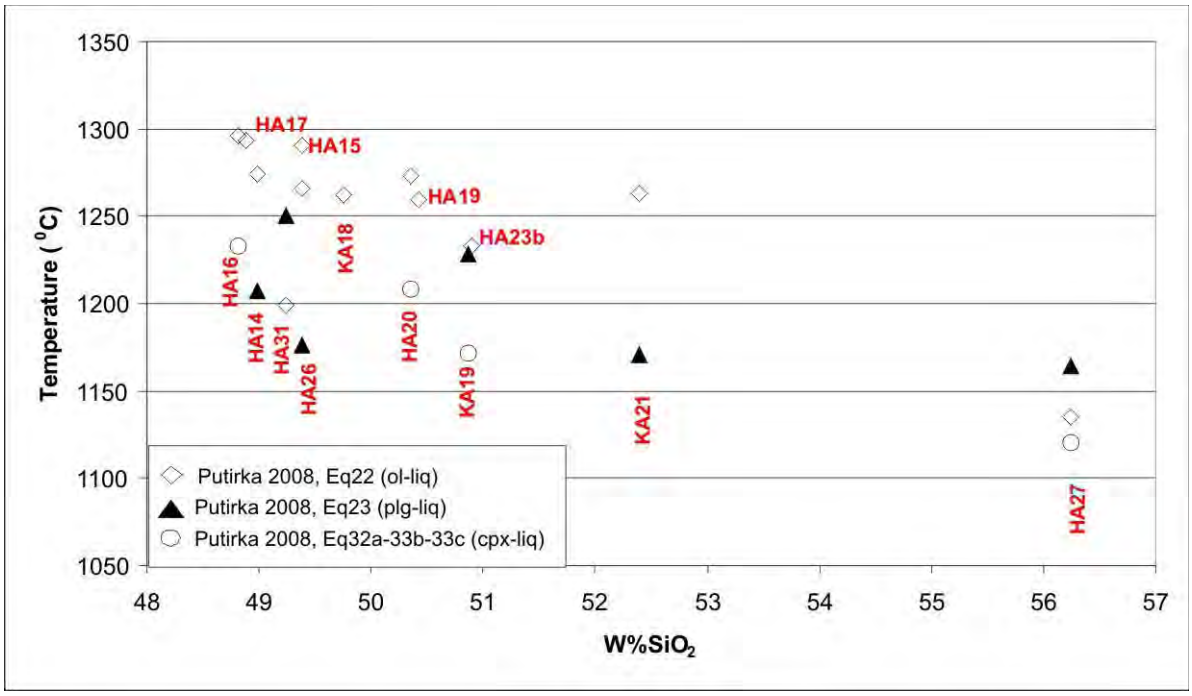

Figure 4.22: Temperature vs. SiO_2 of Southwestern Cappadocia volcanics

4.4.2.1. Olivine- Liquid Geothermometer

As mentioned in 4.4.1.1 the composition of the olivine and olivine–liquids pairs of equilibrium (Figure 4.18) are important, making clearer of relationship of equilibrium and fractional crystallization in basaltic magmas. Based on this information, estimated geothermometers are calculated for Southwestern Cappadocia volcanics.

- ✓ **Hasandağ stratovolcano**

The minimum and the maximum calculated temperatures are 1199 ^{o}C and 1273 ^{o}C for HA31 and HA20, respectively (Table 4.3). These temperatures are in accord with the samples chemistry. Due to HA13b and HA18 are not in equilibrium field, there isn't any geothermometer calculation made for them.

- ✓ **Obruk-Zengen**

All Obruk-Zengen samples are suitable for geothermometer calculations. Each sample is plotted in equilibrium field. Except HA27, the other Obruk-Zengen samples SiO_2 range is very restricted. The less differentiated sample HA16 has the maximum temperature (1296 ^{o}C) and the more differentiated sample HA27 has the minimum temperature (1135 ^{o}C). The others range between these values.

- ✓ **Karapınar**

According to olivine-liquid equilibria, except KA19 the calculations were performed with the samples KA18 and KA21 (Figure 4.18). As can be seen from the Table 4.3, both samples temperatures are very close to each other, 1262 ^{o}C for KA18 and 1263 ^{o}C for KA21.

4.4.2.2. Clinopyroxene- liquid geothermometer

The details about the clinopyroxene- liquid geothermometer were presented in section 4.4.1.2. Estimated temperatures and pressures are listed in Table 4.3.

- ✓ **Hasandag stratovolcano**

Mostly the cpx phenocrysts and microcrysts of Hasandag stratovolcano are out of the equilibrium field (Figure 4.19). However, the samples HA19 and HA31 only have cpx microlites (Figure 4.7) due to that they are not used for thermometer calculations. HA20 is the only ideal sample for thermometer and barometer estimation. Cpx-liquid temperature of HA20 is 1208 ^{o}C and the cpx-liquid barometer is 4.66 kbar (Table 4.3). According to Putirka (2008) the depth of HA20 was estimated about 18km.

- ✓ **Obruk-Zengen**

Only the phenocrysts and microcrysts of HA16 and HA27 are under equilibrium conditions (Figure 4.19). The samples HA14, HA15 and HA17 only have microlites and the phenocrysts and microcrysts of HA26 are not in equilibrium conditions (Figure 4.19). Cpx geothermometer of the oldest and the less differentiated sample HA16 is 1233 ^{o}C. On the other hand more differentiated and the second youngest sample HA27 temperature is 1135 ^{o}C. The estimated barometer of HA16 is 7.79 kbar and its depth 28km. The estimated barometer values of HA27 are not rational, than it is not on the Table 4.3.

- ✓ **Karapınar**

In Karapınar, KA19 is the only sample that exhibits cpx phenocrysts in equilibrium (Figure 4.19). The calculated temperature of KA19 is 1172 ^{o}C. The other two samples, KA18 and KA21 are out of the equilibrium field.

For this reason there isn't any cpx geothermometer calculation made for these samples. The estimated barometer and the depth of KA19 is 5.30 kbar and 21 km, respectively.

4.4.2.3. Plagioclase - liquid geothermometer

The models of plagioclase-liquid pairs by previous workers indicated in section 4.4.1.4. By using plagioclase-liquid equilibria, estimated geothermometers are calculated (Table 4.3).

- ✓ **Hasandag stratovolcano**

HA31 is the only sample under equilibrium condition (Figure 4.20) and its estimated temperature is 1250 ^{o}C (Table 4.3).

- ✓ **Obruk-Zengen**

The plg phenocrysts and microcrysts of the samples HA14, HA26 and HA27 are in the equilibrium field (Figure 4.20). Their estimated temperatures are 1207 ^{o}C, 1176 ^{o}C and 1164 ^{o}C, respectively (Table 4.3).

- ✓ **Karapınar**

Except KA18, phenocrysts and microcrysts of KA19 and KA21 are in the equilibrium field (Figure 4.20). In Table 4.3, the results are 1228 ^{o}C for KA19 and 1171 ^{o}C for KA21.

4.4.3. Conclusion

According to the microprobe analyses, we are trying to find out the conditions and constraints of the magma. Estimated temperatures, barometers and depths are calculated (Table 4.4). A summary of mineral chemistry and mineralogy and petrography is presented below.

Table 4.4: Estimated geothermometer and geobarometer values for the four groups volcanics.

Temperature (°C)					Pressure (kbar)	Depths(km)
(Putirka, 2008)						
Study Area	Eq (32d-33-34) cpx-liq	Eq 22 ol-liq	(Eq 36-37) two-pyroxene	Eq 23 plg-liq	(Eq 32a-32b-32c) cpx-liq	
ES	**1138-1167**	**1160-1260**	**1024**	**1146-1183**	**4.20-4.90**	**10.5-17**
HS	**1208**	**1199-1273**	**—**	**1250**	**4.66**	**18**
OZ	**1120-1233**	**1135-1296**	**—**	**1164-1207**	**7.79**	**28**
K	**1172**	**1262-1263**	**—**	**1171-1228**	**5.30**	**21**

1. Plagioclase is the common mineral of all four studied areas. Mostly, plg occurs as a phenocryst and ES differs from the 3 other studied areas with its wide range plg phenocrysts.

2. Normal and reverse zoning plg occur in ES, OZ and K.

3. Erciyes stratovolcano is the only region that has opx.

4. The occurrence of both plg and ol, in equilibrium and disequilibrium, emphasizes that the genesis conditions were variable and related to magma mixing processes.

5. Estimated temperatures and barometers are proposed are 10.5-17 km, 18 km, 19-28 km and 21 km for ES, HS, OZ and K, respectively (Table 4.4). According to these results, the depths of ES are shallower than for the other studied areas. OZ gives the highest cpx-liq temperature, pressure and depth.

6. The evolution of temperatures does not change systematically with SiO_2 contents in the 4 studied areas.

7. The mean value of ol-liq temperatures and depths are increasing from NE to SW.

All these differences may be explained by multistage crystallization of minerals in magma chambers located at different depths.

5. GEOCHEMISTRY

Detailed geochemical features of the subjected associations from studied area, including isotopic data, are given in the following sections with their interpretations. Representative samples for major, trace and rare earth elements analysis were carried out from Erciyes stratovolcano (ES) (n=19), Southwestern Cappadocia Volcanism (n=15), that embraces the Hasandağ stratovolcano (HS) (n=6), Obruk-Zengen (OZ) (n=6), and Karapınar (K) (n=3) areas. Moreover, 29 Sr-Nd, 28 Pb and 28 O isotopic analyses were performed and discussed in detail below. Procedures of the analytical techniques can be found in the section 1.4.2.

5.1. Major, Trace and Rare Earth Element (REE) Analysis

In this section, major, trace and REE analytical results, which were separated from the studied field by their composition and their locations, will be given in individual sub-sections.

5.1.1 Erciyes Stratovolcano

Major element and CIPW normative data are given in Table 5.1. Most of the samples are intermediate in composition (52% <SiO_2< 63%), while the loss of ignition (LOI) values of the samples varies between 0.32% and 1.14%. MgO contents range between 6.65 and 3.00 wt%, with Mg# between 53 and 69.The major element values, that are recalculated according to anhydrous basis, are plotted in the total alkaline (Na_2O% + K_2O%) vs. silica (SiO %) diagram of Le Bas et al. (1986) (Figure 5.1). The samples of ES are plotted in the trachybasalt, basaltic andesite, basaltic-trachyandesite, andesite and dacite areas (Figure 5.1). According to the alkaline-subalkaline separation line (Miyashiro, 1978), 2 of the samples present alkaline characteristics while the remaining 17 samples are subalkaline. It is determined that the trachybasalt and basaltic-trachyandesite samples are respectively hawaiite (Na_2O-2>K_2O) and mugearite (Na_2O-2>K_2O). The subalkaline samples are calcalkaline in the FeOt, Na_2O+K_2O and MgO (AFM) diagram of Irvine and Baragar (1971) (Figure 5.2). In Peccerillo and Taylor's (1976) K_2O vs. SiO_2 diagram, these samples show also a calcalkaline characteristic, except, ER29 sample that is high calcalkaline (Figure 5.3). According to the Al_2O_3 > Na_2O+K_2O+CaO values, Erciyes lavas display dominantly per aluminous features.

Table 5.1: Major element results and CIPW norm values of ES

	ER1	ER2	ER3	ER4	ER5	ER9	ER10	ER11	ER13	ER16	ER17	ER20	ER22	ER25	ER26	ER27	ER29	ER30	ER32
Major element(%)																			
SiO_2	54.34	55.33	53.13	62.02	60.25	57.34	53.09	56.70	48.89	62.70	55.46	54.53	57.37	57.15	56.43	55.01	52.45	55.07	56.22
Al_2O_3	17.17	17.32	16.52	16.67	16.19	17.64	16.95	17.65	17.06	16.38	17.57	17.56	18.24	17.57	17.98	17.42	17.68	17.40	17.78
Fe_2O_3	6.88	6.97	8.24	4.87	5.55	7.07	8.39	7.22	11.99	4.85	7.27	7.24	6.27	6.70	6.57	6.81	8.96	7.94	6.55
MgO	6.10	5.62	6.54	3.00	4.06	4.21	6.65	4.04	5.44	2.86	4.95	5.88	4.67	4.59	4.59	5.62	4.78	4.84	5.12
CaO	8.32	8.13	8.54	6.14	6.74	7.18	8.54	7.06	8.46	5.95	7.54	8.22	8.03	7.58	8.20	8.28	7.54	7.42	7.93
Na_2O	3.48	3.66	3.62	3.72	3.67	4.08	3.81	4.08	4.17	3.71	3.97	3.70	3.52	3.74	3.80	3.64	4.31	4.06	3.65
K_2O	1.24	1.37	1.02	1.67	1.63	1.23	0.96	1.24	0.94	1.74	1.54	1.36	1.10	1.18	1.31	1.14	1.65	1.62	0.95
TiO_2	0.96	1.04	1.30	0.66	0.78	1.07	1.36	1.05	2.40	0.65	1.11	1.10	0.79	0.89	1.04	1.01	1.54	1.39	0.94
MnO	0.11	0.11	0.13	0.08	0.09	0.12	0.13	0.12	0.18	0.08	0.12	0.12	0.10	0.11	0.11	0.11	0.15	0.13	0.10
P_2O_5	0.36	0.33	0.37	0.19	0.23	0.37	0.40	0.45	0.51	0.19	0.38	0.36	0.25	0.37	0.34	0.33	0.66	0.41	0.28
LOI	0.23	0.28	-0.16	1.14	0.99	-0.19	-0.10	0.30	-0.32	1.09	0.30	0.29	0.47	0.50	0.08	0.42	0.15	0.50	0.58
Mg#	69.06	66.99	66.61	61.59	65.60	60.78	66.60	59.28	53.29	61.38	63.17	67.13	66.00	64.08	63.72	67.27	58.18	61.34	66.31
Total	99.19	100.15	99.25	100.15	100.19	100.12	100.18	99.91	99.73	100.22	100.20	100.36	100.81	100.39	100.42	99.79	99.87	100.79	100.09
CIPW norm																			
Q	3.04	3.54	0.86	16.40	12.75	7.13	-	6.89	-	17.56	3.09	1.85	8.33	7.85	5.46	3.94	-	2.49	6.62
Or	7.43	8.17	6.13	9.99	9.78	7.28	5.71	7.40	5.63	10.42	9.14	8.10	6.50	7.03	7.74	6.81	9.82	9.62	5.66
Ab	29.96	31.14	31.01	31.88	31.43	34.60	32.37	34.85	34.49	31.82	33.80	31.48	29.86	31.86	32.18	31.12	36.82	34.49	31.19
An	27.99	26.97	26.14	24.21	23.17	26.27	26.39	26.43	25.26	23.16	25.76	27.42	30.74	27.83	28.20	28.11	24.28	24.53	29.64
Ne	-	-	-	-	-	-	-	-	0.616	-	-	-	-	-	-	-	-	-	-
Di	9.33	9.27	11.57	4.39	7.44	5.69	10.94	4.85	11.27	4.40	7.60	9.04	6.09	6.12	8.36	9.06	7.47	7.84	6.67
Hy	17.40	15.98	18.37	9.71	11.47	13.68	17.60	13.97	-	9.04	15.34	16.92	14.23	14.40	13.28	16.11	9.48	14.66	15.74
Ol	-	-	-	-	-	-	0.87	-	13.23	-	-	-	-	-	-	-	4.50	-	-
Mt	2.15	2.16	2.57	1.71	1.95	2.46	2.60	2.53	3.73	1.89	2.25	2.24	2.18	2.34	2.03	2.14	3.14	2.77	2.04
Il	1.86	1.99	2.50	1.27	1.50	2.04	2.59	2.02	4.60	1.26	2.13	2.11	1.50	1.71	1.97	1.94	2.95	2.64	1.80
Ap	0.84	0.77	0.87	0.45	0.53	0.86	0.92	1.05	1.18	0.45	0.89	0.84	0.58	0.87	0.79	0.77	1.54	0.62	0.65

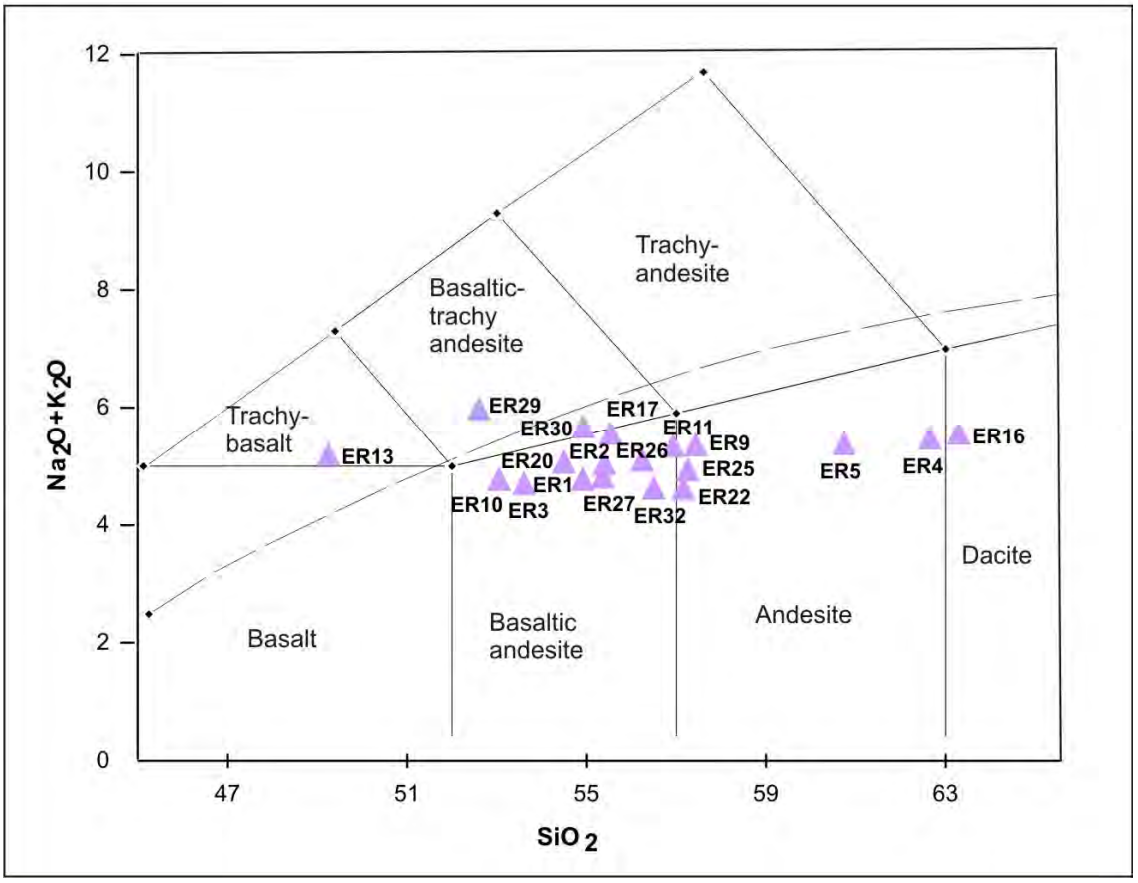

Figure 5.1: Total Alkaline-SiO_2 diagram of Erciyes (Le Bas et al., 1986; Miyashiro,1978)

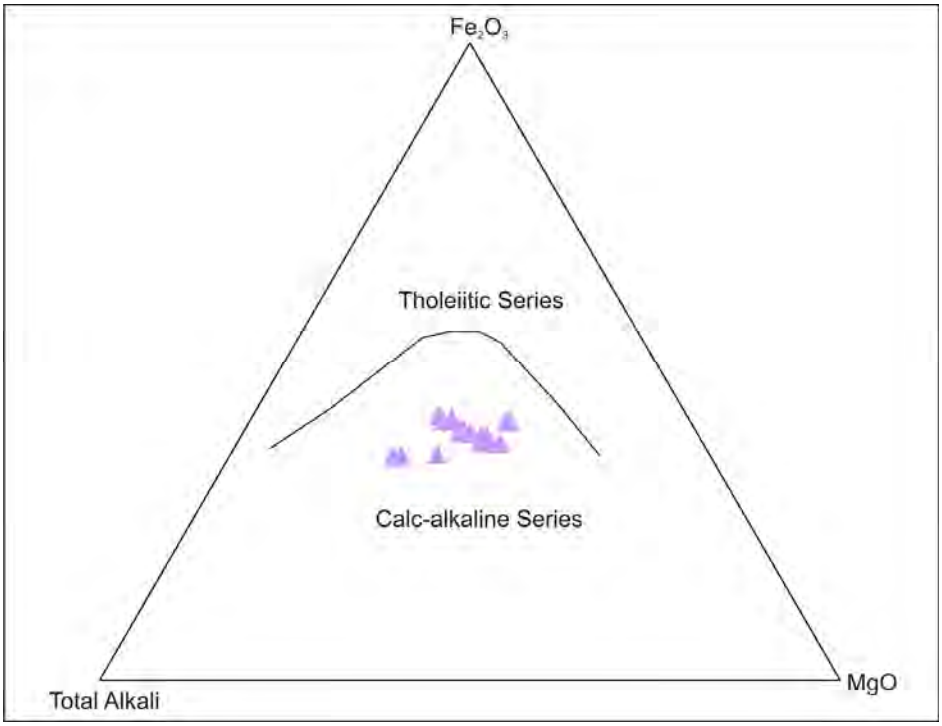

Figure 5.2: AFM diagram for the volcanic rocks of Erciyes, indicating their subalkaline characteristics (Irvine and Baragar, 1971)

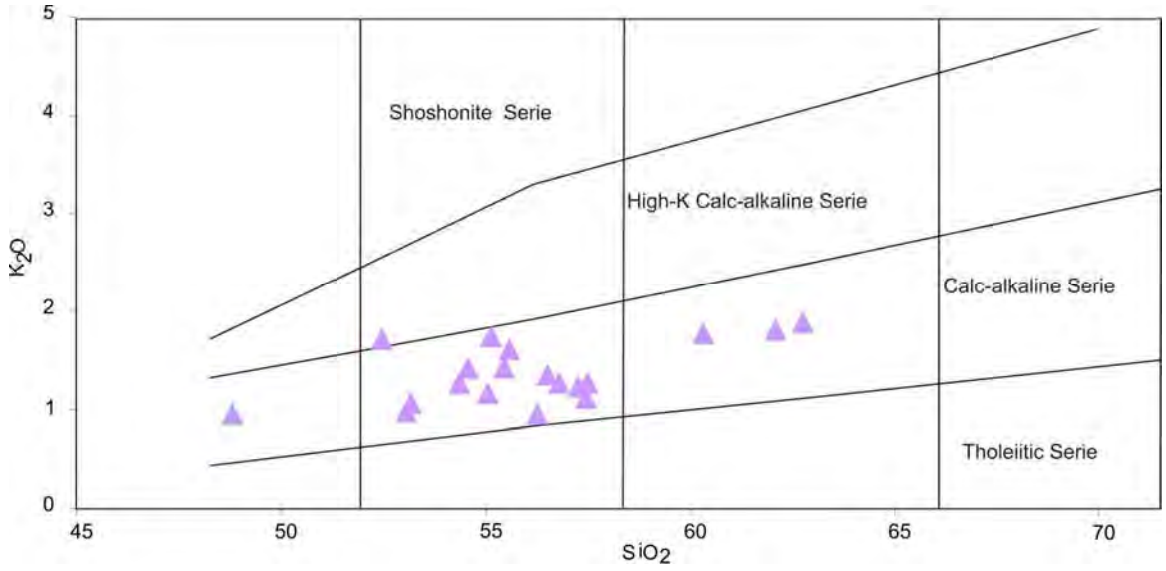

Figure 5.3: K_2O-SiO_2 diagram (Peccerillo and Taylor, 1976)

CIPW norm values are given in Table 5.1. All samples exhibit normative Plg, diopside and accessory minerals (apatite, magnetite and ilmenite). ER13 sample exhibits nepheline normative while the others exhibit normative hypersthene. All samples exhibit normative quartz, except the samples ER10, ER13 and ER29, which are olivine normative.

Variation diagrams based on selected major oxides vs. MgO are given in Figure 5.4. The diagrams clearly indicate that SiO_2, Al_2O_3, Na_2O and K_2O values increases with the MgO decrease. However, CaO, Fe_2O_3, MnO, P_2O_5 and TiO_2 exhibit a positive trend (Figure 5.4).

In the Harker diagrams, the trends emphasize the fractional crystallization process. In the initial phase, olivine, pyroxene, Ca-plagioclase and opaque minerals (apatite, magnetite, and ilmenite) were formed. In the later phases, the formation of amphibole occurs.

Trace element compositions of 19 samples from Erciyes are shown in Table 5.2. Selected trace elements vs. Th are proposed, according to the more stable characteristic of Th, compared to the other incompatible elements such as Rb, K, Ba, etc. (Figure 5.5).

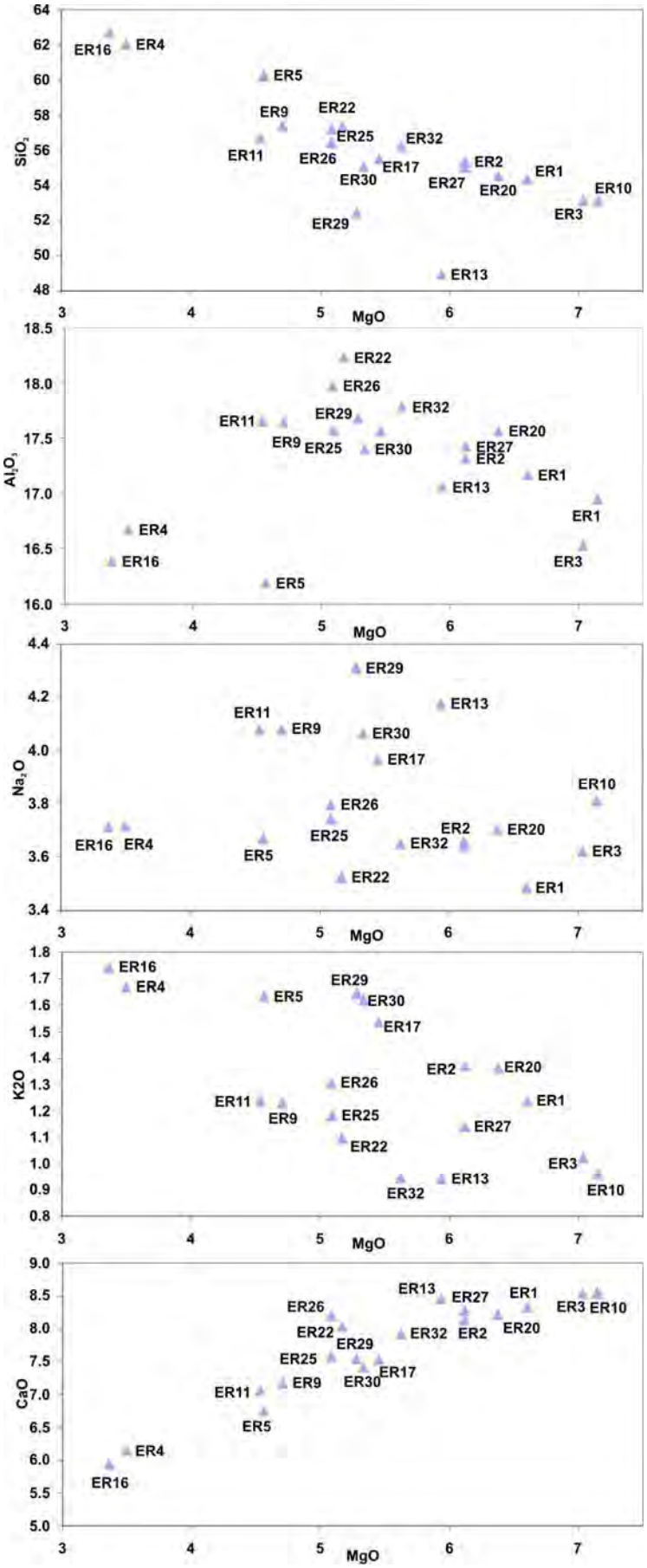

Figure 5.4: Major oxide variation diagrams of Erciyes

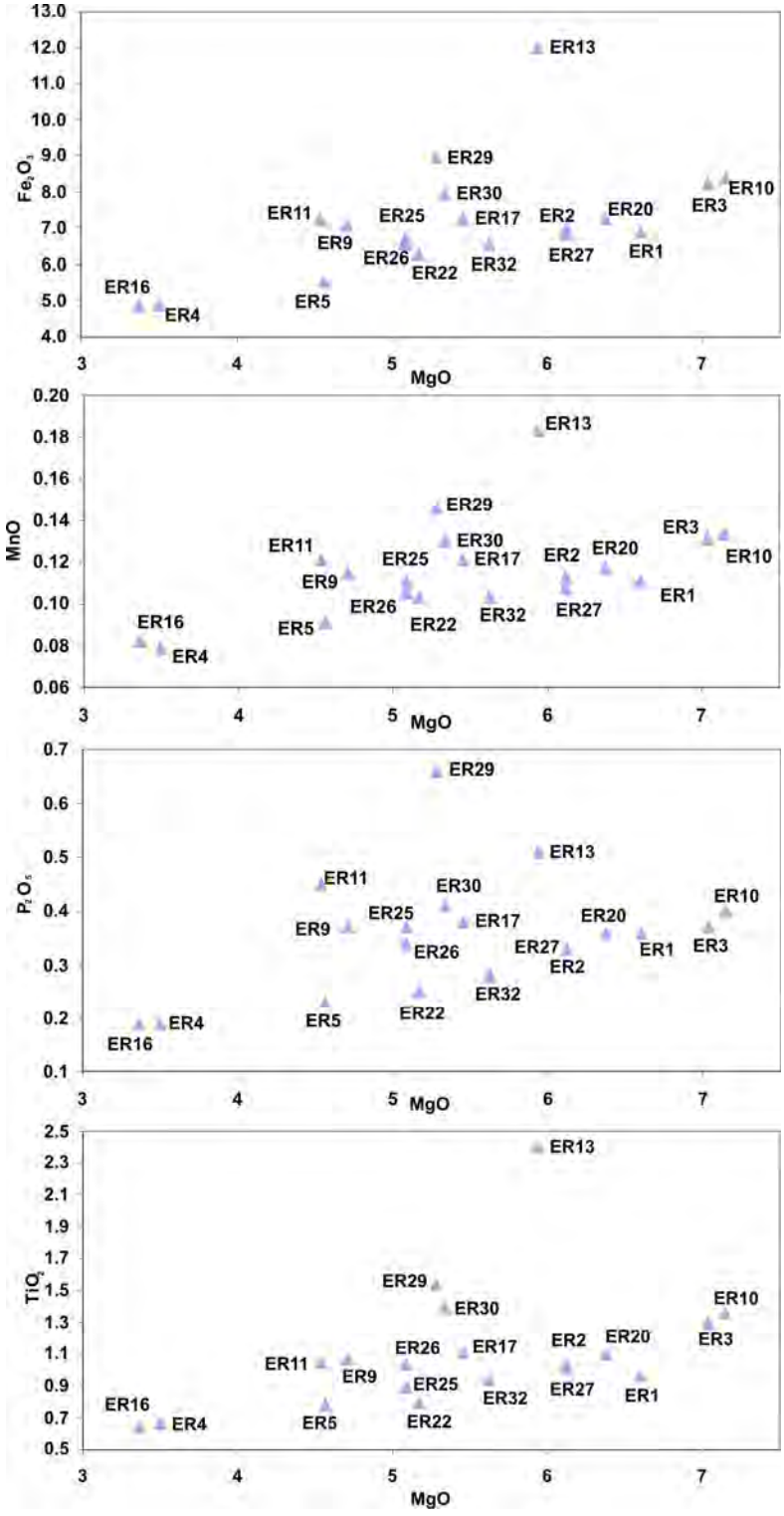

Figure 5.4: (*continued*)

A positive trend is observed in U, Ba and Rb while Sr, Hf, Y and Eu are decreasing with the increase of Th (Figure 5.5).The decrease in Sr can be related to the fractionation of the first Ca-plagioclases. The negative trends in Hf and Y are related to the lack of accessory minerals, such as ilmenite, apatite and zircon in the samples.

As concluded for major element distribution, trace elements diagrams also emphasize the predominant role of fractional crystallization.

Primitive Mantle (PM) (Sun and McDonough, 1989) normalized multi-element diagrams are given in Figure 5.6 a-b. To understand similarities or differences between the samples, we separated LDDS (Less differentiated dated samples) and MDDS (More differentiated dated samples). LDDS (ER1, ER3, ER10, ER13 and ER 29) and MDDS (ER2, ER9, ER11, ER17, ER20, ER22, ER25, ER26, ER27, ER30, ER32) ages (Table 2.3) and TAS diagram (Figure 5.1) were given in previous sections. Multi-element patterns display enrichment in all *Large Ion Lithophile (LIL) Elements* (Rb, Ba, Th, U and Pb) and clear depletion in Nb, Ta, Ti and P.

Similarities and some variances in separated LDDS and MDDS groups are:

i) In the LDDS group, except Pb, Nb and Ta contents, the samples vary in multi-element contents (Figure 5.6 a). The oldest sample ER13 is the only one in LDDS that exhibits Rb, Ba, U and Th depletions and P, Sm, Zr, Hf, Dy, Y, Yb and Lu enrichment. In the sample ER1 and particularly in the youngest sample ER29, Ba, Th, U and Pb elements are displaying enrichments. In contrast, Nd, Zr, Hf, Sm, Eu, Ti, Dy, Y, Yb and Lu are more depleted in ER1. Although ER3 and ER10 have a similar pattern; Ba, Th and U elements are enriched and Ta is depleted in ER3 more than ER10 (Figure 5.6a).

ii) MDDS group displays mostly depleted patterns, except Th, U and Pb (Figure 5.6b). Negative anomalies in Nb, Ta, P and Ti elements are characteristic of this group. The sample ER30, that exhibits a moderate differentiation, shows

enrichment in Ba, K, and depletion in Ti unlike other samples. ER9 sample is more enriched in Zr and Hf, while ER11 is more enriched in P and Nd.

Enrichment in highly incompatible element contents such as Ba, Rb, Th and K is a typical characteristic of active continental margins or within plate magmatisms (Wilson, 1989). During subduction, the subducted plate plunges into the mantle and partially melts. This partial melting favors enrichment in volatile components and fluids (Wilson, 1989). Highly incompatible elements (such as Ba, Rb, Th and K) will merge into the melt. High-Field Strength (HFS) elements will be kept in the mineral stable phases that remain in the source after partial melting, such as rutile, titanite, ilmenite and apatite (Gill, 1981; Fitton et al., 1988; McCulloch and Gamble, 1991). According to Lustrino and Wilson (2007), negative Nb–Ta and positive Pb anomalies can be related to two different processes: i) shallow level crustal contamination by addition of subducted sediment into the mantle source, ii) fluid-induced enrichment of the elements adjacent to Nb–Ta in the trace element pattern (will be discussed in 6th chapter).

Besides, the elements trends in spidergrams or multielement diagrams, the element ratios such as Ba/Nb, Ce/Y, La/Nb helps to understand the features of the magmas. According to Fitton et al. (1988), the ratio Ba/Nb >28 is characteristic of arc magmatisms. Ba/Nb ratios vary between 17.46 to 21.69 in LDDS and 21.53 to 26.73 in MDDS (Table 5.3).

Table 5.2: Trace element composition of Erciyes

Trace element (ppm)	ER1	ER2	ER3	ER4	ER5	ER9	ER10	ER11	ER13	ER16	ER17	ER20	ER22	ER25	ER26	ER27	ER29	ER30	ER32
As	< L.D.	< L.D.	< L.D.	2.49	2.20	1.65	< L.D.	1.81	< L.D.	2.04	1.83	< L.D.	1.97	< L.D.	1.54	2.51	1.63	2.74	1.75
Ba	343.65	331.22	260.93	314.00	339.60	317.80	225.70	355.70	228.20	351.20	347.90	296.30	260.60	317.40	292.10	246.90	519.50	413.30	252.30
Be	< L.D.	< L.D.	< L.D.	< L.D.	< L.D.	< L.D.	< L.D.	1.51	1.90	< L.D.	1.53	< L.D.	< L.D.	< L.D.	< L.D.	1.48	1.75	< L.D.	< L.D.
Bi	< L.D.	< L.D.	< L.D.	< L.D.	< L.D.	< L.D.	< L.D.	< L.D.	< L.D.	< L.D.	< L.D.	< L.D.	< L.D.	< L.D.	< L.D.	< L.D.	< L.D.	< L.D.	< L.D.
Cd	< L.D.	< L.D.	< L.D.	0.17	0.18	0.18	0.20	0.19	0.29	0.18	0.24	0.17	0.17	0.18	0.24	< L.D.	0.21	0.18	0.17
Ce	50.63	49.52	46.09	43.63	45.76	50.26	45.35	54.56	48.59	46.77	52.51	47.91	39.83	50.78	46.57	39.43	70.27	45.77	38.13
Co	< L.D.	< L.D.	< L.D.	15.17	18.80	22.48	32.14	20.70	37.90	14.16	24.12	26.73	22.49	21.91	21.51	26.48	28.12	24.48	23.98
Cr	< L.D.	< L.D.	< L.D.	52.65	116.80	67.92	186.70	61.49	27.43	53.94	105.60	144.00	68.76	83.45	77.08	132.90	55.74	85.95	114.60
Cs	< L.D.	< L.D.	< L.D.	1.63	1.56	0.71	0.63	0.91	< L.D.	1.42	0.70	0.66	1.20	1.04	1.09	1.16	1.05	0.67	0.67
Cu	< L.D.	< L.D.	< L.D.	27.80	23.92	30.69	30.78	29.83	30.78	26.41	32.55	33.71	34.81	34.81	31.76	37.34	31.49	28.81	31.00
Dy	3.43	3.68	4.37	3.32	3.59	4.27	4.57	4.13	6.04	3.57	4.14	3.71	3.12	3.68	3.53	3.13	4.73	4.21	3.30
Er	1.89	2.05	2.46	1.86	1.99	2.41	2.54	2.28	3.47	2.08	2.33	2.07	1.72	2.04	1.94	1.70	2.54	2.37	1.81
Eu	1.18	1.22	1.34	1.04	1.18	1.50	1.57	1.54	2.13	1.10	1.46	1.39	1.11	1.37	1.29	1.14	1.92	1.60	1.21
Ga	< L.D.	< L.D.	< L.D.	18.24	18.20	19.65	18.94	19.95	22.82	18.11	18.65	18.61	19.62	19.92	19.12	17.05	20.40	19.39	18.46
Gd	3.56	3.88	4.47	3.62	3.91	4.59	4.76	4.59	6.29	3.81	4.50	3.99	3.29	3.98	3.81	3.51	5.41	4.59	3.57
Ge	< L.D.	< L.D.	< L.D.	1.21	1.28	1.35	1.40	1.32	1.69	1.22	1.31	1.22	1.29	1.24	1.18	1.23	1.30	1.34	1.17
Hf	3.15	3.53	3.72	4.06	4.01	4.57	4.09	4.13	5.36	4.27	4.45	3.79	3.12	3.89	3.49	3.10	4.34	3.79	3.40
Ho	0.70	0.76	0.92	0.66	0.70	0.85	0.90	0.81	1.23	0.72	0.83	0.73	0.61	0.72	0.70	0.62	0.92	0.83	0.65
In	< L.D.	< L.D.	< L.D.	< L.D.	< L.D.	< L.D.	< L.D.	< L.D.	0.10	< L.D.	< L.D.	< L.D.	< L.D.	< L.D.	< L.D.	< L.D.	< L.D.	< L.D.	< L.D.
La	27.34	25.04	21.96	23.22	24.42	25.76	22.49	28.05	21.92	24.87	27.11	24.91	21.35	26.59	24.50	19.70	36.35	22.86	20.00
Lu	0.30	0.33	0.38	0.31	0.32	0.38	0.39	0.36	0.52	0.34	0.37	0.33	0.28	0.34	0.31	0.27	0.39	0.37	0.28
Mo	< L.D.	< L.D.	< L.D.	1.60	1.57	1.39	1.20	1.40	1.16	1.60	1.51	1.30	1.21	1.18	1.23	1.25	1.35	1.24	1.15
Nb	15.99	14.85	12.12	8.92	9.86	12.04	11.39	15.06	13.07	9.11	14.76	13.76	10.17	13.17	12.83	10.06	23.95	14.92	9.44
Nd	19.69	20.96	21.79	18.64	20.42	23.09	22.32	24.53	26.59	20.07	23.47	21.68	17.29	22.13	20.48	17.63	31.36	22.47	17.92

Table 5.2: *(continued)*

	ER1	ER2	ER3	ER4	ER5	ER9	ER10	ER11	ER13	ER16	ER17	ER20	ER22	ER25	ER26	ER27	ER29	ER30	ER32
Ni	< L.D.	< L.D.	< L.D.	40.55	59.79	53.37	123.30	49.24	38.28	35.45	71.90	97.00	58.63	66.85	46.39	84.86	45.67	57.33	97.27
Pb	9.94	9.01	7.70	9.89	9.28	7.57	5.68	8.23	3.88	10.40	7.72	6.57	7.71	8.59	7.34	6.06	8.31	6.20	6.83
Pr	5.31	5.47	5.43	4.54	4.93	5.64	5.30	6.12	6.10	5.27	6.12	5.63	4.57	5.83	5.39	4.63	8.30	5.61	4.54
Rb	23.27	27.44	18.15	44.50	43.46	24.53	18.49	24.29	8.51	43.78	27.28	23.52	27.87	25.99	29.62	25.37	29.30	26.18	20.21
Sb	< L.D.	< L.D.	< L.D.	0.29	0.25	< L.D.	< L.D.	< L.D.	< L.D.	0.26	< L.D.	< L.D.	0.20	< L.D.	< L.D.	0.17	< L.D.	< L.D.	< L.D.
Sm	3.84	4.17	4.61	3.80	4.23	4.74	4.83	4.89	6.21	4.15	4.75	4.42	3.58	4.48	4.16	3.68	6.12	4.85	3.71
Sn	< L.D.	< L.D.	< L.D.	1.42	1.39	1.43	1.48	1.29	2.01	1.45	1.41	1.31	1.12	1.26	1.27	1.35	1.54	1.27	1.16
Sr	491	477	473	311	382	397	465	448	478	304	428	463	381	412	465	424	610	476	407
Ta	0.84	0.89	0.70	0.81	0.85	0.97	0.86	1.13	1.04	0.81	1.16	1.04	0.83	1.06	1.02	0.82	1.72	1.16	0.72
Tb	0.59	0.64	0.78	0.55	0.60	0.71	0.75	0.69	1.02	0.60	0.70	0.64	0.51	0.62	0.60	0.53	0.81	0.71	0.56
Th	5.81	4.58	3.79	6.11	6.02	3.31	3.19	3.78	1.84	6.19	3.44	3.75	4.71	4.49	4.84	4.79	4.91	3.08	3.35
Tm	0.30	0.30	0.34	0.29	0.30	0.36	0.39	0.34	0.51	0.31	0.35	0.32	0.26	0.32	0.29	0.26	0.38	0.36	0.27
U	1.50	1.33	1.03	1.89	1.85	1.08	0.92	1.19	0.56	1.80	1.05	1.06	1.55	1.42	1.37	1.46	1.28	0.99	1.00
V	< L.D.	< L.D.	< L.D.	79.18	96.05	113.80	148.00	111.60	207.40	76.37	111.90	122.60	113.90	113.20	119.40	112.90	152.80	133.40	110.80
W	< L.D.	< L.D.	< L.D.	1.18	1.06	0.90	0.55	0.95	< L.D.	1.06	0.86	0.71	0.98	0.94	0.87	0.80	0.64	0.53	0.85
Y	18.27	19.94	24.36	19.43	20.68	25.05	25.93	23.85	34.95	21.42	24.21	21.36	17.53	21.10	19.84	17.88	26.57	24.10	18.17
Yb	1.91	1.98	2.33	1.99	2.07	2.45	2.52	2.31	3.38	2.14	2.39	2.11	1.77	2.13	1.98	1.71	2.55	2.39	1.81
Zn	< L.D.	< L.D.	< L.D.	63.26	67.74	78.56	85.69	84.68	115.60	66.74	78.17	75.45	73.40	79.38	73.38	63.33	94.67	86.46	69.01
Zr	153.46	175.35	191.98	169.40	167.60	212.60	193.50	194.30	264.70	182.90	214.40	181.00	138.00	178.10	160.60	128.20	212.90	172.70	153.90

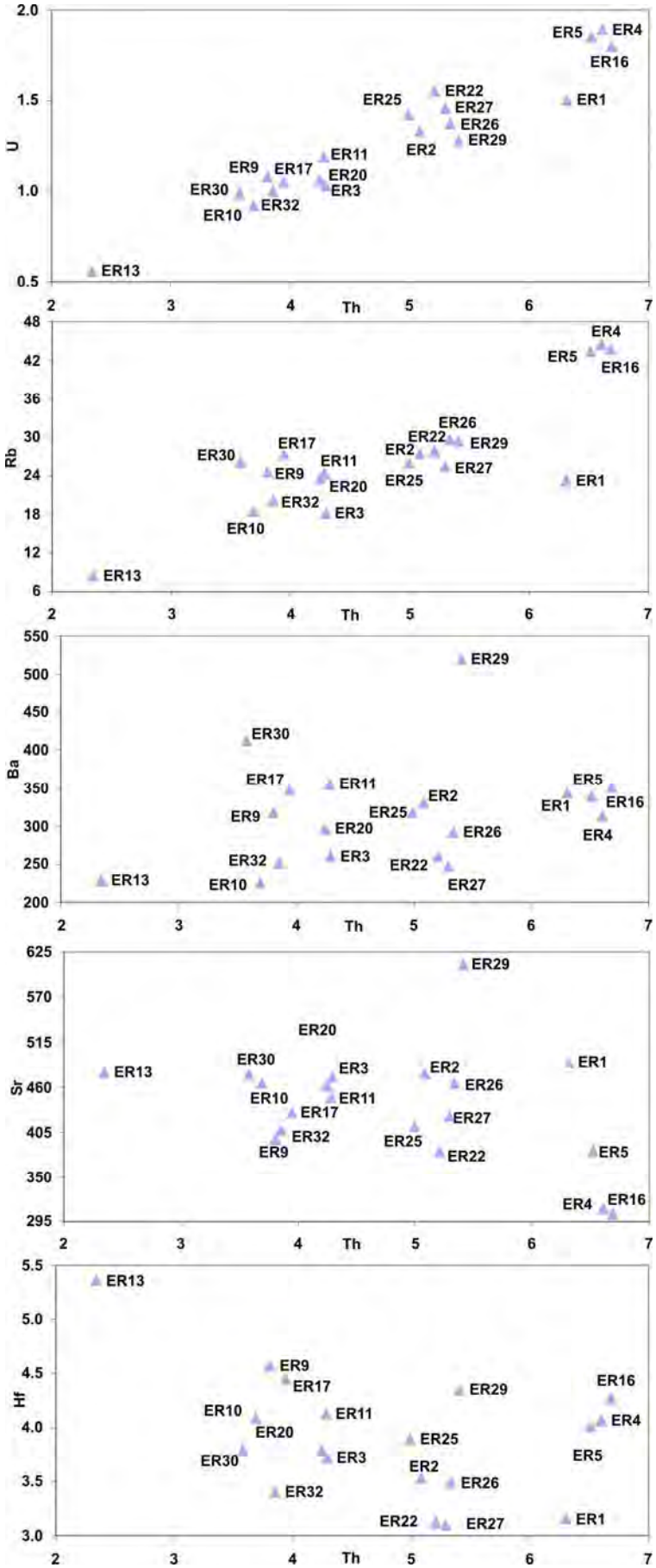

Figure 5.5: Trace element variation diagrams of Erciyes

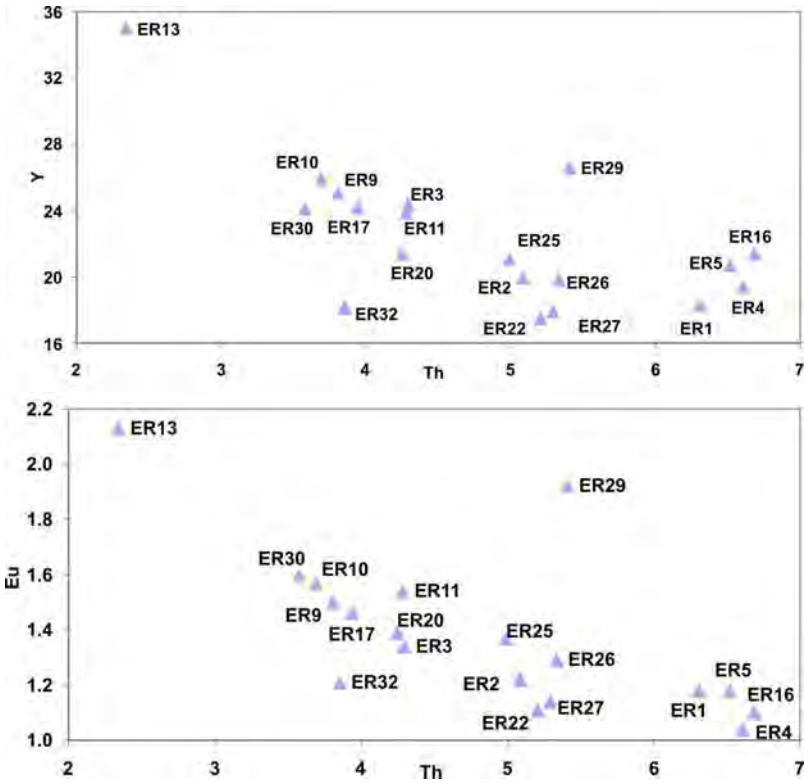

Figure 5.5: (*continued*)

Moreover, Ce/Y ratios are 1.39-2.77 in LDDS and 1.90-2.48 in MDDS. Variance in Zr/Nb ratios are 8.89-20.25, and 11.58-17.66 in LDDS and MDDS, respectively that support the continental crust effect. La/Nb ratios are (1.52-1.97) in LDDS and MDDS (1.53-2.14) are greater than 1. That means the existence of lithospheric mantle source is not deep (De Paolo and Daley, 2000).

According to Shaw et al. (2003), the lithospheric mantle comprises spinel and garnet. However, the mantle melting beneath intra-plate OIB probably begins in a garnet-bearing peridotite (Niu et al., 2011). Niu et al. (2011) suggest, the strong fractionation between primitive-mantle normalized LREE and HREE $(Sm/Yb)_N$ > 1 ratio of the volcanic rocks indicate that garnet was stable in the residue during partial melting. These ratios are (2.04-2.67) and (2.15-2.39) for LDDS and MDDS, respectively.

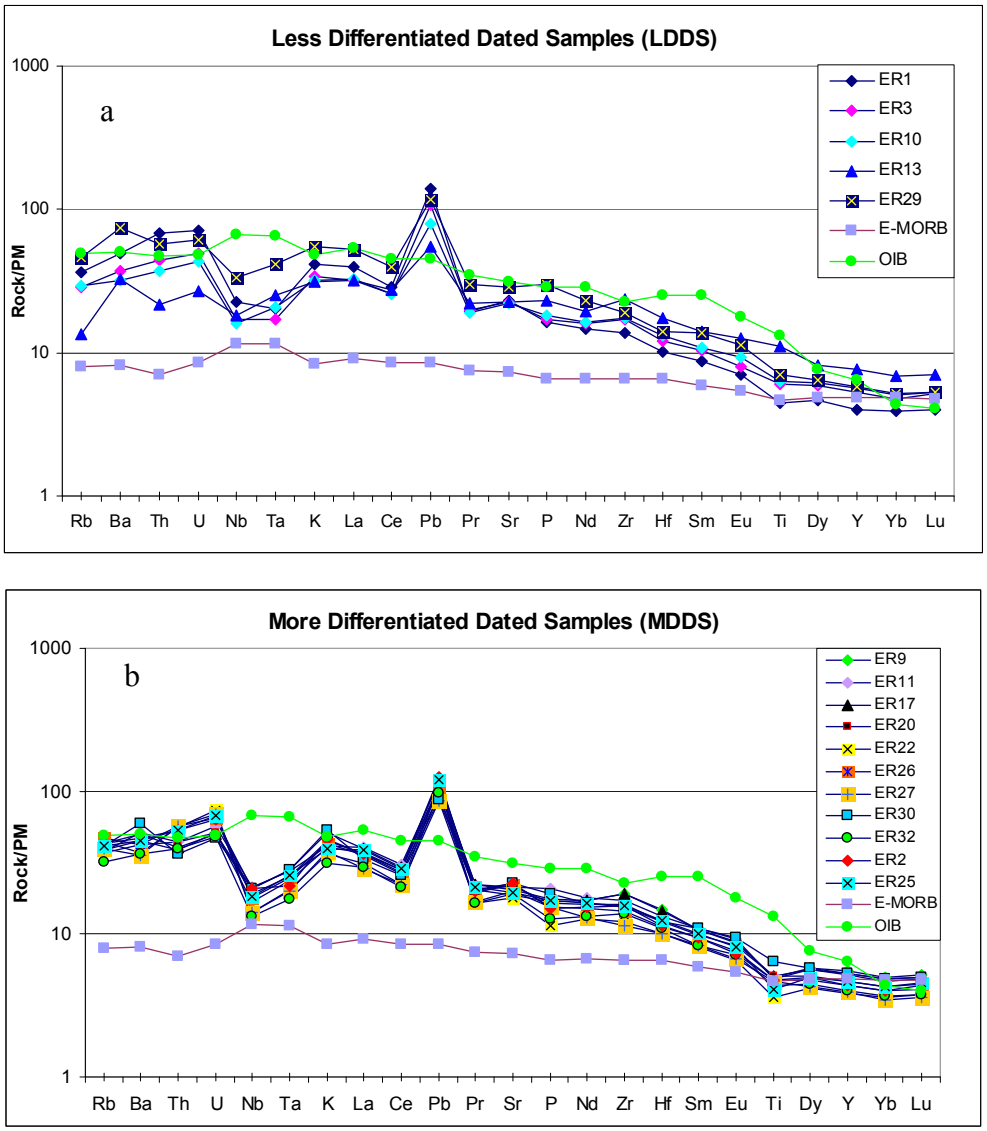

Figure 5.6: (a) Less differentiated dated samples *(LDDS*), (b) More differentiated dated samples (MDDS). Normalized in accordance with PM- spider diagram of Erciyes volcanic rocks (normalized values from Sun and McDonough (1989))

On the other side, negative anomaly for HFS elements (Y, Yb) cannot be seen on our multi-element diagrams (Figure 5.6a-b). Thus we can consider that the garnet phase is not efficient and the source is more likely at shallow depths. Additionally, calculated depths from cpx-liquid geobarometer are between 17 and 10.5 km (section 4.4.1.2). These results support the results given above.

Chondrite normalized Rare Earth Elements (REE) spider diagrams indicate that the ES samples are enriched in Light Rare Earth Elements (LREE) and exhibit flat patterns in MREE and HREE (Figure 5.7). In the following, E-MORB and OIB

normalized patterns and ES volcanics (LDDS, MDDS) are compared (Figure 5.7 a-b).

In Chondrite normalized spider diagram, ER29, the youngest sample of LDDS is enriched in LREE and some trace elements present similar pattern with OIB (Figure 5.7a). ER13, the oldest sample in this group, is relatively more enriched in HREE than other samples and OIB. ER1 is the most depleted sample in HREE, and ER3 and ER10 present similar trends. All the samples, especially the youngest ones (ER9, ER11, ER17) of MDDS, are significantly enriched in LREE (Figure 5.7 b). The oldest ER32 sample displays more depletion in HREE.

Eu/Eu* value varies between 0.90 and 1.04 in LDDS and 0.92-1.03 in MDDS group. According to Zhu et al. (2007), if plagioclase separation is inefficient from the residual melts, plagioclase phenocrysts accumulation would be left as a residue in the melt. Therefore, more plagioclase in the rock gives higher Al_2O_3 while the bulk rock has a lower Mg# and the absence of a negative Eu anomaly.

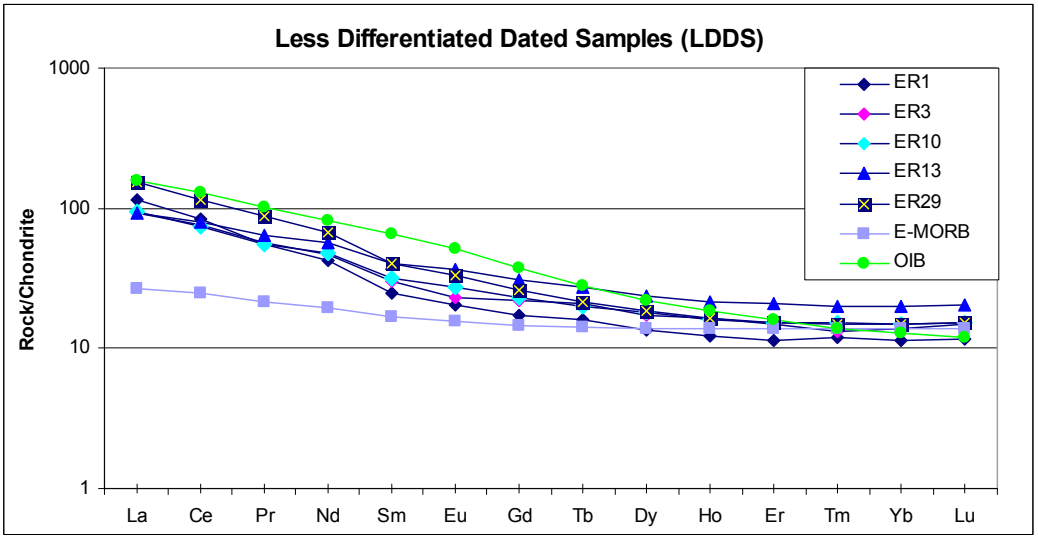

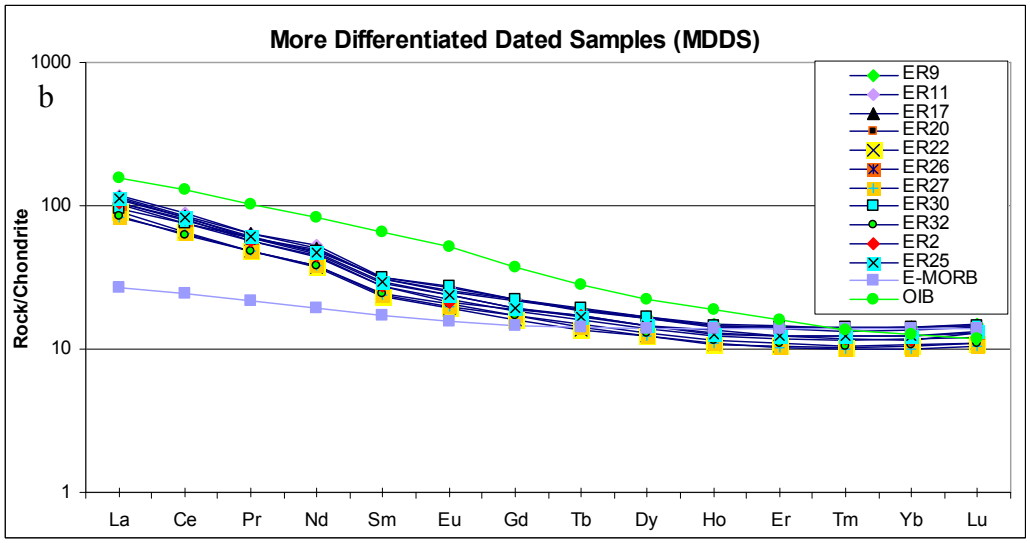

Figure 5.7: (a) Less differentiated dated samples (LDDS), (b) More differentiated dated samples (MDDS). Normalized in accordance with Chondrite - rare earth element diagram of ES volcanics (normalized values and average OIB and E-MORB values are taken from Sun and McDonough, (1989)

According to Sun and McDonough (1989), in LDDS group, the lowest ratio of (La/Yb) is in ER13 (4.65), and slightly higher ratios between 6.76 and 6.39 are in ER3 and ER10's respectively (Table 5.3). ER1 and ER29 have relatively highest ratios of $(La/Yb)_N$ (10.26-10.24). In MDDS, $(La/Yb)_N$ ratios vary between 7.56 to 9.08, except ER30 (6.86) (Table 5.3).

Low Zr/Ba, high Th/Y, and Ta/Th ratios are related to low grade partial melting. Therefore, in LDDSs these ratios are changing between 0.41 and 1.16 for Zr/Ba, 0.05 and 0.32 for Th/Y, 0.14 and 0.56 for Ta/Th. The sample ER13 has the highest Zr/Ba and Ta/Th ratios (Table 5.3) and the lowest Th/Y. On other hand, in MDDSs they vary between 0.42 and 0.67 for Zr/Ba, 0.13 and 0.27 for Th/Y, 0.13-0 and 38 for Ta/Th. Based on this ratio variance, different graded partial melting occurred in these two groups.

According to Fitton et al. (1988), LREEs are more incompatible than HREEs and they prefer entering into molten phase during igneous differentiation or partial melting. The enrichment observed in LREEs may occur at low grade partial melting or crustal contamination. The grade of partial melting that occurred in the mantle may be obtained by using high and low LREE/HREE ratios. LREE/HREE enrichment may particularly followed through the ratio of $(La/Yb)_N$. High $(La/Yb)_N$ ratio gives us the idea that alkaline basalts occurred from an enriched mantle source of magma due to a low grade partial melting.

5.1.2. Southwestern Cappadocia Volcanism

Southwestern Cappadocia Volcanism is examined in 3 different locations: i) Hasandağ stratovolcano (HS) and ii) Obruk-Zengen (OZ), iii) Karapınar (K) dispersed volcanism. In the following section, geochemical results including major, trace, REE, and isotopic data of the Southwestern Cappadocia Volcanism will be given by using the names above.

Major element and CIPW normative values of 6 samples from HS, 5 samples from OZ and 3 samples from K are obtained and given in Table 5.4. HS samples exhibit basic characteristic ($49\% < SiO_2 < 51\%$) with the MgO values of $6\% < MgO < 9\%$. (Table 5.4). In OZ and K samples, basic character is also observed: $49\% < SiO_2 < 56\%$ and $49\% < SiO_2 < 53\%$ respectively, (Table 5.4).

In the nomenclature diagram of Le Bas et al. (1986) in which the major element values are recalculated according to anhydrous basis, most of samples of HS are plotted in the basalt area, except one sample plotted in the trachybasalt field (Figure 5.8).

Table 5.3: Selected trace elemet ratios of Ercives

Trace element (ppm)	ER1	ER2	ER3	ER4	ER5	ER9	ER10	ER11	ER13	ER16	ER17	ER20	ER22	ER25	ER26	ER27	ER29	ER30	ER32
Zr/Nb	9.60	11.80	15.84	18.98	16.99	17.66	16.99	12.90	20.25	20.08	14.53	13.15	13.57	13.52	12.52	12.74	8.89	11.58	16.30
Zr/Ba	0.45	0.53	0.74	0.54	0.49	0.67	0.86	0.55	1.16	0.52	0.62	0.61	0.53	0.56	0.55	0.52	0.41	0.42	0.61
Th/Y	0.32	0.23	0.16	0.31	0.29	0.13	0.12	0.16	0.05	0.29	0.14	0.18	0.27	0.21	0.24	0.27	0.18	0.13	0.18
Ta/Th	0.14	0.19	0.19	0.13	0.14	0.29	0.27	0.30	0.56	0.13	0.34	0.28	0.18	0.24	0.21	0.17	0.35	0.38	0.22
La/Nb	1.71	1.69	1.81	2.60	2.48	2.14	1.97	1.86	1.68	2.73	1.84	1.81	2.10	2.02	1.91	1.96	1.52	1.53	2.12
Ba/Nb	21.49	22.30	21.53	35.19	34.43	26.40	19.82	23.62	17.46	38.56	23.57	21.53	25.62	24.10	22.77	24.54	21.69	27.70	26.73
Ce/Y	2.77	2.48	1.89	2.25	2.21	2.01	1.75	2.29	1.39	2.18	2.17	2.24	2.27	2.41	2.35	2.21	2.64	1.90	2.10
(La/Yb)N	10.26	9.08	6.76	8.36	8.46	7.56	6.39	8.71	4.65	8.32	8.13	8.46	8.65	8.98	8.87	8.26	10.24	6.86	7.93
(La/Sm)N	4.60	3.88	3.08	3.95	3.73	3.51	3.01	3.71	2.28	3.88	3.69	3.64	3.86	3.84	3.81	3.46	3.84	3.05	3.48
(Dy/Yb)N	1.20	1.24	1.26	1.11	1.16	1.17	1.21	1.20	1.20	1.11	1.16	1.18	1.18	1.16	1.19	1.22	1.24	1.18	1.22
(Sm/Yb)N	2.23	2.34	2.20	2.12	2.27	2.15	2.12	2.35	2.04	2.15	2.20	2.32	2.24	2.34	2.33	2.39	2.67	2.25	2.28
Eu*	20.84	22.70	25.60	20.91	22.95	26.31	27.04	26.71	35.25	22.41	26.06	23.69	19.34	23.81	22.45	20.27	32.46	26.61	20.52
Eu/Eu*	0.97	0.92	0.90	0.86	0.88	0.98	1.00	0.99	1.04	0.84	0.96	1.01	0.99	0.99	0.99	0.97	1.02	1.03	1.02

Eu/Eu*=[Eucn/(Smcn*Gdcn)0,5]; oxides are given in weight percentage, trace elements are in ppm

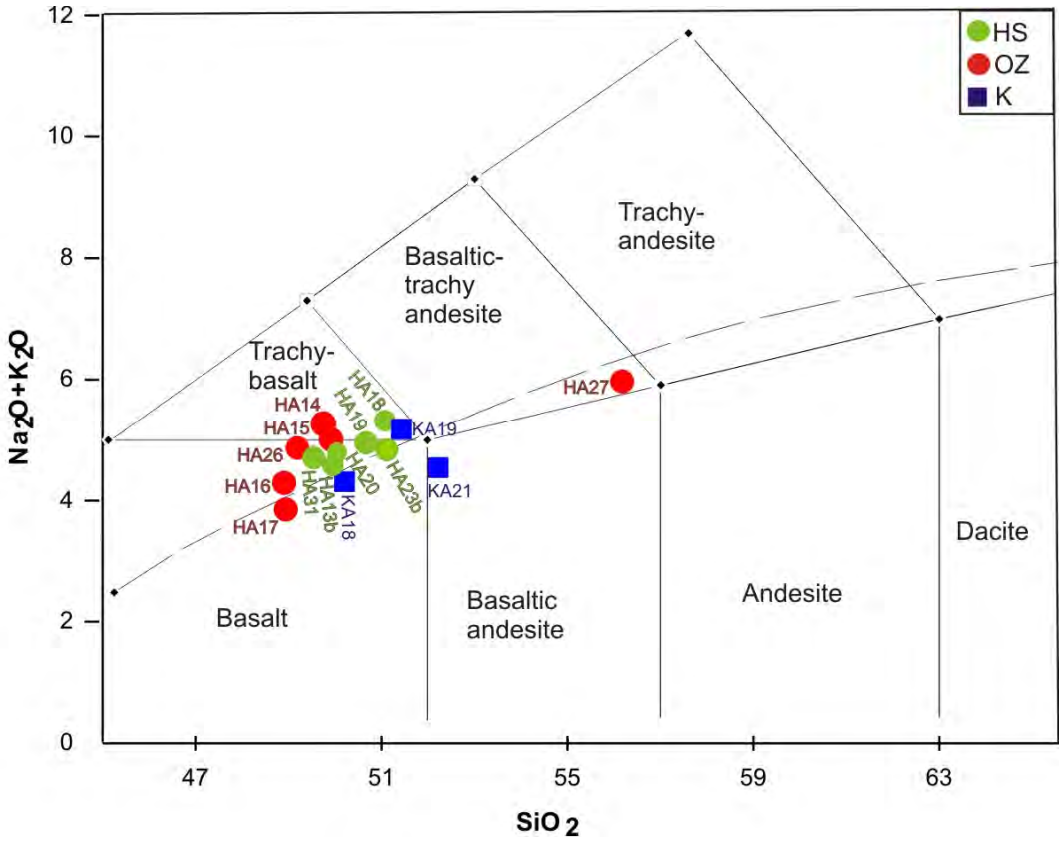

Figure 5.8: Southwestern Cappadocia Volcanism basic samples in the total Alkaline vs. SiO_2 diagram (Le Bas et al., 1986; Miyashiro, 1978)

Samples of OZ are also plotted in the basalt area, but one sample is in the trachybasalt field and another one in the basaltic-trachy andesite field (Figure 5.8). K samples are gathered in the trachybasalt, basalt and basaltic andesite areas (Figure 5.8).

According to Miyashiro (1978) the samples of Southwest Cappadocia volcanics show dominant alkaline characteristic, except slightly sub-alkaline features in some OZ and K samples (Figure 5.8). Moreover, the subalkaline characteristic of these samples exhibit calcalkaline features.

The HS samples in the trachybasalt area is a hawaiite (Na_2O_2>K_2O). In OZ and K, some samples also are hawaiite and mugearite. All the alkaline samples of the Southwestern Cappadocia Volcanism are plotted in the sodic series area, according to the K_2O vs. Na_2O graphic of Middlemost (1975) (Figure 5.9).

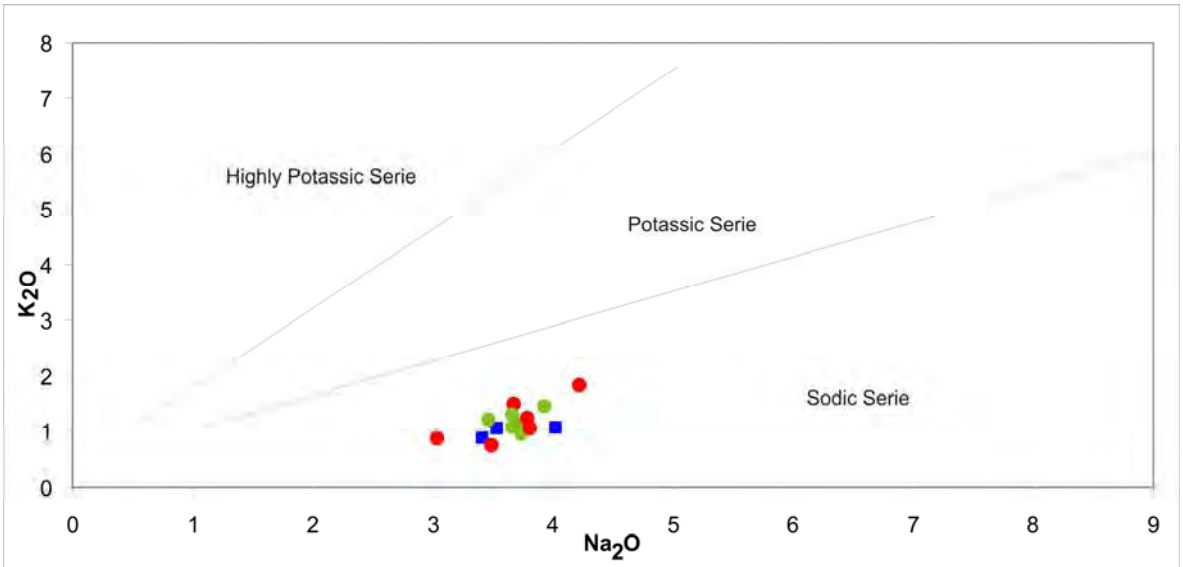

Figure 5.9: K_2O vs. Na_2O diagram (Middlemost ,1975).
(Symbols as in Figure 5.8).

In HS, CIPW norm values indicate occurrence of nepheline normative, except the hypersthene normative of HA18 and HA23b samples (Table 5.4). All samples exhibit high amount of plagioclase normative, diopside, olivine and low amount of normative alkaline feldspar, magnetite, ilmenite and apatite (Table 5.4). Occurrence of normative nepheline is dominant in OZ, except HA27 sample, which is one of the most differentiated samples and display a calcalkaline characteristic with normative quartz and hypersthene (Table 5.4).

In K also, all of the samples consist of dominantly normative plagioclase, diopside, olivine and low amount of alkaline feldspar, magnetite, ilmenite and apatite minerals. In KA21 sample indicates hypersthene normative, but KA18 and KA19 have nepheline normative (Table 5.4).

Aluminous data (Al_2O_3 > Na_2O+K_2O+CaO) indicate that all the samples from Southwestern Cappadocia volcanism are strongly per-aluminous.

As seen in the Figure 5.10, Harker variation diagrams of HS, OZ and K. In Al_2O_3, Na_2O, TiO_2 vs. MgO, variation patterns are more likely positive while negative trends are observed in the CaO, Fe_2O_3, P_2O_5 vs. MgO variation diagrams (Figure 5.10).

In the samples of the HS, from oldest to youngest (HA18, HA19 and HA20), K_2O values tend to decrease compare to MgO values (Figure 5.10), moreover the youngest sample of HA31, which is located on the west side of Hasandağ stratovolcano represent the highest Al_2O_3, CaO, Fe_2O_3, MnO values, and the lowest MgO, SiO_2, P_2O_5, K_2O values (Figure 5.10). Except the samples HA 16 and HA 17, the negative trend in the major oxides are observed and it is more likely noted that, the samples from OZ do not display clear trends. (Figure 5.10).

Although negative trends are observed in Al_2O_3, Na_2O, Fe_2O_3, MnO and TiO_2 of K, there is no significant tendency for SiO_2, K_2O, CaO and P_2O_5 (Figure 5.10).

According to major element distribution of the Southwestern Cappadocia Volcanism, HS experienced strong fractional crystallization even more dominant compared to ES. However, this strong fractional crystallization pattern is not observed in OZ and K dispersed volcanism. Early crystallization of olivine, pyroxene, Ca-plagioclase and accessory minerals (apatite, magnetite, and ilmenite) is related to the depletion of CaO, MgO, Fe_2O_3, P_2O_5 and TiO_2. In addition, occurrence of a negative trend in K element, with the increase of MgO, also supports the dominance of fractional crystallization during the magma genesis.

The trace element analyses of the volcanic rocks of HS, OZ and K are summarized in Table 5.5. Variation diagrams of the Southwestern Cappadocia Volcanism based on selected trace elements versus Th are given in Figure 5.11. In the samples of HS, a positive trend in the incompatible elements Ba, Rb, U, Sr, and a linear decreasing of Hf and Y are observed with increasing Th (Figure 5.11). The increasing trend of Ba, Rb and U elements is related to the differentiation. Increase in Sr and no significant tendency in Eu indicate that Ca-plagioclase fractionation is less effective during the melt formation (Figure 5.11). Moreover negative trends in Hf and Y versus Th is more likely pointing out the latter phases of fractionalization. In contrast to HS, the samples of OZ and K present nearly no systematic trends (Figure 5.11). Irregular scatters in the diagrams are seen and only significant increase in U vs. Th is noted in the OZ group (Figure 5.11). This evidence with

major elements variation diagram clearly addresses that the fractional crystallization was not effective in the genesis of OZ magmas.

Similar to OZ group, samples of K area display no significant trends; however a slightly increase in Ba, Rb and a noticeable positive trend in U with negative Sr, Eu and Y trends are observed (Figure 5.11).

Mg# contents of the Southwestern Cappadocia samples vary in the range of 66 to 72. Relatively to the OZ and K dispersed volcanism, the HS samples display slightly more effect of fractional crystallization. However in the whole associations, it is noted that these samples are derived from peridotite according to their high Mg# > 68-70 range (Frey et al., 1978) and fractional crystallization is not the main process during the magma genesis.

Primitive mantle (PM) normalized multi-element diagrams of HS, OZ and K areas are compared to OIB and E-MORB (Figure 5.12 a-b-c). Characteristically in the HS group, samples are enriched in LILEs, and show a negative anomaly in Nb, Ta, Ti and P and a positive anomaly in Pb (Figure 5.12 a). Samples of the HS display significant depletion in P, Nd, Zr, Hf, Sm, more than in OIB. General multi-element patterns of the HS group exhibit similar patterns as in OIB, such as Rb, Ba, Th, U, K, La, Sr, Ce, Y, Yb and Lu. However Nb, Ta depletion, Pb spikes, and slightly differences in Hf, Sm, Eu and Ti data, are not truly in agreement with OIB values (Figure 5.12a).

All the samples belonging to OZ group are enriched in LILEs as HS group, and they present relatively higher negative anomaly in Nb, Ta, Ti and P (Figure 5.12b). Especially, two samples that are quite enriched in MgO (HA16 and HA17) present a high negative anomaly in Nb and Ta. The most differentiated samples (HA26, HA27) present the highest Pb positive anomaly. OZ group resembles OIB in terms of (Ba, Th, U, K, La, Ce, Pr, Sr, Nd, Y, Yb, Lu) elements.

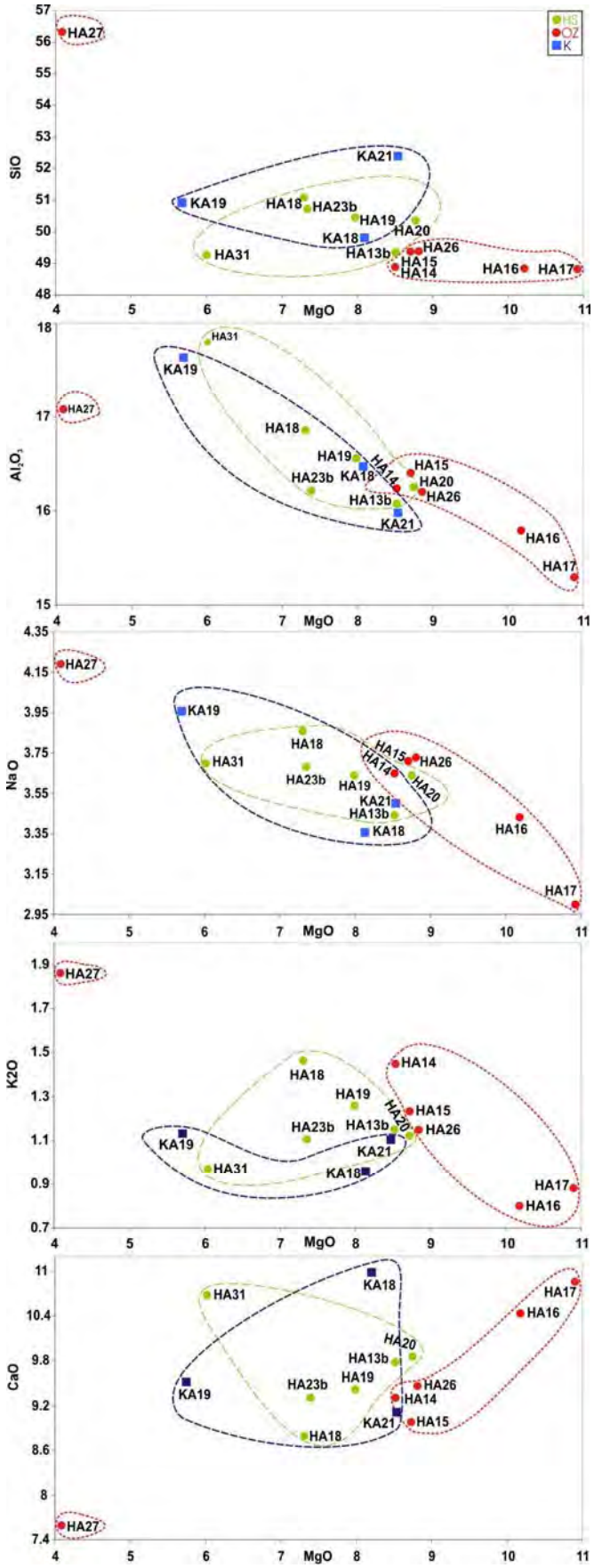

Figure 5.10: Major element oxide variation diagrams of Southwestern Cappadocia Volcanism

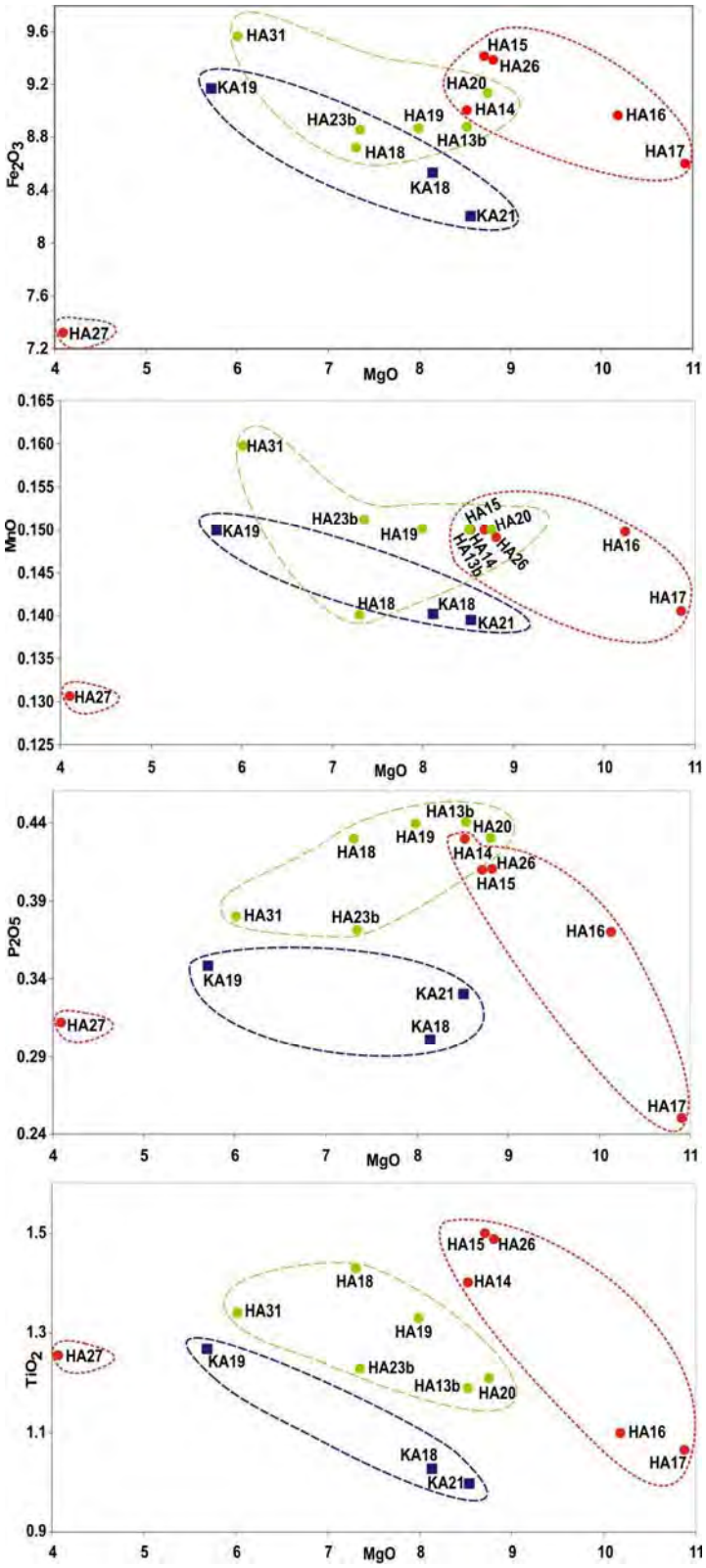

Figure 5.10: (*continued*)

Table 5.4: Major element analysis and CIPW normative values of Southwestern Cappadocia Volcanism

	Hasandağ stratovolcano						Obruk-Zengen						Karapınar		
	HA13 b	**HA18**	**HA19**	**HA20**	**HA23b**	**HA31**	**HA14**	**HA15**	**HA16**	**HA17**	**HA26**	**HA27**	**KA18**	**KA19**	**KA21**
Major element(%)															
SiO_2	49.33	51.06	50.43	50.36	50.90	49.24	48.99	49.38	48.81	48.88	49.39	56.24	49.75	50.87	52.40
Al_2O_3	16.08	16.86	16.56	16.25	16.22	17.80	16.24	16.40	15.79	15.30	16.23	17.08	16.48	17.65	15.99
Fe_2O_3	8.88	8.72	8.87	9.14	8.86	9.57	9.01	9.42	8.97	8.60	9.39	7.31	8.53	9.17	8.20
MgO	8.52	7.31	7.99	8.75	7.35	6.01	8.52	8.71	10.18	10.92	8.81	4.07	8.12	5.69	8.54
CaO	9.78	8.76	9.42	9.85	9.32	10.68	9.28	8.98	10.43	10.86	9.47	7.57	11.02	9.52	9.11
Na_2O	3.44	3.86	3.64	3.64	3.68	3.70	3.65	3.71	3.43	3.00	3.73	4.19	3.36	3.96	3.50
K_2O	1.15	1.46	1.26	1.12	1.10	0.97	1.45	1.23	0.80	0.88	1.15	1.86	0.95	1.13	1.12
TiO_2	1.19	1.43	1.33	1.21	1.23	1.34	1.40	1.50	1.10	1.06	1.49	1.25	1.03	1.27	1.00
MnO	0.15	0.14	0.15	0.15	0.15	0.16	0.15	0.15	0.15	0.14	0.15	0.13	0.14	0.15	0.14
P_2O_5	0.44	0.43	0.44	0.43	0.37	0.38	0.43	0.41	0.37	0.25	0.41	0.31	0.30	0.35	0.33
LOI	-0.14	-0.43	-0.58	-0.27	0.00	-0.06	-0.35	-0.28	-0.32	-0.23	0.22	0.24	-0.32	-0.38	0.12
Mg#	69.16	67.82	67.79	69.11	65.98	59.50	70.41	68.37	72.62	74.80	68.68	59.19	68.99	60.97	72.38
Total	98.72	99.88	99.72	100.64	98.97	99.51	98.69	99.32	99.75	99.83	100.42	100.23	99.35	99.38	100.43
CIPW norm															
Q	-	-	-	-	-	-	-	-	-	-	-	3.518	-	-	-
Or	6.92	8.70	7.49	6.63	6.619	5.77	8.71	7.33	4.76	5.24	6.837	11.051	5.67	6.76	6.64
Ab	27.16	32.86	29.76	27.52	31.706	26.57	25.75	27.64	23.18	21.35	26.339	35.649	25.18	33.50	29.71
An	25.49	24.53	25.29	24.66	24.932	29.41	24.03	24.69	25.51	25.90	24.282	22.426	27.37	27.31	24.69
Ne	1.34	-	0.68	1.76	-	2.72	3.05	2.19	3.28	2.30	2.93	-	1.91	0.16	-
Di	16.95	13.17	15.23	17.24	15.952	17.64	16.00	14.18	19.45	21.48	16.368	10.815	20.90	14.72	14.85
Hy	-	0.11	-	-	2.164	-	-	-	-	-	-	10.878	-	-	10.76
Ol	16.80	14.17	16.00	16.88	13.38	12.31	15.93	18.03	18.85	19.19	17.354	-	14.37	11.45	8.14
Mt	2.00	2.71	1.98	2.02	1.995	2.14	2.82	2.10	2.00	1.92	2.088	2.552	1.91	2.86	2.53
Il	2.30	2.74	2.54	2.30	2.378	2.57	2.70	2.88	2.10	2.03	2.847	2.387	1.98	2.43	1.91
Ap	1.04	1.01	1.03	1.00	0.873	0.89	1.01	0.96	0.86	0.58	0.954	0.723	0.71	0.82	0.77

Table 5.5: Trace element analysis of the Southwestern Cappadocia Volcanism

	Hasandağ stratovolcano						Obruk-Zengen						Karapınar		
Trace element (ppm)	**HA13 b**	**HA18**	**HA19**	**HA20**	**HA23b**	**HA31**	**HA14**	**HA15**	**HA16**	**HA17**	**HA26**	**HA27**	**KA18**	**KA19**	**KA21**
As	< L.D.	< L.D.	< L.D.	< L.D.	< L.D.	< L.D.	< L.D.	< L.D.	< L.D.	< L.D.	1.41	1.63	< L.D.	< L.D.	< L.D.
Ba	391.00	375.80	349.00	383.10	307.90	350.30	360.00	301.00	290.00	260.00	252.80	432.80	343.41	346.16	369.90
Be	< L.D.	< L.D.	< L.D.	< L.D.	1.25	< L.D.	< L.D.	< L.D.	< L.D.	< L.D.	1.37	1.55	< L.D.	< L.D.	1.48
Bi	< L.D.	< L.D.	< L.D.	< L.D.	< L.D.	< L.D.	< L.D.	< L.D.	< L.D.	< L.D.	< L.D.	< L.D.	< L.D.	< L.D.	< L.D.
Cd	< L.D.	0.17	0.15	0.19	0.15	0.20	< L.D.	< L.D.	< L.D.	< L.D.	0.20	0.15	< L.D.	< L.D.	0.13
Ce	61.56	53.92	54.06	58.90	48.59	53.74	66.02	50.26	49.87	35.80	48.21	50.64	56.34	56.15	56.03
Co	< L.D.	33.36	35.42	38.05	35.24	32.99	< L.D.	< L.D.	< L.D.	< L.D.	38.87	23.25	< L.D.	< L.D.	33.44
Cr	< L.D.	205.70	275.10	346.30	285.70	19.72	< L.D.	< L.D.	< L.D.	< L.D.	295.70	43.51	< L.D.	< L.D.	288.30
Cs	< L.D.	0.45	0.24	0.45	0.14	0.53	< L.D.	< L.D.	< L.D.	< L.D.	0.36	1.41	< L.D.	< L.D.	0.98
Cu	< L.D.	32.98	40.36	38.28	44.15	54.10	< L.D.	< L.D.	< L.D.	< L.D.	37.15	38.24	< L.D.	< L.D.	33.63
Dy	4.27	4.27	4.41	4.35	4.51	4.42	4.47	4.14	3.74	3.39	4.35	4.11	3.84	4.46	3.50
Er	2.42	2.33	2.45	2.38	2.55	2.49	2.38	2.23	2.17	1.91	2.44	2.36	2.19	2.57	2.01
Eu	1.57	1.63	1.62	1.64	1.55	1.64	1.83	1.61	1.36	1.15	1.73	1.42	1.31	1.54	1.29
Ga	< L.D.	17.95	17.71	17.96	18.15	19.65	< L.D.	< L.D.	< L.D.	< L.D.	17.13	18.57	< L.D.	< L.D.	15.48
Gd	4.65	4.64	4.65	4.72	4.81	4.79	5.13	4.44	3.82	3.32	5.03	4.43	4.04	4.63	3.76
Ge	< L.D.	1.25	1.41	1.36	1.37	1.25	< L.D.	< L.D.	< L.D.	< L.D.	1.36	1.30	< L.D.	< L.D.	1.36
Hf	3.45	3.56	3.64	3.49	3.61	3.15	3.84	3.43	2.65	2.21	3.73	3.87	2.82	3.13	2.97
Ho	0.86	0.82	0.85	0.85	0.90	0.87	0.90	0.83	0.79	0.69	0.85	0.82	0.79	0.95	0.70
In	< L.D.	< L.D.	< L.D.	< L.D.	< L.D.	< L.D.	< L.D.	< L.D.	< L.D.	< L.D.	< L.D.	< L.D.	< L.D.	< L.D.	< L.D.
La	31.02	28.30	27.73	31.01	23.99	28.14	31.46	24.20	25.94	18.07	22.50	25.75	29.92	28.31	29.72
Lu	0.37	0.36	0.38	0.37	0.41	0.38	0.36	0.35	0.35	0.28	0.37	0.38	0.36	0.41	0.32
Mo	< L.D.	1.02	0.62	0.77	0.90	0.72	< L.D.	< L.D.	< L.D.	< L.D.	1.08	1.24	< L.D.	< L.D.	0.90
Nb	17.29	16.25	16.09	14.88	11.73	12.70	13.53	14.88	11.72	7.78	12.44	12.16	9.96	10.76	8.41
Nd	26.67	25.32	25.60	26.83	23.39	24.80	31.85	23.73	21.37	16.96	25.64	22.93	22.97	25.20	23.48

Table 5.5: *(continued)*

	Hasandağ stratovolcano						Obruk-Zengen						Karapınar		
	HA13 b	**HA18**	**HA19**	**HA20**	**HA23b**	**HA31**	**HA14**	**HA15**	**HA16**	**HA17**	**HA26**	**HA27**	**KA18**	**KA19**	**KA21**
Trace element (ppm)															
Ni	< L.D.	127.90	145.30	177.40	129.50	48.51	< L.D.	< L.D.	< L.D.	< L.D.	156.00	26.61	< L.D.	< L.D.	135.10
Pb	6.16	5.72	5.52	6.03	7.18	5.58	5.10	4.40	4.86	4.63	5.02	8.72	4.17	6.06	6.91
Pr	6.84	6.43	6.54	6.89	5.39	6.41	7.73	5.83	5.47	4.09	5.64	5.41	6.06	6.29	6.39
Rb	18.40	26.91	21.06	22.47	16.51	19.51	23.40	17.10	12.20	13.20	17.24	44.02	20.85	23.06	27.01
Sb	< L.D.	< L.D.	< L.D.	< L.D.	< L.D.	< L.D.	< L.D.	< L.D.	< L.D.	< L.D.	0.14	0.25	< L.D.	< L.D.	< L.D.
Sm	5.13	4.96	5.08	5.18	4.92	5.08	6.11	4.89	4.22	3.51	5.32	4.59	4.30	4.95	4.27
Sn	< L.D.	1.35	1.34	1.27	1.01	1.19	< L.D.	< L.D.	< L.D.	< L.D.	3.95	1.28	< L.D.	< L.D.	1.20
Sr	577.00	609.30	548.70	598.10	589.90	593.90	679.00	527.00	532.00	514.00	695.50	547.40	616.51	605.23	556.10
Ta	0.99	1.25	1.23	1.06	0.79	0.89	0.78	0.88	0.59	0.43	0.93	0.98	0.52	0.59	0.65
Tb	0.76	0.72	0.73	0.73	0.75	0.74	0.79	0.72	0.65	0.57	0.74	0.68	0.66	0.78	0.58
Th	4.48	4.23	3.56	4.48	3.59	4.65	5.32	3.51	4.35	3.51	5.29	9.01	6.70	6.23	9.24
Tm	0.35	0.35	0.37	0.36	0.38	0.37	0.36	0.33	0.33	0.28	0.35	0.35	0.32	0.40	0.29
U	1.00	1.05	0.77	0.97	0.93	1.02	1.17	0.82	0.94	0.77	1.10	2.08	1.46	1.21	2.06
V	< L.D.	160.90	169.30	180.00	172.30	221.20	< L.D.	< L.D.	< L.D.	< L.D.	181.00	141.10	< L.D.	< L.D.	153.40
W	< L.D.	0.38	< L.D.	0.33	0.29	< L.D.	< L.D.	< L.D.	< L.D.	< L.D.	0.32	0.70	< L.D.	< L.D.	0.37
Y	22.60	23.63	24.73	24.05	25.81	24.76	22.60	21.30	20.30	17.70	24.60	23.95	21.31	24.55	19.90
Yb	2.35	2.32	2.42	2.33	2.59	2.45	2.32	2.18	2.19	1.85	2.35	2.41	2.23	2.62	2.02
Zn	< L.D.	80.75	87.10	88.27	83.90	92.22	< L.D.	< L.D.	< L.D.	< L.D.	93.15	67.66	< L.D.	< L.D.	66.02
Zr	167.00	167.80	173.40	159.30	156.50	134.80	186.00	166.00	126.00	97.00	164.00	162.40	134.34	141.82	116.60

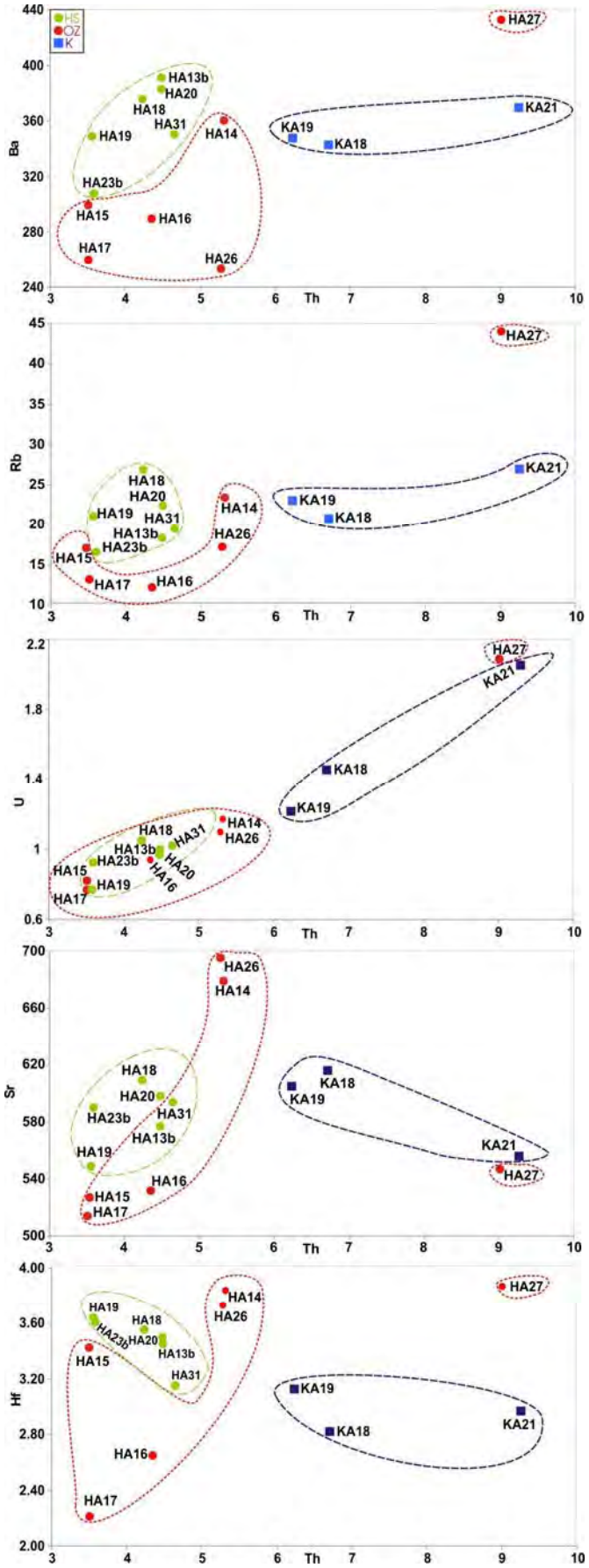

Figure 5.11: Trace element vs. Th variation diagrams of Southwestern Cappadocia Volcanism

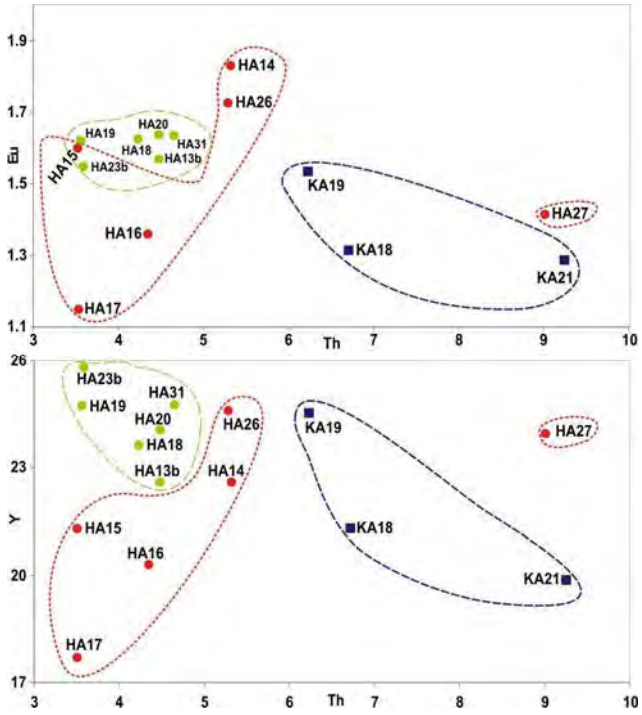

Figure 5.11: (*continued*)

Although the depletion in HFS elements in K group is typical, KA19 sample exhibits the slightly higher concentrations of these elements among these samples (Table 5.5). Samples of the K display similarities with OIB values, especially in Rb, Ba, Sr, Y, Yb and Lu are particularly enriched in Th and U from incompatible elements. Moreover their negative anomaly in Nb, Ta, Ti and P is also notable (Figure 5.12c).

Proportional relative trace element values such as Ba/Nb>28 ratios are typical indicators for subduction magmatisms environment. In the Southwestern Cappadocia volcanism Ba/Nb values are (22-28), (20-36), (32-44) for HS, OZ and K group samples, respectively (Table 5.6). The ratios of Ba/Nb are 28 for HA31 sample and lower than 28 for all other samples in the HS group. In addition to that, a Ba/Nb value are 33 for the most primitive sample and 36 for the most differentiated sample of HA27 in OZ group and is not higher in K group.

Consequently, these samples mentioned above are more likely linked to the partial melting of a non homogeneous mantle, which was metasomatized by an ancient subduction process rather than a stronger one and/or experienced a crustal contamination during its formation. Ce/Y ratios of the HS and OZ groups vary

between 1.88 and 2.72, and 1.96-2.92 respectively. Zr/Nb ratios range from 9.66 to13.34 and 10.75 to 13.75 for HS and OZ groups (Table 5.6).

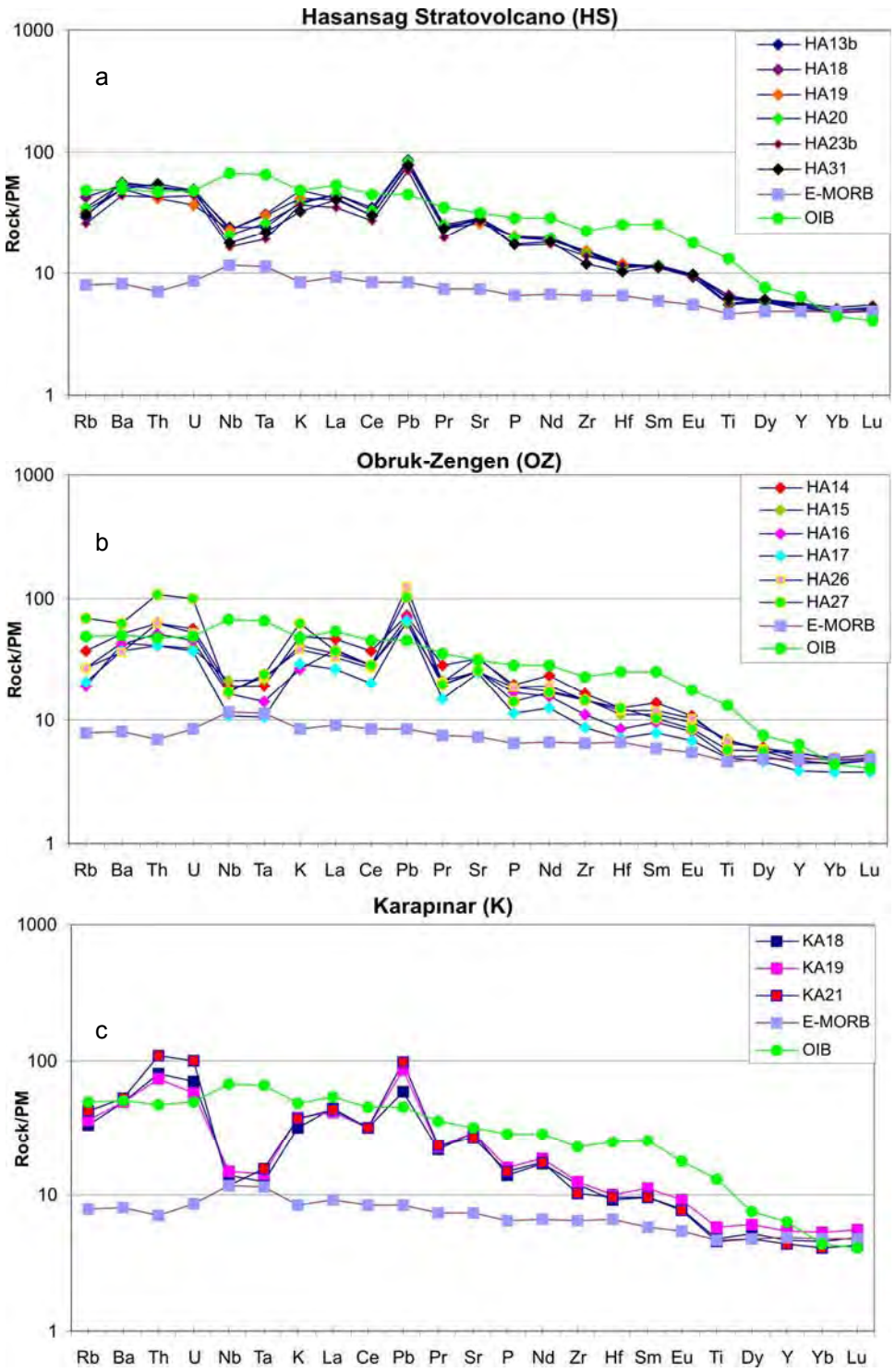

Figure 5.12: Normalized -according to PM- spider diagrams of the samples belonging to Southwestern Cappadocia Volcanism (a) HS, (b) OZ, (c) K (Normalized values and average OIB and E-MORB values are taken from Sun and McDonough (1989))

In the HS group, La/Nb values are between 1.72 and 2.22, and are relatively similar to the 1.63 to 2.33 related to the OZ group, in which lithospheric mantle source values (La/Nb>1) are reported in the literature (De Paolo and Daley, 2000). In K group, Ce/Y, Zr/Nb, and La/Nb values are 2.29-2.82, 13.19-13.86, 2.63-3.53 respectively (Table 5.6). Variable low Zr/Ba ratios (0.32 to 0.65) in HS, OZ and K groups point out a lithospheric source enriched by Ba and mixed to the melting during the subduction processes, as reported in Menzies et al. (1991). In addition, lack of the depletion in garnet phases from the multi-element diagrams (Figure 5.12) related to the lower amount of Y and Yb, favor shallow lithospheric source for the Southwestern Cappadocia Volcanism.

The samples of the whole Southwestern Cappadocia Volcanism, which are normalized to PM, exhibit typical enrichment in LILEs (Rb, Ba, Th, U, K, Sr) indicating an active continental margin magmatisms environment, Nevertheless, OZ and K are more enriched in these elements, and moreover a negative anomaly in Nb, Ta, Ti and P generally occurs, related to the accretion of the fluids resulting of the dehydration of a subducted plate (Saunders and Tarney, 1979; Pearce, 1982; Wilson, 1989). Negative anomaly in HFS element increase relatively from HS to K (Figure 5.12).

Chondrite normalized (Sun and McDonough, 1989). REE diagrams compared to OIB and E-MORB patterns are shown in Figure 5.13. The Southwestern Cappadocia magmas are enriched in LREE more than HREE. Their REE patterns display more likely similar chemical characteristic as OIB, especially in HREE and LREE. HA17 sample from OZ group has the lowest LREE concentration and HA14 has the highest (HS and K). A significant Eu anomaly is not observed in the samples of HS, OZ and K. Eu/Eu* ratios of the three groups are between (0.97-1.04), (0.96-1.06), (0.86-0.98) respectively. According to the PM normalized (Sun and McDonough, 1989) LREE/HREE ratios of the groups in the Southwestern Cappadocia, the ratios are between 6.64 and 10.54, indicating the higher $(La/Yb)_N$ values were the result of low grade partial melting. It is also in agreement with the low Zr/Nb, Zr/Ba and high Th/Y, Ta/Th and La/Nb ratios (Table 5.6). Overall LREE values address the low-grade partial melting of the source can be related to an ancient subduction in the region.

Table 5.6: Trace element ratios of the volcanics belonging to Southwestern Cappadocia Volcanism

Trace element (ppm)	Hasandağ stratovolcano						Obruk-Zengen						Karapınar		
	HA13b	**HA18**	**HA19**	**HA20**	**HA23b**	**HA31**	**HA14**	**HA15**	**HA16**	**HA17**	**HA26**	**HA27**	**KA18**	**KA19**	**KA21**
Zr/Nb	9.66	10.33	10.78	10.71	13.34	10.61	13.75	11.16	10.75	12.47	13.18	13.36	13.49	13.19	13.86
Zr/Ba	0.43	0.45	0.50	0.42	0.51	0.38	0.52	0.55	0.43	0.37	0.65	0.38	0.39	0.41	0.32
Th/Y	0.20	0.18	0.14	0.19	0.14	0.19	0.24	0.16	0.21	0.20	0.21	0.38	0.31	0.25	0.46
Ta/Th	0.22	0.30	0.35	0.24	0.22	0.19	0.15	0.25	0.14	0.12	0.18	0.11	0.08	0.09	0.07
La/Nb	1.79	1.74	1.72	2.08	2.05	2.22	2.33	1.63	2.21	2.32	1.81	2.12	3.00	2.63	3.53
Ba/Nb	22.61	23.13	21.69	25.75	26.25	27.58	26.61	20.23	24.74	33.42	20.32	35.59	34.48	32.18	43.96
Ce/Y	2.72	2.28	2.19	2.45	1.88	2.17	2.92	2.36	2.46	2.02	1.96	2.11	2.64	2.29	2.82
(La/Yb)N	9.47	8.77	8.23	9.55	6.64	8.24	9.73	7.97	8.50	7.01	6.89	7.66	9.62	7.75	10.54
(La/Sm)N	3.91	3.69	3.53	3.87	3.15	3.58	3.33	3.20	3.97	3.33	2.73	3.62	4.50	3.69	4.50
(Dy/Yb)N	1.22	1.23	1.22	1.25	1.16	1.21	1.29	1.27	1.14	1.23	1.24	1.14	1.15	1.14	1.16
(Sm/Yb)N	2.42	2.38	2.33	2.47	2.11	2.30	2.92	2.49	2.14	2.11	2.52	2.11	2.14	2.10	2.34
Eu*	27.54	27.03	27.38	27.88	27.43	27.83	31.57	26.28	22.64	19.25	29.19	25.44	23.51	27.02	22.58
Eu/Eu*	0.98	1.04	1.02	1.01	0.97	1.01	1.00	1.06	1.04	1.03	1.02	0.96	0.96	0.98	0.98

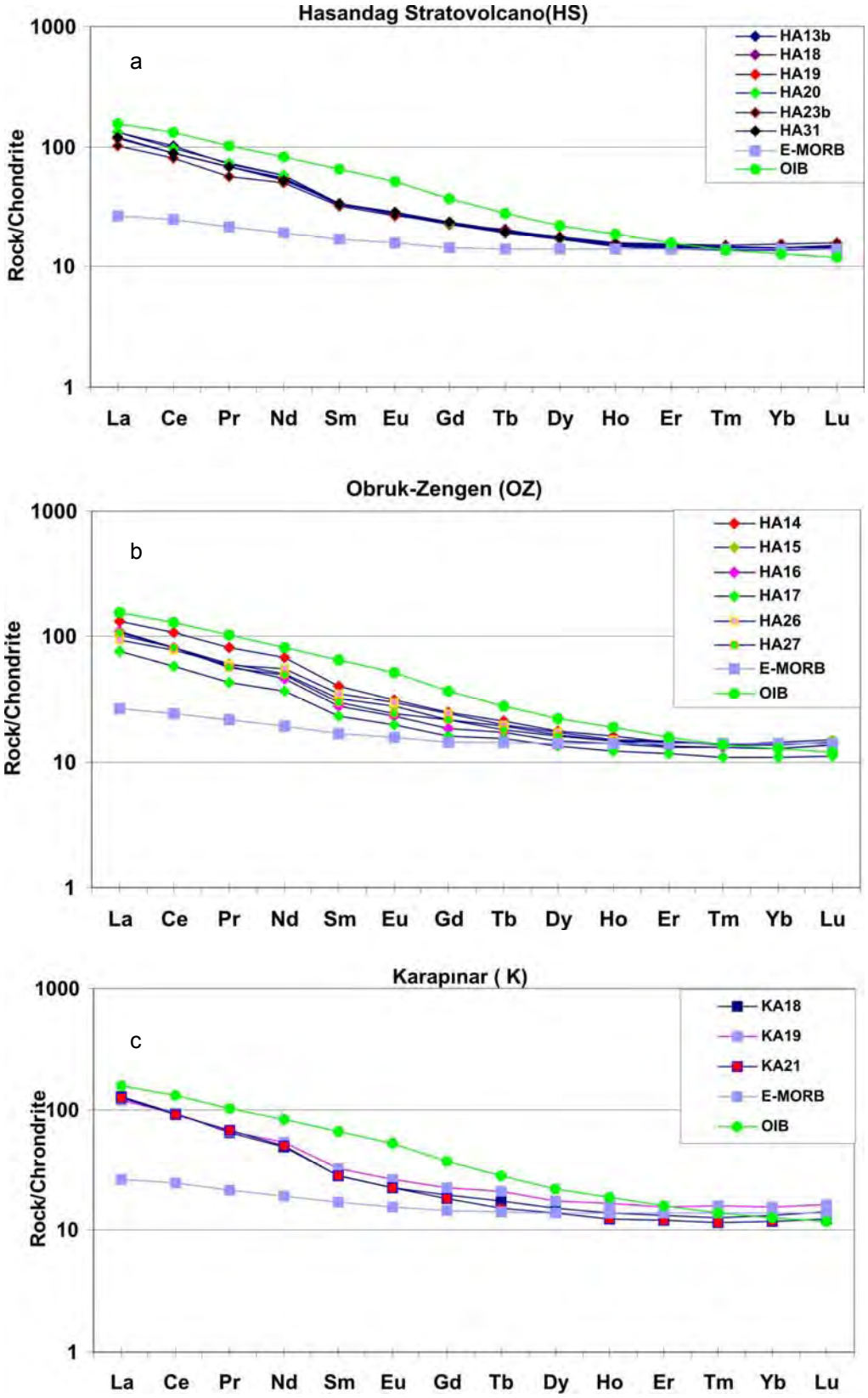

Figure 5.13: Normalized -according to Chondrite- REE spider diagram of the Southwestern Cappadocia Volcanism (a) HS, (b) OZ, (c) K (Normalized values are the same as in Figure 5.12)

5.2. Isotope Geochemistry

Isotopic compositions (Sr-Nd-Pb-O) of the Erciyes stratovolcano (ES) and the Southwestern Cappadocia Volcanism, which consists of Hasandağ stratovolcano (HS), Obruk-Zengen (OZ), Karapınar (K) were analyzed and details of the results are given below. The detailed steps of the regarded analytical techniques can be found in the section 1.4.2. Isotopic features of the samples in the region will be presented related to their region following the same order as in the major, trace and REE analysis section 5.1.

5.2.1. Sr-Nd-Pb-O Isotope Geochemistry

This section will be given in 2 major groups as previously given in major, trace and REE elements. These groups are: i) ES, which is presented in 2 groups as LDDS *(Less differentiated dated samples)* and MDDS *(More differentiated dated samples),* ii) Southwestern Cappadocia volcanism (HS, OZ and K).

5.2.1.1. Erciyes Stratovolcano

From dated 14 samples of the ES with 2 different sections of the sample ER27 were analyzed for Sr-Nd isotopes, the results are given in Table 5.7. $^{87}Sr/^{86}Sr$ isotope and $^{143}Nd/^{144}Nd$ isotope ratios vary between (0.703609-0.705084) and (0.512652- 0.512875) in LDDS, and (0.704509- 0.704875) and (0.512685 -0.512718) in MDDS, respectively.

The Sr-Nd ratios of ES with the volcanics from different regions (Society Islands, Dewey et al., (1990); Kerguelen oceanic island basalts; Gautier et al., (1990); MORB, Cohen et al., (1992); Big Pine, Ormerod et al., (1988); Andean basaltic rocks, Hickey et al., (1986); West Anatolian basaltic volcanics, Aldanmaz et al., (2000); basalts form Mount Nemrut -Eastern Anatolia-, Çubukçu, (2008) (are shown together in (Figure 5.14). ES volcanics present a clear Sr negative trend while Nd ratios are in slightly increasing (Figure 5.14). In addition to that, the samples are plotted in the mantle area and according to the diagram, their only source material is mantle. The oldest sample ER13 (1695 ka) represents the most possible depleted mantle source compare to other younger phases of the magmatisms.

Isotopic compositions of Erciyes stratovolcano have relatively higher $^{87}Sr/^{86}Sr$ and lower $^{143}Nd/^{144}Nd$ values than OIB and bulk earth (Figure 5.14). Samples of the ES show more likely similar values with Kerguelen island basalts (Gautier et al., 1990) and Society island lavas (Dewey et al., 1990). Kerguelen Islands' samples have a higher $^{87}Sr/^{86}Sr$ and lower $^{143}Nd/^{144}Nd$ values than oceanic island basalts (OIB) and bulk earth composition. It's unlikely that these volcanics were contaminated from continental crust especially considering their oceanic derivation environment. This is related to the enriched parts of the mantle from the volatiles and mantle metasomatism during the subduction (Gautier et al., 1990).

Table 5.7: Age (ka), SiO_2 , isotope (Sr, Nd, Pb, O) values of ES

Samples	Groups	Age (ka)	SiO_2	εNd	$^{87}Sr/^{86}Sr$	$^{143}Nd/^{144}Nd$	$(^{206}Pb/^{204}Pb)$	2sigma	$(^{207}Pb/^{204}Pb)$	2sigma	$(^{208}Pb/^{204}Pb)$	2sigma	d18OWR	2sigma
ER 1	LDDS	93±11	54.34	0.28	0.705084	0.512652	18.8976	0.0008	15.6715	0.0010	39.0187	0.0033	6.89	
ER 2		—	55.33	—	—	—	—	—	—	—	—	—	—	—
ER 3	LDDS	352±9	53.13	1.65	0.704537	0.512722	18.8756	0.0012	15.6551	0.0012	38.9547	0.0033	6.82	
ER4		—	62.02	—	—	—	—	—	—	—	—	—	—	—
ER5		—	60.25	—	—	—	—	—	—	—	—	—	—	—
ER9	MDDS	< 1 (*TU-ER -23*)	57.34	1.41	0.704511	0.512710	18.9158	0.0008	15.6626	0.0008	39.0074	0.0023	6.51	
ER10	LDDS	297±15	53.09	1.78	0.704587	0.512729	18.8962	0.0008	15.6662	0.0008	38.9897	0.0025	6.46	
ER11	MDDS	<1	56.70	1.14	0.704710	0.512696	18.9201	0.0010	15.6808	0.0009	39.0520	0.0032	6.37	
ER13	LDDS	1695±37	48.89	4.63	0.703609	0.512875	18.9497	0.0014	15.6458	0.0013	38.9330	0.0036	6.05	
ER16		—	62.70	—	—	—	—	—	—	—	—	—	—	—
ER17	MDDS	45±5	55.46	1.13	0.704534	0.512696	18.8966	0.0016	15.6726	0.0015	39.0013	0.0039	6.79	
ER20	MDDS	115±7	54.53	1.02	0.704697	0.512690	18.8926	0.0009	15.6723	0.0009	39.0055	0.0027	6.80	
ER22	MDDS	40±7	57.37	0.95	0.704769	0.512686	18.9133	0.0010	15.6835	0.0009	39.0562	0.0027	6.47	
ER25		—	57.15	—	—	—	—	—	—	—	—	—	—	—
ER26	MDDS	25±8 (*TU-ER-45*)	56.43	0.93	0.704875	0.512685	18.8979	0.0012	15.6745	0.0011	39.0206	0.0037	6.51	
ER27(1)	MDDS	—	55.01	1.10	0.704796	0.512695	18.8930	0.0020	15.6725	0.0016	39.0139	0.0041	6.15	
ER27(2)	MDDS	—	55.01	1.13	0.704817	0.512696	18.8931	0.0022	15.6723	0.0021	39.0126	0.0052	6.15	
ER29	LDDS	13±5	52.45	0.63	0.704876	0.512670	18.9099	0.0014	15.6850	0.0014	39.0548	0.0044	6.63	
ER30	MDDS	102±6.6 (*TU-ER-30*)	55.07	1.57	0.704509	0.512718	18.9452	0.0008	15.6641	0.0009	39.0371	0.0028	7.12	
ER32	MDDS	707±20	56.22	1.19	0.704557	0.512699	18.9022	0.0019	15.6748	0.0015	39.0246	0.0044	6.00	

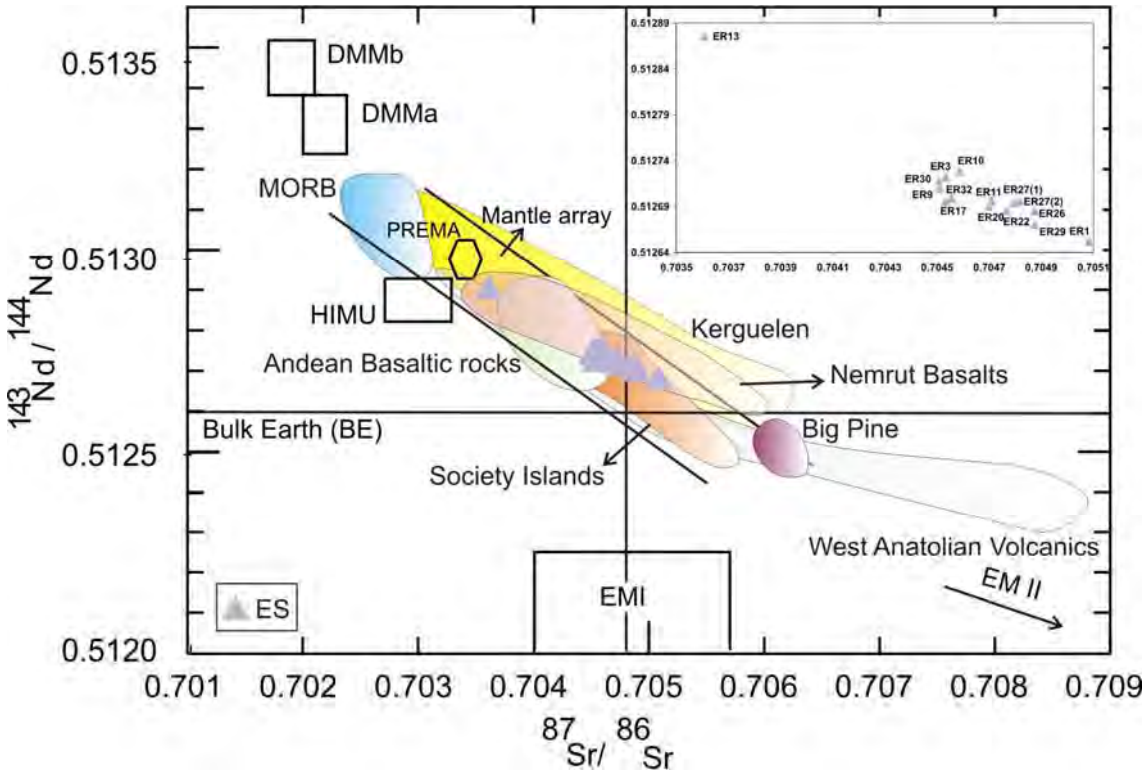

Figure 5.14: Presentation of Erciyes stratovolcano on Sr-Nd correlation diagram (Data sources; Ito, White and Göbel (1987); Chaffey, Cliff and Wilson (1989); Gautier et al.,1990; Dewey et al., 1990; Cohen et al.,1992; Ormerod et al.,1988; Hickey et al.,1986; Aldanmaz et al., 2000; Çubukçu, 2008. Mantle array and Bulk Earth, Wassenburg et al., (1981) and Faure (1986); EMI and EMII, Zindler and Hart (1986))

Age and isotope data have a great importance to understand spatio-temporal evolution of the region. Detailed examination is performed inter groups of the all ES samples (Figure 5.15).

In LDDS, except the oldest sample (ER13), Sr-isotopes are increasing, and the Nd-isotopes are decreasing by younger volcanism (Figure 5.15a-c). LDDS samples (ER3; ER10), which are in similar age interval and similar tendencies on major-trace element variation diagrams present different isotopic ratios. Sr and Nd isotope ratios are increasing from NE (ER3) to SW (ER10) (Figure 2.2; Figure 5.15 a-c).

In MDDS, all samples present calcalkaline features and except ER32 they have limited age interval (Table 5.7). The youngest samples ER9 and ER11, which have slightly different $^{87}Sr/^{86}Sr$ ratios and $^{143}Nd/^{144}Nd$ ratios from each other, respectively (Table 5.7; Figure 5.15b-d).

Another same age interval sample couples are ER17 and ER22. ER22 is more radiogenic in terms of $^{87}Sr/^{86}Sr$ than ER17 (Figure 5.15b). No significant differences in Nd-isotopes (Figure 5.15d).

According to the age vs. Sr-Nd isotope diagrams, slightly different trends are seen between LDDS and MDDS groups (Figure 5.15). LDDS age interval is more extended than MDDS (Table 5.7). Sr-Nd isotopes vs. Age relations are more systematic in LDDS than MDDS. Calcalkaline ER26 (MDDS) and alkaline ER29 (LDDS) are the same age interval and $^{87}Sr/^{86}Sr$ isotope ratio, but ER29 is less radiogenic $^{143}Nd/^{144}Nd$ than ER26 (Figure 5.15c-d).

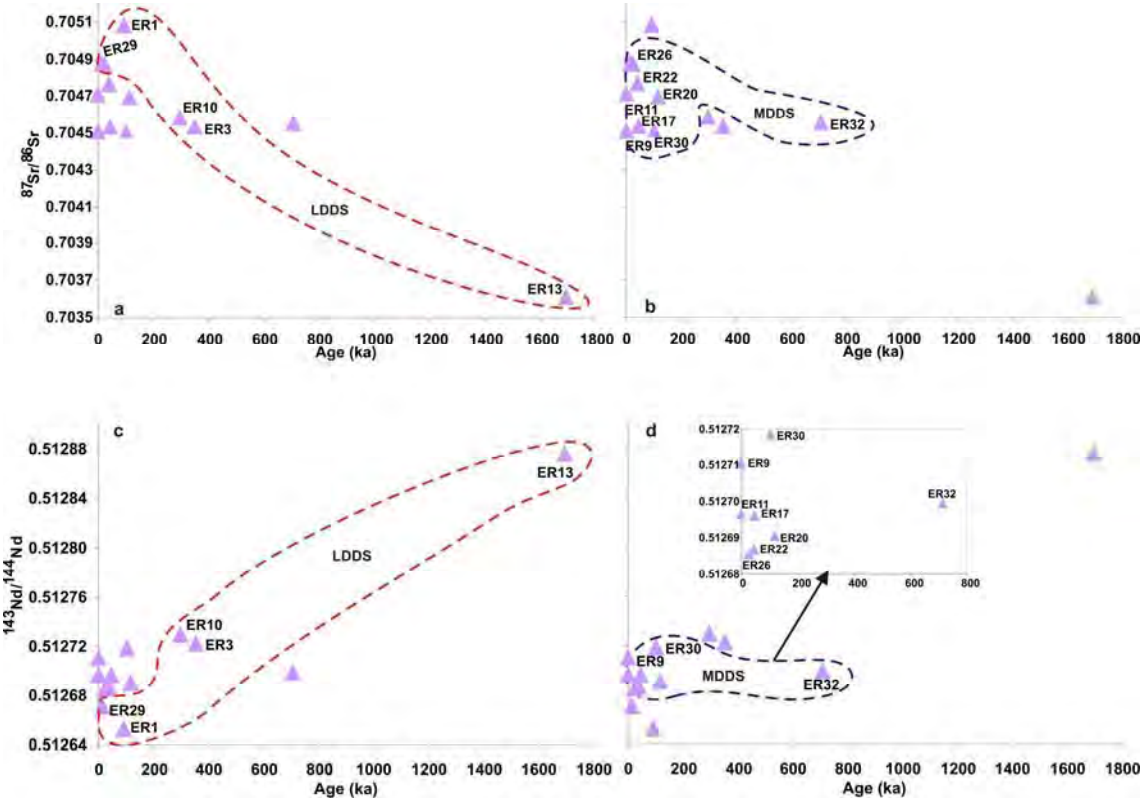

Figure 5.15: (a) $^{87}Sr/^{86}Sr$ vs. Age (ka) of LDDS group, (b) $^{87}Sr/^{86}Sr$ vs. Age (ka) of MDDS group, (c) $^{143}Nd/^{144}Nd$ vs. Age (ka) of LDDS group, (d) $^{143}Nd/^{144}Nd$ vs. Age (ka) of MDDS group

In Figure 5.16a, samples from ES are plotted to age vs differentiation diagram to point out the general differentiation differences by variable age data. In addition to understand possible involvement of crust, Sr and Nd isotopic data plotted against SiO_2 (Figure 5.16b-c). In LDDS group, except the youngest sample ER29, SiO_2 and $^{87}Sr/^{86}Sr$ values are increasing, and $^{143}Nd/^{144}Nd$ values are decreasing from

older to younger (Figure 5.16). Except the oldest sample ER32 (MDDS), SiO_2 increasing, from older to younger (Figure 5.16a). In MDDS group, regardless of age data, a small dispersion is observed in Sr-Nd vs. SiO_2 plots (Figure 5.16b-c). According to the age, Sr-Nd vs. SiO_2 diagrams (Figure 5.16), slightly different trends are seen between LDDS and MDDS groups like their major element values.

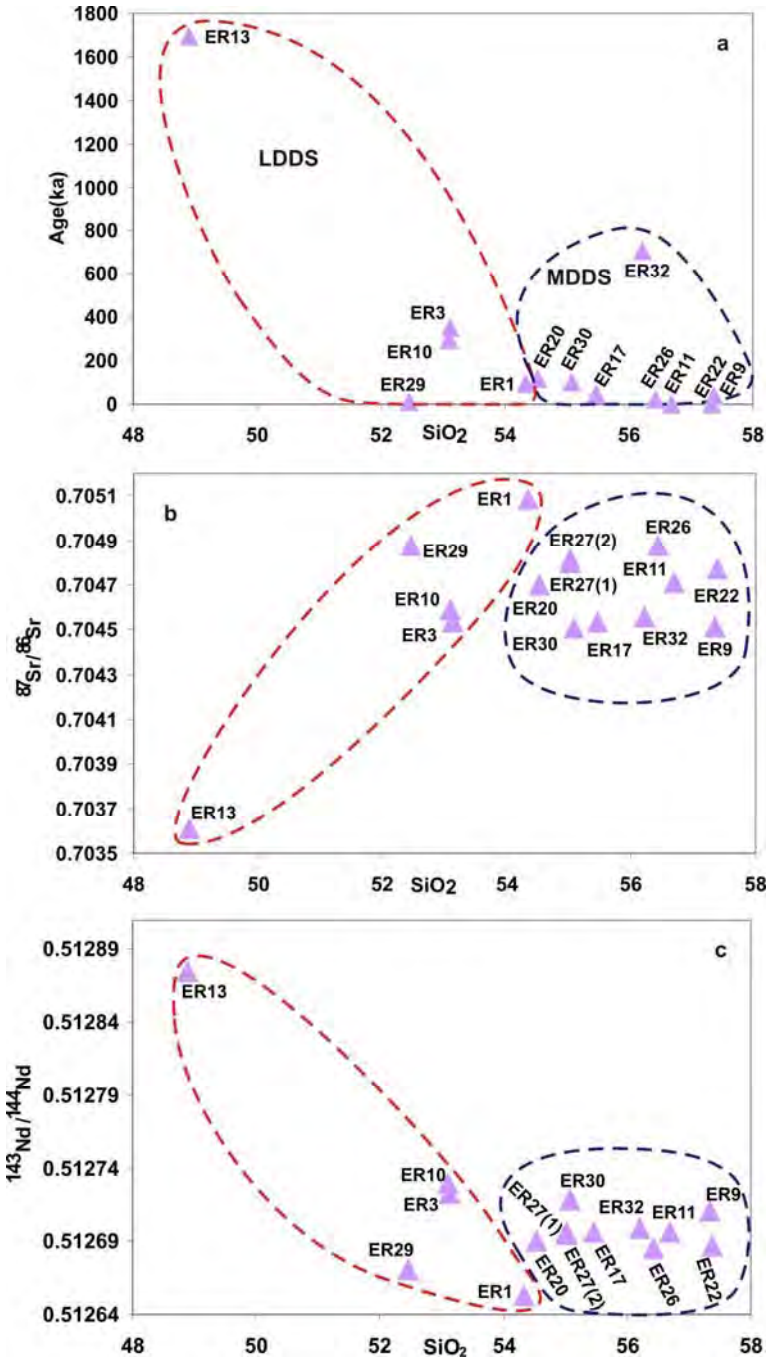

Figure 5.16: (a) Age(ka) vs. SiO_2, (b) $^{87}Sr/^{86}Sr$ vs SiO_2, (c)$^{143}Nd/^{144}Nd$ vs. SiO_2 diagram of ES

15 samples from ES were analyzed for $^{206}Pb/^{204}Pb$, $^{207}Pb/^{204}Pb$, $^{208}Pb/^{204}Pb$ and details are given in Table 5.7. As mentioned previous sections, the sample ER27 analyzed such as ER27 (1) and ER27 (2) due to its banded texture. Samples from the ES, which are separated to their different differentiation level, were examined in two groups (MDDS and LDDS) in terms of their Pb-isotopes. $^{206}Pb/^{204}Pb$, $^{207}Pb/^{204}Pb$ and $^{208}Pb/^{204}Pb$ isotope ratios vary in between 18.90-18.95; 15.65-15.68; 38.93-39.05 for LDDS and 18.89-18.95; 15.66-15.68; 39.00-39.06 respectively (Table 5.7).

Samples of the ES plotted in the $^{207}Pb/^{204}Pb$ vs. $^{206}Pb/^{204}Pb$ diagram indicating that Enriched Mantle (EMII) area above the Northern Hemisphere Reference Line (NHRL) is characteristic for the region (Figure 5.17). This EMII area is known as the enriched mantle source which is enriched by compounds such as sediment, continental crust, altered oceanic crust (Rollinson, 1993; Zindler and Hart, 1986).

Furthermore, Pb isotope data are also evaluated with Sr and Nd isotopic data mentioned in detail above (Figure 5.14). In $^{87}Sr/^{86}Sr$ vs. $^{206}Pb/^{204}Pb$ diagram only ER13 (LDDS) is seen to the border of the MORB composition, other LDDS and MDDS samples show a linear distribution (Figure 5.18). $^{143}Nd/^{144}Nd$ vs. $^{206}Pb/^{204}Pb$ diagram point out that, except ER13 others are plotted out the MORB area (Figure 5.19).

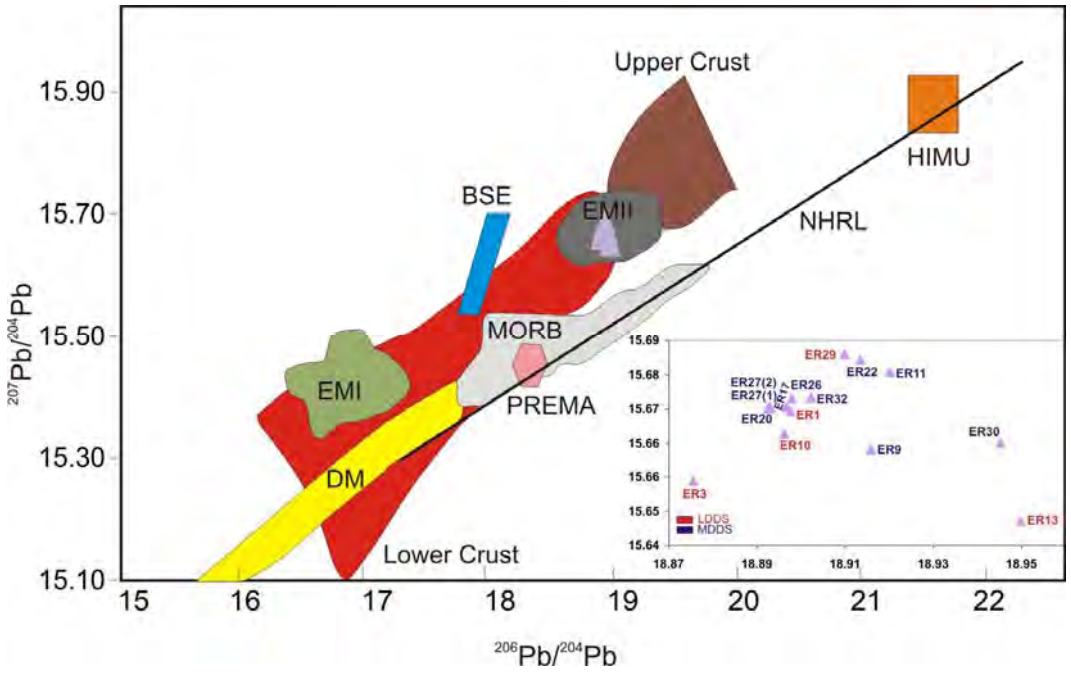

Figure 5.17: Erciyes stratovolcano $^{206}Pb/^{204}Pb$ vs. $^{207}Pb/^{204}Pb$ isotope correlation diagram (Data sources: Rollinson, 1993 (MORB: Mid-oceanic Ridge Basalts EMI and EMII: Enriched Mantle, DM: Depleted Mantle, PREMA: Prevalent Mantle, HIMU: High μ Mantle, BSE: Bulk Earth, Lower and Upper Crust, NHRL: Northern Hemisphere Reference Line)

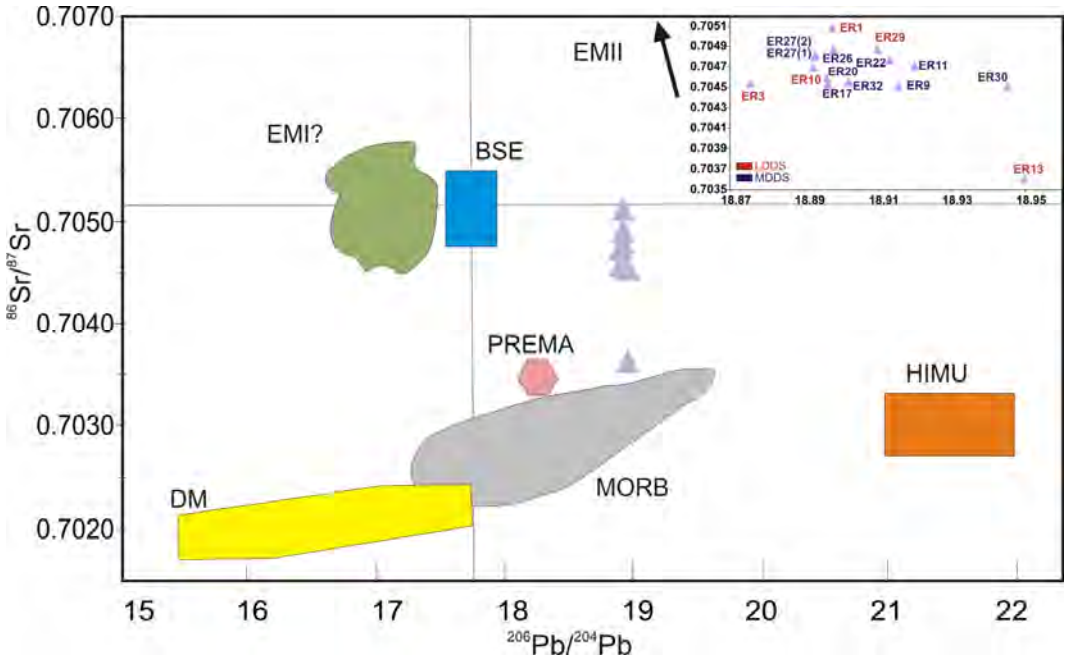

Figure 5.18: Erciyes stratovolcano $^{206}Pb/^{204}Pb$ vs. $^{86}Sr/^{87}Sr$ isotope correlation diagram. (Data sources and symbols are the same as given in Figure 5.17)

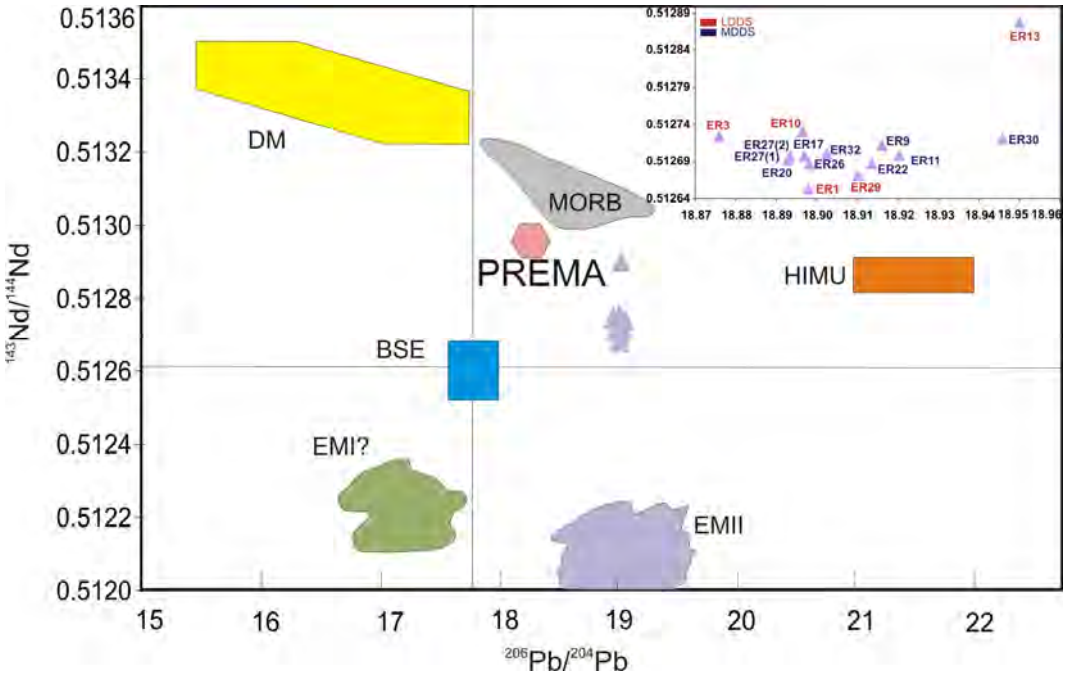

Figure 5.19: Erciyes stratovolcano $^{206}Pb/^{204}Pb$ vs. $^{143}Nd/^{144}Nd$ isotope correlation diagram. (Data sources and symbols are the same as given in Figure 5.17)

Correlation diagram based on $^{206}Pb/^{204}Pb$ vs. Age (ka) is given in Figure 5.20. According to the diagram, more regular trend is noted than observed in $^{87}Sr/^{86}Sr$ vs. Age (ka) (Figure 5.15). From oldest sample to the youngest one, positive trend in $^{206}Pb/^{204}Pb$ isotope ratio is characteristic in LDDS group, except sample ER13 (Figure 5.20). In LDDS group, $^{87}Sr/^{86}Sr$ is relatively higher, in where $^{206}Pb/^{204}Pb$ ratio of the sample ER29 spikes. It is also likely that, by the younger ages in MDDS except sample ER32, $^{206}Pb/^{204}Pb$ ratio increases as seen in $^{87}Sr/^{86}Sr$ vs. Age (ka) (Figure 5.15). Along the similar age samples ER9 (<1ka) and ER11 (<1ka), and same age interval couples, from older to younger, (ER17 (45±5 ka)→ER22 (40±7ka) and ER20 (115±7ka)→ER30 (102±7ka) positive correlation in $^{206}Pb/^{204}Pb$ isotopes are common (Figure 5.20).

$^{206}Pb/^{204}Pb$ vs. SiO_2 diagram (Figure 5.21) is shown to understand the magmatic differentiation effect on the magmatic evolution of the samples. In this diagram, negative Pb isotope correlation in LDDS and positive correlation in MDDS are observed. In addition to that, the correlation is not regular in contrast to the age data of the ES samples.

Pb-isotope ratios are known as fingerprints of crustal contamination Ellam and Harmon, 1990) as O-isotopes. Especially, positive correlation of Pb-isotopes vs. differentiation in the MDDS group is likely pointing out crustal contamination took place during the formation of the magma.

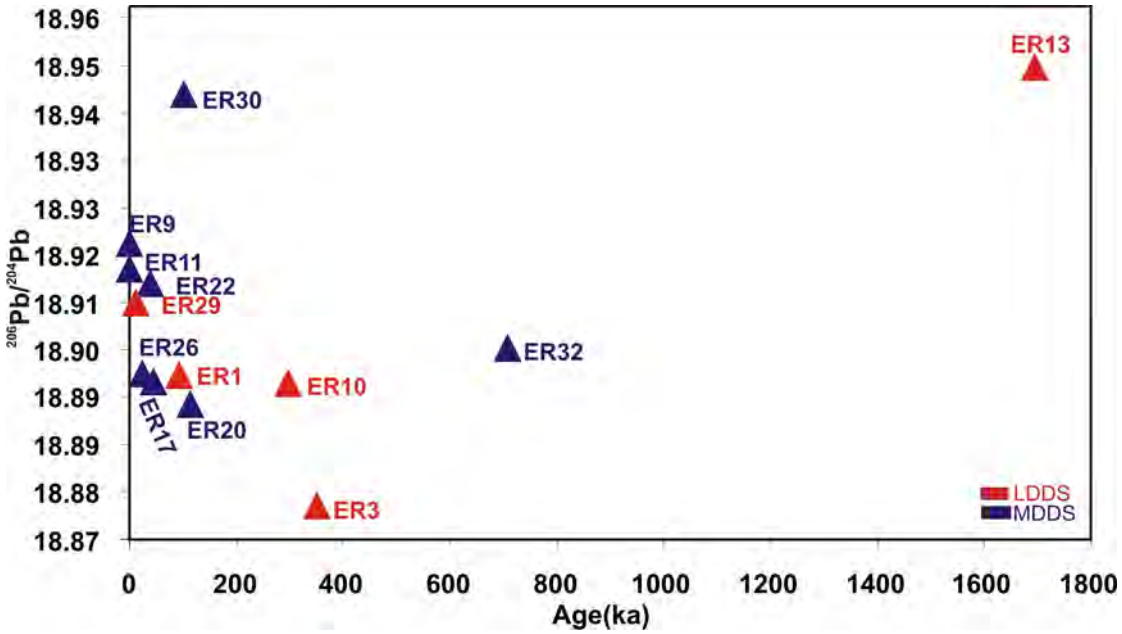

Figure 5.20: Erciyes stratovolcano $^{206}Pb/^{204}Pb$ vs. Age (ka) diagram

In some special cases, such as tracing the sub-levels of the upper mantle (e.g. Sub-Continental Lithosphere) with Sm/Nd and Pd-isotopic systems are not the most effective isotopic fingerprints. To discuss the details of the source, additional tracers as O-stable isotope systematic are needed. Therefore, isotope results are also combined and compared with O-isotopes (WR). $\delta^{18}O$ distributions of the ES is given in (Table 5.7). $\delta^{18}O$ values of the LDDS vary range about +6.05-6.89‰ and +6.00-7.12‰ for MDDS (Table 5.7). The highest $\delta^{18}O$ value (7.1‰) is seen in the sample ER30 indicating a possible alteration observed in thin sections (Table 3.1) and higher LOI values support this as well (Table 5.1).

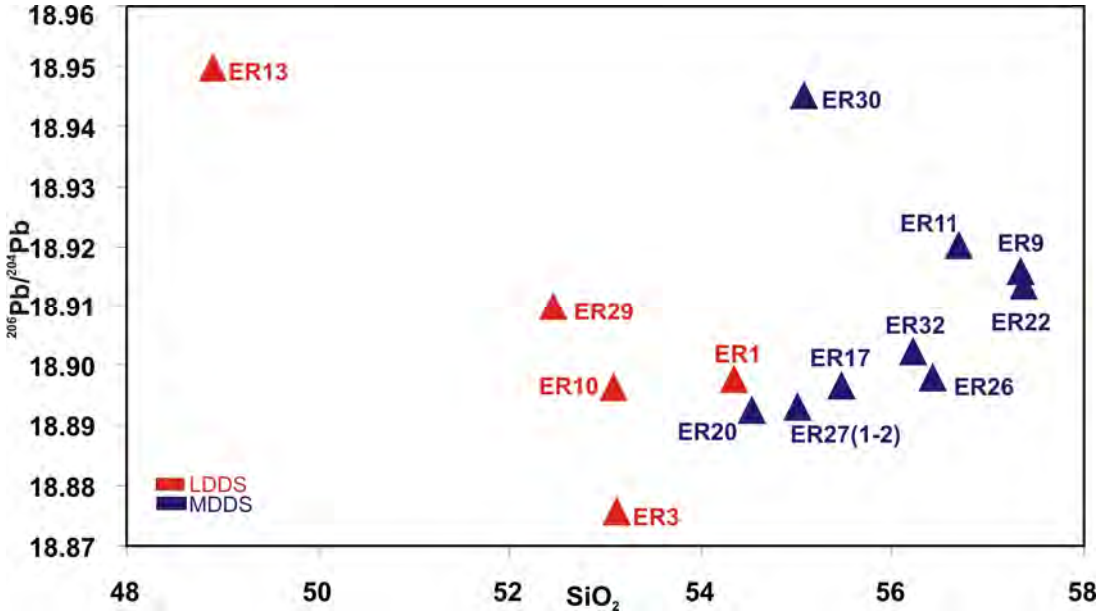

Figure 5.21: Erciyes stratovolcano SiO_2 vs. $^{206}Pb/^{204}Pb$ isotope diagram

To compare and understand the spatio-temporal evolution of the ES samples, O isotope variation vs. Age (ka) diagram is shown in Figure 5.22. According to the diagram, no significant correlation is observed in LDDS group, however the oldest sample ER13 plots in the lowest O-isotope side, when the sample ER1 display highest $\delta^{18}O$ value (Figure 5.22). In the similar age group samples of LDDS, ER3 displays higher $^{18}O/^{16}O$ isotope ratios than ER10 (Table 5.7). The oldest sample (ER32) in MDDS group has the lowest $\delta^{18}O‰$ value as seen the oldest sample of LDDS (ER13). $\delta^{18}O‰$ values decrease in the older sample couples of ER30—ER20 to the to younger sample couples of ER17—ER22 and ER9—ER11 (Figure 5.22).

$\delta^{18}O$ vs. $^{87}Sr/^{86}Sr$ diagram of the ES samples display co-variation, however it is clearly noted that LDDS group samples tend positive correlation against Sr-isotopes (Figure 5.23a), in where similar tendency is seen against SiO_2 variation (Figure 5.23b). In MDDS group, the similar age samples disperse in terms of $\delta^{18}O‰$ and present slightly negative correlation in contrast to Sr-isotopes and SiO_2 (Figure 5.23b).

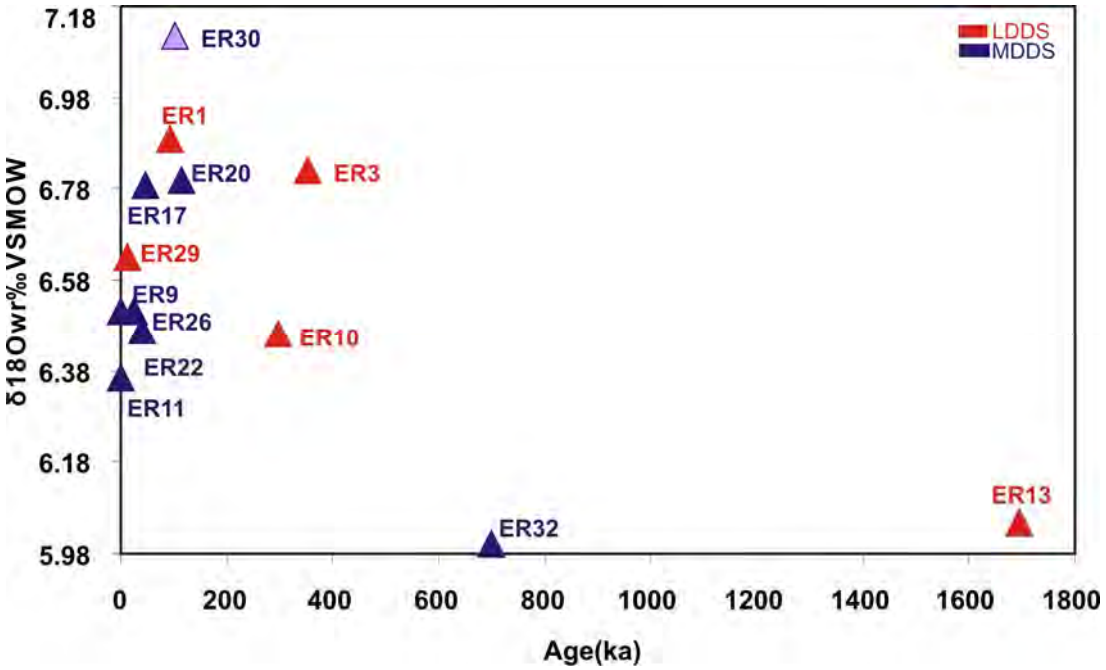

Figure 5.22: $\delta^{18}O‰VSMOW$ vs. Age (ka) correlation diagram of Erciyes stratovolcano

According to $\delta^{18}O‰$ vs. $^{206}Pb/^{204}Pb$ isotope correlation diagram, $^{206}Pb/^{204}Pb$ isotope ratio increases with $\delta^{18}O‰$ decrease in LDDS group (Figure 5.24). In MDDS group, possible positive tendency is seen between O-Pb isotopes (Figure 5.24).

Based on analysis of O-isotope data for ES samples, $\delta^{18}O‰$ variation of + 6.00 to +7.12‰ points out these values are slightly higher than MORB (+ 5.3- 6.2‰ [142]), and OIB (+4,9-6‰ Eiler et al.,1996a ; Zindler and Hart ,1986) values, moreover these values do not fit in the scattered $\delta^{18}O$ values (+4,8-12‰ Harmon et al.,1981; Davidson and Harmon,1989) of subduction related volcanism.

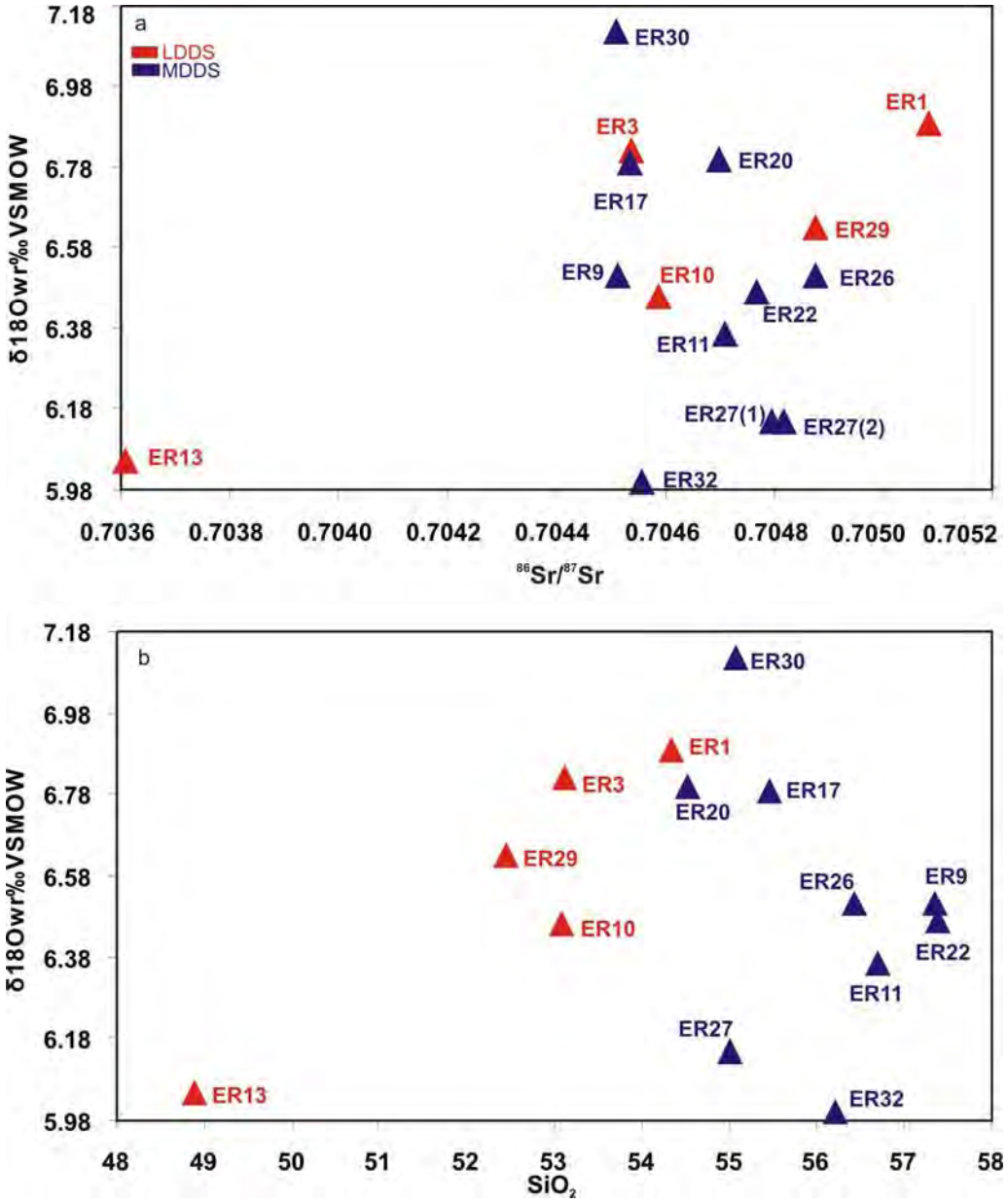

Figure 5.23: (a) $\delta^{18}O‰$ VSMOW vs. $^{87}Sr/^{86}Sr$ isotope correlation diagram, (b) $\delta^{18}O‰$ VSMOW vs. SiO_2 diagram of Erciyes stratovolcano

Based on similar age samples, no significant variation is observed, besides negative correlation in LDDS is more likely related to a contamination resulted by the lower Pb bearing crustal material (Ellam and Harmon, 1990).

5.2.1.2. Southwestern Cappadocia Volcanism

Sr, Nd, Pb, and O-isotope analysis of the Southwestern Cappadocia Volcanism consisting of three different volcanic areas (HS, OZ and K) are given in Table 5.8.

Based upon isotopic analytical results of the $^{87}Sr/^{86}Sr$ and $^{143}Nd/^{144}Nd$ isotopic geochemistry, ratios for HS vary (0.704625-0.704976; 0.512657-0.512718), OZ (0.704153-0.704711; 0.512723-0.512826), and K (0.705188-0.705502; 0.512602-0.512633), respectively (Table 5.8).

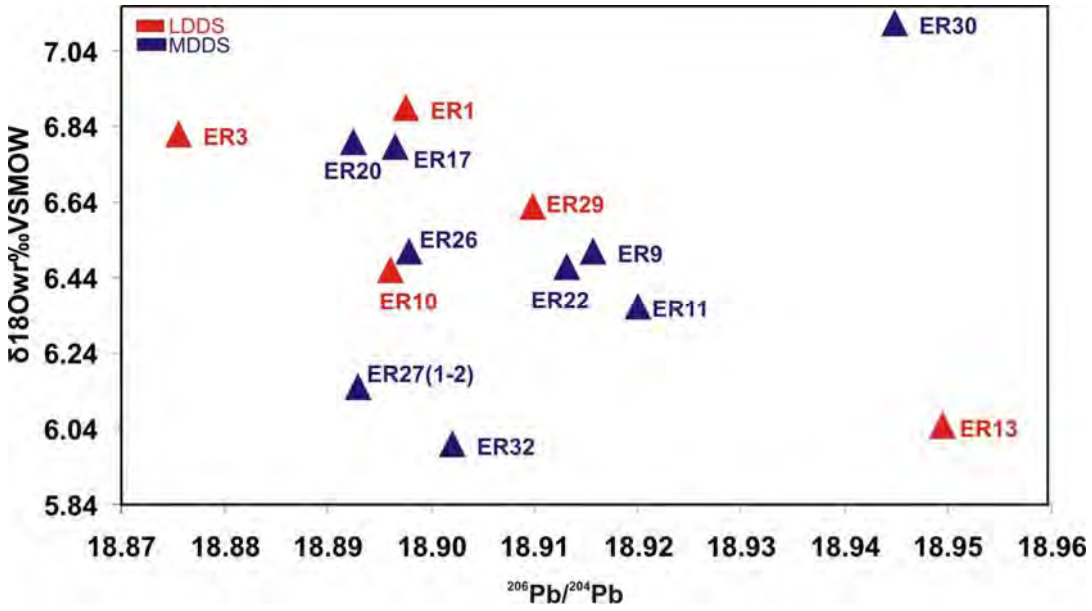

Figure 5.24: $\delta^{18}O‰VSMOW$ vs. $^{206}Pb/^{204}Pb$ isotope diagram of Erciyes stratovolcano

In comparison with other selected isotope data of the volcanic rocks from different parts of the earth. In $^{87}Sr/^{86}Sr$ vs. $^{143}Nd/^{144}Nd$ diagram, samples of the Southwestern Cappadocia are plotted in the mantle area presenting a clear negative correlation (Figure 5.25). Samples of the HS yield higher $^{87}Sr/^{86}Sr$ and lower $^{143}Nd/^{144}Nd$ isotopic ratios compare to OIB and bulk earth isotopic compositions.

HS samples have a higher, and exhibit similarities with Kerguelen (Gautier et al., 1990) and Society island (Dewey et al., 1990) lavas. OZ group is plotted along the mantle array (Figure 5.25). K samples comprise lowest end of the whole group in terms of Nd-isotopic values, besides they are plotted in highest Sr-isotope values as seen Society Islands' samples (Figure 5.25). Isotope values of ES have a higher $^{87}Sr/^{86}Sr$ and lower $^{143}Nd/^{144}Nd$ values (Figure 5.14) than OIB and bulk earth from the comparison data that are given in Figure 5.25. In addition to this, they show similarities with Kerguelen (Gautier et al., 1990), Society island (Dewey et al., 1990) and And basalts (Hickey et al., 1986).

Table 5.8: Age(ka),SiO2, isotope (Sr, Nd, Pb, O) and trace elements of Southwestern Cappadocia Volcanism

Samples	Groups	Age (ka)	SiO_2	εNd	$^{87}Sr/^{86}Sr$	$^{143}Nd/^{144}Nd$	$(^{206}Pb/^{204}Pb)$	2sigma	$(^{207}Pb/^{204}Pb)$	2sigma	$(^{208}Pb/^{204}Pb)$	2sigma	d18OWR
HA13b	HS	19±5	49.33	0.83	0.704952	0.512680	18.8997	0.0011	15.6704	0.0010	39.0109	0.0028	6.79
HA14	OZ	395±10	48.99	3.15	0.704333	0.512799	18.8602	0.0018	15.6411	0.0018	38.8905	0.0054	6.57
HA15	OZ	404±10	49.38	2.75	0.704319	0.512779	18.8800	0.0014	15.6557	0.0014	38.9507	0.0041	6.58
HA16	OZ	799±20	48.81	1.67	0.704711	0.512723	18.8913	0.0013	15.6567	0.0013	38.9699	0.0037	6.61
HA17	OZ	66±7	48.88	2.14	0.704472	0.512748	18.9134	0.0019	15.6536	0.0016	38.9799	0.0041	6.38
HA18	HS	105±5	51.06	1.57	0.704636	0.512718	18.8762	0.0014	15.6587	0.0015	38.9619	0.0046	6.73
HA19	HS	79±4	50.43	1.32	0.704729	0.512705	18.8871	0.0012	15.6568	0.0012	38.9646	0.0034	6.62
HA20	HS	57±5	50.36	0.38	0.704908	0.512657	18.8967	0.0014	15.6649	0.0018	38.9932	0.0043	6.63
HA23b	HS	543±12	50.69	1.47	0.704625	0.512714	—	—	—	—	—	—	6.92
HA26	OZ	675±16	49.39	3.67	0.704153	0.512826	18.8791	0.0015	15.6422	0.0021	38.9070	0.0041	5.88
HA27	OZ	331±7	56.24	1.74	0.704542	0.512727	18.9040	0.0021	15.6614	0.0017	38.9858	0.0050	7.27
HA31	HS	2±7	49.24	0.67	0.704976	0.512672	18.8979	0.0015	15.6598	0.0017	38.9910	0.0045	6.68
KA18	K	280±7.1 (*CK89-19*)	49.75	-0.18	0.705320	0.512629	18.9795	0.0011	15.6857	0.0009	39.1376	0.0027	6.75
KA19	K	<1	50.87	-0.10	0.705188	0.512633	18.9739	0.0016	15.6851	0.0015	39.1338	0.0038	6.59
KA21	K	163±10	52.40	-0.69	0.705502	0.512602	18.9960	0.0009	15.6976	0.0009	39.1868	0.0029	6.31

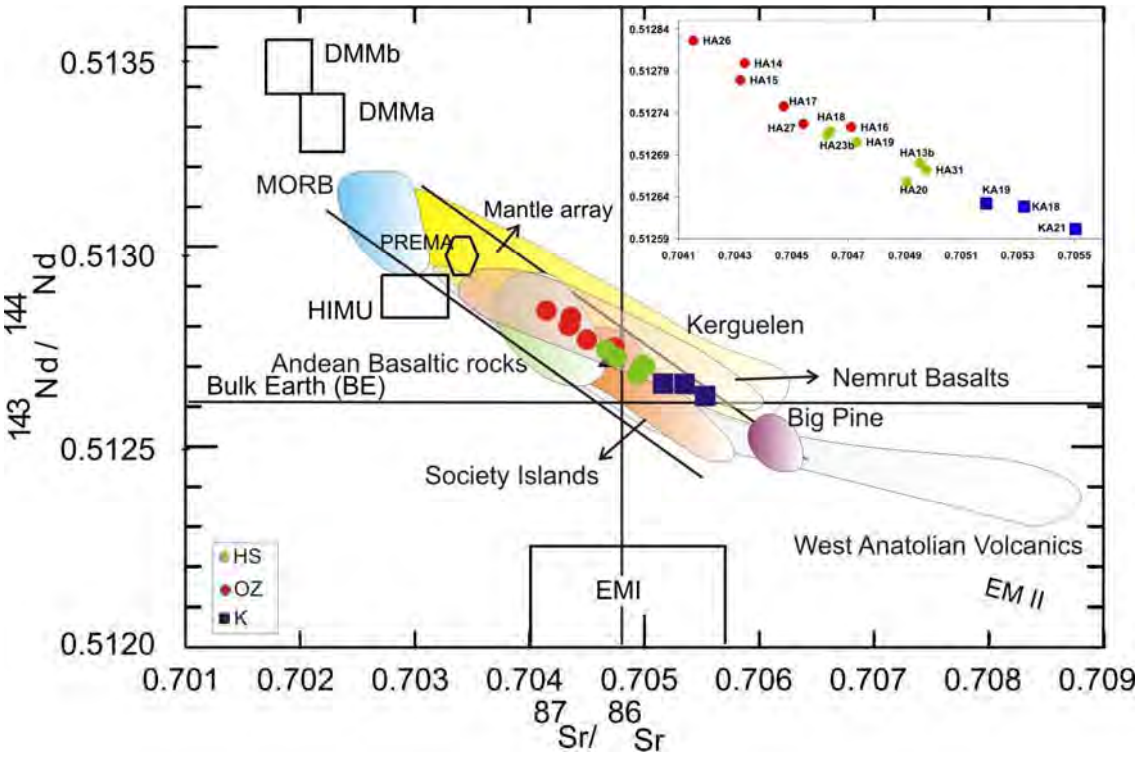

Figure 5.25: Presentation of Southwestern Cappadocia Volcanism on Sr-Nd correlation diagram (Data sources; Ito, White and Göbel(1987); Chaffey, Cliff and Wilson (1989); Gautier et al., 1990; Dewey et al., 1990; Cohen et al., 1992; Ormerod et al., 1988; Hickey et al., 1986; Aldanmaz et al., 2000; Çubukçu, 2008. Mantle array and Bulk Earth belong to Wassenburg et al., (1981) and Faure (1986), EMI and EMII, to Zindler and Hart (1986))

In the spatio-temporal evolution diagrams, as seen in Sr, and Nd-isotopes vs. Age (ka), HS display clear positive trend from oldest to youngest sample (HA23b to HA31) (Figure 5.26). OZ group which represents a wide age range and K samples have relatively constant relationship with the increase of the age. In alkaline HS samples, Sr-isotopes increase by the negative tendency of the SiO_2 (Figure 5.27). This relationship is mostly seen in crustal contaminated magmatic systems and/or another radiogenic contribution occurred in the source, which is enriched in $^{87}Sr/^{86}Sr$. No significant correlation between differentiation and spatio-temporal evolution is seen in OZ group, however similar age samples (HA14 and HA15) display similar SiO_2 values in contrast to Sr and Nd isotopes (Figure 5.26; Figure 5.27). Slightly positive trend in Sr and Nd isotopes is seen in the samples of K by increase of SiO_2 and age (Figure 5.26; Figure 5.27).

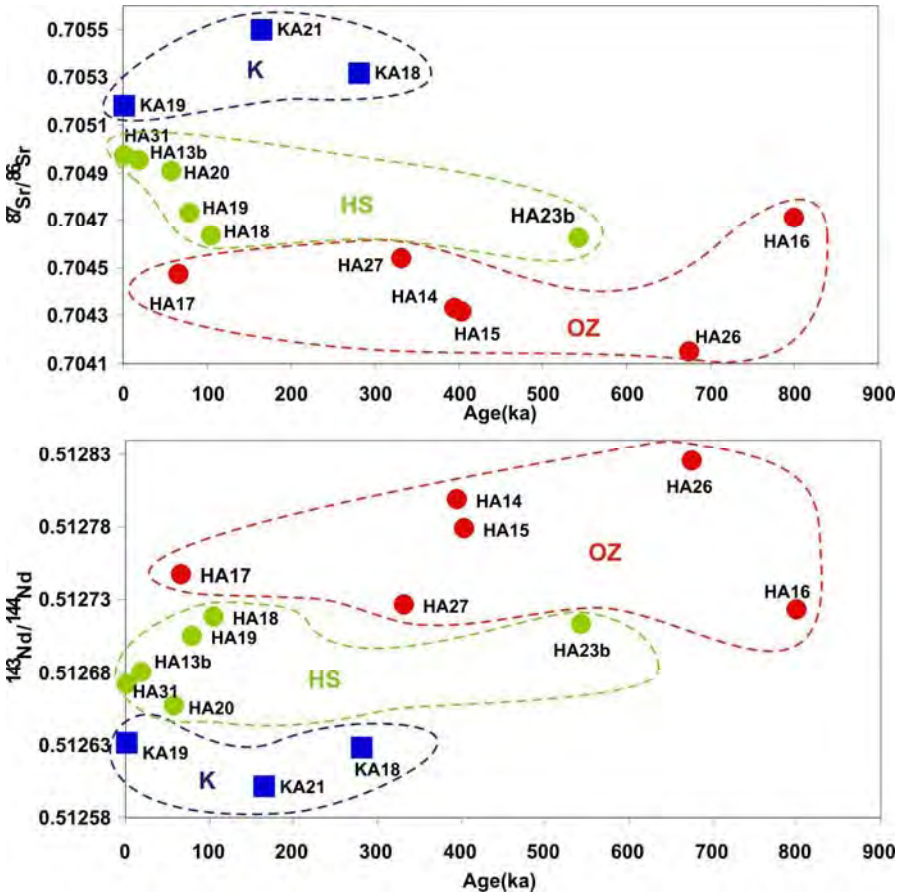

Figure 5.26: (a) $^{87}Sr/^{86}Sr$ vs. Age (ka), (b) $^{143}Nd/^{144}Nd$ vs. Age (ka) diagram of Southwestern Cappadocia Volcanism

From HS, OZ and K, $^{206}Pb/^{204}Pb$, $^{207}Pb/^{204}Pb$, $^{208}Pb/^{204}Pb$ isotope analyzes are performed (5, 6, and 3 samples, respectively) (Table 5.8) In HS samples, $^{206}Pb/^{204}Pb$, $^{207}Pb/^{204}Pb$, $^{208}Pb/^{204}Pb$ isotope ratios vary in between (18.88-18.90); (15.66-15.67); (38.96-39.01) (Table 5.8). Pb-isotope ratios between (18.86-18.91); (15.64-15.66); (38.89-38.98) and (18.97-19.00); (15.69-15.70); (39.13-39.19) are seen in OZ and K samples, respectively (Table 5.8). All the samples of the Southwestern Cappadocia Volcanism are plotted above Northern Hemisphere Reference Line (NHRL) (Figure 5.28). Samples of this volcanism are likely seen in the EMII area, which is defined as the mantle area enriched by sediments, continental crust, altered oceanic crust (Rollinson, 1993; Zindler and Hart, 1986).

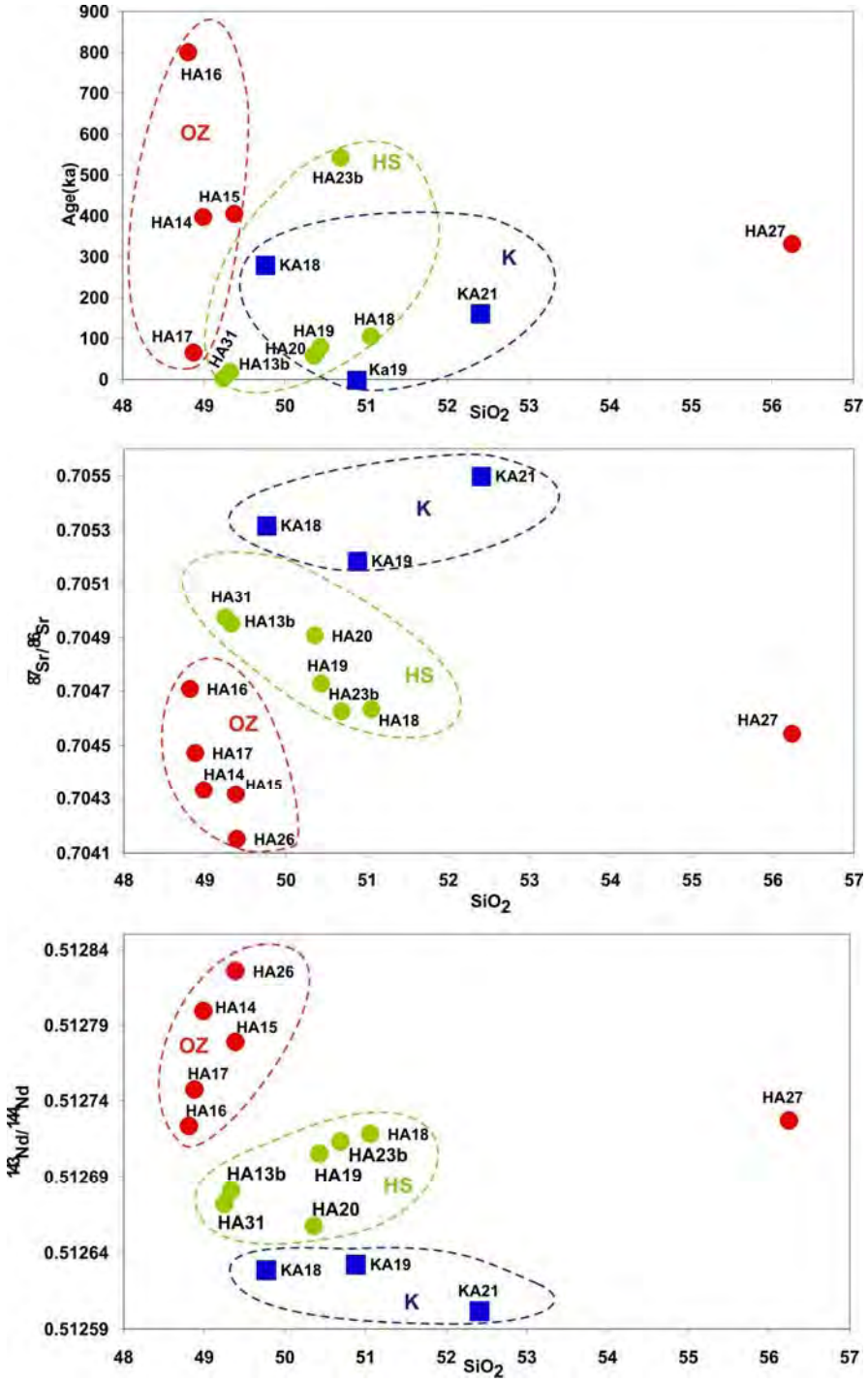

Figure 5.27: Southwestern Cappadocia Volcanism (a) Age (ka) vs. SiO_2 (b) $^{87}Sr/^{86}Sr$ vs. Age (ka) diagram c) $^{143}Nd/^{144}Nd$ vs. SiO_2

In HS and K samples, according to Sr-Pb and Nd-Pb isotope comparison diagrams, the samples of these groups are also compiled in EMII area (Figure 5.29; Figure 5.30). $^{87}Sr/^{86}Sr$ vs. $^{206}Pb/^{204}Pb$ and $^{143}Nd/^{144}Nd$ vs. $^{206}Pb/^{204}Pb$ diagrams of the OZ group display close relationship to MORB area (Figure 5.29; Figure 5.30).

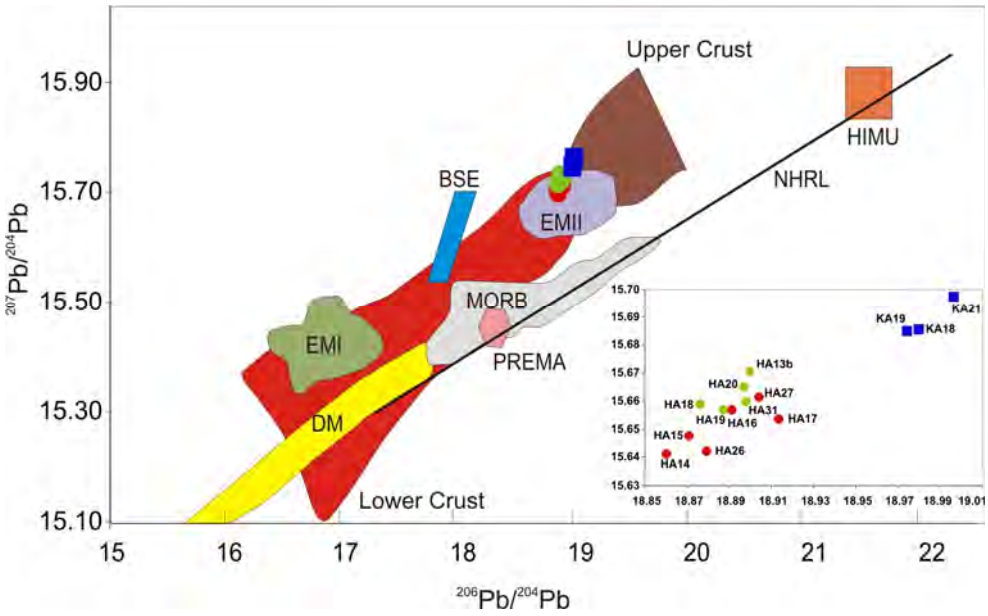

Figure 5.28: $^{206}Pb/^{204}Pb$ vs. $^{207}Pb/^{204}Pb$ isotope correlation diagram of HS, OZ and K samples belonging to Southwestern Cappadocia Volcanism (Data sources: Rollinson, 1993 (MORB: Mid-oceanic Ridge Basalts, EMI and EMII: Enriched Mantle, DM: Depleted Mantle, PREMA: Prevalent Mantle, HIMU: High μ Mantle, BSE: Bulk Earth, Upper-Lower Crust, NHRL: Northern Hemisphere Reference Line (Symbols are the same as given in 5.19)

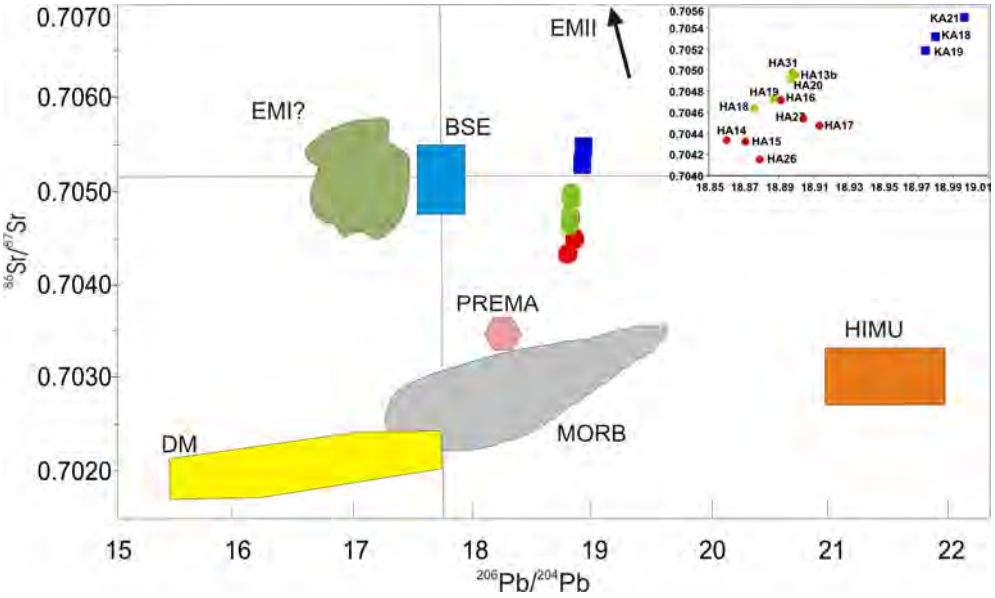

Figure 5.29: $^{206}Pb/^{204}Pb$ vs. $^{86}Sr/^{87}Sr$ isotope correlation diagram of HS, OZ and K samples belonging to Southwestern Cappadocia Volcanism. (Data sources and symbols are the same as given in Figure 5.28)

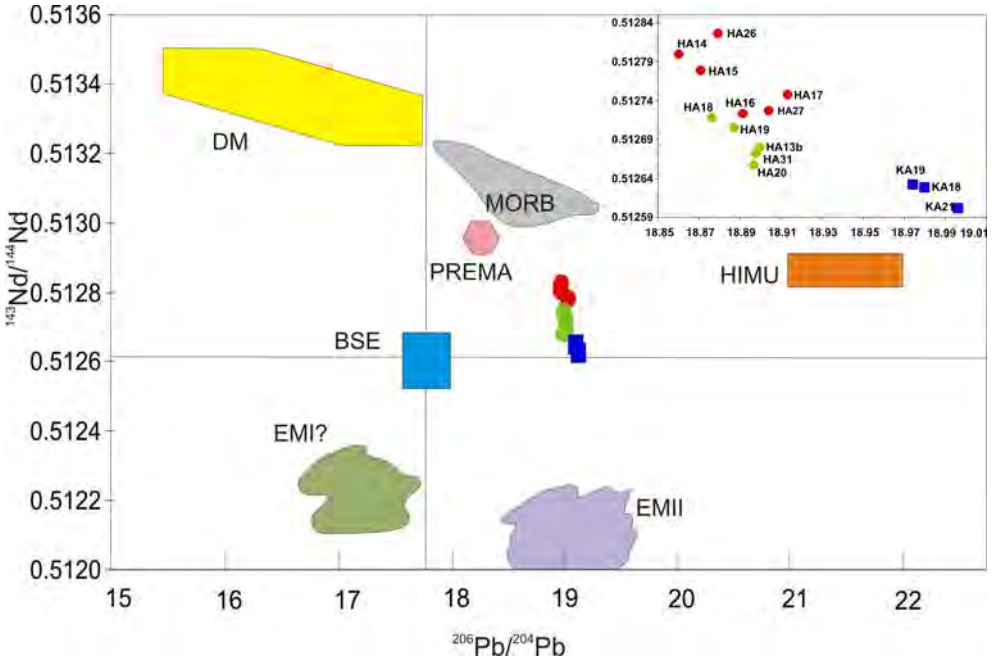

Figure 5.30: $^{206}Pb/^{204}Pb$ vs. $^{143}Nd/^{144}Nd$ isotope correlation diagram of HS, OZ and K samples belonging to Southwestern Cappadocia Volcanism(Data sources and symbols are the same as given in Figure 5.28)

In Figure 5.31, temporal evolution diagram for the HS clearly shows that $^{206}Pb/^{204}Pb$ ratio regularly increases from the oldest sample to the youngest sample and by the decrease of SiO_2 values (Figure 5.32) as well as in Sr-Nd vs. Age diagrams (Figure 5.26). Except the samples of HA14 and HA15 from OZ (Figure 5.31), $^{206}Pb/^{204}Pb$ isotope ratio increases from oldest to youngest samples as seen in Nd-isotope vs. Age diagram (Figure 5.26). In $^{206}Pb/^{204}Pb$ vs. SiO_2 diagram positive correlation is observed regardless of SiO_2 content (Figure 5.32).

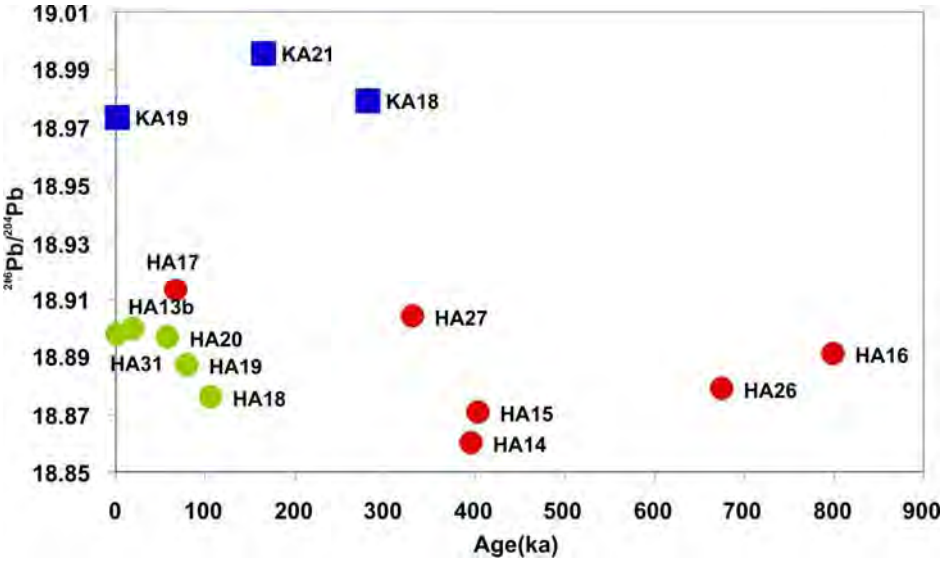

Figure 5.31: $^{206}Pb/^{204}Pb$ vs. Age (ka) diagram of HS, OZ and K samples belonging to Southwestern Cappadocia Volcanism

K group presents not a significant correlation in Pb-isotope vs. Age and SiO_2 diagrams however slightly positive correlation can be seen in the samples of KA18 to KA21 (Figure 5.31; Figure 5.32).

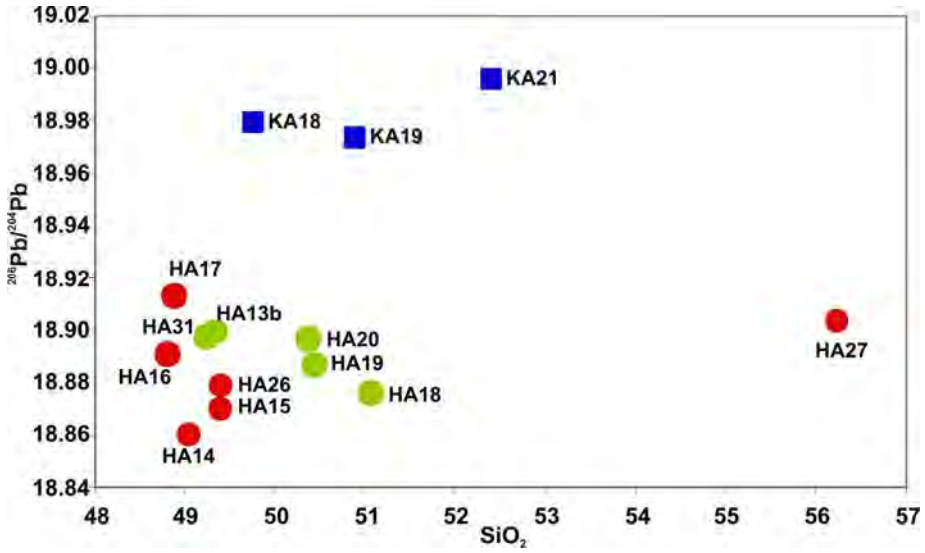

Figure 5.32: SiO_2 vs. $^{206}Pb/^{204}Pb$ isotope diagram of HS, OZ and K samples belonging to Southwestern Cappadocia Volcanism

$\delta^{18}O‰$ VSMOW isotope values of the Southwestern Cappadocia Volcanism (HS, OZ and K) is given in Table 5.8. O-isotope values range from (6.62-6.79); (5.88-7.27); and (6.31-6.75) in HS, OZ and K, respectively (Table 5.8). According to Ito et al., (1987), O-isotope values between 5.3-6.2‰ indicate MORB like signature. In the papers of Eiler et al. (1996) and Zindler et al. (1986) 4.9-6‰ O-isotope values remark OIB areas.

For subduction volcanism, Harmon et al. (1981) and Davidson and Harmon (1989) suggest 4.8-12‰ O-isotope values. Moreover, according to Eiler (2001), typical upper mantle and oceanic basalts' $\delta^{18}O‰$ values are also in between 6-7%. According to literature mentioned above, HS, OZ and K groups indicate upper mantle and oceanic basalt values.

In $\delta^{18}O‰$ VSMOW vs. Age (ka) diagram (Figure 5.33), HS group present no significant change from oldest to youngest samples. Slight differences between inter and intra groups is noted in the samples of the Southwestern Cappadocia Volcanism, however this doesn't affect the evolution history of the group (Figure 5.33). However, in the diagram of $\delta^{18}O‰$ VSMOW vs. $^{87}Sr/^{86}Sr$, clear discrimination due to Sr-isotope variation between the sub-groups of Southwestern Cappadocia Volcanism is seen (Figure 5.34).

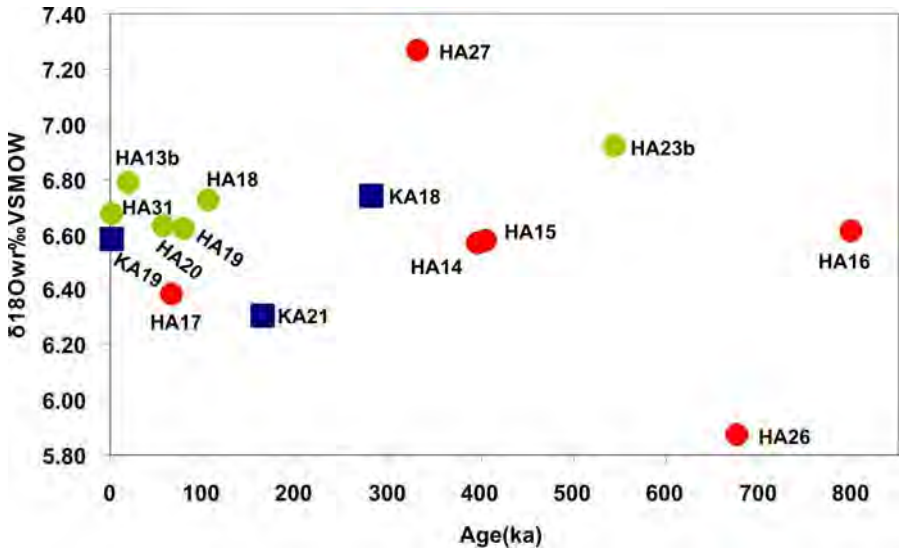

Figure 5.33: $\delta^{18}O‰$ VSMOW vs. Age (ka) diagram of HS, OZ and K samples belonging to Southwestern Cappadocia Volcanism

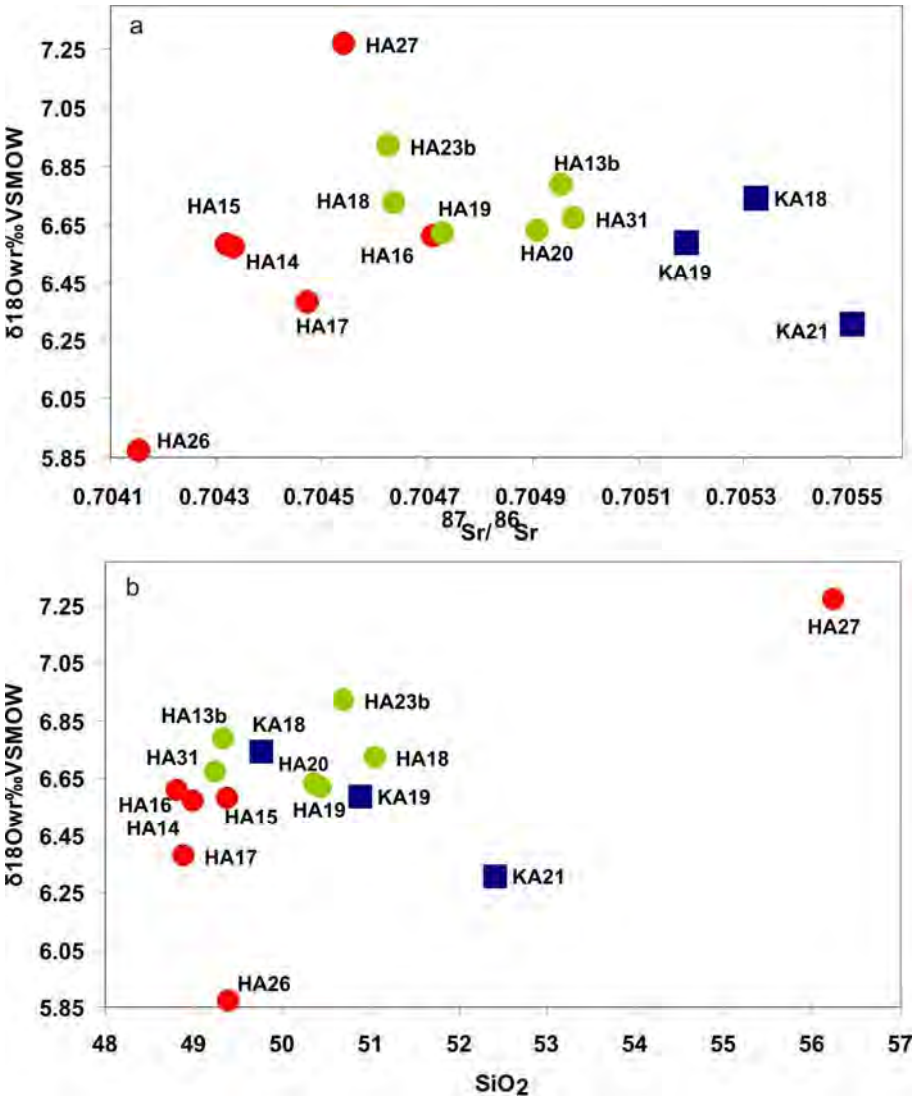

Figure 5.34: (a) $\delta^{18}O‰$ VSMOW vs. $^{86}Sr/^{87}Sr$ isotope correlation diagram, (b) $\delta^{18}O‰$ VSMOW vs. SiO_2 of HS, OZ and K samples belonging to Southwestern Cappadocia Volcanism

No significant correlation in HS can be observed when $\delta^{18}O‰$ VSMOW vs. $^{206}Pb/^{204}Pb$ isotope diagram is examined (Figure 5.35).

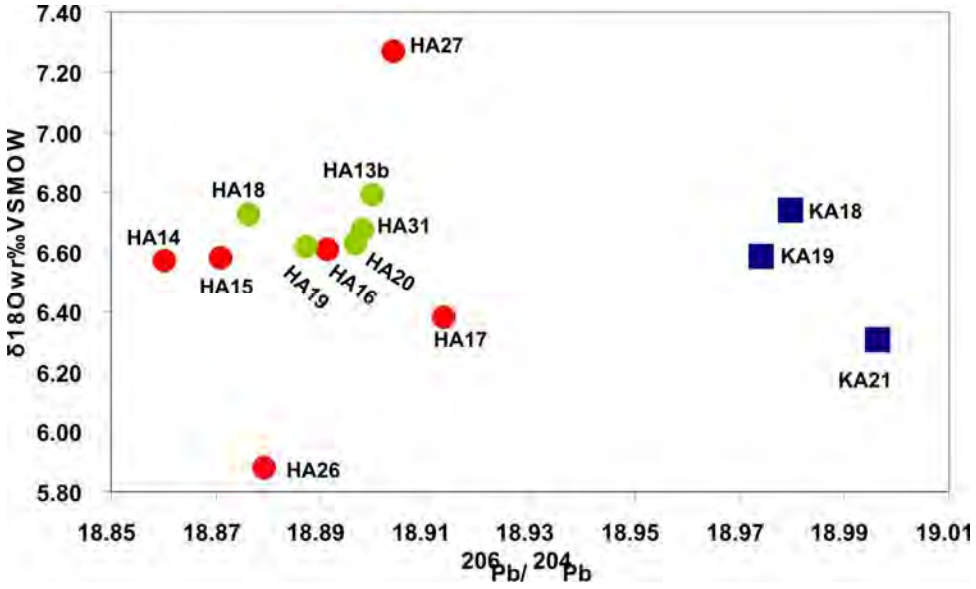

Figure 5.35: $\delta^{18}O‰$ VSMOW vs. $^{206}Pb/^{204}Pb$ isotope diagram of HS, OZ and K samples belonging to Southwestern Cappadocia Volcanism

5.3. Conclusion

Representative samples for geochemical analysis of major elements were carried out from Erciyes stratovolcano (ES) (n=19), Hasandag stratovolcano (HS) (n=6), Obruk-Zengen (OZ) (n=6), and Karapınar (K) (n=3) areas. Besides, 29 Sr-Nd, 28 Pb and 28 O isotopic analyses were performed. The purpose of these analyses is to present new geochronological and geochemical (major, trace and isotope elements) data on the Quaternary post collisional basaltic volcanism of Central Anatolia.

1. Most of the samples from ES are intermediate in composition (52% <SiO_2<63%). The samples of ES are plotted in the trachybasalt, basaltic andesite, basaltic-trachyandesite, andesite and dacite areas (Figure 5.1). Two of the samples present alkaline characteristics while the remaining (17) samples are subalkaline.

2. All samples exhibit normative Plg, diopside and accessory minerals (apatite, magnetite and ilmenite) (Table 5.1). ER13 sample exhibits nepheline normative while the others exhibit normative hypersthene. All samples exhibit normative quartz, except the samples ER10, ER13 and ER29, which are olivine normative.

3. Harker diagrams emphasize the predominant role of fractional crystallization.

4. We separated the ES samples, LDDS (Less differentiated dated samples) and MDDS (More differentiated dated samples).

5. In LDDS group, except Pb, Nb and Ta contents, the samples vary in multi-element contents (Figure 5.6a). MDDS group displays mostly depleted patterns, except Th, U and Pb (Figure 5.6b). Negative anomalies in Nb, Ta, P and Ti elements are characteristic of this group.

6. Negative anomaly for HFS elements (Y, Yb) cannot be seen on multi-element diagrams (Figure 5.6a-b). Probably, the garnet phase is not efficient and La/Nb ratios are (1.52-1.97) in LDDS and MDDS (1.53-2.14) are greater than 1. That means the source is in shallow depths

7. Chondrite normalized Rare Earth Elements (REE) spider diagrams indicate that the ES samples are enriched in Light Rare Earth Elements (LREE) and exhibit flat patterns in MREE and HREE (Figure 5.7).

8. The low Zr/Ba, high Th/Y, and Ta/Th ratios are related to low grade partial melting. Based on different ratios of this ratio variance, different graded partial melting occurred in these two groups.

9. The samples of HS exhibit basic characteristic (49% < SiO_2 < 51%), OZ and K samples are basic in compositions 49% < SiO_2< 56 % and 49% < SiO_2 < 53% respectively, (Table 5.4).

10. Most samples of HS are in the basalt area, one sample is in the trachybasalt field (Figure 5.8). Samples of OZ are also plotted in the basalt area, but one sample is in the trachybasalt field and another one in the basaltic-trachy andesite field (Figure 5.8). K samples are spread in the trachybasalt, basalt and basaltic andesite areas (Figure 5.8). The samples of Southwestern Cappadocia volcanics show dominant alkaline characteristic.

11. All the alkaline samples of the Southwestern Cappadocia Volcanism are plotted in the sodic series area, according to the K_2O vs. Na_2O (Figure 5.9).

12. In HS, all samples exhibit high amount of plagioclase normative, diopside, olivine and low amount of normative alkaline feldspar, magnetite, ilmenite and apatit Occurrence of normative nepheline is dominant in OZ and in K, all of the samples consist of dominantly normative plagioclase, diopside, olivine and low amount of alkaline feldspar, magnetite, ilmenite and apatite minerals (Table 5.4).

13. According to major element distribution of the Southwestern Cappadocia Volcanism, HS experienced strong fractional crystallization even more dominant compared to ES. However, this strong fractional crystallization pattern is not observed in OZ and K dispersed volcanism.

14. Primitive mantle (PM) normalized multi-element diagrams of HS, OZ and K exhibit enrichment in LILEs. OZ and K have negative anomaly in Nb, Ta, Ti and P and negative anomalies in HFS element increase relatively from HS to K (Figure 5.12 a-b-c).

15. Chondrite normalized REE diagrams show that HS, OZ and K are enriched in LREE more than HREE (Figure 5.13).

16. Variable low Zr/Ba ratios in HS, OZ and K groups point out a lithospheric source enriched by Ba and mixed to the melting during the subduction processes, as reported in Menzies et al. [132].

17. Lack of the depletion in garnet phases from the multi-element diagrams (Figure 5.12) related to the lower amount of Y and Yb, favor shallow lithospheric source for the Southwestern Cappadocia Volcanism.

18. ES volcanics present a clear Sr isotope negative trend while Nd ratios are in slightly increasing (Figure 5.14). The samples are plotted in the mantle area.

19. In LDDS, except the oldest sample (ER13), Sr-isotopes are increasing, and the Nd-isotopes are decreasing by younger volcanism (Figure 5.15a-c). In MDDS, there isn't any systematic Sr vs. Nd isotopes. The young samples (ER9, ER11,

ER17 and ER22) have slightly different $^{87}Sr/^{86}Sr$ ratios, and $^{143}Nd/^{144}Nd$ ratios from each other, (Table 5.7; Figure 5.15b-d).

20. According to the Age vs. Sr-Nd isotope diagrams, slightly different trends are seen between LDDS and MDDS groups (Figure 5.15). LDDS age interval is more extended than MDDS (Table 5.7). Sr-Nd isotopes vs. Age relations are more systematic in LDDS than MDDS.

21. According to the age, Sr-Nd vs. SiO_2 diagrams (Figure5.16), slightly different trends are seen between LDDS and MDDS groups like their major element values.

22. Samples of the ES are plotted in Enriched Mantle (EMII) area which is above the Northern Hemisphere Reference Line (NHRL) (Figure 5.17).

23. In LDDS group, except ER13 from oldest sample to the youngest one, positive trend has seen in $^{206}Pb/^{204}Pb$ isotope ratio (Figure 5.20). Moreover, by the younger ages in MDDS except sample ER32, $^{206}Pb/^{204}Pb$ ratio increases as seen in $^{87}Sr/^{86}Sr$ vs. Age (ka) (Figure 5.15).

24. $^{206}Pb/^{204}Pb$ vs. SiO_2 diagram, negative Pb isotope correlation in LDDS and positive correlation in MDDS are observed. The correlation is not regular in contrast to the age data of the ES samples. Especially, positive correlation of Pb-isotopes vs. differentiation in the MDDS group is likely pointing out crustal contamination took place during the formation of the magma.

25. No significant correlation is observed in LDDS group, $\delta^{18}O$ vs. $^{87}Sr/^{86}Sr$ diagram of the ES samples display co-variation, however it is clearly noted that LDDS group samples tend positive correlation against Sr-isotopes and SiO_2 variation. In MDDS group, the similar age samples disperse in terms of $\delta^{18}O‰$ and present slightly negative correlation in contrast to Sr-isotopes and SiO_2 (Figure 5.23b). $^{206}Pb/^{204}Pb$ isotope ratio increases with $\delta^{18}O‰$ decrease in LDDS group and in MDDS group, possible positive tendency is seen between O-Pb isotopes (Figure 5.24).

26. In $^{87}Sr/^{86}Sr$ vs. $^{143}Nd/^{144}Nd$ diagram, samples of the Southwestern Cappadocia are plotted in the mantle area presenting a clear negative correlation (Figure 5.25) from OZ, HS and K, respectively.

27. HS display clear positive trend from oldest to youngest sample (Figure 5.26), OZ group which represents a wide age range and K samples have relatively constant relationship with the increase of the age.

28. All the samples of the Southwestern Cappadocia Volcanism are plotted above Northern Hemisphere Reference Line (NHRL) (Figure 5.28). Samples of this volcanism are likely seen in the EMII area.

29. Temporal evolution diagram shows that $^{206}Pb/^{204}Pb$ ratio of HS regularly increases from the oldest sample to the youngest sample and by the increase of SiO_2 values (Figure 5.32) as well as in Sr-Nd vs Age diagrams (Figure 5.26). In OZ, except the samples of HA14 and HA15 (Figure 5.31), $^{206}Pb/^{204}Pb$ isotope ratio increases from oldest to youngest samples as seen in Nd-isotope vs. Age diagram (Figure 5.26). K, presents not a significant correlation in Pb-isotope vs. Age and SiO_2 diagrams however slightly positive correlation can be seen in the samples of KA18 to KA21 (Figure 5.31; Figure 5.32).

30. $\delta\ ^{18}O‰$ VSMOW isotope values of the HS, OZ and K groups indicate upper mantle and oceanic basalt values.

31. In $\delta^{18}O‰$ VSMOW vs. Age (ka) diagram (Figure 5.33), HS group present no significant change from oldest to youngest samples. Slight differences between inter and intra groups is noted in the samples of the Southwestern Cappadocia Volcanism, however this doesn't affect the evolution history of the group (Figure 5.33). However, in the diagram of $\delta^{18}O‰$ VSMOW vs. $^{87}Sr/^{86}Sr$ shows clearly Sr-isotope variation between the sub-groups of Southwestern Cappadocia Volcanism (Figure 5.34).

6. DISCUSSION and CONCLUSION

In previous chapters, volcanic rocks from Erciyes and Hasandağ stratovolcanoes, Obruk-Zengen and Karapınar dispersed volcanism were presented with inter and intra-group comparisons. Whereas, in this chapter the spatio-temporal evolution of the Quaternary basaltic volcanism in Central Anatolia have been discussed, using geological, geochronological, mineralogical, petrographical and geochemical results.

6.1. Erciyes stratovolcano

In the Sr-Nd isotope correlation diagram (Figure 5.14), Erciyes stratovolcano data plots within both the enriched and depleted mantle areas. As mentioned previously, these results are similar to those obtained in the Kerguelen area with an OIB-EMI source (Gautier et al., 1990) and in the Society Islands area with an OIB-EMII source (Devey et al., 1990). $^{206}Pb/^{204}Pb$ vs. $^{207}Pb/^{204}Pb$ isotope correlation diagram (Figure 5.17) reveals that Erciyes samples are related to an enriched mantle source such as EMII. EMI and EMII fields are defined as mantle fields enriched with the addition of sediments, continental crust and altered oceanic crust (Rollinson, 1993; Zindler and Hart, 1986).

The geochemical analysis given in Chapter 5 was used to characterize this enriched mantle source. Asthenospheric mantle Sr isotopic ratios (0.7022-0.7028), La/Nb (~0.7), Nb/La>1.3 (Haase et al., 2000) and ε Nd (+8) values (De Paolo and Daley, 2000) are (0.703609-0.705084), (1.52-2.73), (0.47-0.66) and (+0.70-+5.05) respectively for Erciyes stratovolcano. High Nb/La (~>1) [154] and Nb/U (~47) [155] values are one of the typical characteristics of rocks that evolved from an OIB-like asthenospheric mantle source and were not exposed to crustal contamination. Nb/La values of Erciyes stratovolcano samples were in the range of (0.51-0.66), (0.47-0.65) respectively for LDDS and MDDS, while Nb/U values were in the range of (10.64-23.34), (6.57-15.12), respectively.

Zr/Ba ratio is a parameter used to distinguish lithospheric sources (Zr/Ba: 0.3- 0.5) from asthenospheric sources (Zr/Ba >0.5) (Menzies et al., 1991; Kürkçüoğlu, 2010). Zr/Ba ratio is (0.4-1.2) for LDDS and (0.4-0.7) for MDDS at Erciyes.

Multi element diagrams (Figure 5.6) reveal no negative anomaly in the HFS elements Y and Yb. This demonstrates that the garnet phase that contains these elements during partial melting and related to a deep source was not effective. According to Jung et al. (2006, a Dy/Yb ratio that is greater than 2 is an indicator of residual garnet phase. Dy/Yb ratio is between (1.66-1.73) for differentiated samples and (1.73-1.86) for other samples. All samples have Dy/Yb ratios that are less than 2, which show the garnet phase was not highly effective. In light of the geochemistry data, it is considered that the Erciyes source of basalts s.l. is mainly lithospheric and/or associated to a minor interaction with a deeper source.

6.1.1. Partial Melting

Erciyes volcanics generally have high LILE and LREE content but low HFSE and HREE content (Figure 5.6 and Figure 5.7). This is related to magmatic differentiation processes (subduction, crustal contamination, etc.) or shows LILEs and LREEs tendency to shift into liquid phase during partial melting. Higher or lower LREE/HREE ratio is informative of the melting degree of the source. As a result of partial melting at low degrees, low Zr/Nb, Zr/Ba and high Th/Y, Ta/Th and La/Nb ratios should be observed (Table 5.3), whereas high Zr/Nb, Th/Y; low Zr/Ba, Ta/Th; and relatively high La/Nb ratios are observed in Erciyes volcanic rocks.

Magma is a result of partial melting taking place in the mantle or any solid source due to factors such as an adiabatic decompression, increase in environmental temperature and addition of volatile components. Basalt genesis generally occurs as a result of the partial melting of mantle sources (Wilson, 1989). Due to the lack of data in Central Anatolian mantle xenoliths in the literature, the values for spinel peridotite (McDonough, 1990) and garnet peridotite (Frey, 1980) that reflect the composition of the upper mantle, were used. A source with spinel peridotite mineralogy is stated at shallow depth and exhibits lithospheric characteristics (Wilson, 1989; McDonough, 1990, Stern et al., 1999) therefore, a source with garnet peridotite mineralogy indicated a deeper source. The modal mineralogical composition of garnet peridotite is 60% olivine, 21% orthopyroxene, 8% clinopyroxene and 11% garnet whereas that of spinel peridotite is 58% olivine, 27% orthopyroxene, 8% clinopyroxene and 3% spinel (McKenzie and O'Nions, 1991).

Modal bulk/equilibrium melting of any solid rock is a process where the liquid phase formed during partial melting of source rock reaches equilibrium by reacting continuously with the other solid phase until it begins to rise diapirically, and rises from the magma source, due to the difference in density only after the amount of melt reaches a certain quantity.

This type of partial melting is called modal bulk/equilibrium melting (Wood and Fraser, 1976; Wilson, 1989). The equation used in modal bulk/equilibrium melting modeling is as follows:

- $C_L / C_O = 1 / [D_o + F (1-D_o)]$ (Equation 1)
- C_L=Concentration of element in liquid
- C_o= Concentration of element in original solid source

$D_o = [\Sigma X\alpha Kd]$ (X_α is the percentage of phase in residual source at the moment the melt begins to rise diapirically from solid source. Kd is the crystal-liquid partition coefficient of the respective element for this mineral.)

F=Weight fraction of melt formed.

Initial (C_o) values in Equation 1 used in modeling are from McDonough (1990) and Frey (1980) while mineral/melt partition coefficients of elements (Kd) are from Fujimaki et al. (1984); McKenzie and O'Nions (1991); Rollinson (1993) and www.earthref.org/KDD. Overall partition coefficients of rocks (Do) were calculated by multiplying these values with the modal contents of minerals constituting the rocks.

Yb vs. La (Figure 6.1) bulk melting modeling (Shaw, 1970) was conducted using spinel and garnet peridotite as starting components. In the modeling, basalt samples were used to ensure accurate identification of the source. Values were corrected to MgO using fractionation correction to decrease the effects of fractional crystallization. Most of the basalt samples had 6-15% partial melting degrees similar to that of spinel peridotite between the spinel-garnet peridotite curves. ER13, the oldest and most alkaline of LDDS group, was close to the garnet peridotite curve with a partial melting degree of 8-10%. MREE/HREE ratios (Dy/Yb) are informative of garnet and spinel peridotite sources. Blundy et al.

(1998) stated melts where (Dy/Yb)N <1.06 had evolved from spinel peridotite sources. This ratio is between LDDS (1.17-1.26), MDDS (1.17-1.24) in Erciyes samples.

A modal batch partial melting modeling was conducted with trace element concentrations of spinel peridotite and ES samples. Calculated values obtained from modeling were normalized to Chondrite (Sun and McDonough, 1989) and the multiple element diagram given in Figure 6.2 was plotted. This diagram shows that the samples were formed through partial melting of the spinel peridotite source within the range F=5-15%. Figure 6.2 indicates that spinel peridotite was less effective in the formation of ER13 in comparison to the rest of the samples.

Partial melting modeling results with garnet peridotite as the starting component were not realistic. In the light of geochemistry results, it is considered that Erciyes stratovolcano samples partially melted at various degrees and, as (Dy/Yb)N>1.06 in all samples, garnet peridotite was also effective on the source as well as spinel peridotite.

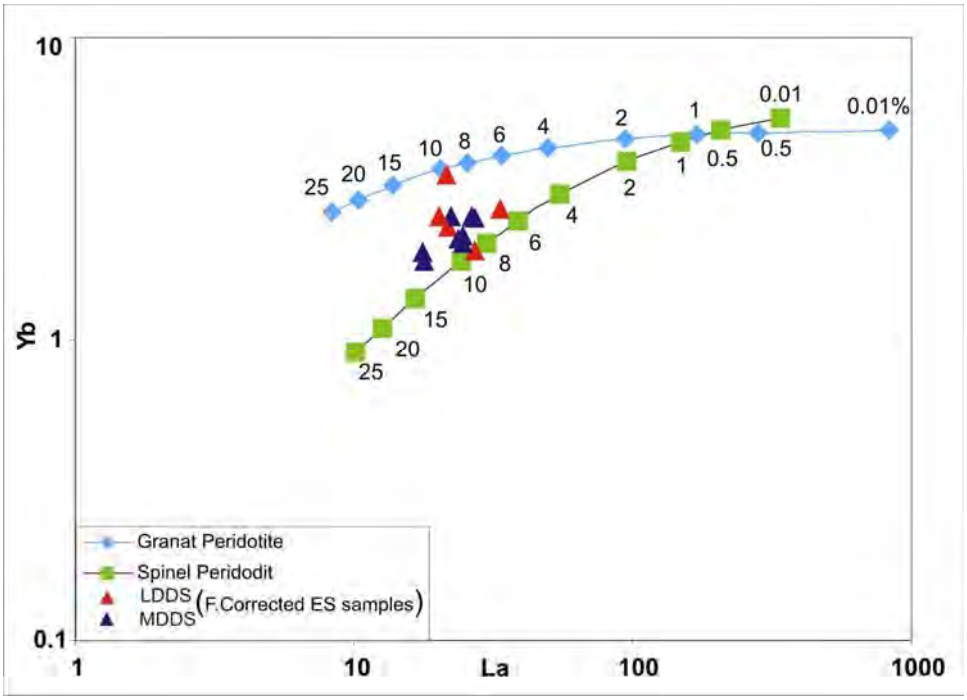

Figure 6.1: Yb vs. La trace element diagram of Erciyes stratovolcano volcanics Garnet peridotite data was obtained from Frey (1980) and spinel peridotite data was obtained from McDonough (1990).

6.1.2. Fractional Crystallization

When fractional crystallization is an effective process, olivine, pyroxene, Ca-plagioclase and oxides are the first components to separate from the cooling melt. The composition of the remaining melt and the composition of the crystals forming from this melt will differ in composition with respect to their stages of generation of magma. Therefore, many values in the melt will vary as long as fractional crystallization continues (i.e. SiO_2 will increase and Mg# will decrease) which allows us to explain the origin of rocks with various compositions forming from a single magmatic source. Modeling studies are carried out to reveal how this process affects rock formation. Fractional crystallization (FC) modeling can be applied when a phase is removed from a homogeneous medium with chemical or isotropic fractionation (Albaréde, 1996).

FC modeling is mainly concerned with trace element fractionation in solidifying magma together with hydrothermal processes or for example, the evaporation of lakes. In this case, while primary magma composition changes with fractionation, mineral phases removed from the environment with fractionation and will have different compositions than parent melt and will be spatially zoned, due to the change in magma composition.

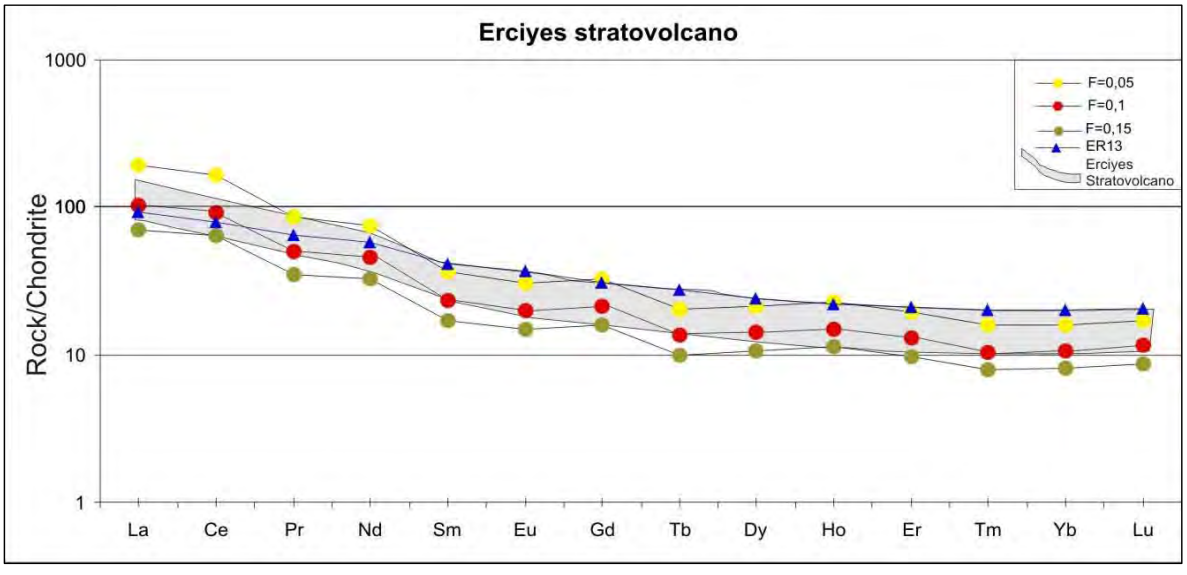

Figure 6.2: Partial melting modeling of Erciyes stratovolcano volcanics using spinel peridotite. (Values were normalized to Chondrite (Sun and McDonough, 1989))

As explained in Chapter 3, it is possible to observe this zoning (normal) in the plagioclases, clinopyroxenes and to lesser degree olivines in both Erciyes and Southwestern Cappadocia (HS, OZ and K) samples. It is postulated that the minerals are in both chemical and isotopic equilibrium at the time of their separation from the magma through FC. FC modeling equations are based on the postulation that there is equilibrium at the solid-liquid interface. The equations used in fractionation crystallization models are as follows:

- $C_L / C_o = F^{(Do-1)}$ (equation used when crystals are removed from environment of formation after crystallization) (Equation 2)
- $C_R / C_o = D_o F^{(Do-1)}$ (equation for the enrichment of a trace element relative to the original liquid) (Equation 3)
- $C_R / C_o = (1-F)^{(Do-1)}$ (equation for the mean enrichment of a trace element in the cumulate) (Equation 4)

$C_{R=}$ Concentration of element (i) in any solid that crystallizes in the magma and is spontaneously removed from the melt (settles with gravitative processes). Other abbreviations are explained in the previous section.

It is possible to speak of an effective fractional crystallization for Erciyes stratovolcano from Harker variation diagrams plotted using major and trace element data, respectively, given in Chapter 5 (Figure 5.4 and Figure 5.5). A negative trend is not observed for Eu (Eu/Eu*=0.90-1.03) in the multiple element diagram (Figure 5.7). On the other hand, in Figure 6.3, Al_2O_3/CaO ratio which remains constant despite the increase in SiO_2 in some samples from LDDS and MDDS groups indicates the occurrence of some plagioclase fractionation. Clinopyroxene fractionation is more apparent especially in MDDS (Figure 6.3). Furthermore, the scattered distribution of some elements in Harker variation diagrams demonstrates that fractional crystallization was not the only effective process (Verma, 1999). As mentioned previously in Chapter 5, the trends in the variation diagrams reveal olivine, plagioclase and pyroxene fractionation.

FC modeling elicited more detailed information on the process. For modeling purposes, samples with high Mg#, Cr, Ni, Fe_2O_3 and MgO and low SiO_2 were

determined as end members and the element contents of these samples were assumed to represent the original liquid given in Equation 2 (Table 6.1). Fractionation degrees of plagioclase, clinopyroxene and olivine were calculated in percentages (Table 6.2). Generally, with cooling and crystallization of magma, Mg# decreases (Zhu et al., 2007).

This is due to the separation of a mafic mineral (olivine, clinopyroxene, etc.) accompanied by plagioclase crystallization. Examination of Mg# contents given in Chapter 5 shows that Mg# value of ER13, the sample with the highest alkalinity, is 53 whereas Mg# values of other samples range between from 58 to 69. Generally, Mg# decreases as SiO_2 increases.

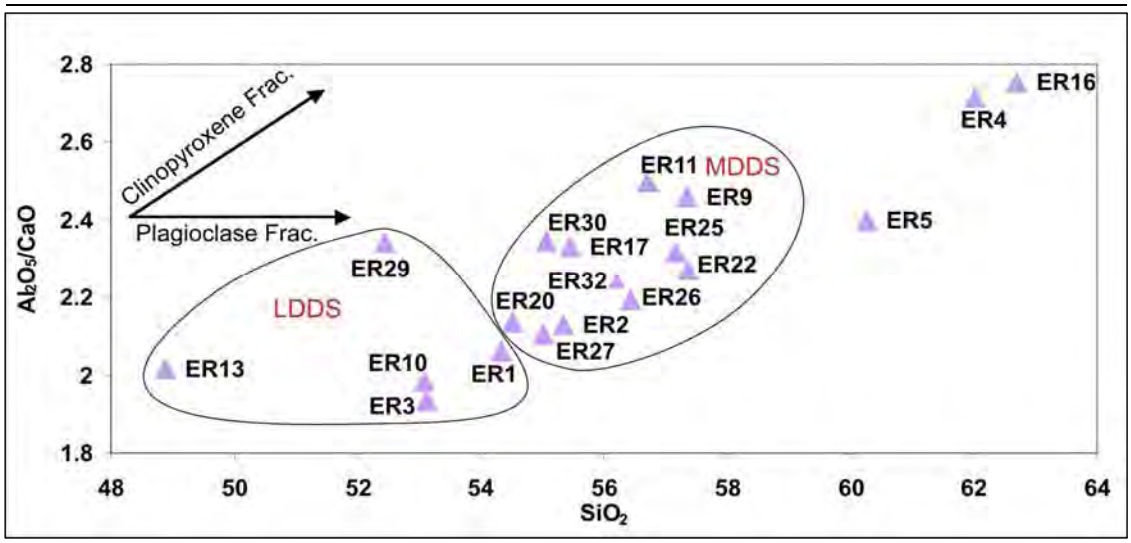

Figure 6.3: Al_2O_3/CaO vs. SiO_2 variation diagram of Erciyes stratovolcano volcanics.

6.1.3. Crustal Contamination and AFC (Assimilation Fractional Crystallization)

Enrichment in LILE and LREE elements can be explained with subduction contributions, crustal contamination or low degree partial melting (Pearce et al., 1990). Multi element diagrams of Erciyes volcanics show LILE and LREE enrichment. This is indicative of magmatic differentiation (subduction, crustal contamination, etc.) or the tendency of LILEs and LREEs to shift into liquid phase during partial melting.

In previous sections, it was demonstrated that fractional crystallization and partial melting was effective. Herein, the modeling of the effect of crustal contamination is proposed.

Table 6.1: SiO_2, Fe_2O, FeO, MgO, Mg#, Cr and Ni element concentrations of Erciyes volcanics.

Samples	SiO_2 %	Fe_2O %	FeO %	MgO %	Mg#	Cr (ppm)	Ni (ppm)
ER1	54.34	6.88	6.19	6.10	69	—	—
ER3	53.13	8.24	7.42	6.54	67	—	—
ER9	57.34	7.07	6.36	4.21	61	68	53
ER11	56.70	7.22	6.50	4.04	59	61	49
ER17	55.46	7.27	6.54	4.95	61	106	72
ER20	54.53	7.24	6.51	5.88	67	144	97
ER22	57.37	6.27	5.64	4.67	66	69	59
ER26	56.43	6.57	5.91	4.59	64	77	46
ER27	55.01	6.81	6.13	5.62		133	85
ER32	56.22	6.55	5.89	5.12	66	115	97

Table 6.2: Olivine, orthopyroxene, clinopyroxene and plagioclase fractionation values of Erciyes volcanics.

Less Differentiated Samples		More Differentiated Samples	Olivine %	Ortopyroxene %	Clinopyroxene %	Plagioclase %
ER3	→	ER11	11	2	7	11
ER20	→	ER17	0.94	—	3	—
ER1	→	ER22	1.14	—	3	1.1
ER27	→	ER32	0.25	3.4	—	4.17
ER17	→	ER11	2.62	1.27	—	7
ER26	→	ER9	—	3.59	—	9.41
ER32	→	ER9	—	6.17	—	10.53
ER1	→	ER27	1.45	—	0.87	1.52

As Th, Ta, Yb elements are incompatible and immobile elements, ratios such as Th/Yb and Ta/Yb will not change during partial melting and fractional crystallization. In Th/Yb vs. Ta/Yb diagram (Figure 6.4), Erciyes samples were mostly compared to Quaternary basalts with similar geodynamic structures from Eastern and Western Anatolia and rest of the world. This diagram (Figure 6.4) reveals that both crustal contamination and subduction related enrichment was effective in Erciyes samples. Erciyes samples are more analogous to Quaternary Süphan, Nemrut and Tendürek basalts in Eastern Anatolia and Quaternary Big Pine basalts in Western North America (Figure 6.4).

Although Quaternary Persani Mountain alkali basalts (Romania) have a strong asthenospheric (OIB-type mantle source) component, their Pb isotopes indicate they were derived from a mantle source affected by an earlier subduction (Downes et al., 1995). On the other hand, Quaternary Karasu basalts, Osmancık-Ceyhan plain basalts, and Huri Hills alkali basalts (Kenya) trace elements and isotope signature indicate asthenospheric mantle source characteristics.

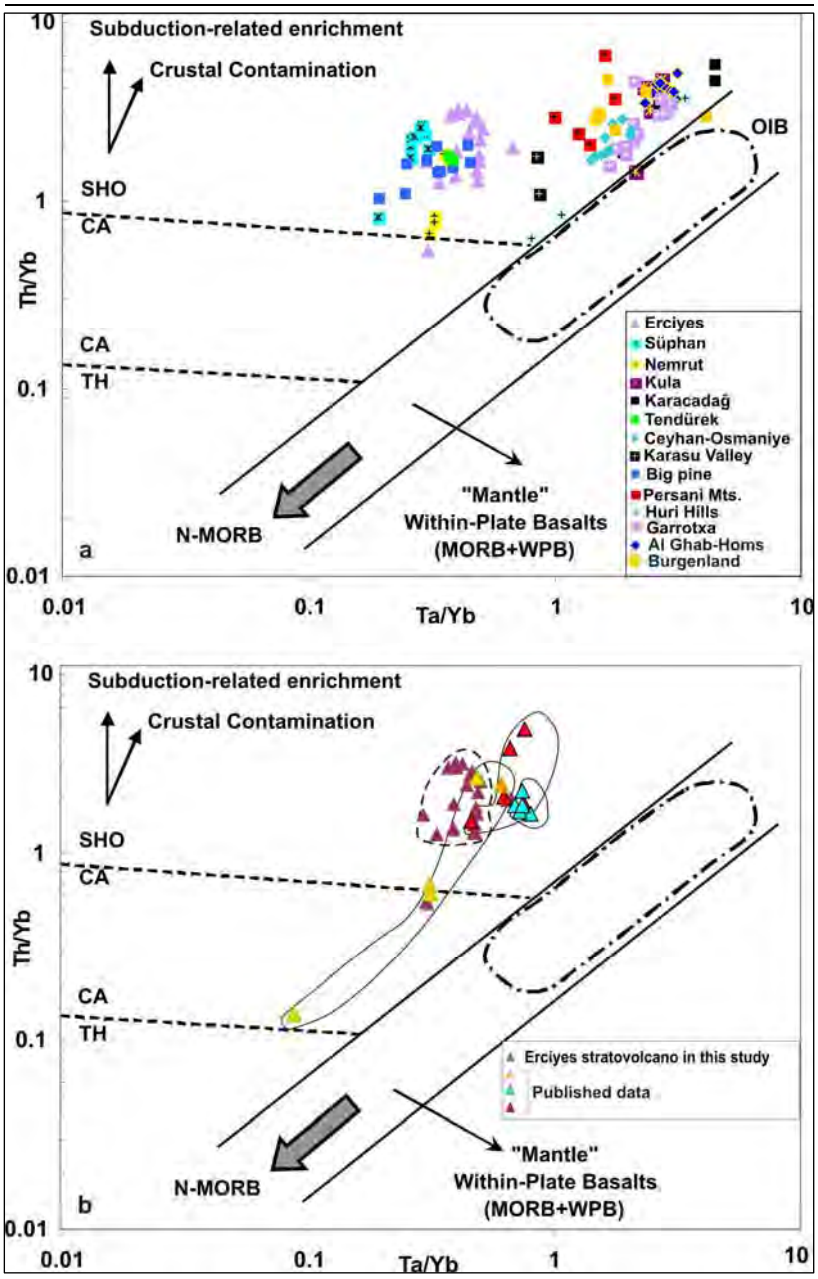

Figure 6.4: Th/Y-Ta/Yb variation diagram of Erciyes volcanics. Data sources (Class et al., 1994; Polat, et al., 1997; Ormerod et al., 1988; Downes et al., 1995; Kürkçüoğlu et al., 1998, 2001; Cebria et al., 2000; Ma et al., 2011; Çubukcu, 2008; Özdemir, 2011; Ali and Ntaflos 2011; Alıcı et al., 2001; Alıcı, 2002; Alıcı Şen et al., 2004; Tang et al., 2006)

Özdemir (2011) reported both lithospheric and asthenospheric mantles were effective in the genesis of lavas from Süphan stratovolcano and other Eastern Anatolian volcanics (Ağrı, Nemrut, Tendürek) and that lithospheric mantle effect increased from Miocene-Pliocene to Quaternary. Özdemir (2011) suggested that the asthenospheric upwelling and widespread volcanism in the area could be due to both slab break off and partial loss of lower lithosphere.

In Figure 6.4b, Quaternary Erciyes stratovolcano samples were compared to Kürkçüoğlu et al. (1998; 2001) and Alıcı-Şen et al. (2004) samples with no radiometric dating. All of the samples in the present study are mostly (Figure 2.7) calcalkaline rocks of Erciyes s.s. (Figure 5.1) whereas Kürkçüoğlu (1998; 2001) and Alıcı Şen (2004) samples mostly consist of Koçdağ and Erciyes calcalkaline basalts and basaltic andesites. Figure 6.4b shows that alkaline and calcalkaline samples from various Erciyes stratovolcano stages did not display a systematic relationship and were affected by both subduction related enrichment and crustal contamination. The similar trend observed in Erciyes samples of the present study to Süphan, Nemrut and Tendürek supports the geochemical data given in Chapter 5. In light of the geochemical data, the Erciyes source is considered to be mainly derived from a mantle source.

$^{87}Sr/^{86}Sr$ vs. SiO_2 and Rb/Sr diagrams (Figure 6.5) show that LDDS samples from old (ER13) to young (ER1), except for ER29, were affected by crustal contamination. On the other hand, although there was no systematic temporal relationship in MDDS group, fractional crystallization and crustal contamination were effective. The increase observed in both charts supports that both fractional crystallization and crustal contamination were effective.

In Th/Y vs. Nb/Y diagram, Erciyes samples range between Th/Nb = 0.1 and Th/Nb = 1. The ratio of Th/Nb is a good tracer of the source of arc lavas because both Nb and Th are relatively immobile in aqueous fluids (Brenan et al., 1995; Elliot et al., 1997). While Th/Y ratio directly is proportional to increasing Nb/Y ratio, suggesting a within plate enrichment, Th/Y increasing in contrast to low Nb/Y is an indicator of subduction enrichment.

In Erciyes samples, both Nb/Y increasing in direct proportion to Th/Y and Th/Y increasing in contrast to Nb/Y is observed (Figure 6.6a).

Comparative data sources given in Figure 6.6a shows that Ceyhan - Osmaniye, Karasu Valley, Huri Hills and Garrotxa basalts reported to have asthenospheric mantle sources all plotted in OIB area. As mentioned previously, although Romanian Persani alkali basalts have a strong asthenospheric mantle source, there are traces of an earlier subduction (Downes et al., 1995).

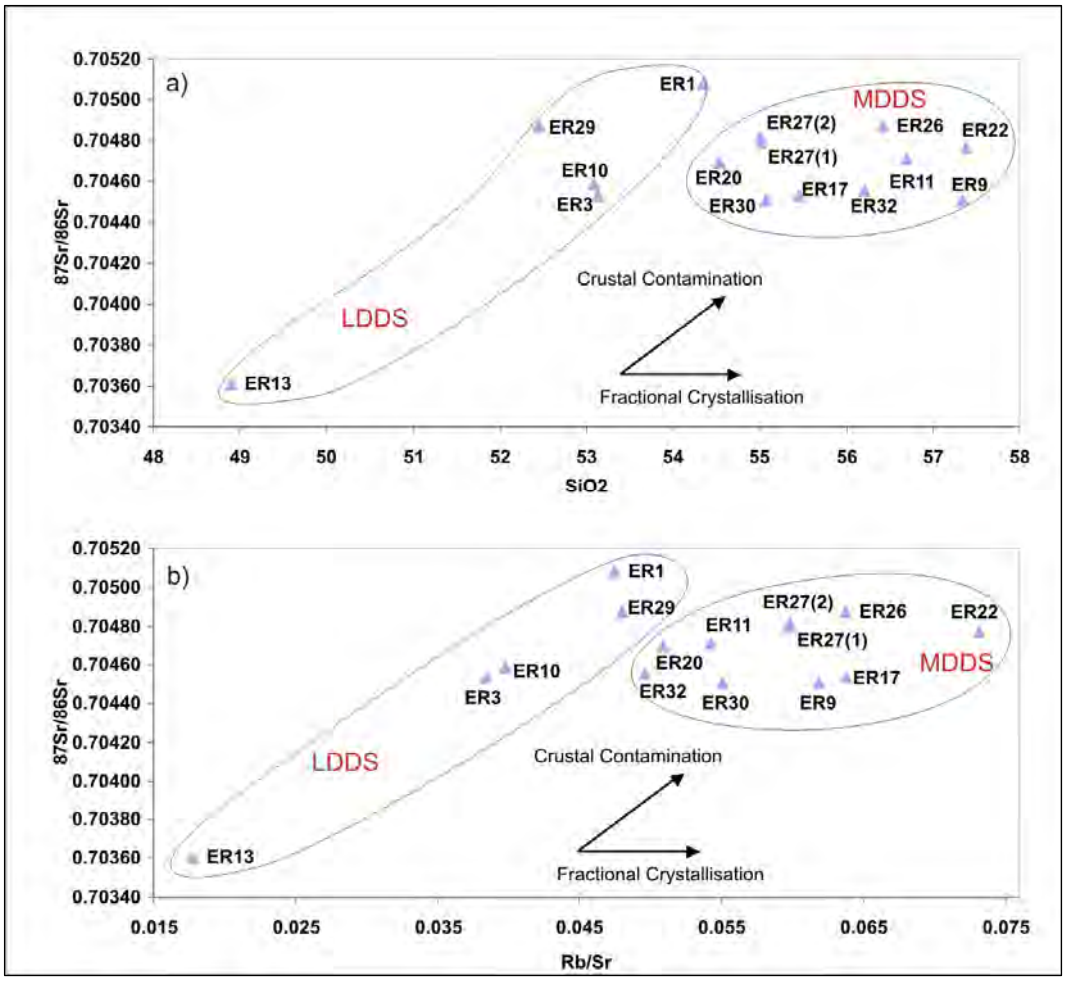

Figure 6.5: (a) $^{87}Sr/^{86}Sr$ vs. SiO_2 (b) $^{87}Sr/^{86}Sr$ vs. Rb/Sr variation diagrams of Erciyes volcanics.

As in Figure 6.4, Erciyes samples once more plotted similarly to Eastern Anatolian volcanics and Western North American Big Pine basalts.

The comparison of Erciyes samples used in the present study to previous researchers is given in Figure 6.6b. These trends show that assimilation-fractional crystallization together with subduction enrichment was effective in Erciyes volcanics (Figure 6.6a-b)

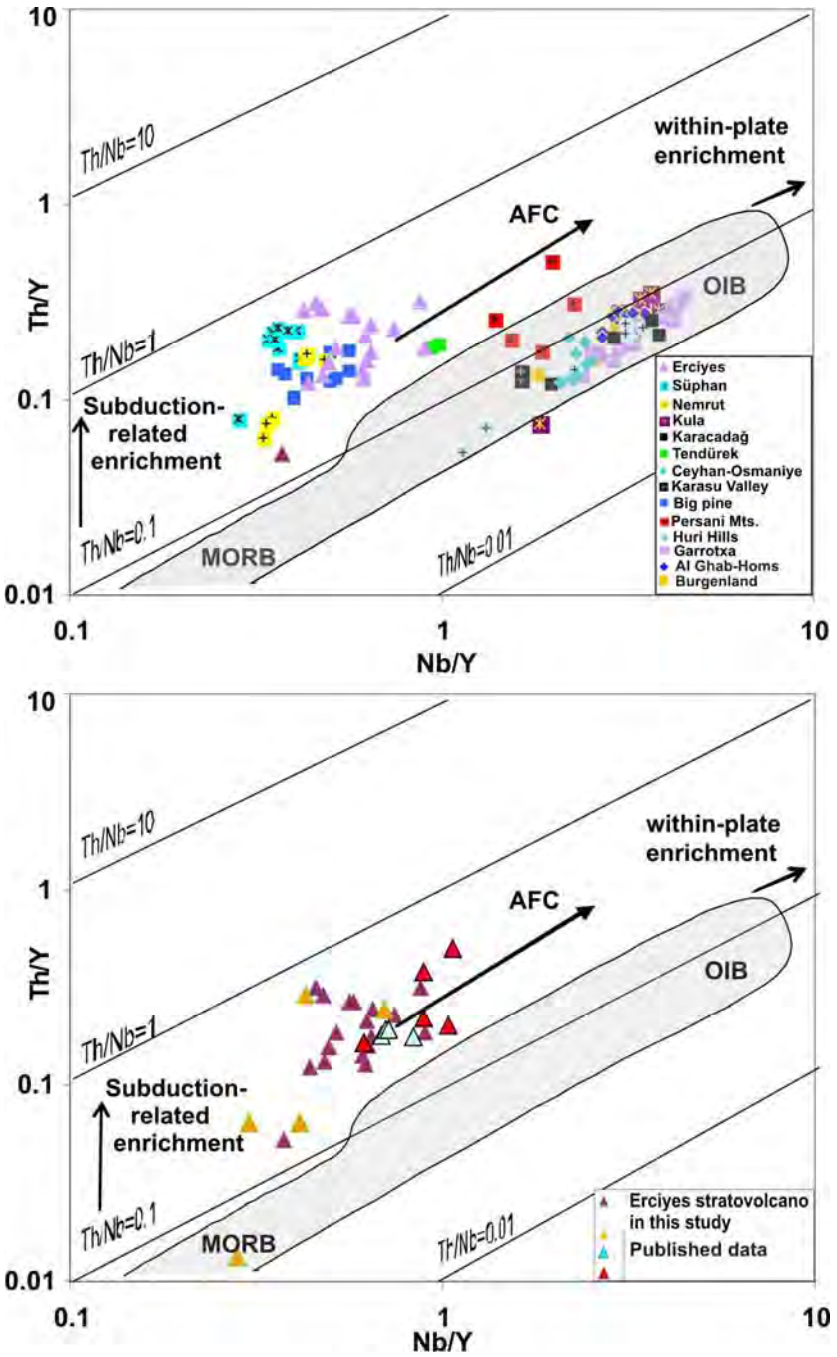

Figure 6.6: Nb/Y-Th/Y variation diagram of Erciyes volcanics. Data sources (Class et al., 1994; Polat, et al., 1997; Ormerod et al., 1988; Downes et al., 1995; Kürkçüoğlu et al., 1998, 2001; Cebria et al., 2000; Ma et al., 2011; Çubukcu, 2008; Özdemir, 2011; Ali and Ntaflos 2011; Alıcı et al., 2001; Alıcı, 2002; Alıcı Şen et al., 2004; Tang et al., 2006)

According to Fitton et al.(1988), Ba/Nb >28 is a typical arc magmatism characteristic. This ratio (Ba/Nb >28) ranges between LDDS (18-22) and MDDS (22-28) (Table 5.3). High Ba/Ta (>450) ratio, which is also typical for arc magmatism, is between LDDS (220-411) and MDDS (285-373). A low La/Nb ratio is indicative of within-plate enrichment (Huang et al.,2000) or an asthenospheric source (De Paolo and Daley, 2000) whereas a high La/Nb ratio is indicative of subduction enrichment (Huang et al.,2000) or a lithospheric source (>1) (De Paolo and Daley, 2000). Hart et al. (1989) suggested that La/Ta should be greater than 22 and La/Nb should be greater than 1.5 in rocks affected by crustal contamination. La/Ta and La/Nb ratios range between 19.71-32.67 and 1.52-2.73, respectively. Furthermore, Nb-Ta-Ti negative and Pb positive anomalies observed in both groups in Figure 5.7 and Figure 5.9c suggest they were affected by both crustal contamination and subduction-related enrichment.

6.1.3.1. Potential Contaminants and AFC modeling

As related in Chapter 2, the primary rocks in Central Anatolian Volcanic complex consist of Paleozoic-Mesozoic metamorphic series (quartzite and crystalline schists), Mesozoic-Early Tertiary (acidic-intermediate granites and granodiorites, intermediate-alkaline granitic and gabbroic intrusives, gabbros and ophiolites) and Lower Pliocene sedimentary rocks (intercalated carbonate sandstones, semi-metamorphosed limestones, sandy and argillaceous marls and gypsum-bearing sediments) (Ayrancı,1991). Due to the small number of isotope and dating analyses of primary rocks in the literature, potential contaminants were selected through a detailed research. The contaminants selected accordingly were i) biotite-moscovite granite found in Agaçören Igneous Association (Köksal et al., 2012) ii) monzonite from subalkaline-transitional Barandağ granitoid (İlbeyli, 2004) found in Central Anatolian Volcanic Province.

The change in composition after assimilation of wall rock and the occurrence of both assimilation and fractional crystallization during the solidification of magma can be identified with AFC modeling. For this purpose, the equations developed by

De Paolo (1981) for assimilation-fractional crystallization (AFC) modeling were used.

These equations revealing both trace element and isotropic effects of AFC modeling are given below:

AFC modeling for trace elements:

$C_m / C_o = f' + (r / (r-1+D_o))^* C_a / C_m^{o*} (1- f')$ (Equation 5)

R= ratio of assimilation rate to fractionation rate

C_a= concentration of trace element in wall rock

C_m^o = initial composition of trace element in original magma

C_m= composition of trace element in assimilated rock

AFC modeling for isotope ratios ($\in$):

$(\in_m - \in_m^o) / (\in_a - \in_m^o) = 1- (C_m^o / C_m) F^{-z}$ (Equation 6)

$z = (r + D_o - 1) / (r - 1)$

$\in_m^o$= initial isotope ratio in magma (starting component)

$\in_m$= isotope ratio in magma exposed to AFC processes

$\in_a$= isotope ratio in wall rock or assimilant rock (assimilant component).

Equation 6 given above was used in isotope AFC modeling for Erciyes stratovolcano. C88-79 (tholeiitic basalt) Kürkçüoğlu (2000) was used as end member and this sample was Paleozoic- with biotite-moscovite granite of Köksal et al., (2012) (Figure 6.7a) and plutonic N-26 (monzonite) of İlbeyli (2004) (Figure 6.7b), respectively.

CIPW norms of C88-79 (55.69% plagioclase, 19.58 % clinopyroxene, 16.06% olivine, 2.81% nepheline, 2.6% ilmenite, 1.06% K-feldspar, 0.12% magnetite) used as end member were obtained from Kürkçüoğlu (2000). Mineral/melt partition coefficients (Kd) for basaltic melts were calculated from Fujimaki et al., (1984), McKenzie and O'Nions (1991), Rollinson (1993) and (www.earthref.org/KDD/). R-values representing the ratio of assimilation rate to fractionation rate given in Equation 6 were determined as illustrated in Figure 6.7 (a-b). Figure 6.7 (a-b) shows that the samples were exposed to crustal contamination within the range of 0.1-0.3 (Figure 6.7a) and 0.2-0.5 (Figure 6.7b) except for ER13, which differs from the rest of the samples.

6.1.4. Mixing Sources

The occurrence of both plagioclases, in equilibrium and out of equilibrium, in the same sample allows us to consider that the genesis conditions were not homogeneous. Besides, the association of both equilibrium and disequilibrium olivines were observed. Temperature (Table 4.2) and depth values in Chapter 4, multiple element diagrams in Chapter 5 (Figure 5.6 and Figure 5.7), Sr-Nd isotope correlation diagram (Figure 5.14) and particularly Pb isotope correlation diagram (Figure 5.17) suggests that Erciyes stratovolcano has an enriched and heterogeneous source. Isotope correlation diagrams (Figure 5.14; 5.17; 5.23; 5.24) and Sr-Nd-Pb and O isotope values (Table 5.7) preponderate the mixing of two sources over the existence of a single source.

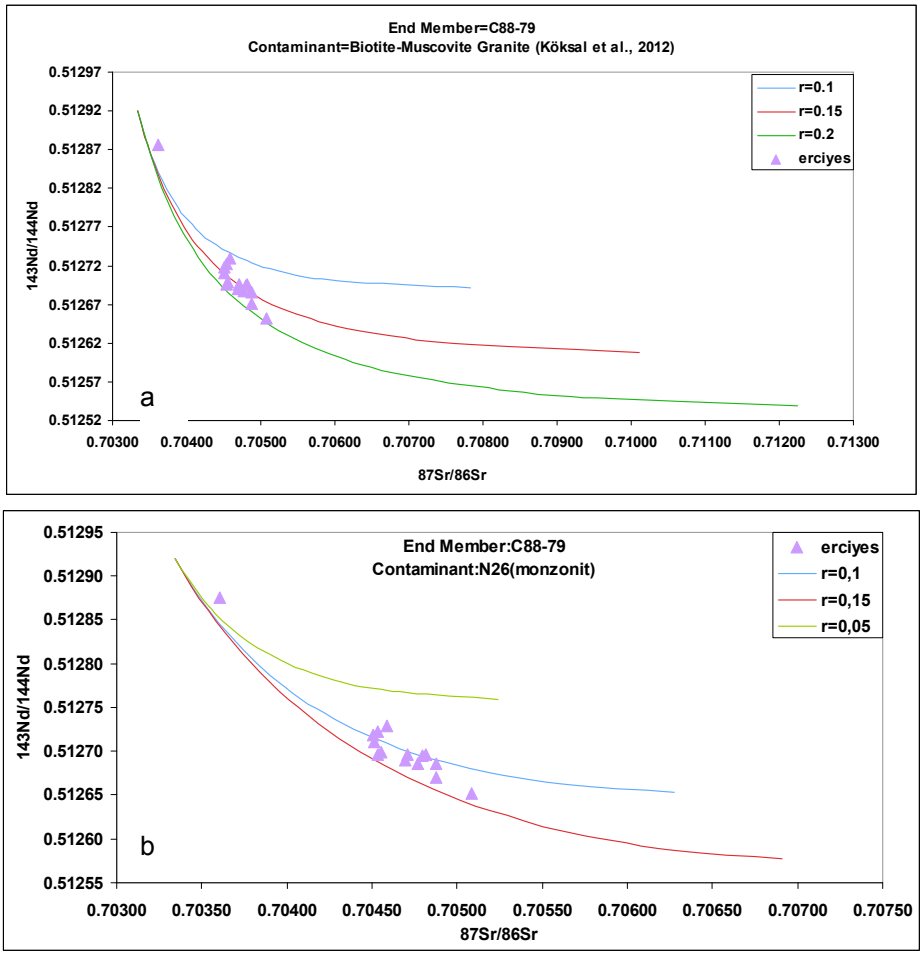

Figure 6.7: $^{143}Nd/^{144}Nd$ vs. $^{87}Sr/^{86}Sr$ AFC modeling diagrams of Erciyes volcanics between end member C88-79 and respectively (a) bmg1 (biotite muscovite granite) and (b) N26 (monzonite). (The values used are as follows: C88-79 (Sr=398.5 ppm, Nd=107 pmm, $^{87}Sr/^{86}Sr$=0.703384,$^{143}Nd/^{144}Nd$=0.512920; Kürkçüoğlu, 2000), bmg-1 (Sr=183 ppm, Nd=35.3 ppm, $^{87}Sr/^{86}Sr$=0.717924, $^{143}Nd/^{144}Nd$=0.512139; [181], and N26 (Sr=911 ppm, Nd=60.12 ppm, $^{87}Sr/^{86}Sr$=0.70804, $^{143}Nd/^{144}Nd$ =0.51227; İlbeyli, 2004).

Using particularly Sr and Pb isotope data, mixing modeling of the sources with high Pb-and Nd- isotopes and low Sr-isotope identified for the first time as FOZO (Focal Zone) by Hofmann, (1997) and as C (common mantle) by Hannan and Graham, (1996) and the EMII source higher in $^{87}Sr/^{86}Sr$ and lower in $^{143}Nd/^{144}Nd$ and $^{206}Pb/^{204}Pb$ in comparison to the other source was conducted (Figure 6.8). Accordingly, all Erciyes samples plot on the mixing curve.

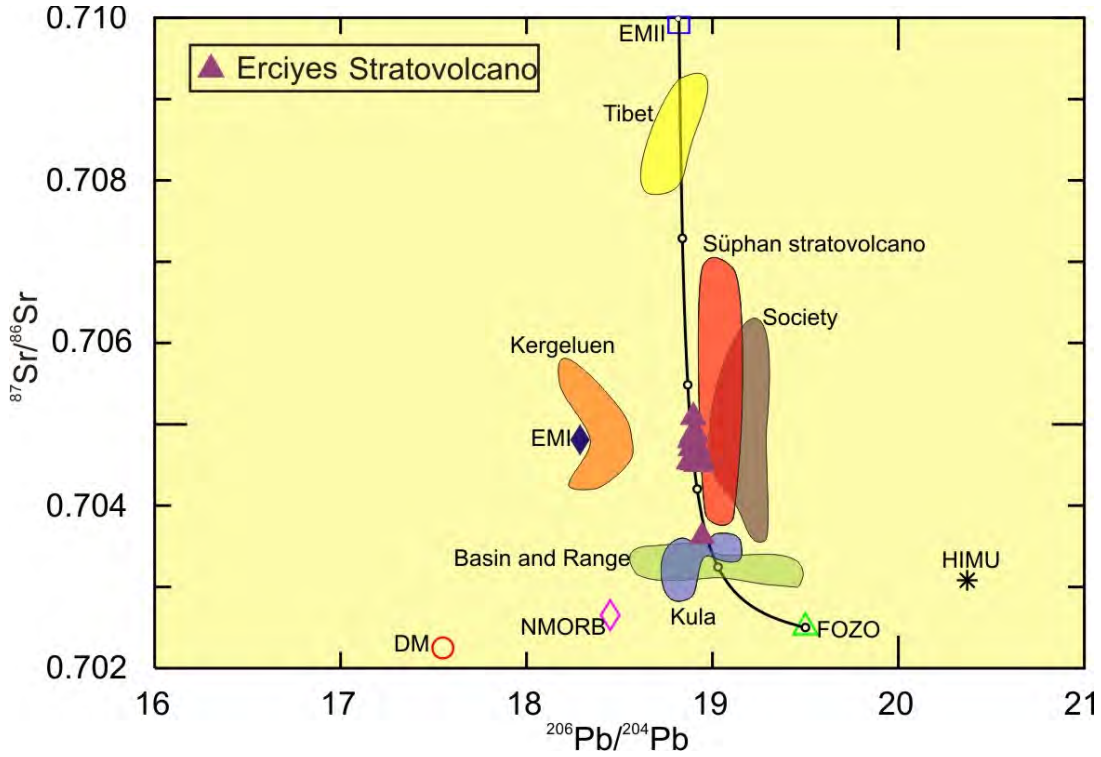

Figure 6.8: $^{87}Sr/^{86}Sr$ vs.$^{206}Pb/^{204}Pb$ mixing diagram of Erciyes volcanics and FOZO-EMII mixing modeling. Data sources: EMII, EMI, HIMU, DM (Zindler and Hart, 1986), NMORB (Okamura et al., 2005), FOZO (Hart et al., 1992), Tibet (Tang et al., 2006), Süphan stratovolcano (Özdemir et al., 2011), Society (Devey et al., 1990), Kula (Alıcı Şen et al., 2004), Basin and Range (Kempton et al.,1991), Kergeluen (Gautier et al., 1990).

In the diagram (Figure 6.8), as in Figure 6.4a and 6.6a, Erciyes volcanics, except for ER13, display similar trends to Süphan stratovolcano samples with a lithospheric + asthenospheric mantle interaction where the lithospheric mantle effect increases as the samples get younger, and Society Islands samples with an enriched mantle source such as EMII. Whereas, ER13 is similar to an asthenospheric mantle source such as Basin and Range (Kempton et al., 1991) where it is not affected by crustal contamination, and Kula volcanics (Alıcı et al.,

2002) postulated to have mostly asthenospheric and limited contribution of a lithospheric mantle component source.

6.2. Southwestern Cappadocia Volcanism

Multi element diagrams of the samples found in Hasandağ stratovolcano (HS) (Figure 5.12a), Obruk-Zengen (OZ) (Figure 5.12b) and Karapınar (K) dispersed volcanism (Figure 5.12c) display a nearly similar pattern. On the other hand, a strongly negative anomaly for Nb-Ta and Ti, as well as, a positive anomaly for incompatible elements such as Th, U and particularly Pb is observed gradually from northeast to southwest in HS, OZ and K; respectively. This indicates effects of subduction or crustal contamination (Downes et al., 1995). In the Sr-Nd correlation diagram (Figure 5.25), all the samples plotted in the mantle array and, therefore, have mantle sources, whereas particularly OZ samples plotted in the depleted mantle array and some HS and K samples plotted in the enriched mantle array. As mentioned previously, these samples are similar to the Kerguelen lavas with OIB-EMI source (Gautier et al., 1990) and Society Islands lavas with OIB-EMII source (Devey et al., 1990). $^{206}Pb/^{204}Pb$ vs. $^{207}Pb/^{204}Pb$ isotope diagram (Figure 5.28) reveals that OZ and HS values are similar to an enriched mantle source such as EMII, while K samples have values more similar to an area between EMII and upper crust. EMI and EMII fields are defined as mantle fields enriched with the addition of constituents such as sediments, continental crust, and altered oceanic crust into the mantle (Rollinson, 1993; Zindler and Hart, 1986).

The chemical composition of the samples was used in the determination of the characteristics of this enriched mantle source. Asthenospheric mantle Sr isotope (0.7022-0.7028), La/Nb (~0.7) and εNd (+8) values (De Paolo and Daley, 2000) are respectively (0.704625-0.704976), (1.72-2.22), (0.38-1.57) for HS, (0.704153-0.704711), (1.63-2.33), (1.67-3.67) for OZ and (0.705188-0.705502), (2.63-3.53), (-0.18 — -0.69) for K. As mentioned previously, high Nb/La (~>1) (Abdel-Rahman and Lease, 2012) and Nb/U(~47) (Hofmann, 1997) values are typical characteristics of rocks that evolved from an OIB-like asthenospheric mantle source and were not exposed to crustal contamination. Nb/La varies between (0.45-0.58), (0.43-0.61), (0.28-0.38) while Nb/U varies (12.43-21.01), (5.83-18.15),

(4.08-8.86) for HS, OZ and K respectively. Zr/Ba ratio ranges between (0.38-0.51) for HS, (0.38-0.65) for OZ and (0.32-0.41) for K. In light of the geochemical data, it is considered that Southwestern Cappadocia volcanism was affected mainly by the lithospheric mantle but, in addition, could have interacted with a deeper asthenospheric source.

6.2.1. Partial Melting

Yb vs. La bulk melting modeling (Shaw, 1970) was conducted using spinel and garnet peridotite as starting components (Figure 6.9). As SiO_2 (49-52%), MgO (7-11%), Cr (288-346 ppm) and Ni (128-177ppm) for the samples whose data sets were used in the diagram, the values were not fractionation-corrected. According to the diagram, HS (%8-9), OZ (%8-12) and K (%8) have varying partial melting degrees. Most of Southwestern Cappadocia samples were close to spinel peridotite curve, which is related to a lithospheric source, whereas some samples plotted between garnet and spinel peridotite curves.

Multi element diagrams (Figure 5.12) reveal no negative anomaly in the HFS elements as Y and Yb, which indicates that garnet phase containing these elements during partial melting had a limited effect. According to Jung et al. (2006), a Dy/Yb ratio greater than 2 is another criterion for residual garnet phase. Dy/Yb ratios ranging between respectively (1.74-1.84), (1.71-1.93) and (1.70-1.73) for HS, OZ and K support the information given above.

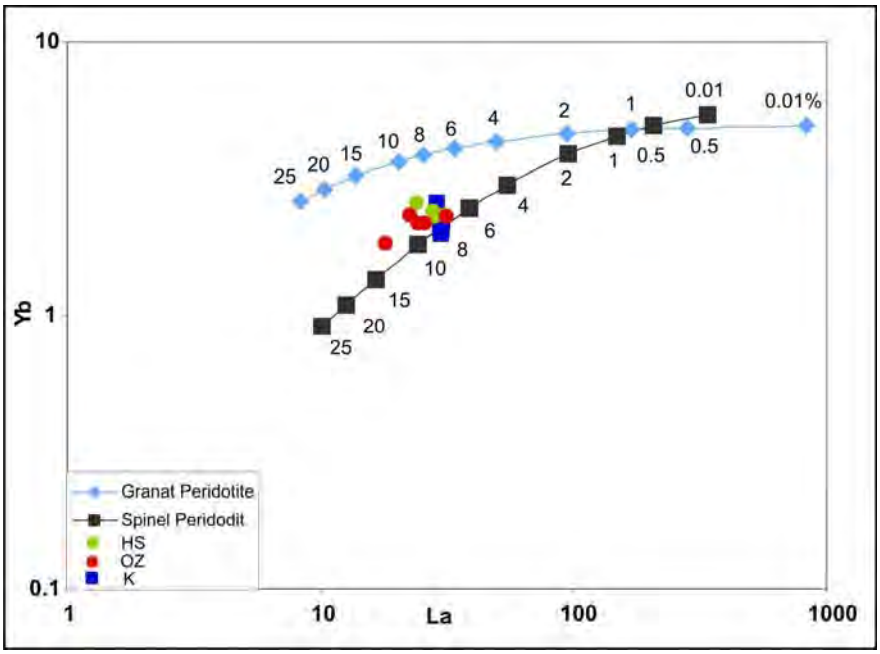

Figure 6.9: Yb vs. La trace element diagram of Southwestern Cappadocia volcanics. (Garnet peridotite data was from Frey, (1980) and spinel peridotite data from McDonough, 1990).

In order to test the values given above, a modal bulk/equilibrium (batch) melting modeling normalized to Chondrite (Sun and McDonough, 1989) was conducted (Figure 6.10).

The modeling revealed that HS (Figure 6.10a) and K (Figure 6.10c) magmas are related to the partial melting of spinel peridotite source at F=5-10% interval whereas OZ (Figure 6.10b) was formed by the partial melting of the same source at F=5-15% interval.

6.2.2. Fractional Crystallization

Major and trace element Harker diagrams of Southwestern Cappadocia samples given in Chapter 5 (Figure 5.10 and Figure 5.11) show that fractional crystallization was not as effective as in Erciyes. Furthermore, plagioclase fractionation was more effective in HS samples than in OZ and K whereas clinopyroxene fractionation was more effective in OZ and K (Figure 6.11). Fractional crystallization modeling was explained in detail in Section 6.1.2. Values factored in the selection of Southwestern Cappadocia volcanics used in modeling are given in Table 6.3.

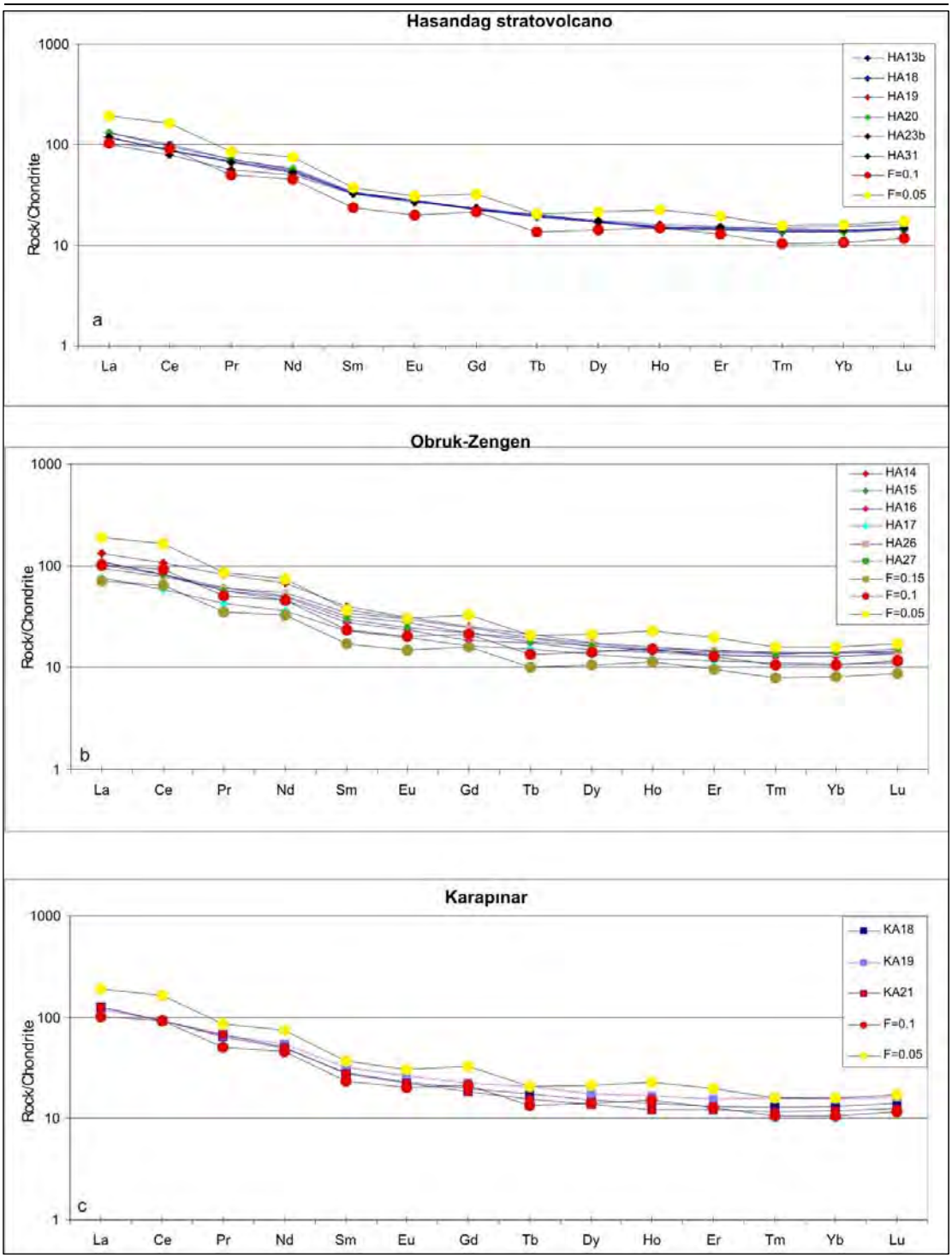

Figure 6.10: Partial melting modeling of Southwestern Cappadocia volcanics (a-b-c) with spinel peridotite. (Values were normalized to Chondrite (Sun and McDonough, 1989))

According to the modeling results (Table 6.4), OZ samples exhibited very little or even none plagioclase fractionation whereas clinopyroxene and olivine fractionation was observed (Figure 6.11). HA31 from HS group, HA27 from OZ group and KA19

from K group have the lowest Mg# (60-61) values while HA16 (Mg#73) and HA17 (Mg#75) from OZ group have the highest Mg# values (Table 6.3).

According to Frey et al. (1978), Mg# values between Mg#>68-70 are values for primary magmas. The fact that many samples have similar Mg# values leads us to think that the effect of fractionation was limited and/or negligible for some samples.

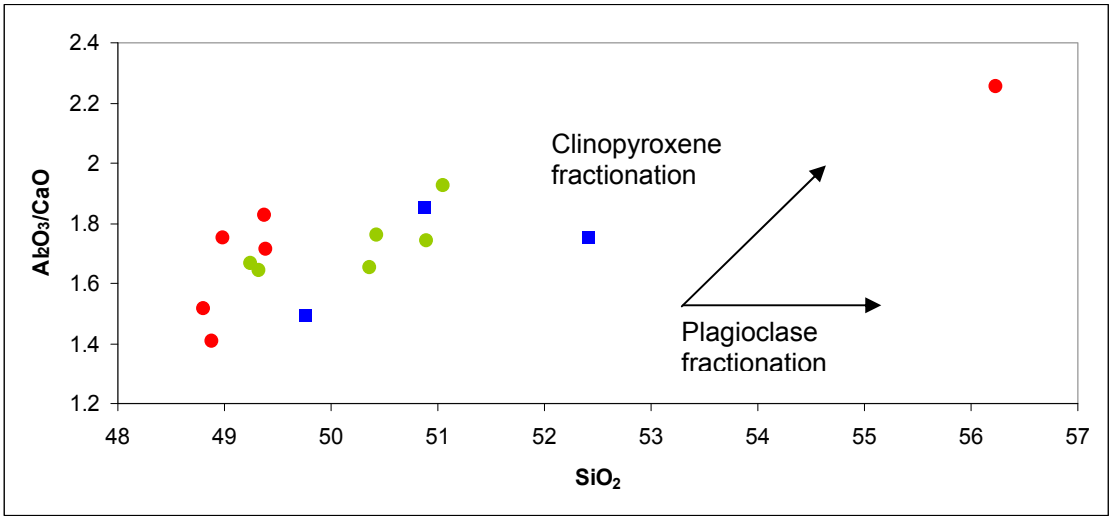

Figure 6.11: Al_2O_3/CaO vs. SiO_2 variation diagrams of Southwestern Cappadocia volcanics. (Symbols given in Figure 6.9)

Table 6.3: SiO_2, Fe_2O, FeO, MgO, Mg#, Cr and Ni element concentrations of Southwestern Cappadocia volcanics.

Samples	SiO2	Fe_2O	FeO	MgO	Mg#	Cr	Ni
Hasandağ stratovolcano							
HA13b	49.33	8.88	7.99	8.52	69	—	—
HA18	51.06	8.72	7.85	7.31	68	206	128
HA19	50.43	8.87	7.98	7.99	68	275	145
HA20	50.36	9.14	8.23	8.75	69	346	177
HA31	49.24	9.57	8.61	6.01	60	20	49
HA23b	50.69	8.86	7.97	7.35	66	286	130
Obruk-Zengen							
HA14	48.99	9.01	8.11	8.52	70	—	—
HA15	49.38	9.42	8.48	8.71	68	—	—
HA16	48.81	8.97	8.07	10.18	73	—	—
HA17	48.88	8.6	7.74	10.92	75	—	—
HA26	49.39	9.39	8.45	8.81	69	296	156
HA27	56.24	7.31	6.58	4.07	60	44	27
Karapınar							
KA18	49.75	8.53	7.68	8.12	69	—	—
KA19	50.87	9.17	8.25	5.69	61	—	—
KA21	52.4	8.20	7.38	8.54	72	288	135

Table 6.4: Olivine, orthopyroxene, clinopyroxene and plagioclase fractionation values of Southwestern Cappadocia volcanics.

Less Differentiated Samples		More Differentiated Samples	Olivine %	Clinopyroxene %	Plagioclase %
HA20	→	**HA18**	3.3	6.34	4.95
HA23b	→	**HA18**	—	4.04	0.67
HA13b	→	**HA19**	2.35	—	2.31
HA20	→	**HA23b**	3.01	2.27	2.44
HA20	→	**HA19**	2.25	—	0.95
HA19	→	**HA18**	1.72	3.79	3.66
HA16	→	**HA26**	4.28	6.35	6.89
HA17	→	**HA26**	5.84	11.56	8.27
KA18	→	**KA19**	4.3	12.05	9.33

6.2.3. Crustal Contamination-AFC

All of Southwestern Cappadocia volcanics have higher LILE (Figure 5.12) and LREE (Figure 5.13) content in comparison to HFSEs vs. HREEs. LILE and LREE enrichment can be explained with magmatic differentiation processes such as subduction-related processes or crustal contamination, or the tendency of LILEs and LREEs to shift into liquid phase during partial melting. Furthermore, high LREE/HREE ratio suggests that the magma was derived from an enriched mantle source or as a result of a low degree partial melting.

As related in Section 6.1.3, ratios of incompatible elements such as Th, Ta and Yb will not change during partial melting and fractional crystallization. In Th/Yb vs. Ta/Yb diagram, OZ displays mainly crustal contamination enrichment whereas K displays both crustal contamination and subduction enrichment. HS does not exhibit a significant trend (Figure 6.12).

HS, OZ and K volcanics from Southwestern Cappadocia plotted similarly to Süphan, Nemrut, Tendürek and Big Pine basalts (Figure 6.12a). Özdemir (2011), reported that both lithospheric and asthenospheric mantles are related to the genesis of Süphan stratovolcano and other Eastern Anatolian volcanics (Ağrı, Nemrut, Tendürek), and that lithospheric mantle effect increased from Miocene-Pliocene to Quaternary. A comparison of Southwestern Cappadocia volcanics to

the data of previous researchers could not be carried out in Figure 6.14, due to the lack of some trace element data.

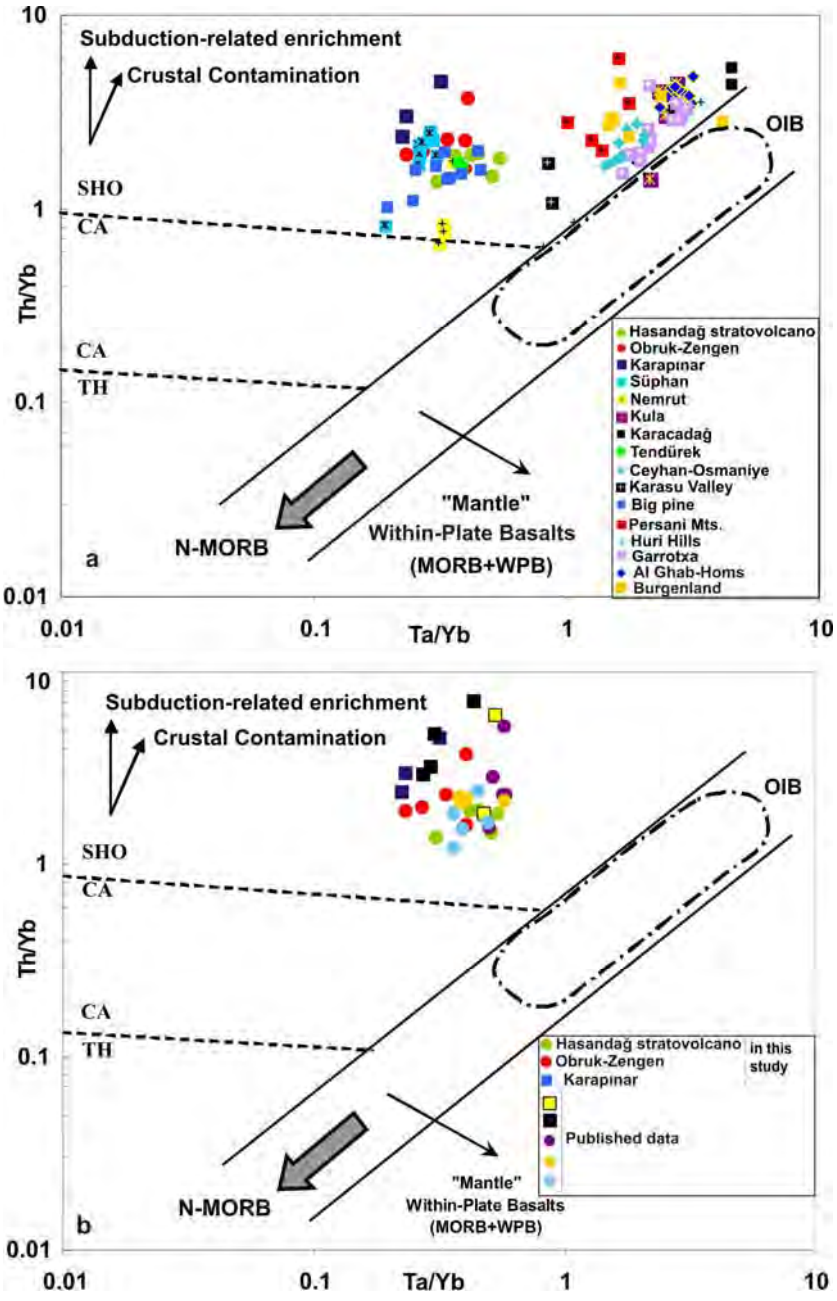

Figure 6.12: Th/Y vs. Ta/Yb variation diagram of Southwestern Cappadocia volcanics. Data sources (Class et al., 1994; Notsu et al., 1995; Polat et al., 1997; Ormerod et al., 1988; Downes et al., 1995; Kürkçüoğlu et al., 1998; 2001; Cebria et al., 2000; Ma et al., 2011; Çubukcu, 2008; Özdemir, 2011; Ali and Ntaflos 2011; Alıcı et al., 2001; Alıcı, 2002; Alıcı Şen et al., 2004; Tang et al., 2006).

HS and OZ that plotted similarly to Eastern Anatolian volcanics may be considered to be related to both lithospheric and asthenospheric mantle sources (Figure 6.12a). While isotope (Sr-Nd-Pb and O) data, trace element ratios and ϵNd values

confirmed that lithospheric mantle was more effective, temporal evaluation of lithospheric mantle interaction could not be demonstrated.

Quaternary Southwestern Cappadocia samples of the present study were compared to other samples without radiometric dating collected from the same volcanic area (Alıcı Şen et al., 2004; Notsu et al., 1995). All of Southwestern Cappadocia volcanics were neovolcanic (Figure 2.8) and most consisted of alkali rocks (Figure 5.10). HS, OZ and K samples of the present study have similar trends with samples of previous researchers (Notsu et al., 1995; Alıcı Şen et al., 2004) (Figure 6.12b). More significant subduction-related enrichment and/or crustal contamination trends in K than in HS and OZ. This trend is also observed in multiple element diagrams in Figure 5.14.

HS, OZ and K have different trends in $^{87}Sr/^{86}Sr$ vs. SiO_2 and Rb/Sr diagrams (Figure 6.13). K was more related to crustal contamination than HS and OZ, and fractional crystallization was more effective in HS (Figure 6.13).

In Th/Y vs. Nb/Y diagram (Figure 6.14), all Southwestern Cappadocia data range between Th/Nb = 0.1 and Th/ Nb = 1. Nb/Y and Th/Y ratios are tracers that can be used for the determination of source heterogeneity and crustal contamination effects (Pearce, 1983) while Th/Nb ratio is a good tracer for arc lavas (Brenan et al., 1995; Elliot et al., 1997). If mantle was enriched by subduction and/or crustal contamination elements, Th/Y is expected to be greater than Nb/Y. However, if the mantle was enriched by an earlier and weak partial melting, it could exhibit within-plate enrichment trends with high Th/Y and Nb/Y ratios. Accordingly, high Th/Y and Nb/Y ratios in HS and OZ samples are indicative of within-plate enrichment, whereas Th/Y increasing Th/Y vs. low Nb/Y in K suggests mainly subduction enrichment. As in Figure 6.12, Southwestern Cappadocia volcanics have a mainly lithospheric mantle source and/or plotted in areas with lithospheric + asthenospheric interaction. A comparison of Southwestern Cappadocia volcanics to the samples of previous researchers could not be carried out in Figure 6.14 due to the lack of some trace element data.

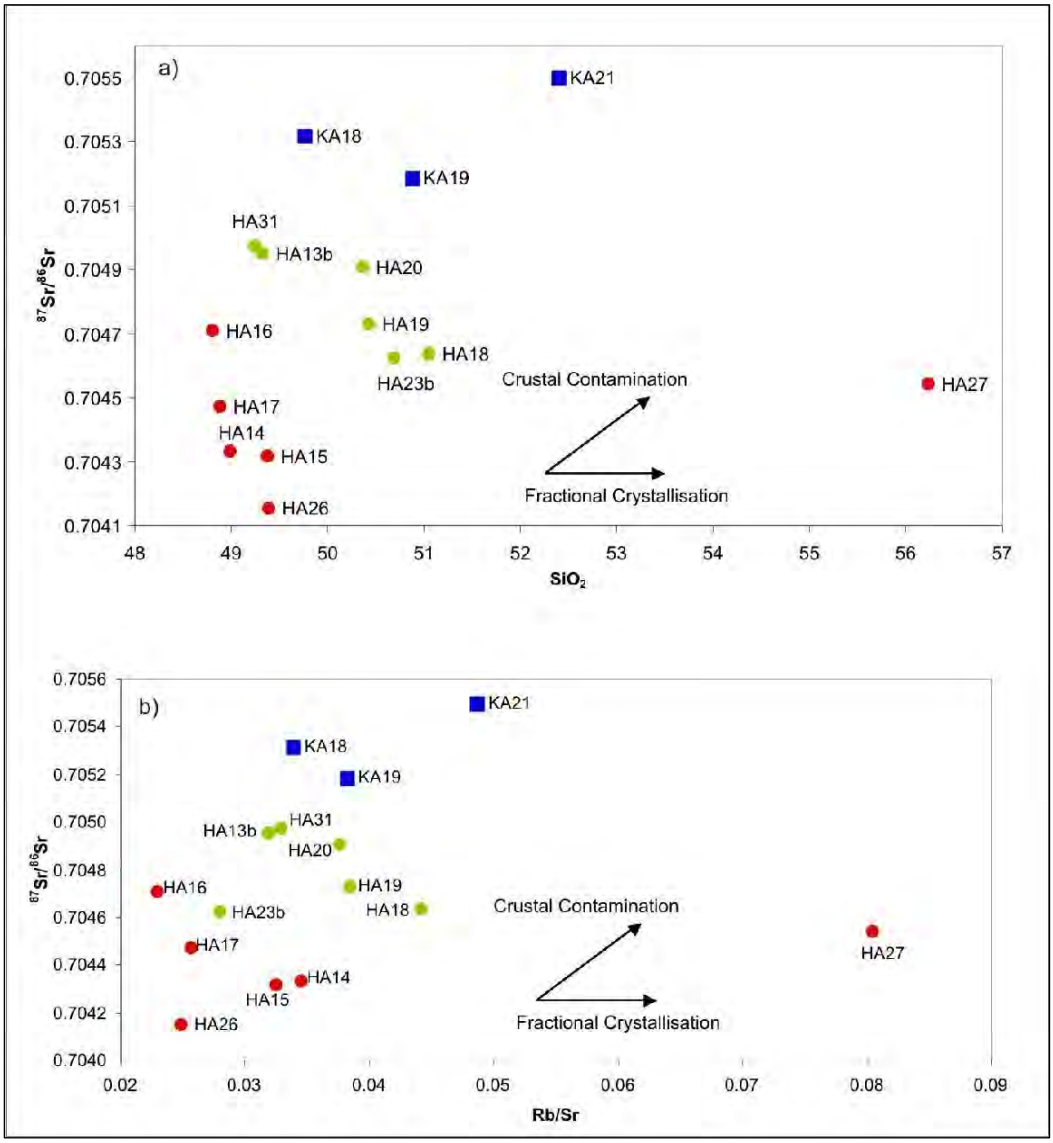

Figure 6.13: (a) $^{87}Sr/^{86}Sr$ vs. SiO_2, (b)$^{87}Sr/^{86}Sr$ vs. Rb/Sr variation diagrams of Southwestern Cappadocia volcanics. (Symbols given in Figure 6.9.)

High Ba/Nb (>28) and Ba/Ta (>450) ratios are typical for subducted-related magma (Fitton et al.,1988 ; Gill,1981) for HS, OZ and K and are respectively (22-28; 20-36; 32-44) and (283-395; 273-462; 573-664). A low La/Nb ratio is indicative of within-plate enrichment (Huang et al.,2000) or an asthenospheric source (De Paolo and Daley, 2000) whereas a high La/Nb ratio is indicative of subduction enrichment (Huang et al.,2000) or a lithospheric source (>1) (De Paolo and Daley, 2000).

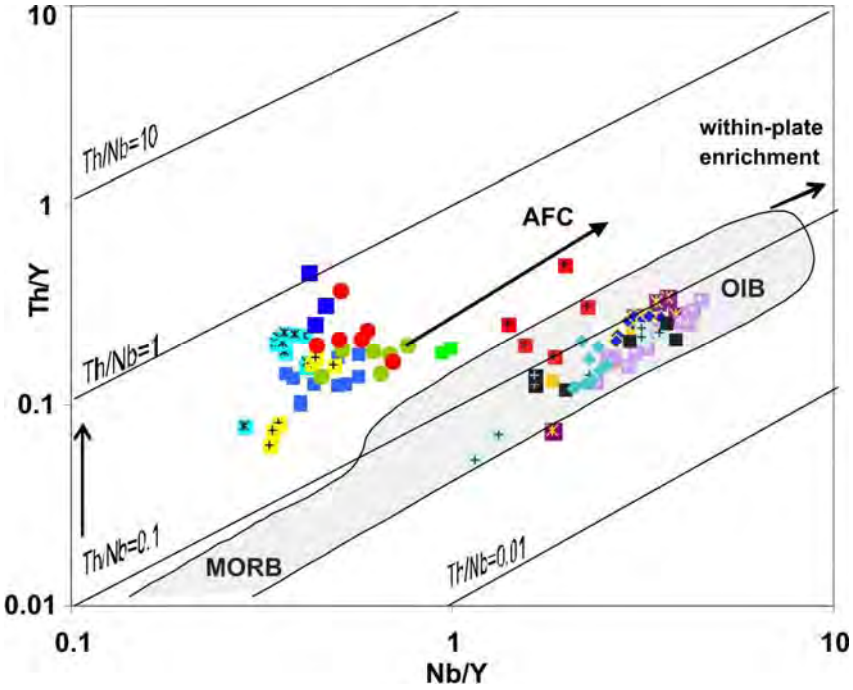

Figure 6.14: Nb/Y vs. Th/Y variation diagrams of Southwestern Cappadocia volcanics. (Symbols are the same as given in Figure 6.12.) (Data sources: Ormerod et al., 1988; Morris et al., 2000; Çubukçu, 2008; Parker, D.F et al., 2010; Özdemir, 2011; Alıcı, 2002; Alıcı Şen et al., 2004; Tang et al., 2006)

Trace element ratios in rocks affected by crustal contamination are La/Ta>22 and La/Nb>1.5 (Hart et al., 1989). Accordingly, HS, OZ and K La/Nb ratios range between (1.72-2.22; 1.63-2.33; 2.63-3.53) and La/Ta ratios range between (23-32; 24-44; 46-58); respectively. All trace element ratios given above gradually increase from HS in the north to K in the southwest. In Figure 5.12, Nb-Ta-Ti negative anomaly and Pb positive anomaly increase gradually from HS (Figure 5.12a) to OZ (Figure 5.12b) and K (Figure 5.12c), thus, supporting the data presented above. This demonstrates that the groups were affected by crustal contamination and/or subduction-related enrichment at different degrees.

6.2.3.1. Potential Contaminants and AFC Modeling

Using AFC modeling and the equations explained in Section 6.1.3.1, isotope AFC modeling was conducted for HS, OZ and K areas. Samples with highest alkalinity in three groups (HA23b, HA26 and KA19) were selected as end members and the same contaminants used for Erciyes stratovolcano AFC modeling, namely biotite-moscovite granite (bmg-1) (Köksal et al., 2012) and plutonic (monzonite) N-26 (İlbeyli, 2004) were employed as contaminants.

CIPW norms of end member samples are given in Table 5.4. References concerning selected contaminants and mineral/melt partition coefficient (Kd) values for basaltic melts are given in Section 6.1.3.1. r values representing the ratio of assimilation rate to fractionation rate given in Equation 6 reveal that exposure to crustal contamination of HS (Figure 6.15a-b), OZ (Figure 6.15c-d) and K (Figure 6.15e-f) ranged between (0.05-0.3), (0.05-0.3) and (0.05-0.1); respectively.

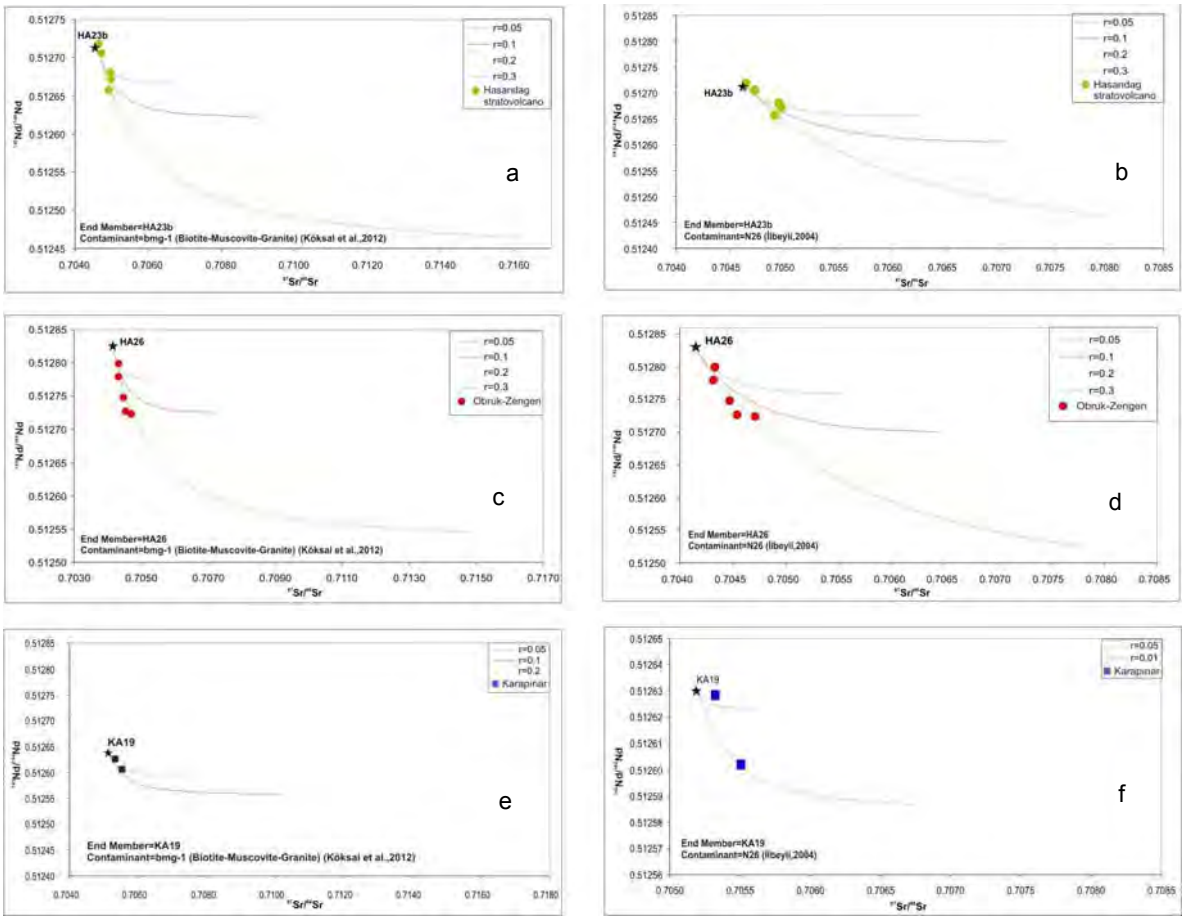

Figure 6.15: $^{143}Nd/^{144}Nd$ vs. $^{87}Sr/^{86}Sr$ AFC modeling diagrams of (a) Hasandağ stratovolcano samples end member HA23b and contaminant bmg1 (biotite muscovite granite), (b) Hasandağ stratovolcano samples end member HA23b and contaminant N26 (monzonite), (c) Obruk-Zengen samples end member HA26 and contaminant bmg1, (d) Obruk-Zengen samples end member HA26 and contaminant N26, (e) Karapınar samples end member KA19 and contaminant bmg1, (f) Karapınar samples end member KA19 and contaminant N26 (Values obtained from (İlbeyli, 2004) are as follows: bmg-1 (biotite muscovite granite) (Sr=183 ppm, Nd=35.3,$^{87}Sr/^{86}Sr$=0.717924,$^{143}Nd/^{144}Nd$=0.512139; (Köksal et al., 2012), and N26 (monzonite) (Sr=911 ppm, Nd=60.12 ppm, $^{87}Sr/^{86}Sr$=0.70804, $^{143}Nd/^{144}Nd$ =0.51227)

6.2.4. Mixing Sources

According to mineralogical and petrographic observations presented in Chapter 3, both equilibrium and disequilibrium plagioclase and olivine minerals were observed in HS, OZ and K basalts, which suggests that the conditions of crystallization were complex. Examination of temperature values of Southwestern Cappadocia volcanics (Table 4.3) reveals that, contrary to ES, olivines exhibit higher temperatures. Depth values calculated using clinopyroxene minerals indicate the existence of a magma chamber and/or magma chambers at a greater depth than ES.

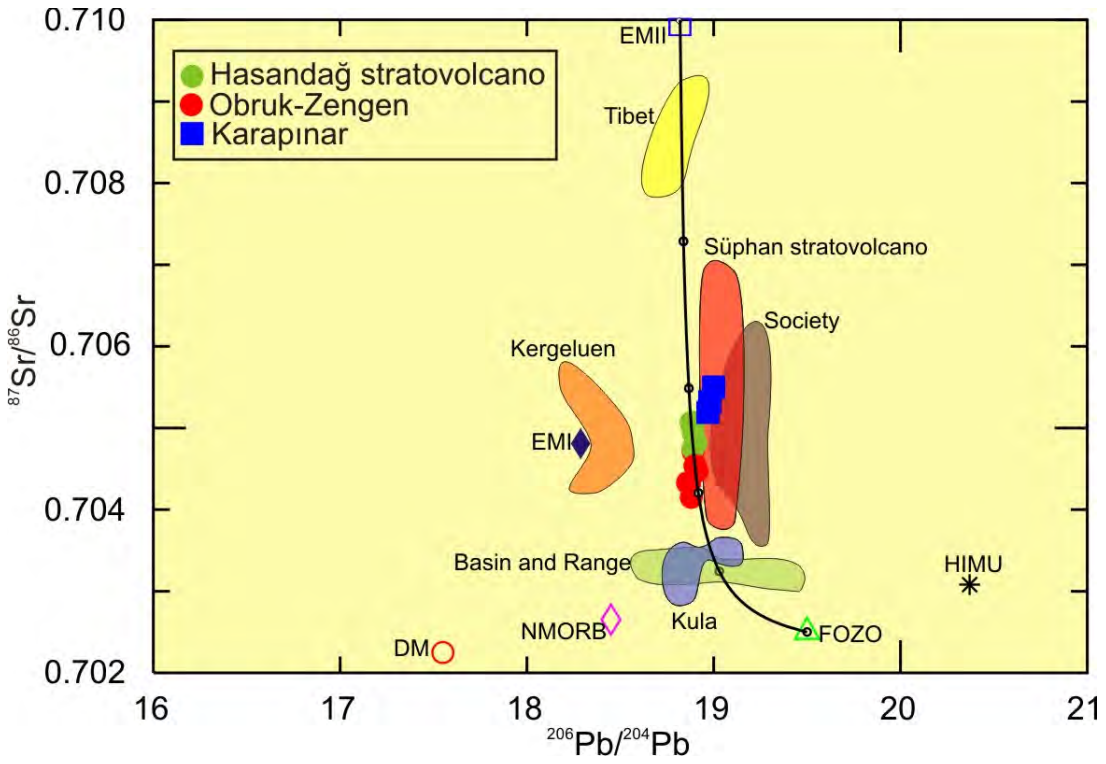

Figure 6.16: $^{87}Sr/^{86}Sr$ vs. $^{206}Pb/^{204}Pb$ mixing diagram of Erciyes volcanics and FOZO-EMII mixing modeling. Data sources: EMII, EMI, HIMU, DM (Zindler and Hart, 1986), NMORB (Okamura et al., 2005), FOZO (Hart et al., 1992), ,Tibet (Tang et al., 2006), Süphan stratovolcano (Özdemir et al.,2011), Society (Devey et al., 1990), Kula (Alıcı Şen et al.,2004), Basin and Range (Kempton et al.,1991), Kergeluen (Gautier et al., 1990)

Multi element diagrams (Figure 5.12), Sr-Nd isotope correlation diagram (Figure 5.25) and Pb isotope correlation diagram (Figure 5.28) of Southwestern Cappadocia volcanics suggest that, similarly to ES, these volcanics also evolved from an enriched heterogeneous source. Mixing modeling of the sources named FOZO (Hofmann, 1997) and/or C (Hannan and Graham,1996), explained in detail

in Section 6.1.4, and EMII source was conducted (Figure 6.16). In the diagram, all HS and OZ samples plotted on the mixing curve whereas K samples plotted near to the mixing curve. In Figure 6.16, HS, OZ and K samples plotted similarly to Süphan stratovolcano samples with a lithospheric + asthenospheric mantle mixture (Özdemir, 2011) and Society Islands samples with an enriched mantle source such as EMII.

6.3. Tectonics

Turkey is a part of the Alpine-Himalayan orogenic belt and one of the most active and complex zones in the world. In order to understand tectonics in Turkey and its structural elements, the Mediterranean Region, especially the Eastern Mediterranean Region, should be examined (Bozkurt, 2001; Faccenna et al., 2003, 2006; Biryol et al., 2011).

The collision of the Eurasian-Arabian plates in the Middle (Early) Miocene changed the Anatolian tectonic regime and initiated the neotectonic period (Şengör, 1980; Şengör and Yılmaz, 1981). This continental collision caused N-S compression in Eastern Anatolia and deformations in the continental crust along the Bitlis Suture Zone. The continental crust shortening and thickening in time, failing to correspond the deformations, enabled the formation of two important transform faults and the Anatolian Block. These are the dextral North Anatolian Fault Zone (NAFZ) and the sinistral East Anatolian Fault Zone (EAFZ).

The development of within plate deformations related to i) collision and ii) subduction roll-back along the Aegean Subduction Zone in the Anatolian Block that lies approximately between NAFZ and EAFZ has been argued (Faccenna 2006; Biryol et al., 2011). Various researchers suggested that, due to the movement of the Arabian, African and Eurasian plates, the Anatolian Block escaping to the west was composed of microplates and that pull-apart basins and thrust faults developed as a result of the mentioned within-plate deformations (Mc Kenzie, 1972; Şengör, 1980; Şengör et al., 1985; Dewey et al., 1986; Lyberis et al., 1992; Yürür and Chorowicz,1998; Dhont et al., 1998). NAFZ is bounded by the Hellenic shear zone near the Gulf of Saros, which slowed its westward escape and

caused a compression in the E-W direction. This compression is balanced with tension stress in the N-S direction and resulted in the development of E-W oriented graben-horst systems in the Western Anatolia Region (McKenzie 1972; Dewey and Şengör, 1979).

Central Anatolia is bounded by Eastern Anatolia subject to the effect of compressional regime since Middle Miocene and Western Anatolia under the influence of tensional regime (Yılmaz, 1990). Various researchers have indicated that the formation of the Central Anatolian volcanism mostly occurred after the collision along the Bitlis Suture Zone (Innocenti et al., 1975, Şengör, 1980, Pasquaré et al., 1988). Besides, the arc volcanism began 10-13 Ma ago and continued until historical times (Innocenti et al., 1975).

The Ecemiş Fault (EF), the Tuzgölü Fault (TF) and local faults are important structural elements of the Central Anatolian Volcanic Province that encompasses the study area. The study of these faults is significant to the association of tectonics and volcanism in the region.

Ecemiş Fault Zone (EFZ)

The Ecemiş Fault was thought to play a significant role in the development of the Erciyes stratovolcano and has been the focus of much research (Arpat and Şaroğlu, 1975; Yetiş and Demirkol, 1984; Pasquaré, 1988; Toprak and Göncüoğlu, 1993; Koçyiğit and Beyhan, 1998). The Ecemiş Fault, denominated differently by various researchers (Bluementhal, 1941; Metz, 1956; Yetiş and Demirkol, 1984, Koçyiğit and Beyhan, 1998) was considered a part of the Central Anatolia Fault Zone (CAVZ) together with the other faults in the region and their segments. CAVZ was defined as a 700 km long, 280 km wide, NE-SW oriented, left-lateral strike-slip fault zone (Koçyiğit and Beyhan, 1998). The age of the Ecemiş fault was estimated as post-Paleocene and pre-Lutetian and it were suggested that EF was a left-lateral strike-slip fault in Quaternary times (Yetiş and Demirkol, 1984)

Parallel segments and different types of related pull-apart basins have developed in the Ecemiş Fault Zone Şengör and Yılmaz, 1981; Yetiş and Demirkol, 1984; Pasquaré et al., 1988, Koçyiğit and Beyhan, 1998). The most important of these

pull-apart basins is *Sultansazlığı* (Şengör and Yılmaz 1981; Pasquaré et al., 1988). The Sultansazlığı pull-apart basin is an S-shaped depression basin that is approximately 35 km wide, 120 km long, and more than 1 km deep. The Erciyes stratovolcano is located at the NNW of Sultansazlığı pull-apart basin and at the center of the Erciyes pull-apart basin.

Pasquaré et al. (1988) and Toprak and Göncüoğlu (1993) stated that EF cuts the main edifice in NE-SW direction. In addition, Koçyiğit and Beyhan (1998) argued that the Develi fault segment in the Ecemiş Fault Zone was the ESE margin of the Erciyes pull-apart basin, and that the Dündarlı-Erciyes fault segment intersected the main edifice.

Kürkçüoğlu (2000) used satellite imaging, digital terrain modeling and aerial photography to identify the NW-SE oriented Göğdağ line, the N-S oriented Yılband line, and other potential faults besides the Ecemiş fault. Furthermore, Genç and Yürür (2011) found three different N-S oriented potential normal faults on the Erciyes stratovolcano. The alkali basalt observed along the Göğdağ line was reported to be the product of the latest activity of the fault (Kürkçüoğlu, 2000). The calcalkaline basaltic andesite ER17 and the alkali basaltic trachyandesite ER29 recovered respectively 2 and 4km NW of Göğdağ in the present study were dated respectively as 45±7 ka and 13±5 ka (Figure 2.2). Moreover, the existence of the calcalkaline andesites ER9 (<1ka), and ER22 (40±7ka), as well as, the calcalkaline basaltic andesite ER11 (<1ka) and ER26 (25±8ka) indicate that northern and northwestern Erciyes was also an active region in historical times.

However, Kürkçüoğlu (2000) later suggested in a verbal correspondence with Dr. Tekin Yürür, that the Ecemiş fault could be lithospheric and could have been responsible for the volcanism in the Erciyes stratovolcano. The coexistence of old, young, alkali and calcalkaline volcanic rocks along the Ecemiş fault and the other mentioned lines substantiates the idea that the faults in the region were active during the Quaternary Period and that it had a significant effect on regional volcanism. However, the last products are not only alkaline but also calcalkaline.

Tuzgölü Fault Zone (TGFZ)

The Tuzgölü Fault is 135 km long and one of the most important faults in the Tuz Gölü Basin. The Tuzgölü Fault is N30–40W oriented and SW and NE dipping fault plane (Erman et al., 2013).

Similar to the EFZ (Ecemiş Fault Zone), TGFZ also comprises parallel segments. The main fault in the TGFZ and the western segment merge in southern Aksaray and are separated by the lavas and cinder cones step-over zones of the Hasandağ stratovolcano (Erman et al., 2013).

TGFZ lays together the basement rocks of the study area and the Plio-Quaternary sediments and cuts the Pliocene limestones and recent alluvials (Erman et al., 2013). In addition, they argued that the contraction in the region ended before 6.81 ± 0.24 Ma and that the N–S to NE–SW extensional tectonic regime began during the Pliocene and has continued until the present times. The traces of two approximately M~6 earthquakes were detected through paleoseismic (trench) studies with a recurrence interval of ~5 ka. The data of the present study also support the existence of, albeit limited, seismic activity along the TGFZ in the Holocene as suggested by Erman et al. (2013). The vertical displacement rates of the limestones in the region along the main fault systems were found to be respectively 0.03-0.05 mm/year and 0.08 to 0.13 mm/year in the western and eastern flanks of the basin.

Pasquaré et al. (1988) argued that the Quaternary monogenic structures in the region had developed as a result of N-S oriented tension cracks, while Toprak and Göncüoğlu (1993) claimed that these tension cracks also caused the development of the structures in the south of Hasandağ and west of Derinkuyu. Consistent with these findings, E-W oriented extension axes can be observed in the Central Anatolia crustal slip vectors map by Genç and Yürür (2011) south of Karapınar and Hasandağ (Dhont et al., 1998).

6.4. Possible Magma Sources

- ***Subduction Component***

Positive anomalies in Ba, Th, Pb and negative anomalies in Nb-Ta-Ti are characteristics of subducting-related magma (Fitton et al. 1988; Saunders et al., 1980). These anomalies are observed in Erciyes and Southwestern Cappadocia (HS, OZ and K) volcanics (Figure 5.6 and 5.12). However, this negative anomaly in Nb-Ta might also indicate crustal contamination of mantle derived magmas rising to the surface (Wilson, 1989). Negative anomaly patterns in Nb-Ta-Ti and positive anomaly patterns in Pb of different scales in Figure 5.6 and Figure 5.12, suggest that these groups were affected by both crustal contamination and subduction related enrichment. Lustrino and Wilson (2007) indicated that negative Nb-Ta and positive Pb anomalies could be observed as a result of two different processes; namely i) crustal contamination occurring at shallow depth with the addition of subducted sediments to the mantle source of the magma ii) fluid-induced enrichment. There are significant differences between a source enriched by fluid components separated from the subduction slab and a source enriched by a subducted sedimentary component (Hawkesworth et al., 1997; Elburg et al., 2002; Chiaradia et al., 2011). According to Chiaradia et al. (2011),, enrichment in aqueous fluid-immobile incompatible elements (Th, La, Zr, Nb) and Th/La, Th/Nb ratios suggest a significant difference in the slab component or in the mantle source. High Th/La ratios (0.28-0.36) and Th values (4-24 ppm) mostly indicate the existence of a subducted sediment component in the mantle source (Plank, 2005).

However, subduction related magmas which strongly have traces of partial melting or have subducted sediments in their sources. Subduction related magmas are separated from fluid metasomatism affected magmas at the mantle source due to their high Th/Ce>0.15, $^{87}Sr/^{86}Sr$, $^{206}Pb/^{204}Pb$ (Hawkesworth et al., 1997; Guo et al., 2006) and low $^{143}Nd/^{144}Nd$, Ba/La (Sheppard and Taylor; 1992 Hawkesworth et al., 1997) ratios.

The Th/La, Th, Th/Ce, $^{87}Sr/^{86}Sr$, and $^{206}Pb/^{204}Pb$ ratios of Erciyes volcanics vary between (0.08-0.24), (1.84-5.81), (0.04-0.12), (0.703609-0.705084) and (18.95-18.88); respectively (Table 6.5). $^{143}Nd/^{144}Nd$ isotope values and Ba/La ratios of the volcanics, except for ER30 (18.08), range between (0.512652-0.512875) and (10.04 -14.299; respectively. Th/La, Th/Ce and Th values of Erciyes samples are mostly lower than designated reference ranges, while Sr, Pb, Nd isotope values are higher and Ba/La ratios are also lower.

Th/La and Th values for HS, OZ and K vary between (0.13-0.17), (0.15-0.35), (0.22-0.31) and (3.56-4.65), (3.51-9.01), (6.23-9.24), respectively. Th/Ce ranges were (0.07-0.09), (0.07-0.18) and (0.11-0.16); while $^{87}Sr/^{86}Sr$ ranges were (0.704734-0.704981), (0.704153-0.704711) and (0.705188-0.705502); and $^{206}Pb/^{204}Pb$ ranges were (18.88-18.90), (18.86-18.91) and (18.97-19.00); respectively, for HS, OZ and K. Whereas their $^{143}Nd/^{144}Nd$ isotope values and Ba/La ratios range between (0.512679-0.512740), (0.512723-0.512826), (0.512602-0.512633) and (12.35-13.28), (11.18-16.81) and (11.48-12.45); respectively.

Th/La and Th/Ce values for HS, OZ and K are generally lower than designated reference ranges, whereas Th values are within designated reference ranges (Table 6.5). These ratios show that the Erciyes stratovolcano was less affected by subducted sediments than HS, OZ and K.

Sr/Th ratio is higher in arc volcanic rocks due to the higher mobility of Sr compared to Th in aqueous fluids (Hofmann et al., 1997). Sr/Th vs. $^{87}Sr/^{86}Sr$ diagrams (Figure 6.17a) reveals that Sr isotope ratio is inversely proportional to Sr/Th ratio except for ER13 of this study from the New Erciyes stage and the alkalibasalt ERC96-116 (Kürkçüoğlu, 1998) from the Koçdağ stage. Whereas, in Figure 6.16b, HS, OZ and K samples of the present study display an alignment from OZ to K exactly as in $^{87}Sr/^{86}Sr$ vs. $^{143}Nd/^{144}Nd$ diagrams. In this diagram (Figure 6.17b), Deniel et al. (1998) samples plotted within the same range as HS.

The samples display a sediment input trend in Ba/La vs. Th/Yb diagrams (Figure 6.17b), and Th/Yb and Ba/La values are lower than $GLOSS_{(average)}$ (Global

subducting sediment). The lack of a correlation between the ages (ka) vs. Sr isotope values of the Erciyes volcanics was stressed previously in Chapter 5 (Figure 5.8a). Isotope and trace element ratios and their distributions indicate that Erciyes volcanism had an enriched and heterogeneous mantle source.

Ba/La vs. Th/Yb diagrams of HS, OZ and K (Figure 6.17c) reveal that, among the samples of the study, especially K has a sediment input trend. These values are generally lower than $GLOSS_{(average)}$ but Miocene basalt and basaltic andesite samples of Deniel et al.,(1998) mainly have a slab derived sediment input trend, with values at approximately at $GLOSS_{(average)}$ (Figure 6.17d).

The research data indicate that the effect of subduction in Central Anatolia decreased from the Miocene to the Quaternary, and the Quaternary samples mainly had a sediment input trend than a slab-derived fluids trend (Figure 6.17d).

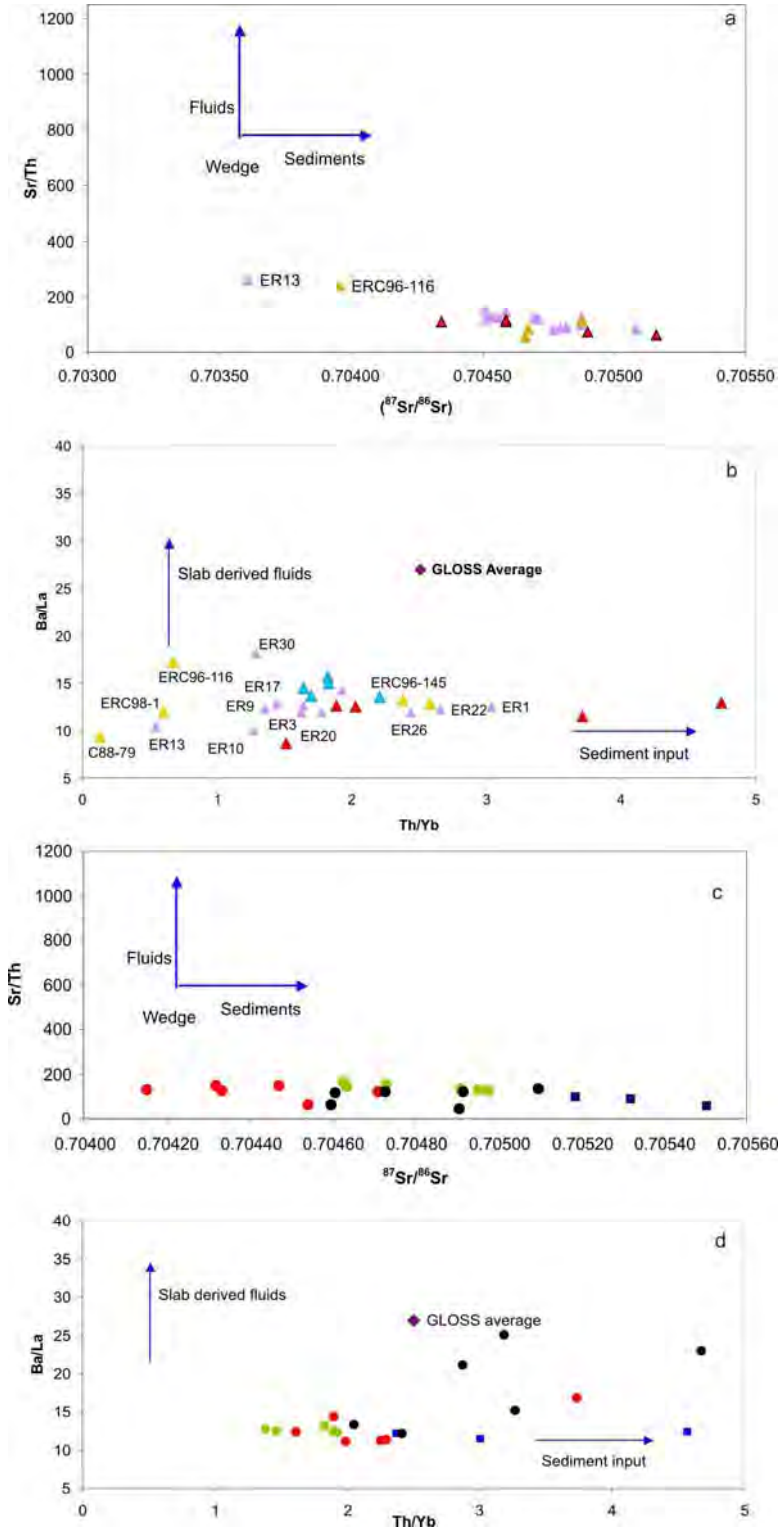

Figure 6.17: Comparison of Erciyes, Southwestern Cappadocia (HS, OZ and K) and previous research samples with GLOSS (average).

Table 6.5: Erciyes stratovolcano and Southwestern Cappadocia (HS, OZ and K) trace element ratios and Sr, Nd, Pb isotope values

	Erciyes stratovolcano														
	ER1	**ER3**	**ER9**	**ER10**	**ER11**	**ER13**	**ER17**	**ER20**	**ER22**	**ER26**	**ER27(1)**	**ER27(2)**	**ER29**	**ER30**	**ER32**
Th	5.81	3.79	3.31	3.19	3.78	1.84	3.44	3.75	4.71	4.84	4.79	4.79	4.91	3.08	3.35
Th/La	0.21	0.17	0.13	0.14	0.13	0.08	0.13	0.15	0.22	0.18	0.20	0.24	0.14	0.13	0.17
Th/Ce	0.11	0.08	0.07	0.07	0.07	0.04	0.07	0.08	0.12	0.10	0.12	0.12	0.07	0.07	0.09
Ba/La	12.57	11.88	12.34	10.04	12.68	10.41	12.83	11.89	12.21	11.92	12.53	12.53	14.29	18.08	12.62
Sr/Th	84.46	124.75	119.96	145.77	118.38	259.55	124.35	123.46	80.94	85.19	96.98	88.49	124.24	154.52	121.41
$^{206}Pb/^{204}Pb$	18.90	18.88	18.92	18.90	18.92	18.95	18.90	18.89	18.91	18.90	18.89	18.89	18.91	18.95	18.90
$^{87}Sr/^{86}Sr$	0.705084	0.704537	0.704511	0.704587	0.704710	0.703609	0.704534	0.704697	0.704769	0.704875	0.704796	0.704817	0.704876	0.704509	0.704557
$^{143}Nd/^{144}Nd$	0.512652	0.512722	0.512710	0.512729	0.512696	0.512875	0.512696	0.512690	0.512686	0.512685	0.512695	0.512696	0.512670	0.512718	0.512699

	Hasandag stratovolcano						Obruk- Zengen						Karapınar		
	HA13b	**HA18**	**HA19**	**HA20**	**HA23b**	**HA31**	**HA14**	**HA15**	**HA16**	**HA17**	**HA26**	**HA27**	**KA18**	**KA19**	**KA21**
Th	4.48	4.23	3.56	4.48	3.59	4.65	5.32	3.51	4.35	3.51	5.29	9.01	6.70	6.23	9.24
Th/La	0.14	0.15	0.13	0.14	0.15	0.17	0.17	0.15	0.17	0.19	0.23	0.35	0.22	0.22	0.31
Th/Ce	0.07	0.08	0.07	0.08	0.07	0.09	0.08	0.07	0.09	0.10	0.11	0.18	0.12	0.11	0.16
Ba/La	12.60	13.28	12.59	12.35	12.83	12.45	11.44	12.44	11.18	14.39	11.24	16.81	11.48	12.23	12.45
Sr/Th	128.79	143.91	154.26	133.53	164.45	127.75	127.63	150.14	122.30	146.44	131.60	60.77	91.96	97.19	60.16
$^{206}Pb/^{204}Pb$	18.90	18.88	18.89	18.90		18.90	18.86	18.87	18.87	18.87	18.88	18.90	18.98	18.97	19.00
$^{87}Sr/^{86}Sr$	0.704952	0.704636	0.704729	0.704908	0.704625	0.704976	0.704333	0.704319	0.704711	0.704472	0.704153	0.704542	0.705320	0.705188	0.705502
$^{143}Nd/^{144}Nd$	0.512680	0.512718	0.512705	0.512657	0.512714	0.512672	0.512799	0.512779	0.512723	0.512748	0.512826	0.512727	0.512629	0.512633	0.512602

- ***Enriched mantle sources in the continental lithosphere***

"The trace element and isotopic compositions of the basalts act as tracers that track the material differentiation and cycling in the mantle" (Iwamori and Nakamura, 2015). Primitive mantle (PM)-normalized trace element diagrams for the samples from ES, HS, OZ and K are enriched in the LILE and LREE, and they show strong Pb spikes (Figure 5.6; Figure 5.12). According to Downes et al. (1995) the strong Pb spikes may be derived by preferential stripping of the lithosphere of Pb during passing to the surface. In addition, the Pb isotopic characteristics of the mantle source of the basalts may have been altered by the introduction of crustal Pb from sediment subduction. Figure 6.16 reveals a sediment input trend rather than a slab-derived fluids trend in the volcanic basalts. The addition of sediment into the mantle has not greatly affected the Sr and Nd characteristics of the mantle, which are still similar to the OIB-source (Downes et al., 2001). Sr, Nd and O isotope values do not suggest a strong contamination in the studied area. The AFC modeling conducted supports this finding (Figure 6.7; Figure.6.15). The extent of crustal contamination varies at different regions within the studied area. The lead isotope ratios display EM2-type character for all four volcanic groups (Figure 5.17; Figure 5.28) and plot above the Northern Hemisphere Reference Line.

Geophysical data indicate the absence of a mantle plume and contemporaneous subduction (Deniel et al., 1998) beneath present-day Central Anatolia. As explained before, all four volcanic groups have high $^{206}Pb/^{204}Pb$, moderately high $^{87}Sr/^{86}Sr$ and $^{143}Nd/^{144}Nd$, and low oxygen ratios.

- ***Asthenosphere –Lithosphere interaction***

In spite of the existence of many major and trace element data related to Central Anatolian Volcanic Province, there isn't much geophysical, age and isotope data. In this study, the Quaternary age basaltic volcanism products show a much more complex pattern than expected. There is no record of any mantle xenoliths that determined in the literature for Central Anatolia. Accordingly, we have less information about asthenosphere - lithosphere interaction beneath Central Anatolia.

Recent geophysical studies in Eastern and Western Mediterranean on Europe and Eurasia plates revealed various scenarios regarding crustal thickness, uplift and uplift time, subduction, slab detachment, slab delamination, slab rollback, and slab break-off processes, as well as, new data on mantle-crust relation and asthenosphere-lithosphere interaction (Govers and Wortel, 2005; Biryol et al., 2011; Consentino et al., 2012; Schidgen et al., 2012; Faccenna et al., 2006, 2013, Aydar et al., 2013).

Faccenna et al. (2013) discussed, how Afar Plume might have affected the Arabian, Anatolian and Aegean systems. According to Cosentino et al. (2012) and Faccenna et al. (2013) the slab window formation at ~8-10 Ma widen westward. The stated event may be the reason of hot material migration from Arabia towards Southeast of Turkey. Karacadağ volcanics are located at the southeast region of Turkey that is lying in the north of Arabian continent. The geochemical data of Karacadağ display both asthenospheric and enriched sub-continental lithospheric mantle source signatures (Keskin et al., 2012). According to Keskin et al. (2012), the situation may be explained by the Afar Plume. However, In Th/Yb vs. Ta/Yb diagrams (Figure 6.4 and Figure 6.12) Karacadağ and this thesis samples (ES, HS, OZ and K samples) do not indicate the same trends. Besides, isotopically, Pb and Nd values of Karacadağ samples are higher than ES, HS, OZ and K. Karacadağ and this thesis samples (ES, HS, OZ and K) do not match at the same area in $^{207}Pb^{204}Pb$ vs. $^{206}Pb/^{204}Pb$ isotope correlation diagram. This result indicates that the effect of the Afar Plume is not being observed in Quaternary basaltic volcanism Central Anatolia according to the findings studied in this thesis. The future studies may help to determine more accurately whether there is a link between Central Anatolia and the Afar Plume or not.

One of the most significant of these data is particularly whether the Cyprus slab could singly generate the volcanism in Central Anatolia from Late Miocene until the Quaternary period (Biryol et al., 2011). Bartol and Govers (2014) showed that the effect of the Cyprus slab, which is presently at 660 km depth, on the surface was limited and proved that it could not generate the Central Anatolian volcanism on its own. Their tomographic results revealed a single slab moving horizontally

from the west towards the east, and they suggested a model where instantaneous delamination occurred beneath both the Eastern Anatolian Plateau (EAP) and Central Anatolian Plateau (CAP). Furthermore, they postulated that the "delamination progressed too fast (on geological time scales) to leave a migration footprint in the geological record" (Bartol and Govers, 2014).

6.5. Comparison of ES, HS, OZ and K

In previous sections, geochronological, geochemical, mineralogical and petrographic information on ES, HS, OZ and K basaltic samples was provided. In this section, the results for the Quaternary basalts from these four regions shall be comparatively discussed. Figure 2.6 reveals that ES basaltic andesites and andesites are calcalkaline whereas the basalts and basaltic andesites from HS, OZ and K are mostly alkaline. In post-collisional volcanisms, generally calcalkaline products surface before alkaline products, whereas the majority of alkaline and calcalkaline products from the studied area had formed in the same time interval (Figure 2.6; Table 2.3; Table 2.4). In Chapter 5, the incompatibility particularly between trace element and isotope data for HS, OZ and K indicate a spatial grouping rather than temporal in Central Anatolia. Table 5.7 and Table 5.8 reveal that the products from these four regions with similar multielement and spidergram patterns (Figure. 6.18) but different isotope values have undergone different magmatic processes.

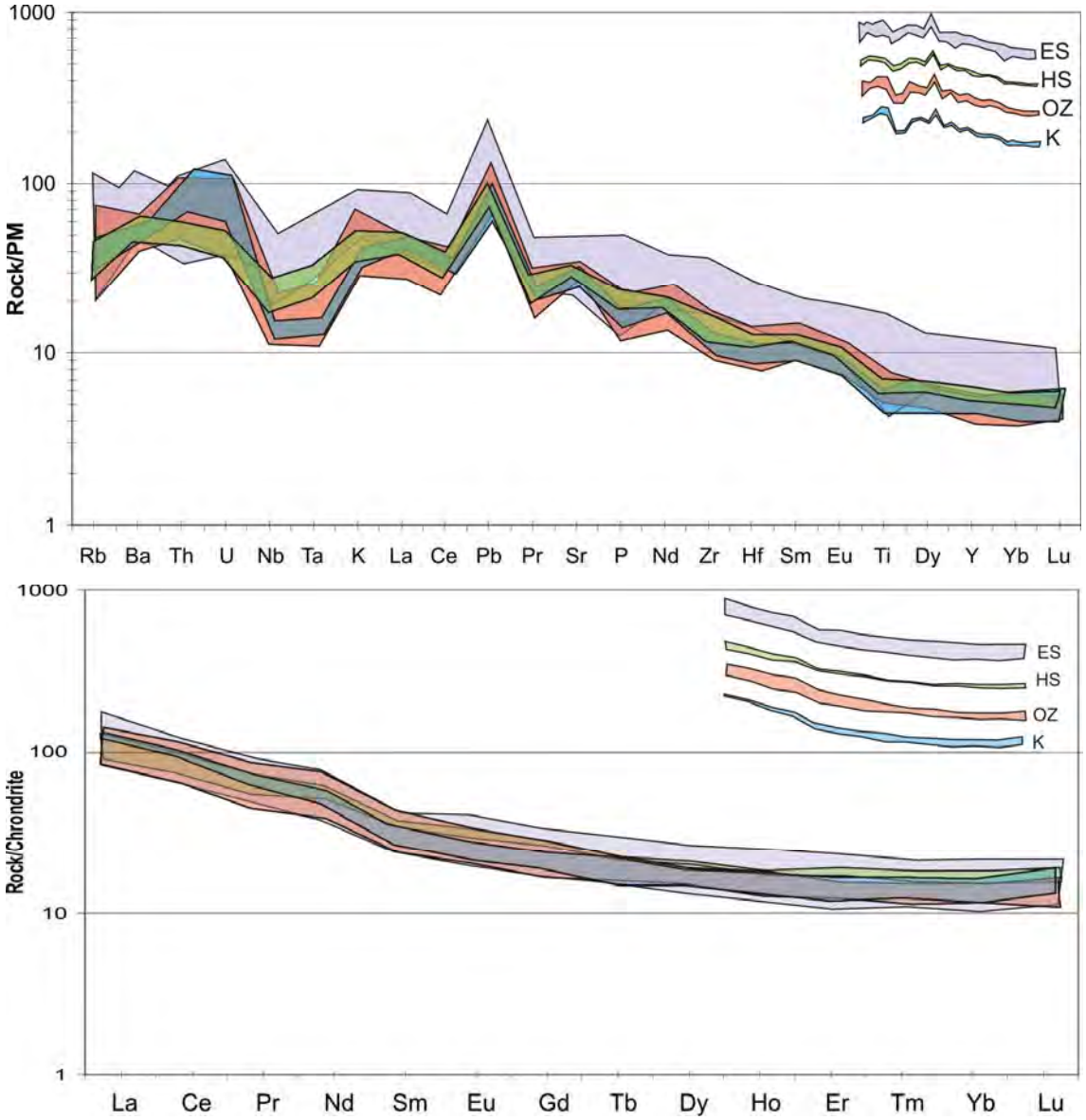

Figure 6.18: (a) Comparison of multielement diagram of ES, HS, OZ and K, (b) Comparison of spidergram of ES, HS, OZ and K. (Values were normalized to Chondrite and PM (Sun and McDonough, 1989)

The modeling revealed that the magma chamber(s) of the Erciyes stratovolcano located in the pull-apart basin are relatively closer to the surface. On the other hand, albeit the existence of isotopic enrichment due to lithosphere - asthenosphere interaction as related in the previous section, the Erciyes stratovolcano was not affected by crustal contamination as much as HS, OZ and K. Whereas, contrary to Erciyes, the Hasandağ stratovolcano samples are rather more alkaline basaltic products and although spidergrams showed that the affect of crustal contamination was lower than in OZ, the isotope data indicated

otherwise (Figure 5.6; Figure 5.12). This substantiates that the source had a heterogeneous chemistry; e.g. the existence of a source mixing (Figure 6.8; Figure 6.16). On the other hand, Obruk-Zengen and Karapınar dispersed volcanism products, with the exception of the stratovolcanoes, have intra-group and inter-group differences. The fact that the majority of Obruk-Zengen alkali products are older than HS and K indicates that deeper magma chamber(s) were active at different periods. However, due to the analogous age range of the samples, it is difficult to speculate on the processes affecting the source(s).

6.6. Temporal and spatial evolution of magma

In post-collisional volcanisms, generally calcalkaline products erupted before alkaline products, whereas the majority of alkaline and calcalkaline products from the studied area had formed in the same time interval. The majority of the alkali basalts and basaltic andesites collected from HS, OZ and K, and ES basaltic andesites have particularly the same age range. The temperature and pressure values calculated using the microprobe analysis data revealed the existence of more than one magma chamber, which previous researchers had also indicated this information (Aydar, 1992; Aydar and Gourgaud, 1997; Güçtekin, 1997). The age data show that spatial evolution was more effective in these four regions than temporal evolution. The analogous age ranges of the samples and the fact that the ages of some samples varied only by a few thousand years hindered the ascertainment of temporal evolution. The data sets of the present study and tomographic images of recent studies indicate that it is not really possible to speak of the existence of a present-day plume in Central Anatolia (Biryol et al., 2011). The geochemical data of the present study suggest that these four regions had mainly evolved from the lithospheric mantle.

Furthermore, the identification of an uplift in Mediterranean in recent studies and the 2 km elevation of the Mut-Ermenek Basin (Cosentino et al., 2012) are indicative of the activity in Eastern Mediterranean. According to the tomographic images of Biryol et al. (2011), the Isparta Angle corresponds to the STEP related tear between the Aegean and Cyprian trenches. The Gölcük volcanism is located immediately above this STEP related tear. Data on Gölcük volcanism indicate a lithospheric mantle source (Alıcı Şen, 1997. Therefore, the traces of the

asthenospheric mantle might have affected the lithospheric mantle not directly but as percolations in Central Anatolia. The model developed by Leat et al. (1989) revealed that the Colorado Quaternary basalts had evolved from three different mantle sources. According to this model, the formation of the Colorado Quaternary basalts had occurred through the partial melting of each of the lithospheric mantles, asthenospheric mantle and the thermal boundary layer of lithospheric mantle.

In this thesis, the spatio-temporal evolution of the Quaternary basaltic volcanism in Central Anatolia has been discussed, using geological, geochronological, mineralogical, petrographical and geochemical data. The basalt ages revealed that the basaltic volcanism is younger than the known data in the geological literature, studied in Central Anatolia. All geochemical data, sources and temporal relations of ES, HS, OZ and K are presented below (Table 6.5).

Table 6.5: Geochemical summary of the studied volcanic centers in Central Anatolia.

Study Area	Sources	Magma Type	Process	Mantle Sources	K-Ar Dating (ka)
Erciyes Stratovolcano (ES)	Enriched Mantle	Excpet ER13 and ER29 Majority of the samples are calc-alkaline basaltic-andesite	*Partial Melting→ F%(6-15) *Fractional Crystallisation→ predominant *AFC→ r=(0.1-0.2)	Spinel peridodite	*The oldest sample ER13 (1695±37) *The youngest samples ER9 and ER11 (<1) * ER32 from Kızıltepe (East of ES) (707±20 ka) *Most samples aged ~45 ka and younger (North and Northwest of ES)
Hasandağ Stratovolcano (HS)	Enriched Mantle	Alkaline basalts	Partial Melting→ F%(8-9) Fractional Crystallisation→more effective than OZ and K AFC→ r=(0.05-3)	Spinel peridodite	* The oldest sample HA23b (543±12) * The youngest sample HA31 (2±7) * Most samples are ~100 ka or younger
Obruk-Zengen dispersed volcanism (OZ)	Enriched Mantle	Except HA27 and HA17 Majority of the samples are alkaline basalts	Partial Melting→ F%(8-12) Fractional Crystallisation→less effective AFC→ r=(0.05-3)	Spinel peridodite	* The oldest sample HA16 (799±20) * The youngest sample HA17 (66±7) * Most samples are ~300 ka or older
Karapınar dispersed volcanism (K)	Enriched Mantle	Except KA19 The other samples are calc-alkaline basalts	Partial Melting→ F%(8) Fractional Crystallisation→less effective AFC→ r=(0.05-0.2)	Spinel peridodite	* The oldest sample KA18 (280±7) * The youngest sample KA19 (<1)

Table. 6.5: continued.

Study Area	Geochemical Features				
	Pb	$^{87}Sr/^{86}Sr$	$^{143}Nd/^{144}Nd$	$\delta^{18}O‰$	Elemantal ratios
Erciyes Stratovolcano (ES)	($^{206}Pb/^{204}Pb$)→ (18.87-18.94) (ER3-ER13) ($^{207}Pb/^{204}Pb$)→(15.64-15.68) (ER13-ER29) ($^{208}Pb/^{204}Pb$)→(38.93-39.05) (ER13-ER22)	(0.70360-0.70508)- (ER13-ER1)	(0.51265-0.51287) (ER1-ER13)	(6.00-7.12) (ER32-ER30)	La/Nb→ (1.52-2.73) Ba/Nb →(17-39) Nb/U→ (7-23) Nb/La→(0.37-0.66) Th/Y→(0.05-0.32) Th/Nb→(0.14-0.68)
Hasandağ Stratovolcano (HS)	($^{206}Pb/^{204}Pb$)→ (18.88-18.90) (HA18-HA13b) ($^{207}Pb/^{204}Pb$)→(15.66-15.67) (HA19-HA13b) ($^{208}Pb/^{204}Pb$)→(38.96-39.01) (HA18-HA13b)	(0.704625-0.704976)-(HA23b-HA31)	0.512657-0.512718 (HA20-HA18)	(6.62-6.79) (HA19-HA13b)	La/Nb→(1.7-2.2) Ba/Nb→ (22-28) Nb/U→(12-21) Nb/La→(0.45-0.58) Th/Y→(0.14-0.20) Th/Nb→(0.22-0.37)
Obruk-Zengen dispersed volcanism (OZ)	($^{206}Pb/^{204}Pb$)→(18.86-18.91) (HA14-HA17) ($^{207}Pb/^{204}Pb$)→(15.64-15.66) (HA14-HA16) ($^{208}Pb/^{204}Pb$)→(38.89-38.98) (HA14-HA27)	(0.704153-0.704711) (HA26-HA16)	(0.512723-0.512826) (HA16-HA26)	(5.88-7.27) (HA26-HA27)	La/Nb→ (1.6-2.3) Ba/Nb→ (20-36) Nb/U→(6-18) Nb/La→(0.43-0.61) Th/Y→(0.17-0.38) Th/Nb→(0.24-0.74)
Karapınar dispersed volcanism (K)	($^{206}Pb/^{204}Pb$)→(18.97-19.00) (KA19-KA18) ($^{207}Pb/^{204}Pb$)→(15.69-15.70) (KA18;KA19-KA21) ($^{208}Pb/^{204}Pb$)→(39.13-39.19) (KA19-KA21)	(0.705188-0.705502) (KA19-KA21)	(0.512602-0.512633) (KA21-KA19)	(6.31-6.75) (KA21-KA18)	La/Nb→2.6-3.5) Ba/Nb→(32-44) Nb/U→(4-9) Nb/La→(0.28-0.33) Th/Y→(0.25-0.47) Th/Nb→(0.58-1.09)

Table. 6.5. continued.

Study Area	Estimated Geothermobarometer		
	Temperature (°C) [98]	Pressure (kbar) [98]	Depth (km)
Erciyes Stratovolcano (ES)	cpx-liq→ 1138(ER26)-1167 (ER10) ol-liq→1160 (ER32)- 1260 (ER3) two pyx→ 1024 (ER3-ER22) plg→1146 (ER30)- 1183 (ER26)	4.20 (ER10) 4.90 (ER22)	10.5 (ER26) 17 (ER10)
Hasandağ Stratovolcano (HS)	cpx-liq→ 1208 (HA20) ol-liq→1199(HA31)-1273(HA20) plg→1250 (HA31)	4.66 (HA20)	18 (HA20)
Obruk-Zengen dispersed volcanism (OZ)	cpx-liq→ 1120 (HA27)-1233 (HA16) ol-liq→1135(HA27)-1296(HA16) plg→ 1164 (HA27)-1207(HA14)	7.79 (HA16)	28 (HA16)
Karapınar dispersed volcanism (K)	cpx-liq→ 1172 (KA19) ol-liq→ 1262 (KA18)-1263(KA21) plg→ 1171 (KA21)- 1228 (KA19)	5.30 (KA19)	21 (KA19)

APPENDIX

Representative microprope analyses of plagioclase minerals from Erciyes Stratovolcano (c:center, r:rim, mic:microlite)

(Calculated for 32O).

Samples	**ER1**													**ER3**	
	Phenocryst								**Microlite**					**Phenocryst**	
	57—c	***58—r***	***59—c***	***60—r***	***72—c***	***73—r***	***87—c***	***88—r***	***64—mic***	***96—mic***	***104—mic***	***105—mic***	***108—mic***	***6—c***	***7—r***
SiO_2	51.73	50.11	52.78	51.80	50.51	47.69	48.85	50.98	53.58	51.40	51.19	53.11	52.26	52.93	53.72
Al_2O_3	29.92	31.24	29.73	29.88	31.06	33.17	32.56	31.23	28.86	30.00	29.86	28.68	29.39	28.84	28.48
FeO	0.52	0.46	0.50	0.48	0.44	0.41	0.15	0.24	0.93	0.74	0.77	0.90	0.76	0.47	0.49
MgO	0.06	0.08	0.05	0.08	0.07	0.08	0.02	0.00	0.05	0.19	0.17	0.15	0.15	0.06	0.05
CaO	13.11	14.69	12.89	13.28	14.47	17.07	15.78	14.49	12.23	13.84	13.43	12.01	13.31	12.11	11.43
Na_2O	3.92	3.13	4.06	3.98	3.29	1.86	2.52	3.47	4.40	3.63	3.78	4.25	4.09	4.58	4.87
K_2O	0.09	0.10	0.09	0.13	0.14	0.05	0.18	0.17	0.25	0.16	0.21	0.26	0.22	0.15	0.18
Total	99.35	99.81	100.09	99.62	100.03	100.36	100.08	100.58	100.33	99.98	99.45	99.38	100.18	99.21	99.23
Si	9.47	9.17	9.57	9.47	9.23	8.74	8.94	9.25	9.71	9.39	9.40	9.71	9.52	9.68	9.80
Al	6.46	6.74	6.36	6.43	6.69	7.17	7.02	6.68	6.16	6.46	6.46	6.18	6.31	6.22	6.12
Fe	0.08	0.07	0.08	0.07	0.07	0.06	0.02	0.04	0.14	0.11	0.12	0.14	0.12	0.07	0.07
Mg	0.02	0.02	0.01	0.02	0.02	0.02	0.01	0.00	0.01	0.05	0.05	0.04	0.04	0.02	0.01
Ca	2.57	2.88	2.50	2.60	2.83	3.35	3.09	2.82	2.38	2.71	2.64	2.35	2.60	2.37	2.24
Na	1.39	1.11	1.43	1.41	1.17	0.66	0.90	1.22	1.55	1.28	1.35	1.51	1.45	1.62	1.72
K	0.02	0.02	0.02	0.03	0.03	0.01	0.04	0.04	0.06	0.04	0.05	0.06	0.05	0.03	0.04
An	64.58	71.76	63.38	64.34	70.25	83.28	76.76	69.10	59.72	67.22	65.44	59.99	63.44	58.86	55.87
Ab	34.91	27.64	36.10	34.93	28.93	16.45	22.22	29.92	38.85	31.87	33.36	38.47	35.32	40.30	43.05
Or	0.51	0.60	0.52	0.73	0.81	0.27	1.02	0.98	1.43	0.91	1.20	1.54	1.23	0.84	1.08

Representative Microprope analyses of olivine minerals from Erciyes Stratovolcano (c:center, r:rim, mic:microlite) (Calculated for 4O).

Samples	**ER1**														
	Phenocryst														**Micro phenocryst**
	51—c	***52—r***	***53—c***	***54—r***	***66—c***	***67—r***	***77—c***	***78—r***	***79—c***	***80—r***	***100—c***	***101—r***	***102—c***	***103—r***	***89—c***
SiO_2	40.99	40.21	40.76	39.78	39.04	38.94	40.86	40.30	40.50	39.34	40.07	39.27	40.46	40.13	40.18
TiO_2	0.01	0.00	0.06	0.00	0.00	0.00	0.00	0.05	0.00	0.01	0.00	0.03	0.01	0.01	0.01
Al_2O_3	0.06	0.03	0.03	0.00	0.02	0.02	0.03	0.03	0.02	0.00	0.02	0.02	0.04	0.03	0.03
FeO	13.49	15.67	12.87	15.70	19.95	22.11	13.15	14.47	15.14	20.58	15.59	20.95	13.26	15.42	14.59
MnO	0.20	0.32	0.12	0.21	0.34	0.37	0.19	0.25	0.22	0.29	0.22	0.31	0.21	0.16	0.26
MgO	45.62	43.27	46.23	44.06	40.73	39.65	45.80	45.17	45.15	40.58	44.23	40.14	46.02	44.79	45.30
CaO	0.12	0.17	0.14	0.09	0.17	0.18	0.12	0.15	0.17	0.17	0.18	0.12	0.11	0.11	0.16
Total	100.55	99.73	100.25	99.96	100.35	101.33	100.20	100.49	101.31	100.98	100.41	100.93	100.17	100.77	100.59
Si	1.01	1.01	1.01	1.00	1.00	1.00	1.01	1.00	1.00	1.00	1.00	1.00	1.00	1.00	1.00
Fe^{+2}	0.28	0.33	0.27	0.33	0.43	0.47	0.27	0.30	0.31	0.44	0.33	0.45	0.28	0.32	0.30
Mn	0.00	0.01	0.00	0.00	0.01	0.01	0.00	0.01	0.00	0.01	0.00	0.01	0.00	0.00	0.01
Mg	1.68	1.63	1.71	1.65	1.56	1.51	1.69	1.68	1.67	1.54	1.65	1.53	1.70	1.67	1.68
Ca	0.00	0.00	0.00	0.00	0.00	0.01	0.00	0.00	0.00	0.00	0.00	0.00	0.00	0.00	0.00
Fo	85.59	82.82	86.38	83.15	78.15	75.86	85.95	84.54	83.97	77.61	83.29	77.09	85.89	83.67	84.46
Fa	14.20	16.83	13.49	16.62	21.48	23.74	13.85	15.19	15.80	22.08	16.47	22.57	13.89	16.16	15.26
Tp	0.21	0.35	0.13	0.23	0.37	0.41	0.20	0.27	0.23	0.32	0.24	0.34	0.22	0.17	0.28

Representative microprope analyses of clinopyroxene minerals from Erciyes Stratovolcano (c:center, r:rim, mic:microlite)
(Calculated for 4 cation and 6O).

Samples	**ER1**														
	Microphenocryst						**Microlite**								
	69—c	***70—r***	***74—c***	***75—r***	***84—c***	***85—r***	***55—mic***	***71—mic***	***81—mic***	***86—mic***	***93—mic***	***97—mic***	***109—mic***	***110—mic***	***107—mic***
SiO_2	51.50	50.08	51.59	50.81	53.23	52.18	50.99	51.14	50.31	51.51	52.51	52.71	52.11	51.26	54.14
TiO_2	0.90	0.78	0.86	1.27	0.39	0.60	0.88	0.78	1.27	0.70	0.74	0.63	1.08	1.09	0.35
Al_2O_3	3.62	4.50	5.26	4.24	2.42	3.79	4.29	4.08	5.48	4.03	1.90	1.77	2.39	3.02	1.06
FeO	7.31	6.23	6.48	7.68	5.73	5.90	7.63	5.95	7.05	6.19	9.91	10.18	11.34	10.33	6.74
MnO	0.22	0.21	0.18	0.24	0.17	0.19	0.14	0.11	0.17	0.18	0.26	0.27	0.34	0.27	0.16
MgO	17.26	15.81	16.17	15.82	18.14	16.87	16.50	16.44	16.71	17.06	16.68	17.79	15.47	17.15	18.17
CaO	18.90	20.37	20.23	19.46	19.58	20.31	18.45	20.69	18.07	19.99	17.75	16.22	16.66	16.27	18.60
Na_2O	0.25	0.35	0.31	0.32	0.27	0.31	0.40	0.31	0.36	0.32	0.29	0.28	0.50	0.29	0.33
Total	100.06	99.01	101.13	100.14	100.22	100.56	99.47	99.91	99.71	100.56	100.15	100.04	100.10	99.85	99.62
Si	1.89	1.86	1.87	1.87	1.93	1.90	1.88	1.87	1.85	1.87	1.94	1.94	1.94	1.90	1.98
Al^{IV}	0.12	0.15	0.13	0.13	0.07	0.10	0.12	0.13	0.15	0.13	0.06	0.06	0.06	0.11	0.02
Al^{VI}	0.04	0.05	0.09	0.05	0.04	0.06	0.07	0.05	0.08	0.04	0.02	0.02	0.04	0.03	0.03
Fe^{+3}	0.04	0.06	0.01	0.02	0.02	0.02	0.03	0.05	0.02	0.05	0.02	0.02	0.01	0.04	0.00
Fe^{+2}	0.18	0.14	0.18	0.22	0.16	0.16	0.21	0.14	0.20	0.14	0.29	0.29	0.35	0.28	0.21
Mn	0.01	0.01	0.01	0.01	0.01	0.01	0.01	0.00	0.01	0.01	0.01	0.01	0.01	0.01	0.01
Mg	0.94	0.87	0.87	0.87	0.98	0.91	0.91	0.90	0.91	0.93	0.92	0.98	0.86	0.95	0.99
Ca	0.74	0.81	0.79	0.77	0.76	0.79	0.73	0.81	0.71	0.78	0.70	0.64	0.66	0.64	0.73
Na	0.02	0.03	0.02	0.02	0.02	0.02	0.03	0.02	0.03	0.02	0.02	0.02	0.04	0.02	0.02
Total	4.00	4.00	4.00	4.00	4.00	4.00	4.00	4.00	4.00	4.00	4.00	4.00	4.00	4.00	4.00
Ae	4.35	5.99	1.24	1.90	1.84	2.17	3.11	4.67	1.89	5.00	1.86	2.48	0.63	4.07	0.00
Aug	91.41	88.66	89.07	92.41	94.26	91.72	89.96	90.24	89.29	90.42	95.98	95.66	95.10	93.11	96.95
Wo	38.71	42.96	42.20	40.82	39.60	41.85	38.86	42.87	38.52	41.06	36.30	33.01	35.21	33.61	37.75
En	49.22	46.41	46.94	46.19	51.09	48.36	48.35	47.36	49.51	48.76	47.47	50.34	45.51	49.32	51.29
Fs	12.07	10.63	10.86	12.99	9.30	9.79	12.79	9.77	11.97	10.17	16.24	16.66	19.28	17.07	10.96
Mg#	80.79	81.89	81.67	78.62	84.96	83.62	79.42	83.13	80.88	83.11	75.00	75.66	70.89	74.76	82.74

Representative microprope analyses of orthopyroxene minerals from Erciyes Stratovolcano (c:center, r:rim, mic:microlite)
(Calculated for 4 cation and 6O).

Samples	**ER1**			**ER3**							**ER9**				
	Microlite			**Phenocryst**					**Microphenocryst**		**Phenocryst**		**Microphenocryst**		
	56—mic	***83—mic***	***99—mic***	***3—c***	***4—r***	***5—r***	***25—c***	***26—r***	***9—c***	***10—r***	***55—c***	***56—r***	***2—r***	***3—c***	***22—c***
SiO_2	54.00	53.90	55.15	54.35	55.43	54.02	54.78	55.08	53.48	53.71	55.01	53.61	54.09	54.36	53.35
TiO_2	0.48	0.35	0.34	0.16	0.12	0.27	0.15	0.13	0.34	0.31	0.25	0.30	0.30	0.35	0.39
Al_2O_3	0.92	0.67	0.88	2.67	2.06	3.49	2.57	2.69	1.10	0.65	1.12	2.31	2.23	1.62	3.43
FeO	16.20	18.20	14.88	12.13	10.13	9.98	10.82	9.88	18.71	18.60	14.82	14.91	15.43	16.22	12.52
MnO	0.46	0.52	0.38	0.25	0.21	0.17	0.28	0.18	0.34	0.34	0.27	0.32	0.34	0.40	0.23
MgO	25.28	24.57	26.48	28.72	29.82	29.48	29.38	29.90	23.84	23.55	27.41	26.98	26.05	26.49	27.10
CaO	2.26	1.80	2.02	1.46	1.38	1.66	1.31	1.43	1.72	1.91	1.59	1.36	1.30	1.30	2.25
Na_2O	0.06	0.07	0.07	0.06	0.04	0.07	0.02	0.03	0.00	0.05	0.03	0.03	0.04	0.04	0.03
Total	99.65	100.11	100.27	99.90	99.46	99.67	99.57	99.88	99.53	99.15	100.58	99.93	99.84	100.82	99.64
Si	1.97	1.97	1.99	1.93	1.97	1.91	1.95	1.94	1.98	1.99	1.97	1.93	1.96	1.95	1.91
Al^{IV}	0.03	0.03	0.01	0.07	0.03	0.09	0.05	0.06	0.02	0.01	0.03	0.07	0.04	0.05	0.09
Al^{VI}	0.01	0.00	0.02	0.04	0.05	0.05	0.05	0.06	0.02	0.02	0.01	0.03	0.05	0.02	0.06
Fe^{+3}	0.00	0.02	0.00	0.02	0.00	0.01	0.00	0.00	0.00	0.00	0.01	0.03	0.00	0.02	0.00
Fe^{+2}	0.49	0.54	0.45	0.35	0.30	0.28	0.32	0.29	0.58	0.58	0.43	0.42	0.47	0.47	0.38
Mn	0.01	0.02	0.01	0.01	0.01	0.01	0.01	0.01	0.01	0.01	0.01	0.01	0.01	0.01	0.01
Mg	1.38	1.34	1.42	1.52	1.58	1.55	1.56	1.57	1.31	1.30	1.46	1.45	1.41	1.42	1.45
Ca	0.09	0.07	0.08	0.06	0.05	0.06	0.05	0.05	0.07	0.08	0.06	0.05	0.05	0.05	0.09
Na	0.00	0.01	0.01	0.00	0.00	0.01	0.00	0.00	0.00	0.00	0.00	0.00	0.00	0.00	0.00
Total	4.00	4.00	4.00	4.00	4.00	4.00	4.00	4.00	4.00	4.00	4.00	4.00	4.00	4.00	4.00
Ae	0.00	1.54	0.00	1.52	0.00	1.23	0.00	0.00	0.00	0.00	0.91	2.76	0.00	1.53	0.00
Aug	98.97	98.36	97.54	94.01	94.82	93.11	94.70	94.27	97.65	97.96	97.66	94.39	94.60	96.53	93.94
Wo	4.46	3.58	3.98	2.88	2.74	3.29	2.59	2.81	3.45	3.87	3.09	2.71	2.59	2.54	4.48
En	69.76	67.54	72.55	78.16	81.45	81.06	80.40	81.75	66.63	66.23	74.05	73.86	72.74	72.08	75.56
Fs	25.77	28.88	23.47	18.96	15.81	15.65	17.01	15.44	29.91	29.91	22.86	23.43	24.68	25.38	19.96

Representative microprope analyses of oxide minerals from Erciyes Stratovolcano (mic:microlite)
(Calculated 3 cation and 4O)

Samples	ti-manyetite						ilmenite	
	ER1	ER11	ER13	ER13	ER17	ER17	Samples	ER13
	Microlite	Microlite	Microlite	Microlite	Microlite	Microlite		Microlite
	65—mic	*37—mic*	*69—mic*	*89—mic*	*139—mic*	*140—mic*		*70—mic*
TiO_2	16.30	15.96	26.18	25.62	16.88	12.43	TiO_2	52.79
Al_2O_3	1.63	1.77	0.43	0.98	3.01	3.05	Al_2O_3	42.80
FeO	42.24	42.34	52.98	52.53	43.70	39.71	FeO	1.77
Fe_2O_3	32.84	34.89	18.79	19.01	26.76	28.16	Fe_2O_3	0.03
MnO	0.49	0.46	0.88	0.76	0.42	0.41	MnO	0.65
MgO	2.29	1.68	1.17	1.27	1.69	1.72	MgO	2.17
Total	93.78	94.04	98.68	98.67	95.08	95.31	Total	100.20
Ti	0.46	0.46	0.73	0.71	0.48	0.35	Ti	0.98
Al	0.46	0.46	0.73	0.71	0.48	0.35	Al	0.03
Fe^{+3}	0.07	0.08	0.02	0.04	0.13	0.13	Fe^{+3}	0.88
Fe^{+2}	0.94	1.00	0.52	0.53	0.75	0.79	Fe^{+2}	0.01
Mn	1.34	1.34	1.64	1.62	1.37	1.24	Mn	0.14
Mg	0.02	0.01	0.03	0.02	0.01	0.01	Mg	0.08
Total	3.01	3.00	3.00	3.00	3.00	3.00	Total	2.00
Usp%	49	46	73	71	48	35	Ilm	98.20

Representative microprope analyses of plagioclase minerals from Southwestern Cappadocia (c:center, r:rim, mic:microlites) (Calculated for 32O).

Samples	**HA13b**												
	Microphenocryst								**Microlite**				
	11—c	***12—r***	***21—c***	***22—r***	***26—c***	***27—r***	***47—c***	***48—r***	***5—mic***	***17—mic***	***20—mic***	***30—mic***	***35—mic***
SiO_2	53.74	53.50	54.41	53.64	54.24	54.54	53.40	53.12	53.75	52.78	53.84	53.72	53.66
Al_2O_3	28.37	28.49	28.32	28.30	28.36	26.98	28.43	28.55	28.53	28.78	28.44	28.77	28.21
FeO	0.81	0.85	0.69	0.96	0.85	1.27	0.84	1.03	0.87	0.91	0.68	0.92	1.03
MgO	0.09	0.07	0.10	0.08	0.10	0.23	0.07	0.07	0.08	0.09	0.10	0.06	0.06
CaO	11.65	12.05	11.61	11.82	11.53	10.50	12.23	12.35	11.92	12.29	11.75	11.71	11.89
Na_2O	4.76	4.52	4.93	4.62	4.78	5.19	4.31	4.28	4.78	4.44	4.86	4.59	4.63
K_2O	0.30	0.22	0.35	0.29	0.33	0.97	0.26	0.26	0.27	0.23	0.29	0.28	0.27
Total	99.71	99.69	100.51	99.83	100.22	99.70	99.54	99.66	100.25	99.53	100.03	100.09	99.81
Si	9.79	9.75	9.82	9.77	9.82	9.97	9.75	9.70	9.75	9.65	9.77	9.75	9.78
Al	6.09	6.12	6.03	6.07	6.05	5.81	6.12	6.14	6.10	6.20	6.09	6.15	6.06
Fe	0.12	0.13	0.10	0.15	0.13	0.19	0.13	0.16	0.13	0.14	0.10	0.14	0.16
Mg	0.03	0.02	0.03	0.02	0.03	0.06	0.02	0.02	0.02	0.02	0.03	0.02	0.02
Ca	2.27	2.35	2.25	2.31	2.24	2.06	2.39	2.42	2.32	2.41	2.28	2.28	2.32
Na	1.68	1.60	1.73	1.63	1.68	1.84	1.53	1.52	1.68	1.57	1.71	1.62	1.64
K	0.07	0.05	0.08	0.07	0.08	0.23	0.06	0.06	0.06	0.05	0.07	0.06	0.06
An	56.48	58.82	55.43	57.59	56.04	49.92	60.11	60.52	57.04	59.66	56.25	57.54	57.72
Ab	41.81	39.90	42.59	40.75	42.05	44.61	38.37	37.98	41.41	39.02	42.11	40.85	40.71
Or	1.70	1.28	1.98	1.66	1.91	5.47	1.52	1.49	1.55	1.33	1.64	1.61	1.57

Representative microprope analyses of olivine minerals from Southwestern Cappadocia(c:center, r:rim, mic:microlite)
(Calculated 4O)

Samples	**HA13b**												
	Phenocryst												**Microphenc**
	3—c	***4—r***	***13—c***	***14—r***	***18—c***	***19—r***	***32—c***	***33—r***	***36—c***	***37—r***	***38—c***	***39—r***	***9—c***
SiO_2	39.50	38.68	40.41	38.86	40.27	39.38	39.92	38.36	40.09	39.54	40.11	39.13	38.54
TiO_2	0.02	0.00	0.02	0.01	0.00	0.04	0.00	0.04	0.00	0.03	0.00	0.04	0.03
Al_2O_3	0.03	0.04	0.02	0.02	0.04	0.00	0.06	0.00	0.04	0.04	0.00	0.02	0.02
FeO	18.88	22.45	15.58	20.69	15.11	19.54	18.09	25.84	15.75	21.10	16.88	19.71	23.07
MnO	0.34	0.36	0.32	0.40	0.24	0.30	0.30	0.46	0.28	0.45	0.37	0.38	0.41
MgO	41.81	38.65	43.98	39.83	44.77	41.34	42.23	35.86	44.12	39.86	43.61	41.44	38.04
CaO	0.28	0.33	0.23	0.34	0.27	0.30	0.25	0.32	0.17	0.30	0.12	0.32	0.32
Total	100.96	100.52	100.66	100.15	100.71	100.94	100.84	100.89	100.53	101.38	101.14	101.09	100.46
Si	1.00	1.00	1.01	1.00	1.00	1.00	1.01	1.01	1.00	1.01	1.00	0.99	1.00
Fe^{+2}	0.40	0.49	0.33	0.45	0.31	0.42	0.38	0.57	0.33	0.45	0.35	0.42	0.50
Mn	0.01	0.01	0.01	0.01	0.01	0.01	0.01	0.01	0.01	0.01	0.01	0.01	0.01
Mg	1.58	1.49	1.64	1.53	1.66	1.57	1.59	1.40	1.65	1.51	1.63	1.57	1.47
Ca	0.01	0.01	0.01	0.01	0.01	0.01	0.01	0.01	0.00	0.01	0.00	0.01	0.01
Fo	79.49	75.12	83.14	77.09	83.86	78.78	80.36	70.84	83.06	76.72	81.83	78.61	74.27
Fa	20.14	24.48	16.52	22.47	15.88	20.90	19.31	28.64	16.64	22.78	17.78	20.98	25.28
Tp	0.37	0.40	0.34	0.44	0.26	0.32	0.32	0.52	0.30	0.50	0.39	0.41	0.45

Representative microprope analyses of clinopyroxene minerals from Southwestern Cappadocia (c:center, r:rim, mic:microlite)
(number of ions)

Samples	**HA13b**										**HA18**			
	Microphenocryst						**Microlite**				**Microphenocryst**			
	24—c	***25—r***	***28—c***	***29—r***	***42—c***	***43—r***	***6—mic***	***15—mic***	***23—mic***	***41—mic***	***167—c***	***168—r***	***181—c***	***182—r***
SiO_2	50.14	51.12	51.04	51.04	52.37	50.89	51.97	50.95	51.15	50.50	50.15	51.93	51.87	51.63
TiO_2	1.18	1.01	1.04	1.35	0.87	1.03	0.99	1.02	1.09	1.26	1.27	1.30	1.05	1.18
Al_2O_3	3.97	3.45	3.84	2.28	2.47	3.24	2.72	3.26	3.12	4.01	4.17	1.63	2.19	2.16
FeO	6.81	7.03	7.06	9.90	6.83	6.84	6.90	6.78	7.55	7.50	6.78	9.76	7.32	8.51
MnO	0.16	0.17	0.17	0.23	0.17	0.12	0.12	0.22	0.22	0.12	0.19	0.30	0.22	0.20
MgO	14.99	15.34	15.16	14.10	15.95	15.12	15.28	14.86	15.49	14.64	14.70	14.41	15.42	14.97
CaO	21.67	21.97	22.17	20.70	21.49	21.77	21.46	21.65	20.84	21.58	21.17	20.32	21.35	20.63
Na_2O	0.36	0.40	0.40	0.56	0.38	0.42	0.37	0.42	0.40	0.43	0.41	0.55	0.45	0.49
Total	99.64	100.74	101.17	100.16	100.68	99.65	99.96	99.38	99.99	100.36	99.55	100.24	100.00	99.87
Si	1.86	1.87	1.86	1.90	1.91	1.88	1.92	1.89	1.89	1.86	1.86	1.93	1.91	1.92
Al^{IV}	0.14	0.13	0.14	0.10	0.09	0.12	0.08	0.11	0.11	0.14	0.14	0.07	0.09	0.08
Al^{VI}	0.03	0.02	0.03	0.00	0.02	0.02	0.04	0.03	0.02	0.03	0.04	0.00	0.01	0.01
Fe^{+3}	0.06	0.08	0.08	0.07	0.04	0.07	0.02	0.05	0.06	0.06	0.04	0.04	0.05	0.04
Fe^{+2}	0.15	0.14	0.14	0.24	0.17	0.15	0.20	0.17	0.18	0.17	0.17	0.27	0.18	0.22
Mn	0.01	0.01	0.01	0.01	0.01	0.00	0.00	0.01	0.01	0.00	0.01	0.01	0.01	0.01
Mg	0.83	0.84	0.82	0.78	0.87	0.83	0.84	0.82	0.85	0.80	0.81	0.80	0.85	0.83
Ca	0.86	0.86	0.87	0.83	0.84	0.86	0.85	0.86	0.82	0.85	0.84	0.81	0.84	0.82
Na	0.03	0.03	0.03	0.04	0.03	0.03	0.03	0.03	0.03	0.03	0.03	0.04	0.03	0.04
Total	4.00	4.00	4.00	4.00	4.00	4.00	4.00	4.00	4.00	4.00	4.00	4.00	4.00	4.00
Ae	6.62	8.03	8.04	6.81	4.04	6.87	1.55	4.69	5.94	6.61	3.84	4.08	5.00	4.38
Aug	90.33	89.99	89.35	93.19	93.89	90.74	94.72	91.87	91.77	89.82	91.58	95.81	94.06	94.58
Wo	45.16	44.91	45.34	42.92	43.74	45.14	44.54	45.29	43.00	45.06	45.00	42.14	43.84	42.75
En	43.48	43.61	43.14	40.69	45.14	43.57	44.07	43.24	44.46	42.52	43.45	41.56	44.05	43.17
Fs	11.36	11.48	11.52	16.39	11.12	11.30	11.39	11.47	12.54	12.43	11.54	16.30	12.10	14.08

Representative microprope analyses of oxide minerals from Southwestern Cappadocia (mic:microlite)
(number of ions calculated based on 3 cation and 4O)

	ti-manyetite													
Samples	**HA13b**	**HA13b**	**HA13b**	**HA15**	**HA15**	**HA15**	**HA15**	**HA19**	**HA19**	**HA19**	**HA19**	**HA23b**	**HA23b**	**HA23b**
	Microlite	**Microlite**	**Microlite**	**Microlite**	**Microlite**	**Microlite**	**Microlite**	**Microlite**	**Microlite**	**Microlite**	**Microlite**	**Microlite**	**Microlite**	**Microlite**
	127—mic	***129—mic***	***130—mic***	***122—mic***	***123—mic***	***126—mic***	***116—mic***	***134—mic***	***135—mic***	***136—mic***	***137—mic***	***10—mic***	***29—mic***	***54—mic***
TiO_2	20.12	20.80	21.44	23.11	21.16	22.90	22.58	21.19	22.19	20.83	18.73	15.48	13.20	12.28
Al_2O_3	2.04	1.06	1.44	0.85	1.66	0.79	1.36	0.81	0.28	0.57	0.65	1.55	1.26	1.35
FeO	45.86	46.21	46.87	48.59	46.09	47.90	48.01	47.52	48.35	46.19	43.51	43.17	39.65	38.79
Fe_2O_3	27.58	28.69	26.86	23.65	24.62	24.06	23.77	26.39	24.92	26.96	25.50	34.54	38.83	40.83
MnO	0.58	0.66	0.68	0.68	0.71	0.62	0.67	0.67	0.87	0.72	0.65	0.29	0.35	0.44
MgO	2.08	2.36	2.31	2.05	2.02	2.34	1.95	1.45	1.31	2.08	1.38	0.99	1.31	1.27
Total	98.40	99.92	99.77	99.14	96.50	98.91	98.83	98.40	98.27	97.87	97.13	97.25	94.85	95.33
Ti	0.56	0.58	0.59	0.65	0.61	0.64	0.63	0.60	0.63	0.59	0.53	0.45	0.39	0.36
Al	0.09	0.05	0.06	0.04	0.07	0.03	0.06	0.04	0.01	0.03	0.03	0.07	0.06	0.06
Fe^{+3}	0.77	0.80	0.74	0.66	0.71	0.67	0.67	0.75	0.71	0.77	0.72	1.00	1.15	1.20
Fe^{+2}	1.43	1.42	1.44	1.51	1.47	1.49	1.49	1.50	1.53	1.46	1.37	1.38	1.30	1.27
Mn	0.02	0.02	0.02	0.02	0.02	0.02	0.02	0.02	0.03	0.02	0.02	0.01	0.01	0.01
Mg	0.12	0.13	0.13	0.11	0.11	0.13	0.11	0.08	0.07	0.12	0.08	0.06	0.08	0.07
Total	3.00	3.00	3.00	3.00	3.00	3.00	3.00	3.00	3.00	3.00	3.02	3.00	3.00	3.00
Usp%	57	58	60	65	61	65	64	61	64	60	62	45	40	37

REFERENCES

Abdel-Rahman, A.F., Lease, N.A. (2012). Petrogenesis of Cenozoic mafic-ultramafic alkaline lavas from the Tigris volcanic field, NE Syria, *Geological Magazine* **149**, 1-18.

Albaréde, F. (1996). Introduction to Geochemical Modelling, *Cambridge University Pres*, 543 p.

Aldanmaz, E., Pearce, J.A., Thirwall, M.F. and Mitchell, J.G. (2000). Petrogenetic evolution of Late Cenozoic post-collision volcanism in Western Anatolia,Turkey, *Journal of Volcanology and Geothermal Research* **102**, 67-95.

Ali, S., Ntaflos, T. (2011). Alkali basalts from Burgenland, Austria: Petrological constraints on the origin of the westernmost magmatism in the Carpathian-Pannonian Region, *Lithos* **121**, 176-188.

Alıcı Şen, P. (2002)**.** *Anadoluda'ki Kuvaterner Yaşlı Bazaltik Vokaniklerin Kökeni*, PhD Thesis, Hacettepe Üniversitesi Fen Bilimleri Enstitüsü, Ankara, Türkiye.

Alıcı Şen, P., Temel, A., Gourgaud, A. (2004). Petrogenetic modelling of Quaternary post-collisional volcanism: a case study of central and eastern Anatolia. *Geological Magazine* **141**-1, 81-98.

Alıcı, P. (1997). *Gölcük (Isaparta) Volkaniklerinin Petrolojik ve Jeokimyasal Özellikleri*, Hacettepe Üniversitesi, Yüksek Lisans Tezi (MSc.).

Alıcı, P., Temel, A., Vidal, P., Gündoğdu, M.N. (2001). Quaternary tholeiitic to alkaline volcanism in the Karasu Valley, Dead Sea Rift Zone, southeast Turkey: Sr-Nd-Pb-O isotopic and trace-element approaches to crust-mantle interaction, *International Geology Review* **43**, 120-138.

Altunkaynak, Ş., Rogers, N.W. and Kelley, S.P. (2010).Causes and effects of geochemical variations in late Cenozoic volcanism of the Foça volcanic centre, NW Anatolia, Turkey, Special Issue: Eastern Mediterranean Geodynamics, Part II, *Geology Review* **52**, 4-6, 579-607.

Ariskin, A.A. and Barmina, G.S. (1990). Equilibria thermometry between plagioclases and basalt or andesite magmas, *Geochemistry International* **27**, 129-134.

Arpat, E., and Şaroğlu, F. (1975). Türkiye'deki bazı önemli genç tektonik olaylar, *Bull. Geol. Soc. Turkey* **18/1**, 91-101.

Aydar, E. and Gourgaud, A. (2002). Garnet-bearing basalts: an example from Mt. Hasan, Central Anatolia, Turkey, *Mineralogy and Petrology* **75***,* 185-201..

Aydar, E. and Gourgaud, A. (1998). The geology of Mount Hasan stratovolcano, Central Anatolia, Turkey, *Journal of Volcanology and Geothermal Research* **85**, 129-152,.

Aydar, E., Çubukçu, E., Akın, L. (2013). Central Anatolian Plateau: incision and paleoalimetry recorded from volcanic rocks, *Turkish Journal of Earth Sciences* **22**, 739-746.

Aydar, E. (1992). *Etude Volcano-Structurale et Magmatologique du Strato-Volcan Hasan Dagı (Anatolie Central-Turquie)*, Thése de doctorat, Université Blaise Pascal, Clermont-Ferrand, France.

Aydar, E., Gourgaud, A., Deniel, C., Lyberis, N., and Gündoğdu, M.N. (1995). Le volcanism quaternaire d'Anatolie central (Turquie): Association de magmatisme calco-alcalin et alcalin en domaine de convergence, *Canadian Journal of Earth Science* **32**,1058-1069.

Aydar, E., Gündoğdu, M. N., Bayhan, H. and Gougard, A. (1994). Kapadokya bölgesinin Kuvaterner yaşlı volkanizmasının yapısal ve petrolojik incelemesi**,** *TÜBİTAK Yerbilimleri Dergisi* **3**, 25-42,.

Aydar, E. (1997). Karataş volkanitlerinin (Orta Anadolu) volkanolojik ve petrolojik özellikleri*, Yerbilimleri* **19**, 41-45.

Ayrancı, B. (1991). The magnificent volcano of Central Anatolia: Mt. Erciyes near Kayseri: *Bulletin of the Technical University of İstanbul* **44**, 375-417.

Ayrancı, B. (1969). *Zur Petrologie und Geologie des Erciyes Vulkangebietes bei Kayseri Zentral Anatolien/Turkei*, Inaugural-Dr. Diss., Universität Würzburg.

Bacon, C.R. and Hirschmann, M.M. (1988). Mg/Mn partitioning as a test for equilibrium between coexisting Fe-Ti oxides. *American Mineralogist* **73**, 57-61.

Bartol, J. And Govers, R. (2014). A single cause for uplift of the Central and Eastern Anatolian plateau? *Tectonophysics* **637**, 116-136.

Batum, I. (1978). Nevsehir guneybatisindaki Göllüdag ve Acıgöl yöresi volkanitlerinin jeolojisi ve petrografisi (Geology and petrography of volcanics in Golludag and Acigol region to the SW of Nevsehir) *Yerbilimleri* **4**, 50–69.

Besang, C., Eckhardt, F.J., Harre, W., Kreuzer, H., und Müller, P. (1977). Radiometrische Altersbestimmungen an Neogenen Eruptivegesteinen der *Turkei. Geol. Jb.B* **25**, 3-36,

Biryol,C.B., Beck, S.L., Zandt, G., Özacar, A.A. (2011). Segmented African lithosphere beneath the Anatolian region inferred from teleseismic P-wave tomography, *Geophys. J. Int*. **184**, 1037-1057,

Blumenthal, M. (1941).Un aperçu de la geologie du Taurus dans les vilayets de Niğde et d'Adana, *Bull. Miner. Res*., Explor, Inst. Turk., 6.

Blundy, J.D., Robinson, J.A.C.,Wood, B.J. (1998). Heavy REE are compatible in clinopyroxene on the spinel lherzolite solidus, *Earth Planet. Sci. Lett*. **160**, 493–504.

Bozkurt, E. (2001). Neotectonics of Turkey–a synthesis, *Geodinamica acta* **1-3**, 3-30.

Brenan, J.M., Shaw, H.F., Ryerson, F.J., Phinney, D.L. (1995). Mineral-aqueous fluid partitioning of trace elements at 900 oC and 2.0 Gpa: constraints on the trace element chemistry of mantle and deep crustal fluids, *Geochimica at Cosmochimica Acta* **59**, 3331-3350.

Cassignol, C. and Gillo, P.Y. (1982). Range and effectiveness of unspiked potassium-argon dating: experimental groundwork and applications. Numerical Dating in Stratigraphy, (eds: Odin, G.S*.), Wiley, Chichester*, 159-179.

Cebria, J.M., Lopez-Ruiz, J., Doblas, M., Oyarzun, R., Hertogen, J., Benito, R. (2000). Geochemistry of the Quaternary alkali basalts of Garrotxa (NE Volcanic Province, Spain): a case of double enrichment of the mantle lithosphere, *Journal of Volcanology and Geothermal Research* **102**, 217-235.

Chaffey D.J., Cliff, R.A. and Wilson, B.M. (1989).Characterization of the St.Helena magma source, *Magmatism in the Ocean basins*, (eds:Saunders, A.D. and Norry, M.J.) Geol.Soc.Spec.Publication **42**, 257-276.

Charbit, S., Guillou, H., Turpin, L. (1998). Cross calibration of K-Ar standard minerals using an unspiked Ar measurement technique, *Chemical Geology* **150**, 147-159.

Chiaradia, M., Müntener, O. And Beate, B. (2011). Enriched Basaltic Andesites from Mid-Crustal Fractional Crystallization, Recharge and Assimilation (Pilavo Volcano, Western Cordillera of Ecuador, *Journal of Petrology* **52**, 6, 1107-1141.

Class, C., Altherr, R., Volker, F., Eberz, G. and McCulloch, M.T. (1994). Geochemistry of Pliocene to Quaternary alkali basalts from the Huri Hills, northern Kenya, *Chemical Geology* **113**, 1-2.

Clayton, R. And Mayeda, T. (1963). The use of bromine pentaflouride in the extraction of oxygen from oxides and silicates for isotopic analysis, *Geochimica et Cosmochimica Acta* **27**, 43-52.

Cohen, R.S. and O'Nions, R.K. (1992). The lead, neodymium and strontium isotopic structure of ocean ridge basalts, *Journal of Petrology* **23**, 299-324.

Coplen, T.B. (1993). The rate and temperature of reaction of ClF3 with silicate minerals, and their relevenace to oxygen isotope analysis, (eds: Alley and W.M), *Van Nostrand Reinhold, New York*, 227-254.

Cosentino, D., Schildgen, T.F., Cipollari, P., Faranda, C., Gliozzi, E., Natália Hudáčková, N., Lucifora, S., Strecker, M.R. (2012). Late Miocene surface uplift of the southern margin of the Central Anatolian Plateau, Central Taurides, Turkey, *GSA Bulletin* **124**, 1-2, 133-145.

Çubukçu, H. E. (2008). *Nemrut Stratovolkanının petrolojik Evrimi: Çarpışma Bölgesinde Peralkali Magmatizma*, Hacettepe Üniversitesi, Doktora Tezi, Türkiye.

Damasceno, D., Scoates, J.S., Weiss, D., Frey, F. And Giret, A. (2002). Mineral chemistry of midly alkaline basalts from the 25 Ma Mont Crozier section, Kerguelen Archipelago: constraints on phenocryst crystallization environments, *Journal of Petrology* **43**, 1389-1413.

Davidson, J.P., Harmon, R.S. (1989) .Oxygen isotope constraints on the petrogenesis of volcanic arc magmas from Martnique, Lesser Antilles, *Earth Planet Sci. Letters* **95**, 255-270.

De Paolo, D.J. (1981). Trace element and isotopic effects of combined wall-rock assimilation and fractional crystallization, *Earth and Planetary Science Letters* **53**, 189-202.

Deniel, C., Aydar, E., Gourgaud, A., (1998). The Hasan Dagı stratovolcano (Central Anatolia, Turkey): evolution from calc-alkaline to alkaline magmatism in a collision zone, *Journal of Volcanology and Geothermal Research*, 87, 275-302.

DePaolo, D.J.and Daley, E.E. (2000). Neodymium isotopes in basalts of the Southwest Basin and range and Lithospheric thinning during extension, *Chemical Geology* **169**, 157-185.

Detection limits and uncertainties intervals for major and trace, elements, http://helium.crpg.cnrs-nancy.fr/SARM/pages/roches.html, (August 2013).

Devey, C.W., Albarede, F., Cheminée, J. ‐ L., Michard, A., Mühe, R. and Stoffers, P. (1990). Active submarine volcanism on the Society hotspot swell (west pacific): A geochemical study, *Journal of Geophysical Research* **95**.

Dewey, J. (1988).Extensional collapse of orogens, *Tectonics* **7**, 1123–1139.

Dewey, J.F. and Sengör, A.M.C. (1979). Aegean and surrounding regions: complex multi-plate and continuum tectonics in a conergent zone, *Geol. Soc. Am. Bull*. **90**, 84-92.

Dewey, J.F., Hempton, M.R.S., Kidd, W.S.F., Şaroğlu, F. and Şengör, A.M.C. (1986). Shortening of continental lithosphere: The neotectonics of Eastern Anatolia, a young collision zone. Collisionc Tectonics, (eds: M.P. Coward and A.C. Ries), *Geological Society Special Publication* **19**, 3-36.

Dhont, D., Chorowicz, J., Yürür, T., Froger, J.L., Köse, O., Gündoğdu, N., (1998). Emplacement of volcanic vents and geodynamics of Central Anatolia, Turkey, *Journal of Volcanology and Geothermal Research* **85**, 33-54.

Dirik, K. and Göncüoğlu M. C. (1996). Neotectonic characteristics of Central Anatolia, *International Geological Review* **38**: 807–817.

Doğan, A.U., Doğan, M., Kilinc, A. (2008). Locke, D., An isobaric-isenthalpic magma mixing model for the Hasan Dagi volcano, Central Anatolia, Turkey, *Bulletin of Volcanology* **70**, 797–804.

Doğan, U. (2010). Climate-controlled river terrace formation in the Kızılırmak Valley, Cappadocia section, Turkey: Inferred from Ar–Ar dating of Quaternary basalts and terraces stratigraphy, *Geomorphology* **126**, 1–2, 66-81.

Dogan, A. U., Peate, D.W., Dogan, M., Yesilyurt-Yenice, F. I.,Unsal, O. (2013). Petrogenesis of mafic-silicic lavas at Mt. Erciyes, central Anatolia, Turkey, *Journal of Volcanology and Geothermal Research* **256**, 16-28.

Downes, H., Seghedi, I., Szakacs, A., Doboski, G., James, D.E., Vaselli, O., Rigby, I.J., Ingham, G.A., Rex., D., Pecskay, Z. (1995). Petrology and geochemistry of late Tertiary/Quaternary mafic alkaline volcanism in Romania, *Lithos* **35**, 65-81.

Downes, H., Thirlwall, Trayhorn, S.C. (2001). Miocene subduction-related magmatism in southern Sardinia: Sr-Nd and oxygen isotopic evidence for mantle source enrichment, *Journal of Volcanology and Geothermal Research* **106**, 1-21.

Drake, M.J (1976). Plagioclase-melt equilibria, *Geochimica et Cosmochimica Acta* **40**, 457-465.

Eiler, J.M., Farley, K.A., Valley, J.W., Hauri, E., Craig, H., Hart, S., Stolper, E.M. (1996). Oxygen isotope variations in ocean island basalt phenocrystals, *Geochim Cosmohim Acta* **61**, 2281-2293.

Eiler, J.M. (2001). Oxygen Isotope Variations of Basaltic Lavas and Upper Mantle Rocks, *Stable isotope geochemistry, Reviews in Mineralogy and Geochemistry*, No.**43**, Mineralogical Society of America, Washington, DC, 319-364.

El Bakkali, S., Gourgaud, A., Bourdier, J.L., Bellon, H. and Gündoğdu, N., (1998). Post-collision neogene volcanism of the Eastern Rif (Morocco): magmatic evolution through time, *Lithos* **45**, 523-543.

Elburg, M.A., Van Bergen, M., Hoogewerff, J., Foden, J., Vroon, P., Zulkarnain, Nasution, A.(2002).Geochemical trends across an arc-continent collision zone : magma sources and slab-wedge transfer processes below the Pantar Strait volcanoes, Indonesia, *Geochimica et Cosmochimica Acta* **66**, 15, 2771-2789.

Ellam, R.M. and Harmon, R.S (1990).Oxygen isotope constrains on the crustal contribution to the subduction-related magmatism of the Aeolian Islands, southern Italy, *Journal of Volcanology and Geothermal Research* **44**, 105-122.

Elliot, T., Plank, T., Zindler, A., White, W.M., Bourdon, B. (1997). Element transport from slab to volcanic front at the Mariana arc, *Journal of Geophysical Research* **102**, 14991-15019.

Ercan, T., Tokel, S., Can, B., Fişekçi, A., Fujitani, T., Notsu, K., Selvi, Y., Olmez, M.,Matsuda, J.I., Ui, T., Yıldırım, T., Akbaşlı, A. (1990). Hasandağı-Karacadağ Orta Anadolu dolaylarındaki Senozoyik yaşlı volkanizmanin kökeni ve evrimi, *Jeomorfoloji Dergisi* **18***,* 39-54.

Ercan, T., Tokel, S., Matsuda, J., Ui, T., Notsu, K., Fujitani, T. (1992). New geochemical, isotopic and radiometric data of the Quaternary volcanism of Hasandagı-Karacadag area (Central Anatolia), *TJK Bulteni* **7**, 8-21.

Ercan, T., Tokel, S., Matsuda, J.I., Ui, T., Notsu, K., Fujitani, T. (1994). Erciyes Dağı Orta Anadolu Pliyo-Kuvaterner volkanizmasina ilşkin yeni jeokimyasal, izotopik, radyometrik veriler ve jeotermal enerji açısından önemi, Türkiye 6. Enerji Kongresi,Teknik oturum tebliğleri.

Faccenna, C., Becker, T.W., Jolivet, L., Keskin, M. (2013). Mantle convection in the Middle-East: Reconciling Afar upwelling, Arabia indentation and Aegean trench rollback, *Earth and Planetary Science Letters* **375**, 254-269.

Faccenna, C., Bellier, O., Martinod, J., Pirolallo, C., Regard, V., (2006). Slab detachment beneath eastern Anatolia: A posible cause for the formation of the Noth Anatolian fault, *Earth and Planetary Science Letters* **242**, 85-97.

Faccenna, C., Jolivet, L., Piromallo, C., Morelli, A. (2003). Subduction and the depth of convection in the Mediterranean mantle, *Journal of Geophysical Research* **108**, B2, 1-10.

Faure, G. (1986). Principles of isotope geology, 2nd ed. *New York: John Wiley*, 589 p.

Feeley, T.C. and Dungan, M.A. (1996).Compositional and dynamic controls on mafic-silicic magma interractions at continental arc volcanoes: evidence from Cordon El Guadal, Tatara-San Pablo Complex, Chile, *Journal of Petrology* **37**, 1547-1577.

Ferla, P. And Meli, C. (2006). Evidence of magma mixing in the "Daly Gap" of alkaline suites: A case study from the enclaves of Pantelleria (Italy), *Journal of Petrology* **47**, 1467-1507.

Fitton, J.G., James, D. and Leeman, W. (1988). The role of lithospheric mantle in the generation of Late Cenezoic basic magmas in the Western United States, *Jour.Petrol. Special Issue* 331-349.

Frey F.A., Green, D.H., Roy, S.D., (1978). Integrated models of basalt petrogenesis study of quartz tholeiited to olivine melilities from south eastern Australia Utilizing geochemical and experimental petrological data, *Journal of Petrology* **19-3**, 463-513.

Frey, F.A. (1980).The origin of pyroxenites and garnet pyroxenites from Salt Lake Creater, Oahu, Hawaii: trace element evidence (eds: Irving,J.),*The Jackson Volume: American Jornal of Science* **280**, 2, 427-449.

Fujimaki, H., Tatsumoto, M. and Aoki, K.I., (1984). Partition coefficients of Hf, Zr, and REE between phenocrysts and groundmasses, *Journal of Geophysical Research* **89**, 662-672.

Garcia, M.O. (1996). Petrography and olivine and glass chemistry of lavas from the Hawaiian Scientific Drilling Project, *Journal of Geophysical Research* **101**, 11701-11713.

Gautier, I., Weis, D., Mennessier, J.-P., Vidal, P., Giret, A. and Loubet, M., (1990). Petrology and geochemistry of Kergulelen basalts (South Indian Ocean): evolution of the mantlesources from ridge to an intrplate position, *Earth and Planetary Science Letters* **100**, 59-76.

Genç, Y. and Yürür, M.T. (2010). Coeval extension and compression in Late Mesozoic- recent thin-skinned extensional tectonics in central Anatolia, Turkey, *Journal of Structural Geology* **32**, 623-640.

Gençalioğlu-Kuşçu, G. and Geneli, F. (2010). Review of post-collisional volcanism in the Central Anatolian Volcanic Province (Turkey), with special reference to the Tepekoy Volcanic Complex, International *Journal of Earth Sciences* **99-3**, 593-621.

Gençalioğlu-Kuşçu, G. (2010). Geochemical characterization of a Quaternary monogenetic volcano in Erciyes Volcanic Complex: Cora Maar (Central Anatolian Volcanic Province, Turkey), International *Journal of Earth Sciences* **100-8**, 1967-1985.

Ghiorso, M.S., Hirschmann, M.M., Reiners, P.W., Kress, V.C III. (2002). The pMELTS: a revision of MELTS for improved calculation of phase relations and major element partitioning related to partial melting of the mantle to 3 Gpa, *Geochemistry Geophysics Geosystems* **3**, 1-36.

Gill, J.B. (1981). *Orogenic andesites and Plate tectonics*, Springer-Verlag, New York.

Glazner, A.F. (1984). Activities of olivine and plagioclase components in silicate melts and their application to geothermometry, *Contributions to Mineralogy and Petrology* **88**, 260-268.

Govers, R. And Wortel, M.J.R (2005). Lithosphere tearing at STEP faults: response to edges of subduction zones, *Earth and Planetary Science Letters* **236 (1)**, 505-523.

Grove, T.L. and Bryan, W.B. (1983). Fractionation of pyroxene-phric MORB at low pressure: An experiment study, *Contributions to Mineralogy and Petrology* **84**, 293-309.

Güçtekin, A. and Köprübaşı, N. (2009). Geochemical Characteristics of Mafic and Intermediate Volcanic Rocks from the Hasandağ and Erciyes Volcanoes (Central Anatolia, Turkey), *Turkish Journal of Earth Sciences* **18**, 1-27.

Güçtekin, A. (1997). *Hasandağ ve Erciyes (Orta Anadolu) Stratovolkanlarının Jeokimyasal ve Petrolojik Evrimi*, PhD Thesis, Kocaeli Üniversitesi.

Guillou,H., Carracedo., J.C. and Day, S. J. (1998). Dating of the Upper Pleistocene-Holocene volcanic activity of La Palma using the unspiked K-Ar technique. *Journal of Volcanology and Geothermal Research* **86**,137-149.

Guo, Z., Wilson, M., Liu, J., Mao, Q. (2006). Post-collisional, potassic and ultrapotassic magmatism of the northern Tibetan Plateau: Constraints on characteristics of the mantle source, geodynamic setting and uplift mechanisms, *Journal of Petrology* **47**, 6, 1177-1220.

Haase, K.M., Mühe, R., Stoffers, P. (2000). Magmatism during extension of the lithosphere: geochemical constraints from lavas of the Shaban Deep, northern Red Sea, *Chemical Geology* **166**, 225-239.

Halloul, N. and Gourgaud, A. (2012). The post-collisional volcanism of northern Tunisia: petrology and evolution through time, *Journal of African Earth Sciences* **63**, 62-76.

Hannan, B.B. and Graham, D.W. (1996). Lead and Helium Isotope Evidence from Oceanic Basalts for a Common Deep Source of Mantle Plumes, *Science* **272**, 991-995.

Harmon, R.S., Thorpe, R.S., Francis, P.W. (1981). Pertrogenesis of Andean andesites from combined O-Sr isotope relationships, *Nature* **290**, 396-399.

Hart, S.R., Hauri, E.H., Oschmann, L.A., Whitehead, J.A. (1992**)**. Mantle plumes and entrainment: isotopic evidence, *Science* **256**, 517-520.

Hart, W.K., Woldegabriel, G., Walter, R.C., Mertzman, S.A. (1989). Basaltic volcanism in Ethiophia: constraints on continental rifting and mantle interractions, *Journal of Geophysical Research* **94**, 7731-7748.

Hawkesworth, C.J., Turner, S.P., McDermott, F., Peate, D.W., Van Calsteren, P. (**1997)**. U-Th Isotopes in Arc Magmas: Implications for element transfer from the subducted crust, *Science* **276**, 551-555.

Hickey, R.L., Frey, F.A., Gerlach, D.C. and Escobar, L.J. (1986). Multiple source basaltic arcrocks from the southern volcanic zone of the Andes (34o-41oS): trace element and isotopic evidence for contributions from subducted oceanic crust. *Journal of Geophysical reaserch* **91** (B6), 5963-5983.,

Hofmann, A.W. (1997). Mantle geochemistry:the mesaage from oceanic volcanism, *Nature* **385**, 219-229.

Hoover, J.D. and Irvine, T.N. (1977). Liquidus relations and Mg-Fe partitioning in part of the system Mg2SiO4-Fe2SiO4-CaMgSi2O6-CaFeSi2O6-KalSi3O8-SiO2, *Carnegie Institute of Washington Yearbook*, **77,** 774-784.

Huang, Y., Hawkesworth, C., Smith, I., Calsteren, P. and Black, P. (2000). Geochemistry of late Cenozoic basaltic volcanism in Northland and Coromandel, New Zealand: implications for mantle enrichment processes, *Chemical Geology* **164**, 219-238.

İlbeyli, N., Pearce, J. A., Thrilwall, M. F. and Mitchell,J. G. (2004). Petrogenesis of collision-related plutonics in central Anatolia, Turkey, *Lithos* **72**, 163–82.

Innocenti, F., Mazzuoli, R., Pasquarè, G., Radicati di Brozolo F. and Villari, L. (1975). The Neogene calc-alcaline volcanic of Central Anatolia: Geochronological data on Kayseri-Niğde area, Geological Magazine **112**: 349-360.

Irvine, T.N. and Baragar, W.R.A., A guide of to the chemical classification of the common volcanic rocks, *Canadian Journal of Earth Science*, 8, 523-548, 1971.

Ito, E.,White, E.M., Gopel, C. (1987). The O,Sr, Nd and Pb isotope geochemistry of MORB, *Chemical Geology* **62**, 157-176.

Iwamori, H., Nakamura, H. (2015). Isotopic heterogeneity of oceanic, arc and continental basalts and its implications for mantle dynamics, Gondwana Research, *Gondwana Research* **27**, 3, 1131-1152.

Jaffey, N., Robertson, A., Pringle, M. (2004). Latest Miocene and Pleistocene ages of faulting, determined by 40Ar/39Ar single crystal dating of airfall tuff and silicic extrusives of the Erciyes Basin, central Turkey: evidence for intraplate deformation related to the tectonic escape of Anatolia. *Terra Nova* **16**, 45–53.

JP Liegeois, J Navez, J Hertogen, R Black. (1998). Contrasting origin of post-collisional high-K calc-alkaline and shoshonitic versus alkaline and peralkaline granitoids. The use of sliding normalization, *Lithos* **45**, 1-28.

Jung, C., Jung, S., Hoffer, E., and Berndt, J. (2006). Petrogenesis of Tertiary Mafic Alkaline Magmas in the Hocheifel, Germany, *Journal of Petrology* **47** 8, 1637-1671.

Keller, J. (1974). Quaternary Maar Volcanism near Karapınar in Central Anatolia, *Bull.Vol* **38**, 378-396.

Kempton, P.D., Fitton, J.G., Hawkesworth, J.C., Ormerod, D.S. (1991). Isotopic and trace element constrains on the composition and evolution of the lithosphere beneath the southwestern United States, *J. Geophys. Res*. **96**, (B8),13,713–13,735.

Keskin, M., Chugaev, A.V., Lebedev, V.A., Sharkov, E.V., Oyan, V., Kavak, O (2012). The Geochronology and Origin of Mantle Sources for Late Cenezoic Intraplate Volcanism in the Frontal Part of the Arabian Plate in the Karacadağ Neovolcanic Arae of Turkey. Part 2. The Result of Geochemical and Isotope (Sr-Nd-Pb) Studies, *Journal of Volcanology and Sesismology* 6, **6**, 361-382,

Koçyiğit, A. and Beyhan, A. (1998). A new intracontinental transcurrent structure : the Central Anatolian Fault Zone, Turkey, Tectonophysics **284**, 317-336.

Koçyiğit, A., Türkmenoğlu, A., Beyhan., A., Kaymakçı, N. and Akyol, E., (1995). Post-Collisional Tectonics of Eskişehir-Ankara-Çankırı segment of İzmir-Ankara-Erzincan Suture Zone: Ankara Orogenic Phase, *TAPG Bulletin* **6**, 69-86.

Koçyiğit, A., Winchester, J.A., Bozkurt, E. and Holland, G. (2003). Saraçköy Volcanic Suite: implications for the subductional phase of arc evolution in the Galatean Arc Complex, Ankara, Turkey, *Geological Journal* **38**, 1, 1-14.

Köksal, S., Möller, A., Göncüoğlu, M., Frel, D., Gerdes, A. (2012). Crustal homogenization revealed by U-Pb zircon ages and Hf isotope evidence from the Late Creataceous granitoids of the Ağaçören intrusive suite (Cental Anatolia/Turkey), *Contribution to Mineralogy and Petrology* **163**, 4, 725-743.

Kudo, A.M. and Weill, D.F. (1970). An igneous plagioclase thermometer, *Contributions to Mineralogy and Petrology* **25**, 52-65.

Kürkçüoğlu , B., Sen, E., Temel, A., Aydar, E., Gourgaud, A. (2001). Trace Element Modelling and Source Constraints for Tholeiitic and Calc-Alkaline Basalts from a Depleted Asthenospheric Mantle Source, Mt. Erciyes Stratovolcano, Turkey, *International Geological Review* **43**, 508–522.

Kürkçüoğlu, B. (2000). *Erciyes stratovolkanı'nın Jeokimyasal Evrimi*, Doktora Tezi, Hacettepe Üniversitesi Fen Bilimleri Enstitüsü, Ankara, Türkiye.

Kürkçüoğlu, B. (2010). Geochemistry and petrogenesis of basaltic rocks from the Develidag volcanic complex, Central Anatolia, Turkey, *Journal of Asian Earth Sciences* **37**, 42–51.

Kürkçüoğlu, B., Şen, E., Aydar, E., Gourgaud, A., Gündoğdu, N. (1998). Geochemical approach to magmatic evolution of Mt.Erciyes stratovolcano Central Anatolia, Turkey, *Journal of Volcanology and Geothermal Research* **85**, 473-494.

Kürkçüoğlu, B., Sen, E., Temel, A., Aydar, E., Gourgaud, A. (2004). Interaction of asthenospheric and lithospheric mantle: the genesis of Calc-alkaline Volcanism at Erciyes Volcano, Central Anatolia, Turkey, *International Geological Review* **46**, 243–258.

Kuzucuoğlu, C., Pastre, J.F., Black, S., Ercan, T., Fontugne, M., Guillou, Hatté, C., Karabıyıkoğlu, M., Orth, P., Türkecan, A. (1998). Identifcation and dating of tephra layers from Quaternary sedimantary sequences of Inner Anatolia, Turkey, *Journal of Volcanology and Geothermal Research* **85**, 153-172.

Le Bas, M.J., Le Maitre, R.W., Streckeisen, A. and Zanettin, B. (1986). A Chemical Classification of Volcanic Rocks Based on the Total Alkali – Silica Diagram, *Journal of Petrology* **27**, 745-750.

Le Pennec, J.L., Bourdier J.L., Froger J.L., Temel A., Camus, G., Gourgaud, A. (1994). Neogene ignimbrites of the Nevşehir plateau, Central Turkey, *Journal of Volcanology and Geothermal Research* **63**, 59-87.

Le Pennec, J.L., Temel, A., Froger, J.L., Sen, S., Gourgaud, A., Bourdier, J.L. (2005). Stratigraphy and age of the Cappadocia ignimbrites, Turkey: reconciling field constraints with paleontologic, radiochronologic, geochemical and paleomagnetic data, *Journal of Volcanology and Geothermal Research* **141**, 45-64.

Leat, P.T, Thompson, R.N., Dickin, A.P., Morrison, M.A., Hendry, G.L., (1989). Quaternary volcanism in Northwestern Colorado: Implications for the roles of asthenosphere and lithosphere in the genesis of continental basalts, *Journal of Volcanology and Geothermal Research* **37**, 291-310.

Location map of the studies areas, http://www2.jpl.nasa.gov/srtm/ (September, **2013**).

Loomis, T.P. (1979). An emprical model for plagioclase equilibrium in hydrous melts, *Geochimica et Cosmochimica Acta* **43**, 1753-1759.

Lustrino, M. and Wilson, M. (2007). The circum-Mediterranean anorogenic Cenozoic igneous province, *Earth and Science Reviews* **81**, 1–2, 1–65.

Lyberis, N., Yürür, T., Chorowicz, J., Kasapoğlu, E., Gündoğdu, N. (1992). The East Anatolian Fault: an oblique collisional belt, *Tectonophysics* **204**, 1-15.

Ma., G.S.K.,Malpas, J., Xenophontos, C., Chan, G.H.N. (2011).Petrogenesis of Latest Miocene-Quaternary Continental Intraplate Volcanism along the Northern Dead Sea Fault System (Al Ghab-Homs Volcanic Field), Western Syria: Evidence for Lithosphere-Astnenosphere Interaction, *Journal of Petrology* **52**, 2, 401-430.

Marsh, B.D., Fournelle, J., Myers, J.D., Chou, I.M. (1990). On plagioclase thermometry in island-arc rocks: experiments and theory, Fluid-Mineral interactions, (eds: Eugster, H.P, Spencer, R.J., Chou, I.M), *Geochemical Society Special Publication* **2**, 65-83.

Masotta, M., Mollo, S., Freda, C., Gaeta, Moore, G. (2013). Clinopyroxene-liquid thermometers and barometers specific to alkaline differentiated magmas, *Contributions to Mineralogy and Petrology* **166**, 1545-1561.

Mathez, E.A (1973). Refinement of the Kudo-Weill plagioclase and its applications to basaltic rocks, *Contributions to Mineralogy and Petrology,* **41**, 61-72.

Maury, R.C., Fourcade, S., Coulon, C., El Azzouzi, M., Bellon,H., Coutelle, A., Ouabadi, A., Semroud, B., Megartsi, M., Cotten, J., Belanteur, O., Louni-Hacini, A., Piqué, A., Capdevila, R., Hernandez, J., Réhault, J.R.. (2000). Post-collisional Neogene magmatism of the Mediterranean Maghreb margin: a consequence of slab breakoff, *Earth and Planetary Sciences* **331**, 159-173.

McCulloch, M.T. and Gamble, J.A. (1991). Geochemical and geodynamic constraints on subduction zone magmatism, *Earth and Planetary Science Letters* **102**, 358-374.

McDonough, W. F. (1990). Constraints on the composition of the continental lithospheric mantle, *Earth and Planetary Science Letters* **101**, 1, 1-18.

McKenzie, D. and O'Nions, R.K. (1991). Partial melt distributions from inversion of rare Earth element concentrations, *Journal of Petrology* **32**, 1021-1091.

McKenzie, D. (1972). Active tectonics of the Mediterranean Region, *Geophysical Journal of the Royal Astronomical Society* **30**, 109-185..

Mellart, J. (1967). Çatal Höyük, *Staat aus der Steinzeit.Lübbe Verl*., Hamburg, 269, Batı Almanya.

Melluso, L., Lustrino, M., Ruberti, E., Brotzu, P., Barros Gomes, C., Morbidelli, L., Morra, V., Svisero, D. P. And D'Amelio, F. (1988). Major and trace element composition of olivine, provskite, clinopyroxene, Cr-Fe-Ti oxides, phlogopite and host kamafugites and kimberlites, Alto Paranaiba, Brazil, *The Canadian Mineralogist* **46**, 19-40.

Menzies, M.A., Kyle, P.R., Jones, M. and Ingram, G. (1991). Enriched and depleted source components for tholeiitic and alkaline lavas from Zuni-Bandera, New Mexico: Inferences about intraplate processes and stratified lithosphere, *Journal of Geophysical Research* **96**, B8, 13645-13671.

Metz, K. (1956). Aladağ ve Karanfil dağının yapısı ve bunların Kilikya torusu tesmiye edilen batı kenarları hakkında malumat husulü için yapılan jeolojik etüd: *MTA Enst. Dergisi* **48**, 63-75.

Middlemost E.A.K. (1975). The basalt clan., *Earth Science Revue*, 11, 337-364.

Miyashiro, A. (1978). Nature of alkalic rock series, *Contributions to Mineralogy and Petrology* **66**, 91- 104.

Moritomo, N. (1989). Nomenclature of pyroxenes, *Bull. Mineral* **111**, 535-550,.

Morris, G.A., Larson, P.B., Hooper, P.R (2000). Subduction style magmatism in a Non-subduction setting: The Colville Igneous Complex, NE Washington State,USA, *J.Petrology* **41**, 1, 43-67.

Nimis, P. and Taylor, W.R., (2000). Single clinopyroxene thermobarometry for garnet peridotites, Part 1: Calibration and testing of a Cr-İn cpx barometer and an enstatite-in-cpx thermometer, *Contributions to Mineralogy and Petrology* **139**, 541-554.

Nimis, P. and Ulmer, P. (1998). Clinopyroxene geobarometry of magmatic rocks, Part 1: an expanded structural geobarometer for anhydrous and hydrous basic and ultrabasic systems, *Contributions to Mineralogy and Petrology* **133**, 122-135.

Nimis, P. (1995). A clinopyroxene geobarometer for basaltic systems based on crystals-structure modeling, *Contributions to Mineralogy and Petrology* **121**, 115-125.

Niu, Y.L, Wilson, M., Humphreys, O'Hara, M.J (2011). The origin of intra-plate ocean island basalts (OIB): the lid effect and its geodynamic implications, *Journal of Petrology* **7-8**, 1443-1468.

Notsu, K., Fujitani, T., Ui, T., Matsuda, J., Ercan, T. (1995). Geochemical features of collision-related volcanic rocks in central and eastern Anatolia, Turkey, *Journal of Volcanology and Geothermal Research* **64**, 217-230.

Okamura, S., Arculus, R.J., Martynov, Y.A. (2005) Cenozoic magmatism of the north-eastern Eurasian margin: the role of lithosphere versus asthenosphere, *Journal of Petrology* **46**, 221-253.

Olanca, K. (1994). *Géochimie des laves quaternaires de Cappadoce (Turquie): les appareils monogéniques*, Thése 3eme cycle, Universite Blaise Pascal, Clermont-Ferrand.

Ormerod, D.S., Rogers, N.W. and Hawkesworth, C.J. (1991). Melting of the lithosphere mantle: Inverse modeling of alkali olivine basalts from the Big Pine volcanic field,California, *Contributions to Mineralogy and Petrology* **108**, 305-317.

Özdemir, Y. (2011). *Volcanostratigraphy and Petrogenesis of Süphan Stratovolcano*, (PhD Thesis) METU.

Özsayın, E., Çiner, T.A., Rojay, F.B., Dirik, R.K., Melnick, D., Fernandez-Blanco, D., Bertotti, G., Schildgen, T.F., Garcin, Y., Strecker, M.R., Sudo, M. (2013). Plio-Quaternary Extensional Tectonics of the Central Anatolian Plateau: A case study from the Tuz Gölü Basin, Turkey, *Turkish Journal of Earth Sciences* **22**, 691-714.

Parker, D.F., Hodges, F.N., Perry, A., Mitchener, M.E., Barnes, M.A., Ren, M. (2010). Geochemistry and petrology of late Ecocene Cascade Head and Yachats Basalt and alkalic intrusions of the central Oregon Coast Range, U.S.A., *Journal of Volcanology and Geothermal Research* **198**, 311-324.

Partition coefficients of elements (Kd), www.earthref.org/KDD (June **2010**).

Pasquarè, G. (1968). Geology of Cenozoic volcanic area of Central Anatolia: *Atti.accad. Naz. Lincei* **9**, 53-294.

Pasquarè, G., Poli, S., Vezzoli, L., Zanchi, A. (1988). Continental arc volcanism and tectonic setting in Central Anatolia, Turkey, *Tectonophysics* **146**, 217-230,

Pearce, J.,A. (1982). Trace element characteristics of lavas from destructive plate boundaries, (eds: Thorpe, R.S.) Andesites, *John Wiley&Sons*, 525-548.

Pearce, J.A., Bender, J.F., De Long, S.E., Kidd, W.S.F., Low, P.J., Güner, Y., Şaroğlu, F., Yılmaz, Y., Moorbath, S. and Mitchell, J.G., (1990). Genesis of collision volcanism in Eastern Anatolia, Turkey, *Journal of Volcanology and Geothermal Reserach* **44**, 189-229.

Pearce, J.A. (1983). The role of the sub-contiental lithosphere in magma genesis at active continental margins. Continental Basalts and Mantle Xenoliths,(eds: Hawkesworth, C. J. and Norry, M. J.), *Shiva Publishing Ltd*., *Cambridge*, Mass., 272 p.

Peccerillo, A. and Taylor, S. R. (1976). Geochemistry of Eocene Calcalkaline volcanic rocks from the Kastamonu area, Northern Turkey, *Contributions to Mineralogy and Petrology* **58**, 63-81.

Peccerillo, A. (1999). Multiple mantle metasomatism in central- southern Italy: geochmeical effects, timing and geodynamic implications, *Geology* **27**, 315-318.

Plank, T. (2005). Constraints from thorium/lanthanum on sediment recycling at subduction zones and the evolution of the continents, *Journal of Petrology* **46**, 921-944.

Platt, J.P. and England, P.C. (1993). Covective removal of lithosphere beneath mountain belts: thermal and mechanical consequences, *American Journal of Science* **293**, 307-336.

Polat, A., Kerrich, R., Casey, J.F. (1997). Geochemistry of Qaternary basalts erupted along the east Anatolian and Dead Sea Fault zones of southern Turkey: implications fro mantle sources, *Lithos* **40**, 55-68.

Putirka, K., Johnson, M., Kinzler, R., Walker, D. (1996). Thermobarometry of mafic igneous rocks based on clinopyroxene-liquid equilibria, 0-30 kbar, *Contributions to Mineralogy and Petrology* **123**, 92-108.

Putirka, K., Mikaelian, H., Ryerson, F., Shaw, H. (2003). New clinopyroxene-liquid thermometers for mafic, evolved, and volatile-bearing lava compositions, with applications to lavas from Tibet and the Snake River Plain, Idaho, American Mineralogist **88**, 1542-1554.

Putirka, K. (2008). Thermometers and Barometers for Volcanic Systems, Minerals, Inclusions and Volcanic Processes, Reviews in Mineralogy and Geochemistry, (eds: Putirka, K., Tepley, F.), *Mineralogical Society of America* **69**, 61-120.

Putirka, K.D**.** (2005). Igneous thermometers and barometers based on plagioclase + liquid equilibria: tests of some existing models and new calibrations, *American Mineralogist* **90**, 336-346.

Putirka, K.D, Perfit, M., Ryerson, F.J, Jackson, M.G. (2007). Ambient and excess mantle temperatures, olivine thermometry, and active vs. passive upwelling, *Chemical Geology* **241**, 177-206.

Roeder, P.L. and Emslie, R.F. (1970). Olivine-liquid equilibrium, Contributions to *Mineralogy and Petrology* **29**, 275-289.

Rollinson, H. R. (1993). Using Geochemical Data: Evaluation, Presentation, Interpretation, *Longman Scientific & Technical*, Essex, 352.

Saunders, A.D. and Tarney, J. (1979). The geochemistry of basalts from a back-arc spreading centre in the East Scotia Sea, *Geochimica et Cosmochimica Acta* **43**, 555-572.

Saunders, A.D., Tarney, J., Weaver, S.D. (1980). Transver geochemical variations across the Antartic Peninsula: implications for genesis of calkalkaline magmas, *Earth and Planetary Sciences* **46**, 4, 344-360.

Schidgen, T.F., Cosentino, D., Caruso, A., Buchwaldt, R., Yıldırım, C., Bowring, S.A., Rojay, B., Echtler, H., Strecker, M.R. (2012). Surface experssion of Eastern Mediterranean slab dynamics: Neogene topographic and structural evolution of the SW margin of the Central Anatolian Plateau, Turkey, *Tectonics* **31**-2,1-21.

Schumacher, R., Keller, J., ve Bayhan, H. (1990). Depositional characteristics of ignimbrites in Cappadocia, Central Anatolia, Turkey. *Proceedings of the International Earth Sciences Congress on Aegean Regions (IESCA)*, (eds: Savaşçın, M.Y. and Eronat, A.H.), Volume II, 435-449.

Şen, E., Aydar, E., Gourgaud, A., Kürkçüoğlu, B. (2002). La phase explosive précédant l'extrusion des dômes volcaniques: exemple du dôme rhyodacitique de Dikkartın Dağ, Erciyes, Anatolie centrale, Turquie, *C.R.Geoscience* **334**, 27-33.

Şen, E. (1997). *Erciyes stratovolkanın'nın (Orta Anadolu) volkanolojik ve petrolojik gelişiminin incelenmesi* ,Yüksek Mühendislik Tezi, Ankara, Türkiye, H.Ü. Fen Bilimleri Enstitüsü.

Şen, E., Kürkçüoğlu, B., Aydar, E., Gourgaud, A. and Vincent, P.M., (2003).Volcanological evolution of Mount Erciyes stratovolcano and origin of the Valibaba Tepe Ignimbrite (Central Anatolia, Turkey), *Journal of Volcanology and Geothermal Research* **125**, 225-246.

Şengör, A.M.C. and Yılmaz, Y. (1981). Tethyan evolution of Turkey: a plate tectonic approach, *Tectonophysics* **75**, 181-241.

Şengör, A.M.C., Görür, N. and Şaroğlu, F. (1985). Strike slip faulting and related basin formation in zones of tectonic escape: Turkey as a case study, Strike-slip Deformation, Basin Formation and Sedimantation, (eds:T.R. Biddle and N. Christie-Blick), *Society* of *Economic Paleontologists* and *Mineral* Special Publication **37**, 227-264.

Şengör, A.M.C. (1980). Türkiyenin Neotektoniğinin Esasları. *Geological Society of Turkey*, 40 pp.

Seyitoğlu, G. and Scott, B. (1992). Late Cnezoic volcanic evolution of the northeastern Aegean region, Journal of Volcanology and Geothermal Research **54**, 157-176.

Seyitoğlu, G., Aktuğ, B., Karadenizli, L., Kaypak, B., Şen, Ş., Kazancı, N., Işık, V., Esat, K., Parlak, O., Varol, B. (2009). A Late Pliocene-Quternary pinched crustal wedge in NW Central Anatolia, Turkey: a neotectonic structure accommodating the internal deformation of the Anatolian plate, *Geol Bull Turkey* **52**, 121-154.

Seyitoğlu, G., Anderson, D., Nowell, G. and Scott, B. (1997).The evolution from Miocene potassic to Quaternary sodic magmatism in western Turkey: Implications for enrichments processes in lithospheric mantle, *Journal of Volcanology and Geothermal Research* **76**, 127-147.

Shaw, D.M. (1970). Trace element fractionation during anatexis, *Geochimica Cosmochimica Acta* **34**, 237-43.

Shaw, J.E, Baker, J.A., Menzies, M.A.,Thirlwall, M, Ibrahim, K. (2003). Petrogenesis of the Largest Intraplate Volcanic Field on the Arabian Plate (Jordan): a Mixed Lithosphere–Asthenosphere Source Activated by Lithospheric Extension, *Journal of Petrology* **44**, 9, 1657-1679.

Sheppard, S. And Taylor, W.R. (1992). Barium and LREE-rich, olivine-mica-lamprophyres with affinities to lamproites, Mt. Bundey, Northern Territory, Australia, *Lithos* **28**, 303-325.

Siebel, W., Schmitt, A.K., Kiemele, E., Danisˇı´k, M., Aydin, F. (2011). Acigöl rhyolite field, central Anatolia (part II): geochemical and isotopic (Sr–Nd–Pb, d18O) constraints on volcanism involving two high-silica rhyolite suites, *Contributions to Mineralogy and Petrolology* **162**,1233–1247.

Sisson, T.W. and Grove, T.L. (1993). Experimental investigations of the role of H2= in calc-alkaline differentiation and subduction zone magmatism, *Contributions to Mineralogy and Petrology* **113**, 143-166.

Stern, C. R., Kilian, R., Olker, B., Hauri, E. H., and Kyser, T.K. (1999). Evidence from mantle xenoliths for relatively thin 100 km continental lithosphere below the Phanerozoic crust of southernmost South America, *Lithos* **48**, 217–235.

Sugawara, T. (2001). Ferric iron partitioning between plagioclase ans silicate liquid: thermodynamics and petrological applications, *Contributions to Mineralogy and Petrology* **141**, 659-686.

Sun, S. S. and McDonough, W. F. (1989). Chemical and isotopic systematics of oceanic basalts: implications for mantle composition and processes, (eds: Saunders, A. D., and Norry, J.) Magmatism in the ocean basin, *Geol.Soc. Lond. Spec. Publ.* **42**, 313-345.

Tang, Y.J., Zhang, H.F., Ying, J.F. (2006). Asthenoshere-litospheric mantle interaction in an extensional regime: Implication from the geochemistry of Cenozoic basalts from Taihang Mountains, North China Craton, *Chemical Geology* **233**, 309-327.

Temel, A., Gündoğdu, M.N., Gourgaud, A. and Le Pennec, J.-L. (1998) Ignimbrites of Cappadocia: Petrology and Geochemistry, *Journal of Volcanology and Geothermal Research* **85**, 447-471.

Temel, A. (1992). *Kapadokya Eksplozif Volkanizmasının Petrolojik ve Jeokimyasal Özellikleri*, Doktora Tezi, Hacettepe Üniversitesi Fen Bilimleri Enstitüsü, Ankara.

Toplis, M.J. and Carroll, M.R. (1995). An experimental study of the influence of oxygen fugacity on Fe-Ti oxide stability, phase relations and mineral-melt equilibria in ferro-basaltic systems, *Journal of Petrology* **36**, 1137-1170.

Toplis, M.J. (2005)The thermodynamics of iron and magnesium partitioning between olivine and liquid: criteria for assessing and predicting equilibrium in natural and experimantal systems, *Contributions to Mineralogy and Petrology* **149**, 22-39.

Toprak, V. and Göncüoğlu, M.C. (1993). Keçiboyduran–Melendiz fayı ve bölgesel anlamı (OrtaAnadolu), *Yerbilimleri* **16**, 55–65.

Turner, S., Arnaud, N., Liu, J., Rogers, N., Hawkesworth, C., Harris, N., Kelley, S., Van Calsteren, P., Deng, W (1996). Post-collision, Shoshonitic Volcanism on the Tibetan Plateu: Implications for Convective Thinning of the Lithosphere and the Source of Ocean Island Baslats, *Journal of Petrology* **37**, 1, 45-71.

Turner, S., Hawkesworth, C., Liu, J., Rogers, N., Kelly, S. And Van Calsteren, P. (1993). Timing of Tibetan uplift constrained by analysis of volcanic rocks*, Nature* **364**, 50-53.

Turner, S., Sandiford, M. and Foden, J.D. (1992). Some geodynamic and compositional constraints on “post orogenic” magmatism, *Geology* **20**, 931-934.

Üstünışık, G. and Kılınç, A. (2011). The role of fractional crystallization, magma recharge, and magma mixing in the differentiation of the Small Hasandag volcano, Central Anatolia, Turkey, *Lithos* **125**, 984-994.

Vennemann, T.W. and Smith, H.S. (1990). The rate and temparature of reaction of ClF3 with silicate minerals, and their relevance to oxygen isotope analysis, *Chemical Geology* **86**, 83-88.

Verma, S. And Haseneka, T. (2005).Sr, Nd and Pb isotopic and trace element geochemical constraints for a veined-mantle source of magmas in the Michoacan-Guanajuato Volcanic Field, west-central Mexican Volcanic Belt, *Geochemical Journal* **38**, 43-65.

Wang, KL., Chung, SL., O'Reilly SY., Sun, SS., Shinjo, R., Chen, CH., (2004). Geochemical constraints for the genesis of post-collisional magmatism and the geodynamic evolution of the northern Taiwan region, *journal of Petrology* **45**, 5, 975-1011.

Wasserburg, G. J., Jacobsen, S. B., De Paolo, D. J., Mc Culloch, M.T. and Wen, T. (1981). Precise determination of Sm and Nd isotopic abundances in Standard solutions, *Geochiminica et Cosmochimica Acta* **45**, 2311-2323.

White, W.M., Albaréde and Télouk, P. (2000). High-precision analysis of Pb isotope ratios by multi-collector ICP-MS, *Chemical Geology* **167**, 257-270.

Wilson, M. (1989). Igneous Petrogenesis, *Unwin Hyman Ltd., London, UK*, 466 pp.

Wood, B.J. and Fraser, D.G. (1976). Elementary thermodynamics for geologists, *Oxford, Oxford University Press*.

Yetiş, C. and Demirkol, C. (1984). Ecemiş fay kuşağının jeo-tektonik evrimi, *Yerbilimleri* **11**, 1-12.

Yılmaz, Y. (1990). Allochthonous terranes in the Tethyan Middle East: Anatolia and the surroundings regions, *R. Soc. Lond. Philos. Transact*., A331, 611-624.

Yürür, T., Chorowicz, J. (1998). Recent volcanism, tectonics and plate kinematics near the junction of African, Arabian and Anatolian plates in the eastern Mediterranean, *J. Volcanol. Geothermal Res*. **85**, 1-15.

Zhu, D.C., Pan, G.T., Mo, X.X., Liao, Z.L., Jiang, X.S., Wang, L.Q., Zhao, Z.D. (2007). Petrogenesis of volcanic rocks in the Sangxiu Formation, central segment of Tethyan Himalaya: A probable example of plume–lithosphere interaction, *Journal of Asian Earth Sciences* **29**, 320-335.

Zindler, A. and Hart, S. (1986). Chemical Geodynamics, *Annual Review of Earth and Planetary Science* **14**, 493-571.